Snow Level Elevation over the Western United States: An Analysis of Variability and Trend

by

Bohumil M. Svoma

A Dissertation Presented in Partial Fulfillment
of the Requirements for the Degree
Doctor of Philosophy

Approved March 2011 by the
Graduate Supervisory Committee:

Randall S. Cerveny, Chair
Robert C. Balling Jr.
Andrew W. Ellis

ARIZONA STATE UNIVERSITY

May 2011

ABSTRACT

Many previous investigators highlight the importance of snowfall to the water supply of the western United States (US). Consequently, the variability of snowpack, snowmelt, and snowfall has been studied extensively. Snow level (the elevation that rainfall transitions to snowfall) directly influences the spatial extent of snowfall and has received little attention in the climate literature. In this study, the relationships between snow level and El Niño-Southern Oscillation (ENSO) as well as Pacific Decadal Oscillation (PDO) are established. The contributions of ENSO/PDO to observed multi-decadal trends are analyzed for the last ~80 years. Snowfall elevations are quantified using three methods: (1) empirically, based on precipitation type from weather stations at a range of elevations; (2) theoretically, from wet-bulb zero heights; (3) theoretically, from measures of thickness and temperature. Statistically significant ($p < 0.05$) results consistent between the three datasets suggest snow levels are highest during El Niño events. This signal is particularly apparent over the coastal regions and the increased snow levels may be a result of frequent maritime flow into the western US during El Niño events. The El Niño signal weakens with distance from the Pacific Ocean and the Southern Rockies display decreased snow level elevations, likely due to maritime air masses within the mid-latitude cyclones following enhanced meridional flow transitioning to continental air masses. The modulation of these results by PDO suggest that this El Niño signal is amplified (dampened) during the cold (warm) phase of the PDO particularly over Southern California. Additionally, over the coastal states, the La Niña signal during the cold PDO is similar to the general El Niño signal. This PDO signal is likely due to more zonal (meridional) flow throughout winter during the cold (warm) PDO from the weakening (strengthening) of the Aleutian low in the North Pacific. Significant trend results indicate widespread increases in snow level across the western US. These trends span changes in PDO phase and trends with ENSO/PDO variability removed are significantly positive. These results suggest that the wide spread increases in snow level are not well explained by these sea surface temperature oscillations.

DEDICATION

To my loving wife Lauren, her love and support has made the completion of this dissertation possible.

ACKNOWLEDGEMENTS

I thank Dr. Randy S. Cerveny for his guidance on this dissertation and throughout my graduate career as well as Dr. Andrew W. Ellis and Dr. Robert C. Balling Jr. for their guidance. In addition, I thank Rich Thompson and John Hart of the National Weather Service Storm Prediction Center for providing the rawinsonde data. Lastly, this material is based upon work supported by a Science Foundation Arizona fellowship.

TABLE OF CONTENTS

Page

LIST OF TABLES……..…viii

LIST OF FIGURES…….xii

CHAPTER

1 INTRODUCTION……..…...1

Significance of Problem……1

Problem Statement and Hypothesis……...1

Brief Overview of Data and Methods……...……3

Organization of Dissertation…….4

2 LITERATURE REVIEW…….5

Introduction…….……...5

Importance of Snowfall…….……6

Global Climate Change and Mountain Snowpack……....…7

Teleconnections and Snowpack in the Western United States……....9

Regional Warming and Snowpack in the Western United States…….....12

Conclusion…….…14

3 DATA…….....17

Introduction…….17

Study Area……...27

Data for Snow Level Quantification……29

Supplementary Data……...….39

Conclusion……...……42

4 METHODS……...…….44

Introduction……...……..44

Wet-Bulb Zero Method……...……45

COOP Snow Level Approximation Method……..…… 46

Reanalysis Method……..……51

Teleconnection Analysis…….……52

Page

CHAPTER

Trend Analysis……65

Control Methods……68

Conclusion……71

5 THE ENSO AND PDO RELATIONSHIP WITH SNOW LEVELS……74

Introduction……74

ENSO/PDO and Upper-Air Thickness/Temperature……75

ENSO/PDO and Wet-Bulb Zero Height……99

ENSO/PDO and Winter Watershed Percentages……107

Similarities in the Three ENSO/PDO Analyses……119

Discussion of the ENSO Results……120

Discussion of the Modulation of ENSO Results by PDO……122

Conclusion……123

6 TRENDS IN SNOW LEVEL ELEVATION……126

Introduction……126

Trends in Winter Wet Day Temperature and Thickness……126

Trends in Winter Wet Day WBZ Height……131

Trends in Estimated Snow Levels……143

Similarities in the Three Trend Analyses……150

Discussion……152

Conclusion……153

7 ARE TRENDS EXPLAINED BY NATURAL VARIABILITY?……155

Introduction……155

Trends with ENSO Variability Removed……155

Trends with ENSO and PDO Variability Removed……160

Trends during Three Different Transitions of PDO……175

Summary of Results……185

Discussion……185

Page

CHAPTER

Conclusion……187

8 CONCLUSION……189

Summary of Research Problem……189

Summary of Data and Methods……190

Summary of Results……191

Future Research……192

REFERENCES

APPENDIX

Supplementary Figures……202

LIST OF TABLES

Table		Page
3.1	The ten rawinsonde sites providing daily wet-bulb zero (WBZ) heights for both the 0000 UTC and 1200 UTC soundings	19
3.2	The ten watersheds adjacent to the rawinsonde sites in Table 3.1	21
3.3	The COOP stations for each of the ten watersheds in Table 3.2	22
3.4	Comparative location information for the ten rawinsonde sites in Table 3.1 and the adjacent COOP sites used as proxies for precipitation data at the rawinsonde sites	41
5.1	Field significance for tests establishing the relationship between SOI and temperature/thickness (1949-2009)	76
5.2	Descriptive statistics for the Pearson product-moment correlation results for the 60 NCEP/NCAR reanalysis grid points (1949-2009)	76
5.3	As in Table 5.2, but for the Kendall's Tau correlation tests	76
5.4	Descriptive statistics for the percent of wet day cold season temperature/thickness values during El Niño events greater than the neutral ENSO median (1949-2009)	78
5.5	As in Table 5.2, but for La Niña events	78
5.6	Descriptions of the regions displaying homogeneous ENSO signals in temperature/thickness introduced in Section 5.2	80
5.7	As in Table 5.1 but for the cold PDO (1949-1976)	84
5.8	As in Table 5.2 but for the cold PDO (1949-1976)	85
5.9	As in Table 5.3 but for the cold PDO (1949-1976)	85
5.10	As in Table 5.4 but for the cold PDO (1949-1976)	86
5.11	As in Table 5.5 but for the cold PDO (1949-1976)	87
5.12	As in Table 5.1 but for the warm PDO (1977-1998)	88
5.13	As in Table 5.2 but for the warm PDO (1977-1998)	88
5.14	As in Table 5.3 but for the warm PDO (1977-1998)	88
5.15	As in Table 5.4 but for the warm PDO (1977-1998)	89

Table Page

5.16 As in Table 5.5 but for the warm PDO (1977-1998)……..……..90

5.17 From 1958-2010, for the ten rawinsonde sites, the test results for establishing the relationship between SOI and WBZ height……...….100

5.18 As in Table 5.17, but for the cold PDO (1958-1976)……..……....105

5.19 As in Table 5.17, but for the warm PDO (1977-1998)……106

5.20 For the ten watersheds, the test results for establishing the relationship between SOI and the percentage of wet days per winter with estimated snow level above the specified elevations……..……..108

5.21 As in Table 5.20, but for the cold PDO (1947-1976)……..……112

5.22 As in Table 5.20, but for the 1925-1946 warm PDO……...……115

5.23 As in Table 5.20, but for the 1977-1998 warm PDO……...….117

6.1 Field significance of trend tests for cold season median wet day temperature and thickness since 1949……..…….128

6.2 Descriptive statistics for the simple linear regression trend test results for cold season median wet day temperature and thickness at the 60 NCEP/NCAR reanalysis grid points since 1949……..……129

6.3 As in Table 6.2, but for Mann-Kendall trend test results……..…129

6.4 Mann-Kendall and simple linear regression trend test results for cold season median wet day WBZ height at the ten rawinsonde sites……...132

6.5 Mann-Kendall and simple linear regression trend test results for the percentage of wet days per winter with snow level estimated as above the specified elevations for the ten watersheds……...139

7.1 Field significance of trend tests for cold season median wet day temperature and thickness with ENSO variability removed……...…..156

7.2 Descriptive statistics for the simple linear regression trend tests on the residuals resulting from regressing cold season median wet day temperature/thickness against fall SOI at the 60 NCEP/NCAR reanalysis grid points……..…157

Table Page

7.3 As in Table 7.2 but for the Mann-Kendall trend test……..……..157

7.4 Results for the Mann-Kendall and simple linear regression trend tests on the residuals resulting from regressing cold season median wet day 0000 UTC WBZ heights against fall SOI……..….159

7.5 Results for the Mann-Kendall and simple linear regression trend tests on the residuals resulting from regressing cold season percentages of estimated snow levels above the given elevations against fall SOI……..160

7.6 Assuming that the PDO has remained in its warm phase, descriptive statistics for the multiple linear regression results for temperature/thickness over the 60 NCEP/NCAR reanalysis grid points……..…….…...162

7.7 As in Table 7.6, but assuming the PDO entered a cold phase in 1999……..….163

7.8 Assuming that the PDO has remained in its warm phase, the multiple linear regression results for cold season median 0000 UTC WBZ heights and the trends in the resulting residuals……..…….……164

7.9 As in Table 7.8, but assuming the PDO entered a cold phase in 1999……..….165

7.10 Assuming that the PDO has remained in its warm phase, the multiple linear regression results for cold season percentages of estimated snow levels above the given elevations and the trends in the resulting residuals……166

7.11 As in Table 7.10, but assuming the PDO entered a cold phase in 1999……..…....167

7.12 Assuming that the PDO has remained in its warm phase, field significance of trend tests for cold season median wet day temperature/thickness with ENSO and PDO variability removed…….……...170

7.13 Assuming PDO as remained in a warm phase, descriptive statistics of residual trends (simple linear regression) when temperature/thickness is regressed against fall SOI (X_1), the PDO phase indicator variable (X_2), and the interaction effects variable……..…..171

7.14 As in Table 7.13, but for the Mann-Kendall trend test……171

7.15 As in Table 7.12, but assuming that the PDO entered a cold phase in 1999……...171

Table Page

7.16 As in Table 7.13, but assuming that the PDO entered a cold phase in 1999……..…..172

7.17 As in Table 7.14, but assuming that the PDO entered a cold phase in 1999……..…..172

7.18 For the three sub-periods (i.e., the first warm to cold PDO transition, the cold to warm PDO transition, and the possible most recent warm to cold PDO transition), simple linear regression trend test results for the ten watersheds……..….177

7.19 As in Table 7.18 but for the Mann-Kendall trend test……...……..181

LIST OF FIGURES

Figure Page

3.1 The ten rawinsonde sites and adjacent COOP sites used as precipitation proxies.……..…...18

3.2 The ten watersheds adjacent to the rawinsonde locations along with the COOP stations providing daily precipitation and snowfall data for each watershed…….…….…….....20

3.3 The USHCN stations providing daily precipitation as proxies for precipitation at the NCEP/NCAR reanalysis grid locations.……..….....22

3.4 The area of study defined by the eleven western most states in the contiguous United States. …….…….....27

5.1 Pearson product-moment correlation coefficients between normalized fall SOI and cold season median wet day temperature and thickness……....79

5.2 As in Figure 5.1, but for Kendall's Tau non-parametric correlation……...81

5.3 The percentage of winter wet day values during El Niño events greater than the median value for neutral ENSO conditions for temperature and thickness……82

5.4 As in Figure 5.3, but for La Niña events……..…83

5.5 As in figure 5.1 but for the cold PDO (1949-1976)……..…91

5.6 As in figure 5.2 but for the cold PDO (1949-1976)…….……92

5.7 As in figure 5.3 but for the cold PDO (1949-1976)…….……93

5.8 As in figure 5.4 but for the cold PDO (1949-1976)…….……94

5.9 As in figure 5.1 but for the warm PDO (1977-1998)…….…..95

5.10 As in figure 5.2 but for the warm PDO (1977-1998)…….……..96

5.11 As in figure 5.3 but for the warm PDO (1977-1998)…….……..97

5.12 As in figure 5.4 but for the warm PDO (1977-1998)…….....…….…...98

5.13 The 850-700 hPa thickness panel from Figure 5.3, Figure 5.7, Figure 5.11, Figure 5.4, Figure 5.8, and Figure 5.12 illustrating the modulation of the El Niño signal and the La Niña signal by the

Figure Page

cold PDO and the warm PDO…….……99

5.14 Correlation results between normalized fall SOI and winter median WBZ height for the entire period of record, the cold PDO and warm PDO…….……101

5.15 Percentage of winter wet day WBZ heights during El Niño events and La Niña events greater than the median value for neutral ENSO conditions for the entire period of record, the cold PDO, and the warm PDO…….…….....103

5.16 Correlation results between normalized fall SOI and winter percentage of winter wet days with snow level above the elevation of the specified station in each watershed…….....109

5.17 The difference in the means of the percentage of precipitation days with snow level above the elevation of the specified station within each watershed for El Niño/La Niña conditions and neutral ENSO conditions…….....…110

5.18 Pearson correlation results between normalized fall SOI and winter percentage of winter wet days with snow level above the elevation of the specified station in each watershed for different PDO phases…….....113

5.19 As in Figure 5.18 but for Kendall's Tau correlations…….....114

5.20 The difference in the means of the percentage of precipitation days with snow level above the elevation of the specified station within each watershed for El Niño conditions and neutral ENSO conditions for different PDO phases……..……116

5.21 As in Figure 5.20 but for La Niña conditions…….118

6.1 From 1949-2009, trends (for simple linear regression) in cold season median wet day temperature and thickness……..127

6.2 As in Figure 6.1, but for the Mann-Kendall test…….130

6.3 Cold season median 0000 UTC WBZ heights and simple linear fits for the rawinsonde sites near Boise, ID and Oakland, CA……...133

Figure Page

6.4 As in Figure 6.3 but for the rawinsonde sites near Albuquerque, NM and Grand Junction, CO……134

6.5 As in Figure 6.3 but for the rawinsonde sites near Tucson, AZ and Salt Lake City, UT…….....……...135

6.6 As in Figure 6.3 but for the rawinsonde sites near Vandenberg Air Force Base, CA and Medford, OR…….....……...136

6.7 As in Figure 6.3 but for the rawinsonde sites near Salem, OR and Spokane, WA…….....….137

6.8 From 1958-2009, trends in cold season median wet day 0000 UTC WBZ height for simple linear regression and Mann-Kendall trend test….....….138

6.9 For the Pend Orielle/Priest /Pend Orielle Lake watershed, observed time series and simple linear regression fits of the percentage of wet days per cold season with snow level estimated above the specified elevations……..……...144

6.10 As in Figure 6.9, but for the Salt/Lower Verde watershed….....145

6.11 As in Figure 6.9, but for the Ventura-San Gabriel /Santa Ana watershed….....146

6.12 As in Figure 6.9, but for the Weber/Jordan watershed.. 146

6.13 As in Figure 6.9, but for the Upper Rio Grande watershed….....147

6.14 As in Figure 6.9, but for the Colorado Headwaters watershed….....147

6.15 As in Figure 6.9, but for the South Salmon/Payette/Weiser watershed….....148

6.16 As in Figure 6.9, but for the San Joaquin watershed….....148

6.17 As in Figure 6.9, but for the Middle/Upper Rogue watershed….....149

6.18 As in Figure 6.9, but for the North Santium/Molalla-Pudding/Clackamas watershed….....149

7.1 From 1949-2009, residual trends (for simple linear regression) in cold season median wet day values resulting from regressing temperature and thickness against fall SOI…….....……158

7.2 Assuming that the PDO has remained in its warm phase, residual trends

Figure Page

(for simple linear regression) when temperature and thickness are regressed against fall SOI, the PDO phase indicator variable, and the interaction effects variable…….....……..169

7.3 As in Figure 7.2, but assuming the PDO entered a cold phase in 1999……...…….....173

Chapter 1: Introduction

1.1 Significance of Problem

The presence of a large and persistent snowpack in the mountains of the western United States (US) is important for alleviating or preventing drought. When considering agricultural drought (e.g., soil moisture deficit; Keyantash and Dracup 2002) or hydrologic drought (e.g., water storage deficit; Keyantash and Dracup 2002), snowfall is important due to its generally slower rate of return to the atmosphere as water vapor than rainfall. Many major cities throughout the western US are dependent on water stored in reservoirs that are filled from high elevation headwaters of major rivers (Rauscher et al. 2008; Hidalgo et al. 2009) and snow melt accounts for at least 75% of the annual discharge for the majority of rivers throughout the western US (Cayan 1996). An average surface air temperature warming of 0.16 ^{o}C dec^{-1} has been observed over the western US during November through March from 1950-1997 (Mote et al. 2005) and trends during December through January range from +0.1 to +0.9^{o}C dec^{-1} since 1979 (IPCC 2007). Additionally, by the mid-21st century, projected temperatures over the western US may range between 0.8 and 1.7^{o}C greater than present values (Barnett et al. 2005). The elevation of snow level (i.e., the elevation that snowfall transitions to rainfall) is sensitive to regional warming and theoretically influences the snow water equivalent (SWE) of spring snowpack (Svoma 2011; Casola et al. 2009).

1.2 Problem Statement and Hypothesis:

In the western US, the relationships between atmospheric teleconnections (i.e., linkages between atmospheric/oceanic phenomena in widely separated parts of the earth (Hushcke 1959)) such as El Niño-Southern Oscillation (ENSO) and Pacific Decadal Oscillation (PDO) and variables such as snowpack, precipitation, and temperature have been studied extensively in recent years (Gershunov and Barnett 1998b; Gutzler et al. 2002; Brown and Comrie 2004; Goodrich 2007). The influence of regional warming (potentially anthropogenic) on the snowpack of the

western US has also received considerable attention in the recent literature; however, the interannual variability of snow level has received little attention.

As the elevation of snow level is directly related to the spatial extent of snow cover resulting from a snowfall event (Svoma 2011; Casola et al. 2009), an explicit focus on the elevation of snow level as it relates to both natural climate variability and anthropogenic climate change is important. This cannot be directly determined by studying snowfall and precipitation trends at individual stations, which has been done by previous investigators (Knowles et al. 2006; Feng and Hu 2007; Kunkel et al. 2009a; 2009b). In addition, the quantification of the elevation of snow level does not require knowledge of the specific snowfall totals recorded on a given day which is beneficial for identifying a potentially subtle climate change signal considering that the accuracy of daily snowfall totals have encountered much scrutiny in the past (Knowles et al. 2006; Kunkel et al. 2007).

Through the use of multiple separate measures of snow level, I seek to answer the following three research questions:

(1) What is the relationship between a set of climatic teleconnections (i.e., ENSO and PDO) and snow level and how does this vary across on the western US?

(2) Considering the changing characteristics of the western US snowpack likely occurring in response to the ongoing buildup of greenhouse gases (Barnett et al. 2008 Pierce et al. 2008), is there a climate change signal in the elevation of snow level and how does this vary across the western US?

(3) Given the existence of a climate change signal in snow level, is this outside the realm of natural climate variability in the form of ENSO and PDO?

My three corresponding hypotheses are:

(1) Considering the higher frequency of maritime air flow into the western US during El Niño events along with more zonal air flow (east-west rather than north-south) during

cold PDO periods (Higgins et al. 2002; Brown and Comrie 2004), I expect snow levels to be the highest during El Niño events occurring in conjunction with the cold PDO.

(2) Based on the numerous studies suggesting trends in twentieth century climate across the western US consistent with large scale warming (e.g., Mote et al. 2008; Rauscher et al. 2008; Barnett et al. 2008, Pierce et al. 2008; Hidalgo et al. 2009), I expect to find predominantly increasing trends in snow level across the western US.

(3) Considering that Knowles et al. (2006) found snowfall to rainfall ratios across the western US to be lower during the more recent warm phase of the PDO (1977-1998) than the earlier warm phase (1925-1946), one should expect increasing snow level outside the realm of variations in PDO. Furthermore, considering the numerous recent studies suggesting that changing climate in the western US is due to increased temperature from anthropogenic forcing (e.g., Barnett et al. 2008; Pierce et al. 2008), I expect increasing snow levels to not be well explained by the potential increase in the frequency and strength of El Niño events alone.

1.3 A Brief Overview of Data and Methods

To evaluate snow level at daily resolution using three separate methods of snow level quantification I created three independent datasets. The first is a collection of daily wet-bulb zero (WBZ) heights from 1957-2010 at ten rawinsonde locations across the western US. The height of WBZ is an estimator of the vertical distance above sea level where frozen precipitation transitions to liquid precipitation (Gedzelman and Arnold 1993; Albers et al. 1996; Bourgouin 2000; Wetzel and Martin 2001). Second, I acquired daily snowfall and precipitation totals from the National Weather Service Cooperative Observer (COOP) Network as a measure of daily precipitation type over various elevations across each of ten watersheds adjacent to the rawinsonde sites. From these data, I empirically estimated snow level at daily resolution from ~1924-2009. Lastly, I obtained upper-air reanalysis data from the National Center for Environmental Prediction/National Center for Atmospheric Research (NCEP/NCAR) at 2.5^{o} resolution across the western US. More

specifically, from 1948-2009, daily temperature and geopotential height (the geopotential height is proportional to the potential energy of a unit mass at that height relative to sea level; e.g., Huschke 1959) were obtained for various equal pressure levels including the 1000 hPa, the 850 hPa, the 700 hPa, and the 500 hPa isobaric surfaces. From the reanalysis data I focused on the 850 hPa temperature, the 1000–500 hPa thickness, the 1000–850 hPa thickness and the 850–700 hPa thickness (Heppner 1992) which have been found to effectively discriminate between frozen and liquid precipitation at the surface (Heppner 1992).

From these data, I created time series representing the interannual variability in these snow level proxies. The time series were subject to various statistical techniques to determine the influence of ENSO/PDO on snow level (e.g., parametric and non-parametric correlations along with bootstrapping techniques), linear trends in snow level (e.g., parametric and non-parametric trend tests), and the likelihood that observed trends in snow level are outside the influences of ENSO/PDO (e.g., residual trends from simple/multiple linear regression and detailed time series analysis). Additionally, the spatially variability of the findings across the western US were examined through the mapping of relevant test statistics and the calculation of local indicators of spatial autocorrelation on these statistics (specifically the local Moran's I).

1.4 Organization of Dissertation

In the remainder of this dissertation I identify the gaps in literature that inspire the research questions above through an extensive review of the literature regarding anthropogenic climate change and natural climate variability in climate variables related to snowpack with an emphasis on the western US (Chapter 2). Following this, detailed discussions regarding the data sources (Chapter 3) and methods (Chapter 4) are given. Subsequently I employ the methods in Chapter 4 to determine the relationship between ENSO/PDO and snow level (Chapter 5), identify trends snow level (Chapter 6) and control for ENSO/PDO in the snow level trends (Chapter 7). Lastly, I summarize my findings and provide direction for future research (Chapter 8).

Chapter 2: Literature Review

2.1 Introduction

As discussed in the previous chapter, the main objectives of this dissertation are to establish the relationship between snow level elevation and natural climate variability as well as anthropogenic climate change in the western United States (US). As a foundation for this dissertation, and future research, it is important to first establish the findings of previous investigations of snowfall, snowpack and other related variables. The western US has received considerable attention in the literature regarding the influence of climate change on the cryosphere. This attention is well justified as (1) the warming over the western US in the late twentieth century has been more rapid than the global warming ($0.16^{o}C\ dec^{-1}$; Mote et al. 2005); (2) the expected continued warming of up to $1.7^{o}C$ by the middle of the twenty-first century (Barnett et al. 2005); (3) snowmelt is the major source of runoff for most rivers and streams in the western US (Cayan 1996); (4) many metropolitan areas throughout the West are dependent on water stored in reservoirs that are recharged from spring snowmelt at higher elevations (Raushcer et al. 2008; Hidalgo et al. 2009). Despite this attention, the elevation of snow level, and the interannual variability thereof, has not been the focus of many previous investigations (e.g., Svoma 2011).

In this chapter, I begin by discussing the importance of snowfall to the human water supply and give a general overview of global climate change and mountain snowpack. I then discuss the known natural interannual variability in the snowpack of the western US, and review previous research on the sensitivity of snowpack in the western US to sustained regional warming. Lastly, I synthesize this information to reveal the contribution that my dissertation will provide to this literature base; specifically, the establishment of natural climate change signals and anthropogenic climate change signals in the elevation of snowfall level throughout the western US.

2.2 The Importance of Snowfall to Human Water Resources

In many mountainous regions, the presence of a large and persistent snowpack is important for human water resources (Minder 2010). One-sixth of the world's population is reliant on glaciers or seasonal snow cover for water supply (Barnett et al. 2005). In these regions, snowfall is a key element for alleviating/preventing agricultural drought (e.g., soil moisture deficit; Keyantash and Dracup 2002) or hydrologic drought (e.g., water storage deficit; Keyantash and Dracup 2002). This is due to snowfall's generally slower rate of return to the atmosphere as water vapor than rainfall. Temperatures are lower over snow-covered surfaces (as opposed to surfaces moistened by rainfall) due to less net radiation from higher albedo and less sensible heat flux (Cohen and Rind 1991). The lower sensible heat flux is due to the (1) additional energy required to melt snow before evaporation and (2) the higher latent heat of sublimation than latent heat of evaporation (Cohen and Rind 1991). In addition, relative to rainfall and discontinuous snow cover, accumulating snowfall increases spring/early summer soil moisture as rainfall and rapid snowmelt result in overland flow while accumulated snow acts as a longer term source of moisture, slowly percolating water into the soil (Williams et al. 2009).

In regards to hydrologic drought, many major cities throughout the world are dependent on water stored in reservoirs that are filled from high elevation headwaters of major rivers (Barnett et al. 2005, Raushcer et al. 2008; Hidalgo et al. 2009; Minder 2010). In these metropolitan areas, water demand is often the highest during the summer and early fall due to hydroelectric power needs and higher potential evapotranspirtaiton (Barnett et al. 2005). When a winter is dominated by accumulating snowfall resulting in a large spring snowpack, the majority of runoff for that water year (October-September) occurs during a time when water demands are higher (i.e., center-timing occurs in early summer; e.g., Stewart et al. 2005; Hamlet et al. 2007; Raushcer et al. 2008; Hidalgo et al. 2009). When winters are dominated by rainfall, or snowfall that ablates very quickly between storms, center-timing occurs earlier in the water year (Barnett et al. 2005). Earlier occurrences of center-timing often result in water lost to the oceans (Barnett et al. 2005; Raushcer

et al. 2008; Hidalgo et al. 2009). In short, snowpack acts as a natural water storage device in addition to man-made reservoirs.

2.3 Global Climate Change and the Mountain Snowpack

It is "extremely unlikely" that global climate change in the previous fifty years is due solely to natural causes and "very likely" that tropospheric warming of the Earth is due to increasing greenhouse gas concentrations (IPCC 2007). The response of the cryosphere to this warming has been the topic of a large body of research (e.g., IPCC 2007). A decline since the mid-twentieth century in Northern Hemisphere snow-covered area is evident in observational records (Brown 2000; IPCC 2007). At a smaller scale, studies focusing on temporal changes in snowfall, the liquid equivalent of melted snowpack per area (termed snow water equivalent or SWE) and other related variables have largely been confined to western North America and Europe as these locations have widespread daily observations extending back to the mid-twentieth century (IPCC 2007).

Trends toward earlier occurrences of snowmelt driven runoff (a proxy for spring snowpack ablation) have been indicated in the Alps (Bavay et al. 2009), the western US (Rauscher et al. 2008; Hidalgo et al. 2009) and the Tarim River basin in western China has seen increased streamflow during the winter, despite stable precipitation (Xu et al. 2010). Bavay et al. (2009) suggest a shift in significant snowmelt driven streamflow from midsummer to spring for certain future climate scenarios in the European Alps and hydrologic simulations with increased European temperatures suggest that the flow in the Rhine River may become dominated by winter rains resulting in periods of low flow in the summer (Barnett et al. 2005). Similarly, in the western US, by the late twenty-first century, significant snowmelt driven runoff may occur more than one month earlier than present (Stewart et al. 2004 Barnett et al. 2005, Rauscher et al. 2008) and trends toward earlier center-timing are evident in observational records (Cayan et al. 2001 Stewart et al. 2005; Hamlet et al. 2007 Rauscher et al. 2008 Hidalgo et al. 2009).

Trends toward less spring snow cover (or related variables) are also evident in climate records throughout many mountainous regions (Mote et al. 2008; Kalra et al. 2008 Barnett et al. 2008; Pierce et al. 2008; Marty 2008; Bavay et al. 2009; Green and Pickering 2009). In the Alps, Bavay et al. (2009) note that below 1,200 meters, continuous winter snow cover is declining in duration and suggest that permanent snow and ice above 3,000 meters may disappear for several future climate scenarios of the next century. Similar results were found in the Austrian Alps (Schoner et al. 2009) and the French Alps (Durand et al. 2009). A recent study in Romanian Carpathians suggests that snow cover duration is decreasing below 1700 meters (Micu 2009). The number of winter days with snow cover has also seen a recent decrease in the Northeast US (Burakowski et al. 2008) and the Swiss Alps (Marty 2008). Green and Pickering (2009) noted a general decline in snowpack in the Snowy Mountains of Australia along with the earlier thaw of snowpack in the last half century. Lastly, recent declines in snowpack in the western US have been observed by numerous researchers (e.g., Mote et al. 2008; Kalra et al. 2008 Barnett et al. 2008 Pierce et al. 2008).

Other researchers have focused on trends in precipitation type in response to climate change (Knowles et al. 2006; Feng and Hu 2007; Schoner et al. 2009; Bavay et al. 2009). In the Alps, the fraction precipitation falling as snow has seen a decrease during the summer at low elevations (Schoner et al. 2009). Bavay et al. (2009) suggest that in future climate scenarios, the Alps may see heavy precipitation events during the fall season in the form of rain instead of snow. In the western US, several researchers have found that snowfall is generally decreasing likely due to higher portions of precipitation falling as rain (Knowles et al. 2006; Feng and Hu 2007; Kunkel et al. 2009a).

While much of the literature indicates declines in snow cover (or other related variables), some results have been sensitive to the time of year, elevation of snow measurements, and precipitation variability (Stewart 2009). Ye and Ellison (2003) found increases in the length of continuous snow cover in northern European Russia despite the earlier melting of snow in the spring. Similar results were found in northern Eurasia by Adam et al. (2009), who indicate a future

increase in snow accumulation due to increased precipitation as determined from a physically based hydrologic model. Ke et al. (2009) found positive trends in winter snowfall in Qinghai, China, likely due to the high elevations of analysis. Similarly, trends in snowpack in the western US have not been uniform, as a few high elevation areas have seen increases in snow depth due to increasing precipitation (Mote et al. 2005; Mote 2006; Casola et al. 2009; McCabe and Wolock 2009).

2.4 Teleconnections and Snowpack in the Western United States

Teleconnections are linkages between atmospheric/oceanic phenomena in widely separated parts of the world (Hushcke 1959). Teleconnections have been found to influence both the mean and extremes of weather events for many regions of the Earth (Stoner et al. 2009). One such teleconnection is the El Niño–Southern Oscillation (ENSO) which is perhaps the most important pattern in global natural climate variability (Stoner et al. 2009). ENSO involves oceanic and atmospheric circulation variations in the tropical Pacific Ocean with a periodicity of 1 to 7 years (Kestin et al. 1998). El Niño events, warm water anomalies over the eastern equatorial Pacific Ocean, strengthen the westerly jets both north and south of the equator (Stoner et al. 2009). Conversely, La Niña conditions favor colder sea surface temperatures in the eastern equatorial pacific and result in a weakening of the westerly jets.

Consequently, previous researchers have linked ENSO to variations in upper-air flow over North America in the context of the Pacific–North American (PNA) pattern which is characterized by differing (i.e., positive versus negative) geopotential height (i.e., the height of an isobaric surface) anomalies between the North Pacific Ocean and western North America (Wallace and Gutzler 1981). Often referred to as positive PNA, anomalously deep troughs over the North Pacific and southeastern US coincident with a stronger than normal ridge over the Rocky Mountains (Renwick and Wallace, 1996; Higgins et al. 2002; Yu and Zwiers, 2007) have been linked to El Niño events (Lau, 1997; Dettinger et al. 1998; Sheppard et al. 2002). Conversely, the negative PNA results in more zonal upper-level flow across the North Pacific and North America

and has been linked to La Niña events (Sheppard et al. 2002). ENSO has also been linked to geopotential height anomalies distinct from the PNA (e.g., Zhang et al. 1996; Straus and Shukla, 2002), specifically, the eastward shift of the of the upper-level ridge generally over the Rocky Mountains during El Niño events (Sheppard et al. 2002; Higgins et al. 2002; Straus and Shukla, 2002) resulting more maritime air flow into the western US and less cold air mass intrusion from Canada (Higgins et al. 2002). Additionally, during El Niño events, the preferred extratropical cyclone track is more likely to split and storms making landfall in southern California are supplied by lower latitude Pacific moisture sources (Sheppard et al. 2002).

The expected resulting influences of ENSO on winter temperature/precipitation over the western US have been extensively studied (e.g., Ropelewski and Halpert, 1986; Kahya and Dracup, 1994; Gershunov, 1998; Gershunov and Barnett, 1998a; Higgins et al. 2002). Over the western US, El Niño events have been linked to anomalously cool/wet winters in the southwestern US and warm/dry winters in northwestern US while La Niña events have been linked to warm/dry winters in the southwestern US and cool/wet winters in the northwestern US (Ropelewski and Halpert, 1986; Kahya and Dracup, 1994; Gershunov, 1998; Gershunov and Barnett, 1998a; Higgins et al. 2002). This spatial pattern is largely due to a southern shift of the jet stream during El Niño events and a northern jet-stream shift for La Niña events (Higgins et al. 2002). Several researchers have noted a recent prominence of El Niño events (Trenberth and Hoar, 1996; Harrison and Larkin, 1997; Rajagopalan et al. 1997; Wunsch, 1999; Solow and Huppert, 2003), and there is debate in the literature regarding the probability that this recent pattern is consistent with stationarity or climate change (Power and Smith, 2007).

Mantua et al. (1997) were among the first to discover a lower frequency sea surface temperature oscillation in the North Pacific Ocean often referred to as the Pacific Decadal Oscillation (PDO). Sea surface temperature anomalies associated with PDO are smaller than those of ENSO but occur over a much larger region (Stoner et al. 2009). During the warm phase of the PDO, waters in the eastern tropical pacific and along the west coast of North America are warmer than normal while waters in the northern and western Pacific are anomalously cool. The converse

of this spatial pattern in sea surface temperatures is apparent during the cold phase of PDO (Stoner et al. 2009). The Pacific Decadal Oscillation changed phase around the years 1925 (cold to warm), 1947 (warm to cold), 1977 (cold to warm) and possibly 1999 (Stewart et al. 2005; Knowles et al. 2006). The potential phase shift of the late 1990s was suggested by earlier researchers (Hare and Mantua 2000; Schwing et al. 2000); however, this shift was not obvious (Bond et al. 2003) and several recent investigators have ignored the potential 1999 phase shift (St Jacques et al. 2010, Ellis et al. 2010).

The mechanisms driving the PDO are not yet known (Stoner et al. 2009), and there is debate in the literature regarding the independence between ENSO and PDO as highlighted by Rodgers et al. (2004) (i.e., PDO may represent decadal variability in ENSO). As such, the PDO has largely been found to have a statistical relationship with precipitation across the western US through its connection with ENSO. The impact of ENSO on southwestern US winter precipitation/temperature is strongest and most spatially coherent during years of El Niño /Warm PDO and years of La Niña/Cold PDO. On the other hand, the ENSO signal tends to weaken during years of El Niño /Cold PDO and La Niña/Warm PDO (Gershunov and Barnett 1998b; Gutzler et al. 2002; Brown and Comrie 2004). Furthermore, Goodrich (2007) found the southwestern US to be drier than normal during winters of neutral ENSO and cold PDO and wetter than normal during the winters of neutral ENSO and warm PDO. Gershonov and Barnett (1998b) suggest that this in phase amplification is likely due to the increased strength of the Aleutian low (i.e., the increased depth of the North Pacific trough resulting more positive PNA and meridional upper-level flow) during the warm phase, shifting the jet stream further south while greater tropical moisture in the eastern pacific during coincident El Niño events provides ample moisture for the associated winter cyclones.

While most investigators have focused on precipitation when exploring the modulation of ENSO effects by the PDO, results displayed by Budikova (2005) suggest that much of the western US experiences warmer winters during the warm PDO phase. This signal appeared most apparent for the Northwest US which experiences warm winters during El Niño conditions and was least

apparent for the Southwest US (Budikova 2005). The variability in surface air temperature explained by ENSO/PDO may be a reasonable proxy for the ENSO/PDO relationship with snow level; however, it would be extremely useful to stratify the temperature data by wet and dry days.

Previous studies that have established relationships between temperature and ENSO/PDO have not discriminated between days with and without precipitation. This represents a significant gap in the literature regarding the relationships between these teleconnections and hydro-climatic variables in the western US. As the elevation of snow level throughout the cold season is one of several critical variables influencing the SWE of spring snowpack (Casola et al. 2009; Svoma 2011; Minder 2010), it is important to understand the interannual and inter-decadal variability in snow level. With established relationships between ENSO/PDO and snow level, any longer term trends, possibly related to anthropogenic forcing, can be put into the context of natural climate variability.

2.5 Regional Warming and Snowpack in the Western United States

The majority of research regarding regional warming and snow in the western US has been focused on SWE and the timing of peak spring runoff (e.g., Cayan et al. 2001; Stewart et al. 2004; Mote et al. 2005; Hamlet et al. 2005; Stewart et al. 2005; Barnett et al. 2005; Mote 2006; Hamlet et al. 2007; Kalra et al. 2008; Mote et al. 2008; Rauscher et al. 2008; Barnett et al. 2008, Pierce et al. 2008; Hidalgo et al. 2009; McCabe and Wolock 2009). There is ample empirical evidence in the literature of trends toward earlier center-timing and the maximum rate of spring snowmelt suggesting that snowpacks are ablating earlier in the spring (Cayan et al. 2001; Stewart et al. 2005; Hamlet et al. 2007; Rauscher et al. 2008; Hidalgo et al. 2009). Stewart et al. (2005) suggest that these trends have endured through changes in PDO phase and numerous model studies also indicate that such hydrological changes are due to anthropogenic influences (e.g., Rauscher et al. 2008; Hidalgo et al. 2009). Furthermore, in the late twenty-first century, significant snowmelt driven runoff may occur more than one month earlier than present over much of the western US (Stewart et al. 2004; Barnett et al. 2005; Rauscher et al. 2008).

Trends toward less spring SWE over the western US are also evident in climate records (Groisman et al. 2004; Mote et al. 2005; Hamlet et al. 2005; Mote 2006; Mote et al. 2008; Kalra et al. 2008; Barnett et al. 2008; Pierce et al. 2008). The trends are likely influenced by the regional warming while precipitation variability can create considerable noise in the SWE records (Hamlet et al. 2005; Mote et al. 2008) and some high elevation areas in the West have experienced increasing SWE due to increasing precipitation (Mote et al. 2005; Mote 2006). Results from Hamlet et al. (2005) suggest that the more widespread decreasing trends resulting from the warming are not well explained by variations in PDO while the noise from precipitation variability appears to be linked to PDO. Recent modeling studies also suggest that the recent decline in western US snowpack is connected to anthropogenic forcing rather than decadal variability (e.g., Barnett et al. 2008; Pierce et al. 2008). Lastly, twenty-first century projections suggest a decrease in snowfall and SWE across the western US except in the higher elevations where an increase may occur due to more precipitation (Kim et al. 2002; Leung et al. 2004).

Surprisingly, very few studies have tried to quantify recent trends in the meteorological conditions during days with precipitation. Knowles et al. (2006) as well as Feng and Hu (2007) conducted this type of study by analyzing trends in snowfall to rainfall ratios over a large network of stations across the west. Decreasing trends were found in the areas where warming rates were the highest and temperatures were generally warm enough to change precipitation form. Geographically, these areas were mainly in the Pacific Northwest and the Southwest. Decreasing trends were also evident in the Rocky Mountains, but there was a definite lack of spatial coherence in this region as suggested by Knowles et al. (2006) who indicate many decreasing trends adjacent to increasing trends. This spatial inconsistency was attributed to the high elevations of the stations in the interior mountains of the western US (Knowles et al. 2006).

Recently, Kunkel et al. (2009a) strictly focused on snowfall and found results consistent with those of Knowles et al. (2006) and Feng and Hu (2007). Specifically, decreasing trends in snowfall totals have been most evident in the Pacific Northwest and the Southwest while the Rocky Mountains have experienced both increases and decreases in snowfall (Kunkel et al.

2009a). In addition, declining snowfall and snow to rain ratios coincide spatially with a reduction in extreme high snowfall seasons and an increase in extreme low snowfall seasons (Kunkel et al. 2009b). Additionally, the extreme snowfall seasons are likely more sensitive to winter temperature than precipitation (Kunkel et al. 2009b). Decreases in snowfall as a result of precipitation changing form solid to liquid form are not explained well by PDO and may be a result of sustained regional warming due to long-term anthropogenic climate change (Knowles et al. 2006).

Snowfall to rainfall ratios as examined by Knowles et al. (2006) and Feng and Hu (2007) are certainly influenced by snow level elevation as are total snowfall and extreme snowfall seasons examined by Kunkel et al. (2009a; 2009b). Previous investigations explicitly examining snow level and long term climate change, however, are scarce in the peer-reviewed literature. This is surprising, considering the numerous studies that imply an important connection between snowfall trends, SWE trends, and elevation (e.g., Mote et al. 2005; Mote 2006; Knowles et al. 2006; Pierce et al. 2008; Casola et al. 2009; Svoma 2011).

2.6 Conclusion

Although climate change signals in snow level have been studied indirectly through snowfall and rainfall trends (Knowles et al. 2006; Feng and Hu 2007; Kunkel et al. 2009a; 2009b), published studies explicitly examining snow level and long term climate change are scarce (Svoma 2011). The relationship between snow level and various teleconnections, such as ENSO and PDO may possibly be inferred by the results of studies regarding teleconnections and temperature (e.g., Gershunov 1998; Gershunov and Barnett 1998a; Higgins et al. 2002); however, investigations directly relating snow level to PDO or ENSO are largely nonexistent.

Considering the numerous studies that imply an important connection between snowfall trends, SWE trends, and elevation (e.g., Mote et al. 2005; Mote 2006; Knowles et al. 2006; Casola et al. 2009; Svoma 2011; Minder 2010) as well as the numerous studies that highlight the importance of SWE for the western US water supply (e.g., Stewart et al. 2005; Hamlet et al. 2007; Raushcer et al. 2008; Hidalgo et al. 2009), it is surprising that the elevation of snow level has not

been given greater attention. With established relationships between snow level and ENSO/PDO, long term snow level trends can be put into the context of natural climate variability. If snow level trends are outside the realm of variations in ENSO/PDO, then the trends may be due to anthropogenic forcing.

Therefore, publications spawned from this dissertation will represent a significant contribution to the literature through answering the following questions:

(1) Does a relationship exist between ENSO, PDO, and snow level and if so, how does this vary across on the western US?

(2) Considering the previous research suggesting that declining western US snowpack is likely in response to the ongoing buildup of greenhouse gases (Barnett et al. 2008 Pierce et al. 2008), do multi-decadal trends exist in the elevation of snow level, and if so, how does this vary across the western US?

(3) Given that there is a climate change signal in snow level, is this outside the realm of natural climate variability related ENSO and PDO?

The previous research detailed in Sections 2.4 and 2.5 above has led me to develop three corresponding hypotheses:

(1) The higher frequency of maritime air flow into the western US during El Niño events along with more zonal air flow (east-west rather than north-south) during cold PDO periods (Higgins et al. 2002; Brown and Comrie, 2004), results in a tendency for snow level to be the highest during El Niño events occurring in conjunction with the cold PDO.

(2) Considering regional warming (Barnett et al. 2008; Pierce et al. 2008), a clear multi-decadal upward trend exists in the snow level elevation across the western US.

(3) Considering that Knowles et al. (2006) found lower snowfall to rainfall ratios across the western US during the more recent warm phase of the PDO (1977-1998) than the earlier warm

phase (1925-1946), I expect that the upward trends in snow level will span multiple PDO phases. Additionally, the numerous recent studies suggesting that changing climate in the western US is due to increased temperature from anthropogenic forcing (e.g., Barnett et al. 2008; Pierce et al. 2008) suggest that increasing snow levels will not be well explained by the potential increase in the frequency and strength of El Niño events.

To examine the validity of these hypotheses, it is important to have accurate estimations of snow level and a quantitative measure of the phase of ENSO. Additionally, as a primary goal of this dissertation is to evaluate multi-decadal trends in snow level, the corresponding data sources must have sufficiently long lengths of record. In the following chapter, the data sources used quantify the interannual variability of snow level and the phases of ENSO and PDO are detailed.

Chapter 3: Data

3.1 Introduction

Snow cover in the western United States as it relates to climate change has received considerable attention by many previous investigators (e.g., Hamlet et al. 2007; Kalra et al. 2008; Mote et al. 2008; Rauscher et al. 2008; Barnett et al. 2008, Pierce et al. 2008; Hidalgo et al. 2009; McCabe and Wolock 2009). Numerous studies imply an important connection between snowfall trends, snow water equivalent trends (SWE) trends, and elevation (e.g., Mote et al. 2005; Mote 2006; Knowles et al. 2006; Pierce et al. 2008; Casola et al. 2009; Svoma 2011), yet relatively few investigations have focused on snow level elevation, as highlighted in the previous chapter. My investigation involves the analysis of temporal snow level patterns as they relate to climate change and natural climate variability in the form of El Niño–Southern Oscillation (ENSO) and Pacific Decadal Oscillation (PDO: see Chapter 2). Additionally, I identify spatial variability in these relationships across the western US. To conduct this investigation, I obtained high-quality datasets capable of quantifying spatial and temporal variations in snow level elevation.

To evaluate snow level at daily resolution from October through April (referred to as the *cold season, winter season*, or *winter* throughout the remainder of this dissertation) using three separate methods of snow level quantification (see Chapter 4), I created three independent datasets. The first is a collection of daily wet-bulb zero (WBZ) heights from 1957-2010 at ten rawinsonde locations across the western US (Table 3.1, Figure 3.1). The height of WBZ is the vertical distance above sea level where the adiabatic wet-bulb temperature is 0^{o}C and is often used as an estimator for snow level elevation (Gedzelman and Arnold 1993; Albers et al. 1996; Bourgouin 2000; Wetzel and Martin 2001).

Figure 3.1: The ten rawinsonde sites (circled dots), and adjacent COOP sites used as precipitation proxies (large ×). Urban areas are displayed as light gray polygons. See Table 3.1 to reference the rawinsonde site labels.

Second, I acquired daily snowfall and precipitation totals from the National Weather Service Cooperative Observer (COOP) Network as a measure of daily precipitation type over various elevations across each of ten watersheds adjacent to the rawinsonde sites (Table 3.2, Figure 3.2). While the lengths of record for each station in the COOP network vary considerably, data from the COOP stations I acquired generally extend from 1924-2009. From these data, I empirically estimate snow level at daily resolution (see Chapter 4).

Table 3.1: The ten rawinsonde sites providing daily wet-bulb zero (WBZ) heights for both the 0000 UTC and 1200 UTC soundings. The percentage of below ground level WBZ heights, missing observations, and missing seasons after quality control for the 0000 UTC (1200 UTC) soundings are with respect to winter defined as October-April. Elevations are given in meters above sea level (msl).

US Location Code	City, State	Lat (^{o}N)	Lon (^{o}W)	Elev (msl)	Period of Record	Percent Below Ground Level 0000 UTC (1200 UTC)	Percent Missing 0000 UTC (1200 UTC)	Missing Seasons 0000 UTC (1200 UTC)
TUS	Tucson, AZ	32.13	110.95	781	1957-2010	0.18 (1.31)	3.65 (8.48)	1 (4)
SLC	Salt Lake City, UT	40.77	111.96	1288	1957-2010	23.61 (37.23)	2.40 (5.13)	1 (4)
ABQ	Albuquerque, NM	35.05	106.61	1619	1957-2010	10.68 (33.40)	3.11 (11.13)	1 (4)
GJT	Grand Junction, CO	39.12	108.53	1474	1957-2010	23.84 (40.54)	2.75 (7.24)	1 (4)
BOI	Boise, ID	43.57	116.21	868	1957-2010	19.20 (32.58)	2.43 (5.23)	1 (4)
OAK	Oakland, CA	37.73	122.20	6	1957-2010	0.00 (0.11)	3.89 (5.54)	1 (4)
VGB	Vandenberg Air Force Base, CA	34.75	120.56	99	1957-2010	0.00 (0.20)	8.33 (9.19)	10 (12)
MFR	Medford, OR	42.38	122.86	402	1957-2010	2.04 (10.91)	2.14 (3.32)	1 (4)
SLE	Salem, OR	44.92	123.01	61	1957-2010	2.02 (6.01)	2.45 (3.39)	1 (4)
OTX/GEG	Spokane, WA	47.62	117.51	722	1957-2010	28.46 (43.91)	2.13 (3.87)	2(2)

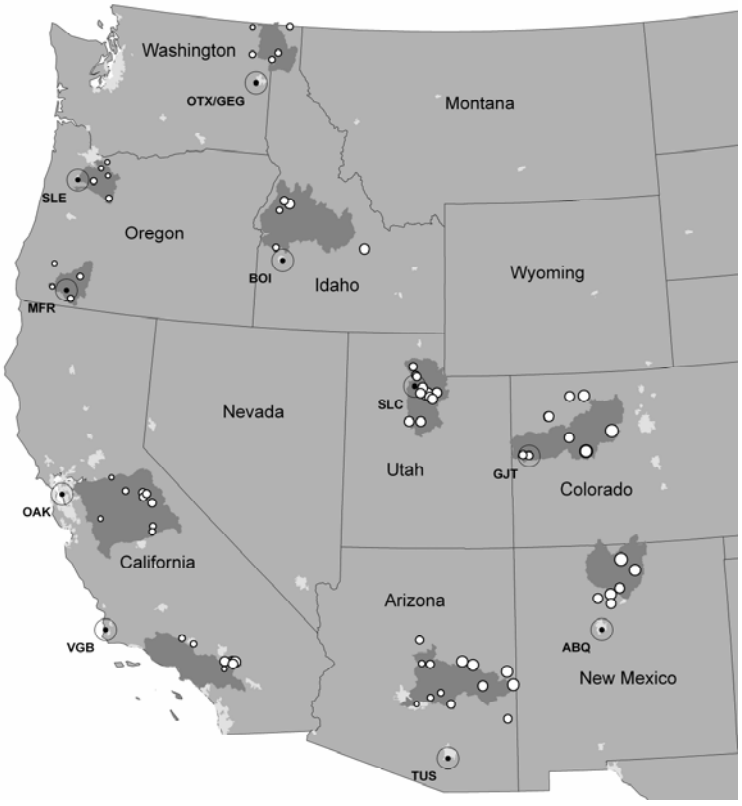

Figure 3.2: The ten watersheds (dark gray polygons) adjacent to the rawinsonde locations (circled dots) along with the COOP stations providing daily precipitation and snowfall data for each watershed (white circles; circle size is roughly proportional to the elevations in Table 3.3). Urban areas are displayed as gray polygons.

Third, upper-air reanalysis data from the National Center for Environmental Prediction/National Center for Atmospheric Research (NCEP/NCAR) were obtained at 2.5^{o} resolution across the western US (Figure 3.3). Specifically, I obtained temperature and geopotential height (relative to sea level, the geopotential height is proportional to the potential energy of a unit mass at that height; e.g., Huschke 1959) for various equal pressure levels including the 1000 hPa, the 850 hPa, the 700 hPa, and the 500 hPa level. From these data I determined the 850 hPa temperature, the 1000–500 hPa thickness, the 1000–850 hPa thickness and the 850–700 hPa thickness (Heppner 1992) where thickness is the difference in geopotential height between two isobaric surfaces. These variables have been found to effectively discriminate between frozen and liquid precipitation at the surface (Heppner 1992).

Table 3.2: The ten watersheds (or contiguous watershed groups) adjacent to the rawinsonde sites in Table 3.1. All values are approximated.

Adjacent US Rawinsonde Location Code	Watersheds as Referred to in Text	Specific Watersheds Spanned by COOP Stations	Elev Range (msl)	Lat Extent (^{o}N)	Lon Extent (^{o}W)	Area (km^{2})
TUS	Salt/Lower Verde	Salt and Lower Verde	300-3400	33.25-34.75	109.2-112.3	~22,900
SLC	Weber/Jordan	Weber and Jordan	1300-3500	39.60-41.40	110.90-112.20	~16,300
ABQ	Upper Rio Grande	Upper Rio Grande	2200-4000	35.70-37.20	105.20-107.00	~17,000
GJT	Colorado Headwaters	Colorado Headwaters	1350-4300	39.00-40.50	105.75-109.10	~25,200
BOI	South Salmon/Payette/Weiser	Little Salmon, Upper Middle Form Salmon, Upper Salmon, South Fork Salmon, Payette, Weiser	650-3600	43.75-45.36	113.90-117.00	~27.900
OAK	San Joaquin	San Joaquin not including Upper-Consumnes, Upper-Mokelumne, Lower Consumnes-Lower-Mokelumne	0-4100	36.60-38.50	118.67-121.92	~35,600
VGB	Ventura-San Gabriel/Santa Ana	Ventura-San Gabriel Coastal and Santa Ana	0-3250	33.57-34.83	116.56-119.47	~18,600
MFR	Middle/Upper Rogue	Middle Rogue and Upper Rogue	250-2750	42.00-43.12	122.15-123.45	~6,600
SLE	North Santium/ Molalla-Pudding/ Clackamas	North Santium, Molalla-Pudding, and Clackamas	50-3050	44.46-45.44	121.67-123.13	~6,800
OTX/GEG	Pend Orielle/Preist/Pend Orielle Lake	Pend Orielle, Preist, and Pend Orielle Lake	500-2200	47.90-49.06	116.20-117.60	~8,500

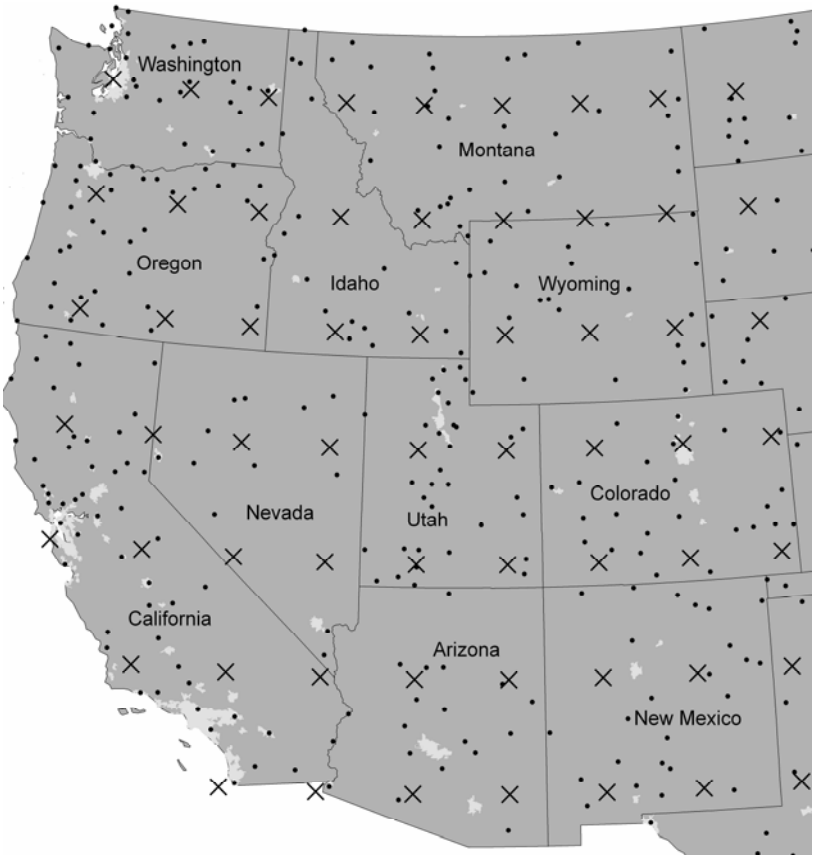

Figure 3.3: The USHCN stations (dots) providing daily precipitation as proxies for precipitation at the NCEP/NCAR reanalysis grid locations (×). Urban areas are displayed as light gray polygons.

In the remainder of this chapter, I give a description of the general area of study, followed by a discussion of the COOP snowfall and precipitation data, the rawinsonde derived WBZ height data, and the NCEP/NCAR reanalysis data. Lastly, I describe supplementary data (e.g., the Southern Oscillation Index and the US Historical Climate Network) essential for the execution of the methods described in the next chapter.

Table 3.3: The COOP stations and station multiples (i.e., stations treated as a single unit as indicated in bold) for each of the ten watersheds in Table 3.2. Elevations are given in ranges due to station relocation. Latitude and longitude ranges are given for the station multiples. The missing data information is with respect to the winter defined as October-April. The number of missing seasons after quality control for each watershed is given below the watershed names. Asterisks and the pound sign (#) indicate the COOP station in each watershed analyzed in Chapter 5 and Chapter 7 respectively.

Salt/Lower Verde (1926-2009) Missing Seasons=17					
COOP Station	**Lat (^{o}N)**	**Lon(^{o}W)**	**Elev (msl)**	**Snow (% missing)**	**Precip (% missing)**
Mesa	33.40	111.82	374	0.52	0.34
Mormon flat	33.55	111.43	524-555	4.42	5.26
Roosevelt	33.67	111.15	674-677	1.03	0.86
Childs	34.33	111.68	807	0.65	0.56
Clifton	33.05	109.30	1054-1061	1.88	1.67
Miami	33.40	110.87	1085-1098	1.56	0.39
Natural bridge/Sedona	34.32-34.88	111.45 - 111.75	1268-1301	3.10	0.89
Whiteriver*#	33.82	109.98	1560-1610	4.01	3.93
Pinedale/Heber	34.30-34.38	110.55 - 110.25	1984-2012	5.86	3.51
Springerville	34.13	109.30	2146-2152	4.84	0.74
Alpine	33.83	109.13	2441-2454	8.98	2.74
Weber/Jordan (1932-2009) Missing Seasons=11					
COOP Station	**Lat (^{o}N)**	**Lon(^{o}W)**	**Elev (msl)**	**Snow (% missing)**	**Precip (% missing)**
Farmington/Ogden Sugar Factory/Farmington 3 NW	40.98-41.22	111.90 - 112.02	1302-1322	2.94	0.16
Cottonwood Weir	40.62	111.78	1512	9.24	3.77
Santaquin Chlorinator	39.95	111.77	1557-1600	8.43	4.70
Mtn Dell Dam#	40.73	111.72	1652-1679	8.85	3.22

Table 3.3 Continued

Heber*	40.48	111.42	1701-1716	1.60	1.01
Snake Creek Powerhouse	40.53	111.50	1817-1832	16.46	1.43
Kamas/Eureka	39.95-40.63	111.28 - 112.12	1953-1993	8.19	1.83
Silver Lake Brighton	40.60	111.58	2655-2667	7.05	5.32
Upper Rio Grande (1925-2009) Missing Seasons=6					
COOP Station	**Lat (°N)**	**Lon(°W)**	**Elev (msl)**	**Snow (% missing)**	**Precip (% missing)**
Cochiti Dam/Espanola	35.63-35.98	106.05-106.32	1695-1735	3.09	2.21
Jemez Springs*#	35.77	106.68	1862-1908	4.89	2.26
Taos	36.38	105.58	2122-2131	3.11	1.14
Los Alamos	36.38	105.60	2234-2262	3.86	2.06
Tres Piedras	35.85	106.32	2457-2481	10.71	5.48
Colorado Headwaters (1935-2009) Missing Seasons=7					
COOP Station	**Lat (°N)**	**Lon(°W)**	**Elev (msl)**	**Snow (% missing)**	**Precip (% missing)**
Fruita	39.15	108.72	1365-1380	7.58	3.71
Grand Junction Walker Fld*#	39.13	108.53	1475-1477	0.62	0.11
Glenwood Spgs #2	39.52	107.32	1752-1800	8.32	4.56
Meeker/Meeker #2/Hayden	40.03-40.48	107.25-107.92	1901-1963	0.51	0.49
Steamboat Springs	40.48	106.82	2060-2085	1.65	1.51
Aspen/Aspen 1 SW	39.18	106.83	2411-2487	3.95	4.43
Dillon 1 E	39.63	106.03	2679-2767	2.50	1.05

Table 3.3 Continued

COOP Station	Lat (°N)	Lon(°W)	Elev (msl)	Snow (% missing)	Precip (% missing)
South Salmon/Payette/Weiser (1925-2009) Missing Seasons=4					
Emmett 2 E	43.85	116.45	722-728	19.04	2.57
Council	44.72	116.42	893-959	13.92	7.86
New Meadows RS*#	44.95	116.28	1176-1179	6.74	5.71
McCall	44.88	116.10	1533	6.43	2.98
Mackay Lost River RS	43.92	113.62	1797-1800	19.08	3.12
San Joaquin (1925-2009) Missing Seasons=8					
COOP Station	**Lat (°N)**	**Lon(°W)**	**Elev (msl)**	**Snow (% missing)**	**Precip (% missing)**
Sonora RS	37.97	120.38	532-557	12.25	5.54
Auberry 2 NW	37.08	119.50	606-651	14.57	0.96
North Fork RS	37.22	119.50	801	19.13	5.78
Hetch Hetchy*	37.95	119.77	1179	6.69	1.56
Yosemite Park HQ	37.75	119.58	1210-1216	11.87	3.68
Mather/Lake Eleanor#	37.86-37.97	119.85-119.88	1377-1420	16.58	4.55
Ventura-San Gabriel/Santa Ana (1932-2009) Missing Seasons=1					
COOP Station	**Lat (°N)**	**Lon(°W)**	**Elev (msl)**	**Snow (% missing)**	**Precip (% missing)**
Redlands	34.05	117.18	402-414	2.45	1.70
Palmdale	34.58	118.08	792-810	0.83	0.30
Fairmont	34.70	118.42	933	9.32	2.37
Seven Oaks/Lake Arrowhead*#	34.18-34.23	116.95-117.18	1523-1593	8.35	2.16

Table 3.3 Continued

Big Bear Lake/Big Bear Lake Dam	34.23	116.90-116.97	2060-2078	11.57	3.45
Middle/Upper Rogue (1925-2009) Missing Seasons=0					
COOP Station	**Lat (°N)**	**Lon(°W)**	**Elev (msl)**	**Snow (% missing)**	**Precip (% missing)**
Riddle	42.95	123.35	201-207	3.93	2.83
Grants Pass	42.42	123.32	280-292	1.89	1.41
Ashland	42.20	122.70	532-542	2.84	0.48
Prospect 2 SW*#	42.73	122.50	755	3.33	1.73
North Santium/Molalla-Pudding/Clackamas (1932-2009) Missing Seasons=1					
COOP Station	**Lat (°N)**	**Lon(°W)**	**Elev (msl)**	**Snow (% missing)**	**Precip (% missing)**
Estacada 2 SE	45.27	122.32	124	1.51	0.83
Headworks Portland Wtr	45.43	122.15	228	1.10	0.01
Three Lynx	45.12	122.07	341	3.16	0.99
Sundown Rch/Marion Frks Fish Hatch*#	44.60-44.95	121.93-122.50	731-755	0.73	0.42
Pend Orielle/Priest/Pend Orielle Lake (1928-2009) Missing Seasons=3					
COOP Station	**Lat (°N)**	**Lon(°W)**	**Elev (msl)**	**Snow (% missing)**	**Precip (% missing)**
Northport	48.90	117.80	402-411	1.97	1.24
Chewelah*#	48.27	117.72	500-512	10.20	1.96
Porthill	48.98	116.50	539-548	9.17	1.88
Newport	48.18	117.03	651	1.82	1.71
Priest River Exp Stn	48.35	116.83	725	0.12	0.05

3.2 Study Area

The general area of study is the eleven western most states in the conterminous US (Figure 3.4). The western US is a region characterized by widely varying topography and climatic conditions. The following basic geographical and climatological information was obtained from the Western Regional Climate Center of the National Oceanic and Atmospheric Administration, derived from data from the National Climatic Data Center, National Weather Service and many other sources such as the Desert Research Institute (http://www.wrcc.dri.edu/).

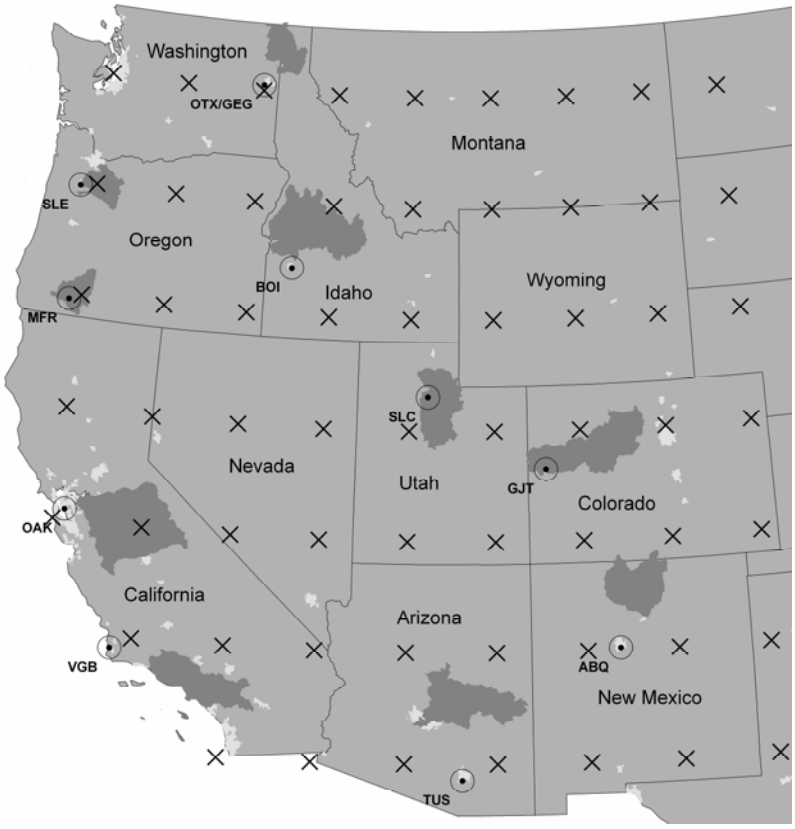

Figure 3.4: The area of study defined by the eleven western most states in the contiguous United States. The ten sub study areas are displayed as the ten watersheds (dark gray polygons) adjacent to the rawinsonde locations (circled dots). The NCEP/NCAR reanalysis grids span the entire study area and are displayed as the × symbol. Urban areas are displayed as light gray polygons.

While both the lowest elevation (85 meters below sea level: Death Valley, California) and highest elevation (4460 meters above sea level: Mt. Whitney, California) in the US occur in California, each of the eleven states have extremely variable topography. All eleven states have

mountain peaks above 3400 meters above sea level (msl) and valleys below 1100 msl with Colorado as the only state entirely above 1000 msl. Therefore, within each state, there are regions with greatly differing annual snowfall totals.

Each state has regions that consistently receive more than 250 cm of snowfall annually. For all states, significant snowfall primarily occurs during October through May. Additionally, there are locations in each state where average maximum snow depths in March exceed 100 cm. Snowfall events are rare in the low elevations immediately adjacent to the West Coast and there are large regions of southern California and southern Arizona where snowfall is extremely rare.

The spatial variability in rainfall across the western US modulates the importance of snowfall for local water supplies. In the Pacific Northwest, there are expansive regions that receive greater than 1000 mm of precipitation annually. Traveling south and further inland, only in the higher elevations does annual precipitation exceed 500 mm and many areas receive less than 250 mm of precipitation annually. Potential evapotranspiration can be high in many areas of the western US, leading to large expanses of arid land. Therefore, snowmelt accounts for most of the runoff into the majority of rivers in the western US (Cayan 1996), and many large metropolitan areas, particularly in the Southwest, are highly dependent on spring snowmelt to replenish water supplies (Raushcer et al. 2008; Hidalgo et al. 2009).

Additionally, I focus on ten sub-areas of the western US. While these ten watersheds—or contiguous watershed groups (Table 3.2, Figure 3.2) —were chosen as focus areas mainly due to adequate data coverage (see Section 3.3 below), these watersheds contain large regions at relatively high elevation that accumulate substantial spring snowpack every year and areas that rarely have significant snow cover in the spring. Therefore, a snow level analysis within these watersheds is not only feasible due to the intra-watershed contrasts in snow accumulation, but also important due to the presumable importance of snowmelt driven runoff.

With exception of the Middle/Upper Rogue, North Santium/Molalla-Pudding/Clackamas, and Pend Orielle/Priest/Pend Orielle Lake watershed, all watersheds have mountains that exceed

3250 msl. The highest watershed in terms of elevation is the Colorado Headwaters watershed with many areas exceeding 4000 msl. Additionally, with the exception of the Colorado Headwaters, Weber/Jordan, Upper Rio Grande, and South Salmon/Payette/Weiser watershed, all watersheds contain land below 500 msl.

The average maximum snow depth in March ranges from 20 cm in the Ventura San-Gabriel/Santa Ana watershed in southern California to over 250 cm North Santium/Molalla-Pudding/Clackamas watershed in Oregon. With the exception of the Salt/Lower Verde, the Upper Rio Grande, and the Ventura San Gabriel/Santa Ana watershed, all watersheds frequently have expansive areas with snow depths of greater than 150 cm in March. Additionally, it is not uncommon for March snow depths to exceed 100 cm in areas of the Salt/Lower Verde, the Upper Rio Grande, and the Ventura-San Gabriel/Santa Ana. The Middle/Upper Rogue and North Santium/Molalla-Pudding/Clackamas watershed are within the expansive region in the Pacific Northwest that receives more than 1000 mm of precipitation annually. Therefore, in these watersheds, runoff is not as highly snowmelt driven as the remaining eight watersheds.

3.3 Data for Snow Level Quantification

The three data sources used to create variables representative of snow level across the western US are detailed in the following sub-sections. I first discuss the collection of daily WBZ heights, detailing the criteria for selecting ten rawinsonde locations for analysis (Table 3.1, Figure 3.1). Then I discuss the selection of ten watersheds for which the precipitation and snowfall characteristics are represented by National Weather Service COOP data. Lastly, recognizing that the regions of the western US covered by the WBZ data and COOP data were selected largely due to adequate data coverage, I introduce the NCEP/NCAR reanalysis data that serve as a spatially unbiased representation of snow level variability over the entire study area. Additionally, I discuss the advantages and disadvantages of each dataset as applied to this study as well as the methods of quality control applied to each dataset.

3.3.1 Rawinsonde-Derived Wet-Bulb Zero Data

When precipitation occurs, the melting/sublimation of frozen precipitation and evaporation of liquid precipitation cause the environment to cool (Gedzelman and Arnold 1993). The extent of cooling can be determined by the isobaric wet-bulb temperature which is the temperature an air parcel would have if cooled adiabatically (i.e., the air parcel does not exchange energy with its surroundings due to temperature contrasts) at a constant pressure through the evaporation of water until the parcel is saturated (Huschke 1959). Another measure of wet-bulb temperature is the adiabatic wet-bulb temperature. This is the temperature an air parcel would have if cooled adiabatically to saturation and then compressed to its original pressure in a moist-adiabatic process (i.e., the lapse rate approximating both a reversible moist-adiabatic process and a pseudoadiabatic process (Huschke 1959)). The adiabatic wet-bulb temperature is always lower than the isobaric wet-bulb temperature; however, the difference is typically only a fraction of a degree Celsius (Huschke 1959).

A surface wet-bulb temperature below 0^{o}C favors precipitation reaching the surface as snow (Gedzelman and Arnold 1993; Albers et al. 1996; Bourgouin 2000; Wetzel and Martin 2001). This is often a better predictor of snowfall occurrence than air temperature because the cooling process in response to precipitation essentially moves the 0^{o}C isotherm to a lower altitude (Gedzelman and Arnold 1993). This altitude is often referred as the wet-bulb zero (WBZ) height (Svoma 2011). WBZ height often overestimates the actual elevation of the melting point of frozen precipitation due to the time needed for complete melting to occur (Gedzelman and Arnold 1993; Albers et al. 1996). Previous investigators have suggested that threshold values for wet-bulb temperatures greater than 0^{o}C are necessary to accurately assess precipitation type (Albers et al. 1996; Bourgouin 2000) and for extreme cases, depending on the size of the snowflakes and environmental lapse rate, snowfall can occur more than100 meters below WBZ altitude (Gedzelman and Arnold 1993). Despite this, there is not a commonly accepted single positive (> 0^{o}C) wet-bulb temperature threshold for discriminating between frozen and liquid precipitation at the surface (Gedzelman and Arnold 1993; Albers et al. 1996; Bourgouin 2000; Wetzel and Martin

2001).

Throughout the western US, there are more than thirty-five upper-air sounding sites with vertical atmospheric profile data archived by the Storm Prediction Center of the National Oceanic and Atmospheric Administration (http://www.spc.ncep.noaa.gov/exper/soundings/). Surface wet-bulb temperatures that are consistently above freezing during the winter is the most important characteristic of a sounding location chosen for analysis in this study. Surface wet-bulb temperatures below 0^{o}C indicate that the WBZ height is below the elevation of the sounding surface and therefore, tangible WBZ heights cannot be calculated. Sounding locations with consistently tangible WBZ heights are generally at lower elevations and/or lower latitudes (i.e., locations with warmer temperatures). Considering this, my initial elimination of sounding locations eligible for analysis was qualitative. For example, I did not consider the sounding site in Flagstaff, Arizona (>2100 msl) or Great Falls, Montana (>1000 msl and ~47.5^{o}N).

As I analyze multi-decadal variability of snow level in this study, I also required sounding locations to have continuous data and relatively long periods of record (to capture large portions of both the 1947-1976 cold PDO phase and the 1977-1998 warm PDO phase (Stewart et al. 2005; Knowles et al. 2006)). Only ten sounding locations with consistently tangible WBZ heights (generally >75% of 0000 UTC soundings; see Table 3.1) had continuous data, relatively long periods of record (~50 years; Table 3.1), and minimal station relocation (R. Thompson 2010, personal communication). Fortunately, most of these sounding sites are located near large cities (Figure 3.1) that are adjacent to mountainous areas that accumulate snow throughout winter. These are ideal sub-areas of the western US to study due to the importance of mountain snowpack for water supply in large metropolitan areas such as Phoenix, Arizona; Los Angeles, California; and San Francisco/Oakland California (e.g., Barnett et al. 2005, Raushcer et al. 2008; Hidalgo et al. 2009; Minder 2010).

For each of the ten locations in Table 3.1 (Figure 3.1), wet-bulb zero (WBZ) heights for every 0000 UTC and 1200 UTC sounding were obtained from the Storm Prediction Center of the

National Weather Service (R. Thompson 2010, personal communication). The WBZ heights were determined from the adiabatic wet-bulb temperature profile derived from the vertical temperature and dew point temperature profiles as measured by the rawinsonde (R. Thompson 2010, personal communication). The adiabatic wet-bulb temperature profile is calculated by determining the adiabatic wet-bulb temperature at each level measured by the sounding through the process described above (i.e., adiabatic expansion until saturation, followed by moist-adiabatic compression to the original pressure). The height above sea level that the adiabatic wet-bulb temperature profile is 0^{o}C is the WBZ height (R. Thompson 2010, personal communication). As seen in Table 3.1, each rawinsonde location dataset was missing less than 10 percent of the daily WBZ heights for the 0000 UTC sounding, with only Albuquerque displaying greater than 10 percent missing data for the 1200 UTC sounding (~11%). For each location, cold seasons with greater than 20% of missing daily observations were not considered for analysis. I found this threshold to be a reasonable compromise between maximizing cold season sample size (i.e., higher thresholds resulting in the elimination of very few seasons) and maximizing the number of observations within each cold season for accurate representation (i.e., lower thresholds resulting in the elimination of many seasons). For nine of the locations, this filtering process resulted in the elimination of at most four seasons for both the 0000 UTC and 1200 UTC soundings (Table 3.1).

Eight out of these ten locations are among the highest quality sounding locations in the western US in terms of station relocation (R. Thompson 2010, personal communication), length of record (extending to 1957), and missing data (Table 3.1). The final two sounding locations analyzed (Spokane, Washington and Vandenberg Air Force Base, California) have extensive lengths of record but with data of lesser quality relative to the eight stations above. However, I elected to retain these two rawinsonde sites for analysis because they provide WBZ values for areas of eastern Washington and southern California (Figure 3.1), which are not covered by the other eight sites.

The first of these two sounding sites with data of lesser quality is located near Spokane, Washington (Figure 3.1). This rawinsonde site underwent relocation in 1994-1995 consisting of a

0.05° shift in latitude to the north, a westward shift of 0.1° in longitude, and an eight meter increase in elevation. Considering that wet-bulb zero is an upper-air variable, changes in local topography and other surface characteristics should not significantly influence the computed wet-bulb zero heights before and after the relocation. The second sounding site of reduced data quality is Vandenberg Air Force Base in southern California (Figure 3.1). Vandenberg Air Force Base had ten cold seasons with greater than 20% of missing data for the 0000 UTC soundings and twelve seasons for the 1200 UTC soundings (Table 3.1). Fortunately, as the data extend back to 1957, Vandenberg Air Force Base had greater than 40 cold seasons with less than 20% of the daily observations missing for both the 0000 UTC and 1200 UTC soundings.

In summary, the ten sounding locations analyzed in this study represent the most useful sites (i.e., warmer sites with consistently tangible winter WBZ heights) in the western US with continuous records of wet-bulb zero heights extending back to 1957 (Table 3.1). While the height of WBZ will rarely represent the exact snow level elevation, WBZ altitudes rarely overestimate snow level by more than 100 meters (Gedzelman and Arnold 1993), and WBZ height is a direct measure of the altitude that frozen precipitation turns to liquid precipitation (i.e., snow level). For a given region, it is reasonable to assume that the interannual variability of snow level would be mirrored by variability in WBZ height.

3.3.2 National Weather Service Cooperative Observer Network

Subsequently, I used information from the United States Geological Survey (obtained from: http://water.usgs.gov/wsc/map_index.html) to choose ten watersheds (or contiguous watershed groups) of focus, each adjacent to a sounding site (Table 3.2; Figure 3.2). Additionally, watershed boundary data for mapping purposes (Figures 3.2 and 3.4) and drainage area information (Table 3.2) were obtained from the United States Department of Agriculture (downloaded from: http://datagateway.nrcs.usda.gov/). I required the watersheds to encompass relatively high elevations (with respect to latitude) capable of receiving consistent winter snowfall. Watershed size was the second criteria I used to select the watershed adjacent to a given sounding

site. Due to the influence of latitude on snow level, a watershed must be limited in latitude extent in order to determine a single snow level elevation over the entire watershed for a given day (Svoma 2011). I qualitatively identified watersheds that are limited in latitudinal extent such that each of the ten watersheds examined are similar in north-south extent (~1.5^{o} latitude) to the Salt/Lower Verde watershed (Table 3.2; Figure 3.2) analyzed by Svoma (2011), a study using methods similar to those utilized in this dissertation. In short, each of the ten watersheds is less than 1.5^{o} latitude in north-south extent and drain high elevation areas that consistently receive winter snowfall. It should be noted that throughout the remainder of the dissertation, each contiguous watershed group will be referred to as a single watershed under the abbreviated name given in Table 3.2.

The National Weather Service Cooperative Observer (COOP) Network consists of more than 18,000 stations across the US and observations are taken by trained weather observers (Baxter et al. 2005). At these stations, new snowfall is measured either once every twenty-four hours, or from the sum of four sets of six hour observations with a goal of measuring the maximum accumulation over the twenty-four hour period (Baxter et al. 2005). Depth is measured either by use of a ruler or snow board. Multiple measurements are taken to determine a mean snow depth so the impacts of wind are minimized (Baxter et al. 2005). The liquid equivalent is obtained by melting the contents collected in a precipitation gauge that is typically unshielded with a mouth diameter of 20 cm (Baxter et al. 2005; Pierce et al. 2008). If there is a noticeable discrepancy between the depth and liquid equivalent, the observer is instructed to take a core sample from a snow board (Baxter et al. 2005).

The accuracy of snowfall depths recorded in the COOP network has been heavily scrutinized in the past (Kunkel et al. 2007) and consequently, detailed quality controls of the snowfall depth observations are commonly implemented by investigators concerned with the measurement of fresh snowfall depths (Knowles et. al. 2006; Kunkel et al. 2009a; 2009b). The most common quality control measure is the removal of days in which a given COOP station reported precipitation that was exactly one-tenth of the measured new snowfall depth. This is in

response to the common occurrence of weather observers dividing the snowfall depth measurement by ten to get the liquid equivalent (Knowles et. al. 2006; Kunkel et al. 2009a; 2009b). Fortunately, an estimation of snow level elevation only requires knowledge of the occurrence of snowfall and not exact snowfall amounts. Therefore, the issues with daily snowfall depths in the COOP network do not apply to this dissertation. It should also be mentioned that many stations (~45 of 60 stations used in this study) in the COOP network have experienced station relocation and/or changes in the timing of observation. Despite this, the network density, daily resolution and long periods of record make this a useful data source for this study.

To estimate daily snow level over the watersheds in Table 3.2 and Figure 3.2, daily precipitation and snowfall data were obtained from the COOP network for multiple (from 4-13) stations in and around each watershed in Figure 3.2 (Table 3.3) from ~1924-2009. The stations were selected based on three criteria in order to create a temporally consistent dataset covering a broad range of elevations within each watershed (Table 3.3). The first and most important criteria required that each station have a long period of record extending back to at least 1934 to capture most of 1925-1946 warm phase of the PDO, and each phase thereafter (Stewart et al. 2005; Knowles et al. 2006). Second, I considered the elevation of each station so that the stations ultimately analyzed cover an extensive range of elevation within each watershed (~370-2500 msl in the lower latitude watersheds and ~200-800 msl in the higher latitude watersheds; see Table 3.3). Lastly, I only considered stations such that changes in elevation due to relocation did not result in a change in the elevation ranks of each station within each watershed.

For each station, I examined the year-to-year variability in cold season percentages of missing daily snowfall and precipitation data. Upon identifying stations with many consecutive years with little or no data, I deemed it appropriate to supplement these stations with data from other stations in order to extend the period of record or to fill in gaps of missing data. This was justifiable based on the adjacency and similar elevations of these multiple stations that were treated as a single station (Table 3.3, Figure 3.2). In Table 3.3, the elevation ranges represent the lowest and highest elevations of each station (or station multiples) during their period of record.

The largest elevation range is 89 meters (at Dillon, Colorado resulting from relocation) which is small when compared to the differences in elevation between the various stations or station multiples (Table 3.3). The percentage of cold season missing daily snowfall and precipitation observations for each station or station multiple is very low, with most displaying less than 5% missing daily observations (Table 3.3). The highest percentage of missing data was 7.86% (Council, Idaho) for precipitation and 19.13% (at North Fork Ranger Station, California) for snowfall.

In summary, as only the occurrence of snowfall is critical for determining snow level elevation, exact snowfall amounts are not important for this study. This negates the impacts of a large weakness in the COOP data network (i.e., the accuracy of daily snowfall amounts). To combat the issues in the COOP network regarding station location, I did not examine stations that underwent a major change in elevation due to relocation. Therefore, the extensive periods of record, density of stations at various elevations, and daily resolution make the COOP network an ideal data source for the quantification of snow level over each watershed (Figure 3.2; Table 3.3).

3.3.3 NCEP/NCAR Reanalysis

The mean temperature of a vertical layer in the atmosphere is directly related to the thickness of that layer (Zhang et al. 2001). Thickness can be defined as the difference in geopotential height (the height, relative to sea level, proportional to the potential energy of a unit mass at that height; e.g., Huschke 1959) between two equal pressure (isobaric) surfaces. Consequently, various thickness values of certain isobaric surfaces have been used as predictive discriminators between frozen and liquid precipitation. For example, a thickness of 5400 geopotential meters (gpm) has been commonly used by operational meteorologists as a critical thickness threshold for the 1000–500 hPa layer (Heppner 1992). Smaller thickness values (<5400 gpm) indicate colder mean air temperatures of the 1000–500 hPa layer and suggest conditions more favorable for frozen precipitation to reach the surface. Several other upper-air variables are useful for discriminating between frozen and liquid precipitation including 1000–850 hPa

thickness, 850–700 hPa thickness and 850 hPa temperature (Heppner 1992).

Recognizing that the sub-areas of the western US covered by the WBZ altitude data and COOP data (Figure 3.2) were chosen mainly due to adequate data coverage, rather than theory, I also selected variables from the NCEP/NCAR upper-air reanalysis to represent the thickness measures and temperature measures discussed above. NCEP/NCAR reanalysis data are available on a regular grid across the western US. The reanalysis project by NCEP/NCAR involves the spatial and temporal interpolation of numerous variables from observational datasets including global rawinsonde data, marine surface data, satellite data, and aircraft data (Kalnay et al. 1996). These data are subject to extensive quality control, supplemented by the predictions from the NCEP global operational model, and interpolated through various techniques to provide output of numerous surface and upper-air variables on several different grid systems (Kalnay et al. 1996). A majority of the variables are output to a regular global grid of 2.5^{o} at sub-daily resolution extending back to 1948 with no missing values (Kalnay et al. 1996).

From 1948-2009, daily NCEP/NCAR reanalysis temperatures (for the 850 hPa isobaric surface) and geopotential heights (for the 1000 hPa, 850 hPa, 700 hPa, and 500 hPa isobaric surfaces) were obtained for the western US (47.5^{o} N to 27.5^{o}N and 97.5^{o}W to 125.0^{o}W) from the Earth Systems Research Laboratory of the National Oceanic and Atmospheric Administration (http://www.cdc.noaa.gov/ data/gridded/). Temperature and geopotential height are considered class ‘A’ variables from the reanalysis output (Kalnay et al. 1996), indicating that these variables are heavily influenced by observational data as opposed to the NCEP/NCAR interpolation techniques/model and are therefore the most reliable reanalysis variables. It is important to note that the results derived from the reanalysis data are only given for 60 grid locations (Figure 3.3) extending from 47.5^{o} N to 32.5^{o}N and 102.5^{o}W to 122.5^{o}W, however, I also performed the methods in Chapter 4 on the adjacent grids (e.g., extending east to 97.5^{o}W, south to 27.5^{o}N and west to 125.0^{o} W) as a means of reducing edge effects when calculating local Moran’s I statistics as illustrated in Chapter 4 below.

From the daily geopotential height NCEP/NCAR reanalysis data, for each grid, I calculated daily values of 1000–500 hPa thickness, 1000–850 hPa thickness and 850–700 hPa thickness. These variables were calculated as the difference in geopotential height (in gpm) between the isobaric surfaces of interest (e.g., the 1000-500 hPa thickness is simply the 1000 hPa geopotential height subtracted from the 500 hPa geopotential height). Along with 850 hPa temperature, these variables have been found to effectively discriminate between frozen and liquid precipitation at the surface (Heppner 1992).

In summary, major benefits of the NCEP/NCAR reanalysis data include high horizontal resolution (e.g., 60 grid locations across the study area Figure 3.3) and daily temporal resolutions with no missing values. A shortcoming of the reanalysis data is that the data are not purely observational like the WBZ height data and the COOP data. However, the upper-air data that I analyze are the most reliable NCEP/NCAR reanalysis variables, as they are heavily influenced by observational values (Kalnay et al. 1996).

3.3.4 Summary of Data for Snow Level Quantification

Three datasets—rawinsonde-derived WBZ heights, daily precipitation and snowfall from the COOP network, and geopotential height and temperature data from 1000 hPa to 500 hPa from NCEP/NCAR reanalysis data—are used to quantify snow level over the western US. The ten sites providing WBZ data are each located near COOP sites and these two data sources provide comparable results, as they are representing snow level over the same regions (i.e., the watersheds). To overcome the limited areal representation of the western US by these two data sources, I use the NCEP/NCAR reanalysis data that are ideal for spatial analysis and unbiased representation of snow levels across the western US.

Each dataset spans multiple phases of the PDO—WBZ data 1957-2010, COOP data ~1924-2009, NCEP/NCAR reanalysis data 1948-2010—which is essential for this study as I seek to establish the relationship between these variables and ENSO/PDO. Additionally, the purely observational data sets—WBZ data and COOP data—have relatively low portions of missing data

(Table 3.1 and Table 3.3) and the temperature and geopotential height data are the variables that are least influenced by modeling and interpolations techniques from the NCEP/NCAR reanalysis project.

These three sources provide data for three separate methods of snow level quantification discussed in Chapter 4. The results derived from these data can provide insight into snow level variability across the entire western US as well as ten specific sub-regions of the West (Figure 3.4). Lastly, convergent results derived from these three independent data sources can strengthen general conclusions regarding snow level variability in the western US.

3.4 Supplementary Data

To examine the relationships between El Niño–Southern Oscillation (ENSO) and the snow level variables calculated from the above data sets, the monthly Southern Oscillation Index (SOI) was used as a measure of ENSO. The SOI values were obtained from the Australian Bureau of Meteorology from the inclusive period of January 1876 to December 2009 (http://www.bom.gov.au/climate/current/soihtm1.shtml). While there are a few slight variations in the calculation of the SOI, the Australian Bureau of Meteorology uses the SOI as defined by Troup (1965). Let $\mu_{\Delta MSLP}$ be the average difference in the mean sea level pressure between Tahiti and Darwin, Australia for a given month and ΔMSLP be the actual difference in the mean sea level pressure between Tahiti and Darwin for that month. If $\sigma_{\Delta MSLP}$ is the long term standard deviation of the month in question, then

$$\text{SOI}=10\frac{\Delta\text{MSLP}-\mu_{\Delta\text{MSLP}}}{\sigma_{\Delta\text{MSLP}}} \tag{3.1}$$

where the multiplier of 10 enables the SOI to be quoted as a whole number typically ranging from -35 to 35. Extreme negative values of the SOI are indicative of El Niño conditions (warm water anomalies over the eastern equatorial Pacific) and extreme positive values are suggestive of La Niña conditions (cold water anomalies over the eastern equatorial Pacific), while values near zero

are representative of neutral ENSO conditions (Troup 1965). For example, previous researchers have used normalized SOI values of less than -0.4 to represent El Niño conditions and greater than 0.4 to represent La Niña conditions (Brown and Comrie 2004).

Many previous researchers have used SOI as a measure of ENSO (e.g., Redmond and Koch 1991; Hamlet and Lettenmaier 1999; Harshburger et al. 2002; Brown and Comrie 2004; Svoma et al. 2010). Due to its continuous and extensive period of record, the SOI is preferable over many other sea surface temperature based indices such as multivariate ENSO index, Niño-1+2, Niño-3, Niño-3.4, Niño-4, the Japan Meteorological Agency Index, and the trans-Niño index (for a more detailed discussion of these indices see Hanley et al. (2003)). These indices require reconstructed sea surface temperatures to be comparable to the SOI in terms length of record (Hanley et al. 2003). Additionally, for the identification of El Niño and La Niña events, the SOI compares well with many of these indices (Hanley et al. 2003).

As a proxy for daily precipitation at the sounding sites, daily precipitation data were obtained from the COOP network at sites nearby the rawinsonde locations (Figure 3.1). The length of record, latitude, longitude, and elevation display a good measure of similarity between the rawinsonde stations and the COOP stations (Table 3.4). Finally, the US Historical Climate Network (USHCN) version 2 (largely extending back to 1900) obtained from the National Climatic Data Center was used to identify the occurrence of daily precipitation in the vicinity of NCEP/NCAR reanalysis grid points (Figure 3.3). The USHCN data are a subset of the COOP network consisting of over 1200 stations across the western US and represent stations with the most continuous and extensive records of high quality daily weather observations (Cerveny et al. 2010).

Table 3.4: Comparative location information for the ten rawinsonde sites in Table 3.1 and the adjacent COOP sites used as proxies for precipitation data at the rawinsonde sites.

Rawinsonde Location Code	**Lat (^{o}N)**	**Lon (^{o}W)**	**Elev (msl)**	**COOP Location**	**Lat (^{o}N)**	**Lon (^{o}W)**	**Elev (msl)**
TUS	32.13	110.95	781	Tucson International Airport	32.12	110.95	777
SLC	40.77	111.96	1288	Salt Lake City International Airport	40.77	111.97	1288
ABQ	35.05	106.61	1619	Albuquerque International Airport	35.03	106.60	1619
GJT	39.12	108.53	1474	Grand Junction Walker Field	39.13	108.53	1481
BOI	43.57	116.21	868	Boise Air Terminal	43.57	116.23	858
OAK	37.73	122.20	6	San Francisco International Airport	37.65	122.43	2
VGB	34.75	120.56	99	Santa Maria Public Airport	34.88	120.43	73
MFR	42.38	122.86	402	Medford Rogue Valley Airport	42.37	122.87	395
SLE	44.92	123.01	61	Salem McNary Field	44.90	123.00	62
OTX/GEG	47.62	117.51	722	Spokane International Airport	47.62	117.52	717

3.5 Conclusion

In this dissertation I examine interannual variability in snow level elevation across the western US (i.e., the eleven western most states in the contiguous US). To conduct such a study, I obtained a variety of data with extensive periods of record (ranging from 1924-2009 to 1957-2010) as sources for methods capable of quantifying snow level over this large region (Figure 3.4). Specifically, three datasets are used for the creation and analysis of daily snow level variables across the western US.

(1) The vertical distance above sea level that the adiabatic wet-bulb temperature is 0^{o}C is the height of wet-bulb zero (WBZ) and is often used as an estimator for snow level elevation (e.g., Gedzelman and Arnold 1993; Albers et al. 1996; Bourgouin 2000; Wetzel and Martin 2001). Daily WBZ heights (from 1957-2010) at ten rawinsonde sites across the West (Figure3.1, Table 3.1) serve to directly measure snow level elevation. In terms of data quality, these ten sounding locations are among the best of the more than thirty-five locations in the western US. The WBZ heights are derived from the vertical adiabatic wet-bulb temperature profile calculated from the temperature and dew point temperature profiles for a given sounding.

(2) At the ten adjacent watersheds, National Weather Service Cooperative Observer (COOP) data reporting daily snowfall and precipitation totals (from ~1924-2009) at various elevations (~200-800 meters above sea level in the higher latitude watersheds and ~370-2500 meters above sea level in the lower latitude watersheds) serve as a source for precipitation type (Table 3.3; Figure 3.2). Although the COOP data network has several quality issues including station relocation and the accuracy of daily snowfall amounts (Kunkel et al. 2007), exact snowfall amounts are not important for this study as only the occurrence of snowfall is critical for determining snow level elevation. With regard to station relocation, I did not include stations that underwent a major change in elevation due to relocation. Therefore, the density of stations, extensive periods of record and daily resolution make the selected COOP stations useful for providing comparable results to those derived at the adjacent rawinsonde sites.

(3) Daily reanalysis geopotential height and 850 hPa temperature data (from 1948-2009) from the National Center for Environmental Prediction/ National Center for Atmospheric Research (NCEP/NCAR) serve to increase the spatial resolution of analysis. From these data, thickness values (i.e., the elevation difference between two equal pressure levels) were computed for the 1000-500 hPa layer, 1000-850 hPa layer, and the 850-700 hPa layer. Thickness values between specific isobaric surfaces have been used as predictive discriminators between frozen and liquid precipitation. For example, a thickness of 5400 geopotential meters has been commonly used by operational meteorologists as a critical snow threshold for the 1000–500 hPa layer (Heppner 1992). The data are derived through modeling and interpolation driven by observational data and are output to a 2.5^{o} resolution grid across the globe by the NCEP/NCAR reanalysis project (Kalnay et al. 1996).

Additionally, two supplementary data sources were obtained. First, monthly Southern Oscillation Index (SOI) values extending back to 1876 act as a measure of ENSO phase (http://www.bom.gov.au/climate/current/soihtm1.shtml). The SOI is preferable in this study over other sea surface temperature based indices due to its long period of record. Additionally, the SOI has been found to compare favorably with other indices for identifying El Niño and La Niña events (Hanley et al. 2003). Second, the US Historical Climate Network (USHCN) is a high-quality subset and of the COOP network and serves to identify the occurrence of daily precipitation in the vicinity of the NCEP/NCAR reanalysis grids (Figure 3.3).

Although, as with all datasets, there are several flaws with the data collected for this study (e.g., station relocation, missing data, reliance on model output, etc.), these data also have several beneficial qualities (e.g., high spatial density, high temporal resolution, and extensive length of record). Consequently, they provide the basis for my investigation into the temporal variability of snow level variation. As discussed in the following chapter, these three datasets are used for daily snow level quantification and are subject to three separate examinations of interannual snow level variability.

Chapter 4: Methods

4.1 Introduction

In this dissertation, I examine the interannual variability in snow level over the western United States (US) as related to anthropogenic climate change and natural climate variability (namely, El Niño–Southern Oscillation (ENSO) and Pacific Decadal Oscillation (PDO)). I also examine the spatial variability in these temporal patterns. To accomplish this I obtained three data sources to quantify daily snow levels across the western US as discussed in the previous chapter. The first dataset is a record of daily wet-bulb zero (WBZ) heights at ten rawinsonde locations across the western US (Table 3.1; Figure 3.1). The second is daily precipitation and snowfall data from stations at a wide range of elevations within ten watersheds (each adjacent to a rawinsonde site) across the western US (Figure 3.2) from the National Weather Service Cooperative Observer Network (COOP). The third dataset involves daily temperature and geopotential heights for the 1000 hPa, the 850 hPa, the 700 hPa, and the 500 hPa isobaric surfaces derived from observational data and interpolated to a 2.5^{o} resolution grid over the western US (Figure 3.3) by the National Center for Environmental Prediction/National Center for Atmospheric Research (NCEP/NCAR) reanalysis project.

Correspondingly, with these three datasets, I employed three methods to create variables that are representative of interannual snow level variability across the western US. The first method involved the identification of days with precipitation over the rawinsonde sites to estimate snow level through WBZ heights (Section 4.2). The second involved an estimation of snow level based on daily data reports from cooperative weather observers through the identification of the elevations between which rainfall transitioned to snowfall (Section 4.3). While these two methods explicitly address elevation, a third method was employed across the western US at 2.5^{o} resolution through the calculation of snow level proxies (850 hPa temperatures, 1000–850 hPa thickness, 850–700 hPa thickness and 1000–500 hPa thickness; see Section 4.4) from NCEP/NCAR reanalysis data on days with precipitation. All three methods were applied for the winter season defined as October 1 through April 30. Days in which a snow level or snow level proxy was

calculated over a location of interest are called *wet days* or *precipitation days* throughout the remainder of this dissertation. These days represent those in which a precipitation event, and thus a vertical transition from rain to snow, occurred near a location of interest.

In the sections that follow, these three methods quantifying interannual snow level variability are discussed in detail, followed by descriptions of the procedures used to establish the ENSO and PDO relationship with snow level and the spatial variability thereof. Subsequently, I discuss the means of trend detection and the method to examine the spatial variability of trends. Lastly, I detail the means of determining the importance of ENSO/PDO to any observed trends in the snow level variables.

4.2 Wet-Bulb Zero Method

As snow level elevation is the elevation in which rainfall transitions to snowfall, this study addresses only those days in which precipitation occurred. Therefore, for each of the wet-bulb zero (WBZ) datasets derived from the ten sounding locations detailed in Chapter 3, the only days considered for analysis were days in which precipitation was reported at the adjacent COOP sites (Figure 3.1; Table 3.4). As seen in Table 3.1, several sounding locations had relatively frequent occurrences of WBZ heights that were below ground level during the cold season (i.e., soundings that were taken when the surface adiabatic wet-bulb temperature were below zero.) Therefore, for each sounding site, a record of 0000 UTC and 1200 UTC wet day WBZ heights and a record of wet day 0000 UTC and 1200 UTC soundings producing below ground level WBZ heights were created for the available length of record (1957-2010).

The trend analysis (Section 4.6) and teleconnection analysis (Section 4.5) below were applied to the WBZ data from both the 1200 UTC and 0000 UTC soundings; however, the 0000 UTC soundings were the primary foci for this study (the results derived from the 1200 UTC soundings are shown in the Appendix). This is justifiable for two reasons. First, in the western US, 0000 UTC soundings are taken during a warmer part of the day (the late afternoon); therefore, below freezing surface wet-bulb temperatures are less frequent for the 0000 UTC soundings than

the 1200 UTC soundings. Second, the 1200 UTC soundings in the western US are taken in the early morning when stable atmospheric conditions often lead to local inversions. Therefore, WBZ heights derived during these conditions may not be as representative of snow level in the surrounding mountains as the 0000 UTC soundings measure a more turbulent and mixed atmosphere.

From these records of wet day WBZ heights I created time series representing the interannual variability in snow level as determined from soundings. For each cold season with less than 20% missing data (see Table 3.1), for each site, the median wet day WBZ height (median= $X_{\frac{n+1}{2}}$ if n is odd or median = ($X_{\frac{n}{2}} + X_{\frac{n+2}{2}}$)/2 if n is even, where $X_1, \ldots, X_n$ are sorted and n is sample size) was calculated. It is important to note that for the calculation of each cold season median, soundings with WBZ heights that were below ground level were considered as a constant negative number. This is justifiable because only two sounding sites recorded a single winter with more than half of the 0000 UTC soundings producing below ground level WBZ heights, Spokane, Washington (1965) and Grand Junction, Colorado (1976). Therefore, these were the only two instances when a winter median was unable to be calculated and these winters were not considered for analysis at these two sites (i.e., 1965 was discarded for Spokane and 1976 for Grand Junction). As described in Sections 4.5 and 4.6 below, these times series (covering the cold seasons 1958-2009), along with the daily records of WBZ heights were used to determine relationships between interannual WBZ variability and ENSO/PDO as well as to determine trends in cold season WBZ heights.

4.3 COOP Snow Level Approximation Method

Approximate snow level elevations for each watershed (Figure 3.2; Table 3.2) were estimated based on the elevations of an array of stations at which daily precipitation and snowfall is reported. As discussed in the previous chapter, each watershed is represented by several (four-eleven) COOP stations (or station multiples) a different elevations (Table 3.3). Each station that underwent a change in elevation was assigned an elevation range based on the lowest and highest

elevation throughout the period of record (Table 3.3). Similarly, each station multiple was assigned an elevation range based on the differing elevations of the stations. It should again be noted that within each watershed, the elevation range of each station and station multiple do not overlap (Table 3.3).

I employed an algorithm (detailed below) over each watershed that essentially estimates the elevation of snow level for a given day as above the highest elevation in which it rained and below the lowest elevation in which it snowed. Ideally, snow level should be estimated on days that every station below a certain elevation received rainfall and every station above that elevation received snowfall as indicated by the COOP measurements. It is unreasonable to assume this, however, as there are certainly instances where the recorded daily precipitation and snowfall at the COOP stations over a given watershed indicate that rainfall occurred at an elevation above where snowfall occurred. In these scenarios, I focus on the lowest elevation that received snowfall as reported by the COOP stations which is justifiable because this suggests that snow level lowered to this elevation as some point during the given day.

Snow levels were only estimated for days which met any of the following criteria: (1) all stations reported measurable precipitation of some form; (2) at least half of the stations reported precipitation and different precipitation types occurred at two stations between which (in terms of elevation) no stations failed to record precipitation; and (3) at least half of the COOP stations reported precipitation and for a given station which received snow, there existed a higher elevation station which received rain. Criterion 1 serves to ensure the examination of days where the elevation of the vertical transition from rain to snow is most likely to be detected. Criterion 2 serves to ensure that the estimation of snow level elevation will be as precise as possible and that this precision will be maintained throughout the period of analysis. For example, for a given watershed, let the elevation of station A be 1500 meters above sea level (msl), station B be 1550 msl and station C be 1600 msl such that there is not a station between stations A and B as well as between stations B and C. In my algorithm, snow level can't be estimated as between 1500-1550 msl for one day and between 1500-1600 msl for another day. Criterion 2 also serves to increase

the number of days that a snow level can be estimated since snow level can be detected if only half the COOP stations receive precipitation. Similarly, criterion 3 also serves to increase the number of days in which a snow level could be estimated, as it is less restrictive than criterion 1. This criterion is justifiable because the timing of precipitation at each station on a given day can influence the precipitation type recorded at each station. For instance, a higher elevation station may have received precipitation only during a warmer part of the day while a lower station received its precipitation in the form of snow during a colder period of the day. These instances suggest that snow level was below the elevation of the lower station at some point during that given day.

For each watershed, on a given day in which recorded precipitation and snowfall over the COOP stations met any of the three criteria introduced above, the snow level was estimated by the following process.

Let:

A = the lowest station (in terms of elevation) that received snowfall,

B = the highest station below the elevation of station A,

L_A = the lowest elevation of station A throughout its period of record (i.e., the lower elevation bound),

L_B = the lowest elevation of station B throughout its period of record,

U_A = the highest elevation of station A throughout its period of record (i.e., the higher elevation bound),

U_B = the highest elevation of station B throughout its period of record,

SL = the estimated snow level,

L_{max} = the lower elevation bound for the highest station in the network.

Then for days in which any of criteria 1, 2, or 3 above were met:

$L_B < SL < U_A$ if A is not the lowest station in the network,

$SL < U_A$ if A is the lowest station in the network,

$SL > L_{max}$ if snow was not reported at any station and criterion 1 was met

To make the statistical analyses in Sections 4.5 and 4.6 feasible, it was important to ensure that SL could only be between the same *n*-1 pairs of elevations throughout the period of analysis, where *n* is the number stations (or station multiples) in a given watershed. Therefore, I put a premium on accuracy over precision by estimating snow level on a given day as between L_B and U_A, regardless of what the elevation of these stations actually were for that given day, ensuring that snow level was actually between those two elevations (i.e., the algorithm does not allow for snow level to be estimated as between U_B and L_A at any point during the period).

It is important to note a specific manner in which station relocation can potentially cause inaccuracies in the snow levels estimated by the above algorithm. This error occurs when the actual snow level occurs within the range of a given station's elevation bounds (e.g., L_A to U_A). For example, let *SL* be the estimated snow level and let *Y* be the actual snow level on a given day such that $L_A < Y < U_A$. Additionally, let *X* be the elevation of station *A* on that day. If $L_A < X < Y$, then $L_A < SL < U_D$ by the above algorithm where D is the next station higher than A. Similarly, if $Y < X < U_A$, then by the above algorithm, $L_C < SL < U_A$ where C is the next station below A. Therefore, the possibility exists for the timing of station relocation to either mask actual trends or create artificial trends in snow level. This possibility is remote because the elevation ranges for

each station are generally very small compared with the vertical distance between stations (Table 3.3). Thus, one would expect days such that $L_A < Y < U_A$ to be isolated cases and not be prominent enough to significantly influence the analysis of datasets with such long periods of record.

It should again be emphasized that although there are multiple stations representing each watershed, per the algorithm above, a single daily snow level is estimated from the precipitation and snowfall reported at the multiple stations. Ultimately, for each watershed, records of daily snow level approximations were created. From these daily records, the percentage of precipitation days (days that a snow level was estimated) in which the snow level was above each station's lowest elevation was calculated. These time series of percentages should be interpreted as the interannual variability in the percentage of wet days per year that snow level was above the specified elevation (e.g., the elevation of the station). Cold seasons containing at least one station with greater than 50% of daily precipitation observations missing were not considered for analysis. I found this threshold to be a reasonable compromise between maximizing the number of observations within each cold season for accurate representation (i.e., lower thresholds resulting in the elimination of many seasons) and maximizing cold season sample size (i.e., higher thresholds resulting in the elimination of very few seasons).Therefore, for a given watershed, the percentage time series for each station cover the same years.

For all watersheds, the length of record extends back to at least the mid 1930s (Table 3.3) with many extending back to 1925 (a transition year from cold to warm PDO (Stewart et al. 2005; Knowles et al. 2006)). After quality control, for half of the watersheds, less than five seasons were discarded from the study. The watershed with the most discarded seasons (17) was the Salt/Lower Verde watershed of central Arizona. As detailed in Section 4.5 and 4.6 below, these time series of percentages were used to determine the relationship between the empirical estimation of snow level from the COOP data, and ENSO/PDO as well as to determine trends in these COOP snow level approximations.

4.4 Reanalysis Method

Previous researchers have suggested that 850 hPa temperature, 1000–500 hPa thickness, 1000–850 hPa thickness and 850–700 hPa thickness are useful for discriminating between frozen and liquid precipitation (Heppner 1992). Smaller thickness values and lower temperatures are indicative of conditions more favorable for frozen precipitation at the surface. For example, a 5400 geopotential meter (gpm) thickness has been commonly used as a critical snow threshold for the 1000–500 hPa layer (Heppner 1992). Therefore, I used the upper-air temperatures and geopotential heights derived from the NCEP/NCAR reanalysis data at 2.5^{o} resolution across the western US (Figure 3.3) to calculate these variables.

As I am only concerned with winter days in which snowfall could have occurred over each grid point, I first determined the days in which precipitation likely fell over each NCEP/NCAR reanalysis grid point. I used the spherical law of cosines to identify USHCN stations within 100 km of each grid point (Figure 3.3). For example, let (lat_1, lon_1) be the latitude and longitude of location 1, and let (lat_2, lon_2) be the latitude and longitude of location 2. The distance D between location 1 and location 2 is given by,

$$D=R*\cos^{-1}(\sin(lat_1)*\sin(lat_2)+\cos(lat_1)*\cos(lat_2)*\cos(lon_2-lon_1)) \quad (4.1)$$

where R is the radius of the earth (~6371 km). Then, from 1948 through 2009, I identified the days in which a USHCN station within 100 km of a given reanalysis grid point received more than 5 mm of rain. I used 5 mm as a subjective criterion indicating the days that a snow level elevation existed in the vicinity of a given grid point. One-tenth of a millimeter is the smallest measureable precipitation amount in the USHCN dataset; however, a threshold for precipitation detection in fractions of millimeters could increase the risk of including a snow level proxy observation for an insignificant winter precipitation event 100 km from a grid point. In such a scenario, these

observed snow level proxies could add considerable noise to the analysis, as there may not be a snow level to quantify in the vicinity of the grid. Finally, for a given grid point, I created a record of 850 hPa temperature, the 1000–500 hPa thickness, the 1000–850 hPa thickness and the 850–700 hPa thickness for each wet day (days that >5 mm precipitation was within at least 100 km of that grid point).

For each grid point and each cold season, I calculated the average (average=$\frac{1}{n}\sum_{i=1}^{n} X_i$, where n is the sample size) and median wet day 850 hPa temperature, 1000–500 hPa thickness, 1000–850 hPa thickness and 850–700 hPa thickness. As described in Sections 4.5 and 4.6 below, these times series (covering the cold seasons 1949-2009), along with the daily records of 850 hPa temperature, 1000–500 hPa thickness, 1000–850 hPa thickness and 850–700 hPa thickness, were used to determine relationships between these variables and ENSO/PDO as well as to determine trends in these snow level proxies.

4.5 Teleconnection Analysis

As the ENSO phase during the fall season is particularly useful for forecasting western US winter characteristics (Harshburger et al. 2002; Brown and Comrie 2004), many previous researchers have used fall SOI as a representation of the ENSO state for the following winter (e.g., Redmond and Koch 1991; Hamlet and Lettenmaier 1999; Harshburger et al. 2002; Brown and Comrie 2004; Svoma et al. 2010). As in Svoma et al. (2010), the fall season three-month average (September–November) of the SOI values from 1896–2009 were calculated and these normalized values of less (greater) than -0.4 (0.4) represented El Niño (La Niña) conditions (Brown and Comrie 2004). The SOI values were normalized by the following procedure.

The probability density function of a normal distribution is given as

$$f(x) = \frac{1}{\sigma\sqrt{2\pi}} \exp\left[\frac{1}{2}\left(\frac{x-\mu}{\sigma}\right)^2\right] \tag{4.2}$$

where μ is the mean of the random variable X, σ is the standard deviation of X, and the area under the curve defined by the integral of $f(x)$ between x_1 and x_2 equals the probability that the random variable X takes on a value between x_1 and x_2. Let $X_1,\ldots,X_n$ be a random sample of n observations from an unknown distribution. To normalize the random sample, first standardize the observations as follows: $Z_i = X_i - \overline{X} / s\{X\}$, where

$$\overline{X} = \frac{1}{n}\sum_{i=1}^{n} X_i \tag{4.3}$$

is the sample mean and

$$\text{s\{X\}} = \sqrt{\frac{1}{n-1}\sum_{i=1}^{n}(X_i - \overline{X})^2} \tag{4.4}$$

is the sample standard deviation. Then let the empirical cumulative distribution function be given as

$$S_n(x) = \frac{1}{n}\sum_{i=1}^{n} Q(X_i, x) \tag{4.5}$$

where $Q(X_i, x)$=1 if $X_i \leq x$ and $Q(X_i, x)$=0 if $X_i > x$ (Hollander and Wolfe 1999). The normalized value for observation i ($Znorm_i$) is the value of z such that $S_n(Z_i)$=F*(z) where F*() is the cumulative normal distribution function (the integral of 4.2) with μ=0 and σ=1.

Two methods were applied to the temperature/thickness variables, WBZ heights, and the COOP snow level approximations calculated via the processes above to ascertain relationships between snow level and ENSO. The first method explores the general monotonic relationship between snow level and the phase of ENSO as quantified by the SOI. The second method identifies the influence of El Niño and La Niña events on these variables. In the following two sub-sections, these methods are introduced.

4.5.1 Monotonic Relationship between ENSO and Snow Level

To establish the monotonic relationship between ENSO and snow level, time series of winter medians were analyzed for the NCEP/NCAR reanalysis variables and WBZ heights. For each watershed, the percentage time series for only one station was analyzed (indicated by asterisks in Table 3.3). This station was subjectively chosen based on the three following list of criteria in order of importance: (1) the station's annual percentages were obviously not consistently bounded by 0% or 100% (to help ensure error normality for significance tests); (2) the station's data was not supplemented with that of another station; and (3) the station experienced a relatively small elevation change due to any station relocation.

The relationships between the autumn SOI values and these times series were assessed through both Kendall's Tau nonparametric correlation (Hollander and Wolfe 1999) and Pearson product-moment correlation as in Hidalgo and Dracup (2003), Brown and Comrie (2004) and Goodrich (2007). I used Kendall's Tau nonparametric correlation adjusted for ties (Hollander and Wolfe 1999). Assuming that n paired observations on random variables X and Y such that $(X_1,Y_1),\ldots,(X_n,Y_n)$ are mutually independent and sampled from identically distributed populations according to a continuous bivariate population, to test for independence of X and Y, the test statistic KT is given as follows:

$$\mathrm{KT}=\sum_{i=1}^{n-1}\sum_{j=i+1}^{n}\Im((X_i,Y_i),(X_j,Y_j)) \tag{4.6}$$

where $\Im((w,x),(y,z))=1$ if $(z-x)(y-w)>0$, $\Im((w,x),(y,z))=0$ if $(z-x)(y-w)=0$ and $\Im((w,x),(y,z))=-1$ if $(z-x)(y-w)<0$. In short, the test statistic KT is simply number of discordant pairs subtracted from the number of concordant pairs. The Kendall's Tau correlation coefficient ranges from -1 to 1 and is given by

$$\tau=2\mathrm{KT}/(n(n-1)) \tag{4.7}$$

To test the null hypothesis that X and Y are independent (i.e., $\tau=0$), I used a large sample ($n>39$) approximation to take advantage of the asymptotic normality of KT when standardized. In the case of ties (i.e., $X_i=X_j$ or $Y_i=Y_j$ for some$1\leq i\neq j\leq n$) under the null hypothesis that KT=0 (and thus $\tau=0$), the variance of KT is given by the following expression:

$$\text{var(KT)}=\{n(n-1)(2n+5)-\sum_{i=1}^{q}w_i(w_i-1)(2w_i+5)-\sum_{j=1}^{s}u_j(u_j-1)(2u_j+5)\}/18$$

$$+\{\sum_{i=1}^{q}w_i(w_i-1)(w_i-2)\}\{\sum_{j=1}^{s}u_j(u_j-1)(u_j-2)\}/9n(n-1)(n-2)\}$$

$$+\{\sum_{i=1}^{q}w_i(w_i-1)\}\{\sum_{j=1}^{s}u_j(u_j-1)\}/2n(n-1)\} \quad (4.8)$$

where q equals the number of tied groups in X, s equals the number of tied groups in Y, w_i and u_j are the size of tied group i and j respectively in X and Y respectively. The standardized version of KT under the null hypothesis is KT*=KT/var(KT). If one chooses $z_{\alpha/2}$ such that the probability of $|KT^*|>z_{\alpha/2}$ is α under the null hypothesis, then one can reject the null hypothesis at the α level.

A firm understanding of Pearson product-moment correlation requires an understanding of simple linear regression and the reverse. Therefore, I detail simple linear regression which is used for trend analysis see (see Section 4.6) followed by Pearson product-moment correlation. The linear regression model is given as follows (Kutner et al. 2005):

$$Y_i=\beta_o+\beta_1X_i+\varepsilon_i \quad (4.9)$$

where:

Y_i is the response variable for trial *i,*

β_o and β_1 are parameters representing the Y intercept and the slope respectively,

X_i is the value of the predictor variable for the trial *i,* a known constant in the case of linear regression,

ε_i is a random error term that is normally distributed with mean μ=0 and standard deviation σ for all *i* =1,…..,n trails. Additionally, for all i=1,…,n and j =1,..,n such that i≠j, the covariance σ{ ε_i , ε_j }=0, where,

$$\sigma\{\varepsilon_i, \varepsilon_j\}=E[\varepsilon_i \varepsilon_j]-\{E[\varepsilon_i]E[\varepsilon_j]\} \quad (4.10)$$

and the operator E[ ] is the expected value of a given random variable (Kutner et al. 2005).

The error term definitions reveal three fundamental assumptions of model 4.9: (1) the error terms must be normally distributed for each trial, (2) the variance of the error terms must be the same for each trial, and (3) each trial must be independent (Kutner et al. 2005). To derive a fit for the above model, the parameters β_o and β_1 can be estimated by least squares estimators, b_o and b_1 respectively. These estimators minimize the sum of the squares of the observed error terms (or residuals) for the above model. The definitions for b_o and b_1 are as follows:

$$b_1=\frac{\sum(X_i-\overline{X})(Y_i-\overline{Y})}{\sum(X_i-\overline{X})^2} \quad (4.11)$$

$$b_o=\overline{Y}-b_1\overline{X} \quad (4.12)$$

where $\overline{X}$ and $\overline{Y}$ are the means of the Y_i and X_i observations, respectively (calculated as by 4.3).

In this study, I am interested in the null hypothesis stating that β_1 equals zero (i.e., there is no relationship between the predictor variable and response variable). Let the standard error of b_1 be given as follows:

let e_i, the residual from the least-square fit, be given by:

$$e_i = y_i - b_0 - b_1 x_i \tag{4.13}$$

and MSE, the mean squared error, be given by ,

$$\text{MSE} = \sum_{i=1}^{n} e_i^{\,2} / (n-2) \tag{4.14}.$$

Then, the estimated standard deviation of b_1 is given by,

$$s\{b_1\} = \sqrt{MSE / \sum_{i=1}^{n} (X_i - \bar{X})^2} \tag{4.15},$$

and the test statistic

$$T^* = b_1 / s\{b_1\} \tag{4.16}$$

is distributed as the student's t distribution with n-2 degrees of freedom (Kutner et al. 2005). If $t_{\alpha/2}$ is chosen such that the probability of $|T^*| > t_{\alpha/2}$ is α under the null hypothesis, then one can reject the null hypothesis wit 100*(1-α)% confidence.

Model 4.9 assumes that the values of X are known constants (e.g., years for trend analyses in Section 4.6). It may not always be appropriate to consider the X values as know constants. For instance, ENSO is a continually changing atmospheric and oceanic phenomenon and values of SOI (the measure of ENSO phase in this study) are continuous and can take any value from ~-35 to 35 as discussed in Chapter 3. Therefore, to relate SOI to a given snow level variable, it is more appropriate to use Pearson product-moment correlation. Let Y_1 and Y_2 be variables that are jointly normally distributed (i.e., given Y_2, Y_1 is normally distributed such that

mean and variance of Y_1 are functions of the covariance between Y_1 and Y_2, and the reverse). Let the covariance between Y_1 and Y_2 (σ_{12}) be given by 4.10. Two variables are said to be independent of one another if the product of their means is equal to the mean of their products (Kutner et al. 2005). Thus when Y_1 and Y_2 are independent, $\sigma_{12}=0$ and the mean and variance of the Y_1 distribution does not depend on variability in Y_2, and the reverse. As a means of determining if $\sigma_{12}=0$, one may calculate the Pearson product-moment correlation coefficient as,

$$r_{12} = r_{21} = \frac{\sum_{i=1}^{n}(Y_{i1} - \overline{Y}_1)(Y_{i2} - \overline{Y}_2)}{\sqrt{\sum (Y_{i1} - \overline{Y}_1)^2 \sum (Y_{i2} - \overline{Y}_2)^2}} \tag{4.17}$$

Furthermore, let $T^* = r_{12}\sqrt{n-2} / \sqrt{1-r_{12}^2}$. Under the null hypothesis that $\sigma_{12}=0$, T* follows the student's t distribution with n-2 degrees of freedom (Kutner et al. 2005). If one chooses $t_{\alpha/2}$ such that the probability of $|T^*| > t_{\alpha/2}$ is α, then one can reject the null hypothesis that $\sigma_{12}=0$ with $100*(1-\alpha)\%$ confidence. The equivalence of simple linear regression and Pearson product-moment correlation follows from the assumption that Y_1 and Y_2 are from a bivariate normal distribution (Kutner et al. 2005). For a given value of Y_2, Y_1 is normally distributed with a mean that is a simple linear function of Y_2, and a variance that is the same for all values of Y_2. If each of the n observations from Y_1 are independent, then the simple linear regression with Y_1 as the response and Y_2 as the predictor, meet error normality and constant error variance assumptions above (Kutner et al. 2005). It can also be shown that the null hypothesis that $\sigma_{12}=0$ is equivalent to $\beta_1 = 0$ for simple linear regression (Kutner et al. 2005).

For all Pearson correlations, error normality was assessed through Lilliefors test for normality (Steinskog et al. 2007). Additionally, constant error variance was assessed through the Breusch-Pagan test (Rackauskas and Zuokas 2007). The Lilliefors test statistic is the same as the Kolmogorov-Smirnov test statistic but with critical values derived by Lilliefors (1967) through

Monte Carlo experimentation. Let $X_1,\ldots,X_n$ be the sample of residuals resulting from regressing a variable X_1 against X_2. The Lilliefors test statistic is given as follows:

$$D=\max|S_n(X)-F^*(X)| \tag{4.18}$$

for all X in the n observations where $S_n(X)$ is the empirical cumulative distribution function of the n observations given by 4.5 and F*(X) is the normal cumulative distribution function with $\mu=\frac{1}{n}\sum_{i=1}^{n} X_i$ and $\sigma^2=\frac{1}{n-1}\sum_{i=1}^{n}(X_i-\mu)^2$ given by the integral of 4.2 (Lilliefors 1967). For $n>30$, if $D>0.886/\sqrt{n}$, then one rejects the hypothesis of a normal population at the 0.05 level (Lilliefors 1967). To examine normality for each correlation test between SOI (Y_1) and a given snow level variable (Y_2), I applied the Lilliefors test on the residuals resulting from regressing Y_1 against Y_2 and Y_2 against Y_1 via simple linear regression.

Similarly, I applied the Brueuch-Pagan test to simple linear regression of $Y=Y_1$ (SOI) and $X=Y_2$ (a snow level proxy) as well as $Y=Y_2$ and $X=Y_1$ through the process as follows (Kutner et al. 2005). Let $\hat{Y}_1(x)$ be the least-squares fit for model 4.9 given by,

$$\hat{Y}_1(x)=b_0+b_1x \tag{4.19}$$

and the residuals from this fit are given by 4.13. The square of a given residual represents the error variance (σ^2) in that the expected value of the average (4.3) of the squared residuals is approximately σ^2. The linear relationship between the squared residuals (e_i^2) and the independent variable (x) is given by,

$$\hat{Y}_2(x)=b_{00}+b_{11}x \tag{4.20}$$

where the values of b_{00} and b_{11} were determined through a least-squares regression as defined by 4.11 and 4.12 respectively (Kutner et al. 2005). The test statistic,

BP= (SSR/2)/(SSE/n)^2 follow a chi-square distribution with 1 degree of freedom (Kutner et al. 2005) where SSR is the sum of squares regression from $\hat{Y}_2(x)$ given as:

$$\text{SSR}=\sum_{i=1}^{n}(\hat{Y}_2(x_i)-\overline{Y})^2 \tag{4.21}$$

and SSE is the sum of squared errors from $\hat{Y}_1(x)$ given as

$$\text{SSE}=\sum_{i=1}^{n}(\hat{Y}_1(x_i)-Y(x_i))^2 \tag{4.22}$$

If BP> $\chi_\alpha{}^2$ where $\chi_\alpha{}^2$ is chosen such that the probability of BP > $\chi_\alpha{}^2$ is less than α, then one can reject the null-hypothesis that σ^2 is constant with changes in the predictor variable (X) with 100*(1-α)% confidence.

4.5.2 Relationship between Snow Level and El Niño /La Niña

As in Gershunov and Barnett (1998a), the medians of the daily values of each variable (e.g., WBZ heights, upper-air reanalysis variables) were calculated for each location (e.g., sounding site or NCEP/NCAR reanalysis grid) in the western US during years of neutral ENSO conditions (-0.4 ≤ $Znorm_i$ ≤ 0.4). Soundings with WBZ heights that were below ground level were considered as a constant negative number. This is justifiable because, even at the coldest rawinsonde locations, much less than 50% of daily WBZ heights were below ground level (Table 3.1). Therefore, even with the inclusion of below ground level values, the medians were tangible WBZ heights in every case. For a given variable, this median can be seen as the center of the probability density function (PDF) for neutral ENSO conditions for a given location. Again following Gershunov and Barnett (1998a), for El Niño conditions ($Znorm_i$ < -0.4) the percentage of daily values that were greater than the ENSO neutral median was calculated for each variable and location. This same procedure was employed for La Niña conditions (0.4 < $Znorm_i$).

The significance of these percent anomalies (which represent the shift in the El Niño and La Niña PDFs relative to the neutral baseline) for each El Niño PDF and La Niña PDF were determined through a bootstrap resampling technique (Gershunov and Barnett 1998a). This bootstrap technique is applied as follows: let *X* be the number of El Niño winters and *Y* be the number of La Niña winters during the period of record (of length T for the total number winters) for each variable. Each El Niño and La Niña winter were chosen at random without replacement from the T winters. The rest of the T-(X+Y) winters were considered neutral ENSO conditions. The percentage anomalies for the random El Niño and La Niña assignments were calculated as above. This procedure was repeated 999 times. For each variable and location, a two-sided pseudo significance level was calculated as follows (Gershunov and Barnett 1998a): for a given El Niño/La Niña anomaly, let K be the number of random anomalies which deviate from 50% (e.g., no shift in the PDF center) by at least as much as the observed anomaly. The pseudo significance of the observed anomaly was therefore (K+1)/1000 (Gershunov and Barnett 1998a). It is important to note that the daily snow level approximations for each watershed derived from the COOP method were not subject to the above analysis as the discrete nature of the daily values (e.g., snow level recorded as between the elevation of two stations) was not suitable for a method applicable to only continuous data.

As a an alternative method, two-sample t-tests were employed as a means of testing for the significance of the difference in the means of COOP derived percentages (i.e., the percentage of wet days for a given winter with snow level above the elevation of stations indicated by asterisks in Table 3.3) between El Niño conditions and neutral ENSO conditions as well as La Niña and neutral ENSO conditions. Two-sample t-tests are equivalent to the linear model given by 4.9 where Y_i is the response variable for trial *i,* X_i is the value of the predictor variable for the trial *i,* where X_i =1 if trial *i* is an El Niño (or La Niña) winter, and X_i =0 if trial *i* is a neutral ENSO winter. The parameter β_o then represents the mean value for neutral ENSO winters and the parameter β_1 represents the change in the mean value for El Niño (or La Niña) winters. The

significance of the deviation of b_1 (i.e., the estimator of β_1) from zero can be determined by the test statistic 4.16.

4.5.3 The modulation of the ENSO relationship with snow level

Several previous researchers have also explored the modulation of the ENSO influence by PDO phase (Gershunov and Barnett 1998b; Gutzler et al. 2002; Brown and Comrie 2004; Goodrich 2007). These investigators examined how the ENSO influence on temperature/precipitation either weakened or strengthened during different phases of the PDO. Therefore, I used similar methods to determine the PDO relationship with snow level.

For each variable, the procedures in Sections 4.5.1 and 4.5.2 were repeated for each recent warm and cold phase of PDO (warm: 1925-1946, cold: 1947-1976, warm: 1977-1998 (Stewart et al. 2005; Knowles et al. 2006)) to explore the combined PDO and ENSO relationship with snow level. As the periods of record for the WBZ time series extend back to winter 1958, the WBZ heights were analyzed for most of the PDO cold phase and the entire recent PDO warm phase for all ten rawinsonde sites (Table 3.1). In addition, the COOP derived percentages generally extend back to before the cold season 1935. Therefore, these time series were analyzed for the entire PDO cold phase, the entire more recent warm phase, and most of the earlier warm phase (Table 3.3). Lastly, the NCEP/NCAR reanalysis time series extend back to cold season 1949 and thus the PDO analysis cover nearly all of the PDO cold phase and all of the recent warm phase.

4.5.4 Statistical Significance for the Entire Study Area

Determining the significance of the relationship between ENSO (represented by fall SOI) and each snow level variable (e.g., 850 hPa temperature, 1000–500 hPa thickness, 1000–850 hPa thickness 850–700 hPa thickness) across the western US as a whole (i.e., the 60 reanalysis grids) cannot be accomplished through traditional statistical techniques such as one-sample t-tests due to a lack of independence between locations from spatial autocorrelation (Wolter et al. 1999).

Therefore, following Wolter et al. (1999), "field significance" was determined through Monte Carlo techniques as follows: for a given variable for a given statistical technique (e.g., bootstrapping technique, Kendall's Tau technique, and Pearson correlation), let J be the number of locations with significant two-sided p-values ($p < 0.05$). Each location across the western US was randomly assigned the same fall SOI value for each winter. The number of locations (J') displaying significant p-values for the random fall SOI assignments was recorded. After this procedure was repeated 999 times, the two-sided pseudo-significance of the relationship between ENSO (represented by fall SOI) and the variable of interest over the entire western US was determined from this empirical probability density function as (K+1)/1000 where K is the number of random trials in which $J' >= J$. This procedure was also employed for results from the analyses of the ENSO relationship with snow level during separate phases of PDO as described in Section 4.5.3. It is important to note that the Monte Carlo derived empirical density functions for the percent anomalies representing the shifts in the El Niño /La Niña PDFs from the neutral ENSO phase baseline were based off only 99 random fall SOI assignments due to the computing time required to repeat each of the 999 random selections of El Niño/La Niña winters (see Section 4.5.2) 99 times.

4.5.5 Spatial Variability

Lastly, spatial patterns in the ENSO influence on snow level, as well as modifications of this influence by PDO, were assessed through the mapping of Kendall's Tau correlation coefficients (4.7), Pearson product-moment correlation coefficients (4.16), and the percent anomalies for El Niño /La Niña conditions (Section 4.5.2) derived from the SOI relationships with the NCEP/NCAR reanalysis data, WBZ height data, and watershed percentages. Additionally, I mapped the local Moran's I for these mapped values (Anselin 1995). The calculation of the local Moran's I is given as,

$$I_i = z_i \sum_{j=1}^{n_i} w_{ij} z_j \tag{4.23}$$

where z_j and z_i are standardized values with respect to all locations (i.e., $z_j = X_j - \overline{X} / s\{X\}$ where $\overline{X}$ is defined by 4.3 and $s\{X\}$ is defined by 4.4), w_{ij} is the weight for the *j*th neighbor for location *i*. For all local Moran's I calculations, each location was considered a neighbor of every other location, and the inverse of the distance squared (determined by 4.1), also called inverse gravity weighting, was used as the weights for each pair of neighbors. I chose to have every location as a neighbor of every other location to reduce edge effects. Inverse gravity weighting was employed to reduce the effects on the calculation of I_i by locations that are extremely far away. It should be noted that the centroid of the COOP stations represented the location of a given watershed for Moran's I calculations. When local Moran's I values are mapped, spatial patterns in the variable of interest are highlighted by the display of statistically significant clusters of high/low values or significant outliers (i.e., low values surrounded by high values or the reverse). A lack of significant clustering in high/lows values along with locations classified as significant outliers indicates that there likely is not an obvious underlying spatial pattern in the variable of interest (Anselin 1995). It is important to note that the mapped values are not spatially de-trended before local Moran's I calculations. Thus, I_i represents a measure of local spatial autocorrelation due to the effects of the spatial variability in the mean of X_i in 4.23.

The significance of each local Moran's I value is based on 9,999 trials in which the neighbors of each location are randomly selected from the remaining *n*-1 locations. This results in an empirical probability distribution function from which a pseudo *p*-value (Anselin 1995) is determined as (K+1)/10,000 where K is the number of random local Moran's I values that are at least as extreme (e.g., absolute deviation from zero) as the observed local Moran's I. Jointly significant cluster cores/outliers at the 5% confidence level are locations which have a local Moran's I significant at the $100(1-(0.95)^{1/n})$ percent level due to the possibility of random significance at the 5% level at each of the *n* locations (Anselin 1995).

4.6 Trend Analysis

Trends in snow level elevation were determined by the analysis of the time series of cold season averages for the NCEP/NCAR reanalysis variables (Section 4.4) and medians for WBZ heights (Section 4.2) as well as the COOP percentages (Section 4.3). It is important to note that median cold season WBZ heights were analyzed as opposed to averages as a meaningful average cannot be calculated with large percentages of below ground level WBZ heights. As discussed in Section 4.2, meaningful medians can be calculated because much less than 50 % of the 0000 UTC soundings were below ground level for each rawindsonde site (Table 3.1). Simple linear regression and the non-parametric Mann-Kendall test were both used for the trend analysis of these time series. The statistical significance of a given trend as determined from the Mann-Kendall test is determined by the same procedure as the Kendall's Tau correlation test described in Section 4.5.1 above (Hollander and Wolfe 1999) where $X_1,\ldots X_n$ represent a measure of time (in this study, the measure of time is years). It is important to note that the Mann-Kendall test has been employed in many previous studies concerned with trends in climate variables and does not require assumptions about error-normality for significance to be determined (Chu and Wang, 1997; Kanae et al. 2001; Garcia et al. 2007 Sheffield and Wood, 2008; Sinha and Cherkauer, 2008).

Simple linear regression has been used in many previous investigations of trends on climate variables (e.g., Mote et al. 2005; Kunkel et al. 2009a; Svoma et al. 2010). I employed simple linear regression through the process detailed in Section 4.5.1 (X=cold seasons) and error normality and constant error variance were assessed for all simple linear regressions through the Lilliefors and Brueuch-Pagan test as described in Section 4.5.1. A common issue with employing simple linear regression on a time series is the relatively high probability of a lack of independence in the error terms (i.e., $\sigma\{\varepsilon_i, \varepsilon_j\}=0$) through autocorrelation (Kutner et al. 2005). First-order autocorrelation ($\sigma\{\varepsilon_i, \varepsilon_{i+1}\} \neq 0$) is a common form of error dependence indicating that the value of an error term is dependent on the previous error term. In this situation, a first-

order autoregressive model (often referred to as AR(1)) can improve upon model 4.9 (Kutner et al. 2005). The first-order autoregressive model is given as in 4.9, but assumes that:

$$\varepsilon_i = \rho\varepsilon_{i-1} + u_i \tag{4.24}$$

where u_i are independent random error terms that are normally distributed with mean μ=0 and standard deviation σ for all i =1,…..,n-1 trails and ρ is the autocorrelation parameter with $|\rho| < 1$ (Kutner et al. 2005). The Durbin-Watson test can be used to determine if null hypothesis of $\rho = 0$ should be rejected for the alternative hypothesis that $\rho > 0$ (Kutner et al. 2005). The test statistic is calculated as follows:

$$D = \frac{\sum_{i=2}^{n}(e_i - e_{i-1})^2}{\sum_{i=1}^{n} e_i^2} \tag{4.25}$$

where e_i are the residuals as in 4.13. It is difficult to obtain exact critical values for D but there are lower bounds (d_u) of D such that if $D > d_u$, the null hypothesis can be definitively be accepted. These bounds are commonly available for various sample sizes in statistical textbooks (e.g., Kutner et al. 2005).

For each time series, I employ the Durbin-Watson test to determine if $\rho > 0$ at the 0.05 significance level. If $\rho > 0$, then I attempt to alleviate the autocorrelation following the Hildreth-Lu procedure (Kutner et al. 2005) as follows:

Consider the transformed model,

$$Y_i' = \beta_o' + \beta_1' X_i' + u_i \tag{4.26}$$

where:

$$Y_i' = Y_i - \rho Y_{i-1} \tag{4.27}$$

$$X_i' = X_i - \rho X_{i-1} \tag{4.28}$$

$$\beta_o' = \beta_o (1 - \rho) \tag{4.29}$$

$$\beta_1' = \beta_1 \tag{4.30}$$

Therefore, under model 4.26, one can use simple linear regression with independent error terms to estimate the regression coefficients (Kutner et al. 2005). To apply model 4.26, however, the value of ρ must be estimated. Let,

$$SSE = \sum \ (Y_i' - b_o' - b_1' X_i')^2 \tag{4.31}$$

where b_o' and b_1' are estimates for the parameters in 4.26 given as 4.12 and 4.11 (Kutner et al. 2005). I employed a computer heuristic to calculate *SSE* in 4.31 for all 100,000 possible estimates of $0<\rho\leq 1$ carried out to nearest 10^5 th. The best estimate of ρ is the one that minimizes *SSE* (per the Hildreth-Lu procedure in Kutner et al. 2005). The coefficients are then transformed back to model 4.9 as (Kutner et al. 2005):

$$b_o = \frac{b_o'}{1 - r} \tag{4.32a}$$

$$b_1 = b_1' \tag{4.32b}$$

$$s\{b_1\} = s\{b_1'\} \tag{4.32c}$$

where r is the estimate of ρ, the operator $s\{\bullet\}$ is given in 4.15, and the significance of the deviation of b_1 from zero follows from the test statistic 4.16. The Durbin-Watson test is then used to determine if the transformation to model 4.26 has eliminated first-order autocorrelation.

The "field significance" of trends over the western US was determined by the same Monte Carlo techniques (Wolter et al. 1999) described in Section 4.5.4 above (e.g., each of the 999 permutations consisted of randomly scrambling the years and testing for trend at each location). The spatial variability of the WBZ trends, reanalysis trends, and watershed percentage trends were assessed through mapping Kendall's Tau correlation coefficients (4.7) and least-squares slopes (4.11) and then computing and mapping the local Moran's I cluster cores/outliers as in Section 4.5.5. As with the teleconnection analysis, all possible neighbor pairs were weighted by inverse squared distance for the local Moran's I calculations.

4.7 Control Methods

With the relationships between ENSO/PDO and snow level established for different regions across the western US, it can be determined if any trends in snow level variables are within the realm of this natural climate variability. As previous researchers have suggested that El Niño events as quantified by SOI have increased in strength (Power and Smith 2007), I first determine the importance of ENSO variability to any observed trends in snow level by testing for trend in snow level variability not accounted for by ENSO. Specifically, I employed the Mann-Kendall test and simple linear regression (I as described in Section 4.6) to $e_{i=} y_i - b_0 - b_1 x_i$ where y_i is the value of a snow level variable (WBZ height, temperature/thickness, or COOP derived percentages) at a given location for cold season i and x_i is the fall SOI for cold season i.

Two methods were then used to determine the influence of the PDO modulation of the ENSO effects on snow level to snow level trends. First, I employ a multiple linear regression to model the snow level variable of interest based on the modulation of the neutral ENSO fit and the snow level variable response to fall SOI by PDO (i.e., β_o and β_1 respectively when the snow level variable is regressed against value fall SOI).

I employ the following model (Kutner et al. 2005):

$$Y_i = \beta_o + \beta_1 X_{i1} + \beta_2 X_{i2} + \beta_3 X_{i1} X_{i2} + \varepsilon_i \qquad (4.33)$$

where:

X_{i1} = normalized fall SOI

X_{i2} = 1 if PDO is in a cold phase and 0 if PDO is in a warm phase

Therefore, when PDO is in its warm phase, the regression fits become

$$\hat{Y}_i = b_o + b_1 X_i \qquad \text{warm PDO} \qquad (4.34)$$

and when PDO is in its cold phase the regression fits become

$$\hat{Y}_i = (b_o + b_2) + (b_1 + b_3) X_i \qquad \text{cold PDO} \qquad (4.35)$$

where b_o b_1 b_2 and b_3 are the estimates of the regression coefficients. The calculation of b_o b_1 b_2 and b_3 (as well as the significance of their deviation from zero) follows logically from simple linear regression (4.11, 4.12, 4.15, and 4.16) (Kutner et al. 2005).

For both simple linear regression and multiple linear regression, a useful metric for determining the effectiveness of the predictors variables is given by

$$R^2 = \frac{SSR}{SSR + SSE} \qquad (4.36)$$

where SSR and SSE are given in 4.21 and 4.22 for simple linear regression. The extensions of 4.21 and 4.22 for multiple linear regression are intuitive. A test statistic derived from 4.36 to test the null hypothesis that $b_1 = b_2 = b_3 = 0$ against the alternative that not all three equal zero is given as follows:

$$F^* = \frac{SSR/3}{SSE/(n-4)} \qquad (4.37)$$

where n is the number of observations and F^* follows the F distribution with 3 degrees of freedom in the numerator and n-4 degrees of freedom in the denominator (Kutner et al. 2005). Another test

statistic of importance determines the significance of the deviation from the null hypothesis $b_2 = b_3=0$ given that X_{i1} is already in the model against the alternative that at least one (i.e., b_2 or b_3) does not equal zero is given as follows:

$$F^* = \frac{(SSR(X_1, X_2, X_3) - SSR(X_1))/2}{SSE/(n-4)} \tag{4.38}$$

where SSR(X_1,X_2,X_3) is derived from model 4.33 and SSR(X_1) is derived from model 4.9 with X_1 representing fall SOI. To determine if trends exist in the snow level variable after ENSO and the PDO modulation of ENSO have been accounted for by model 4.33, I test for trend in the residuals (i.e., $e_{i=} y_i - b_0 - b_1 x_{i1} - b_2 x_{i2} - b_3 x_{i1} x_{i2}$) as described in Section 4.6. It is important to note that the above methods were applied to each temperature/thickness and WBZ height time series analyzed in Chapter 6, however, for the sake of simplicity only one time series of percents were analyzed for each watershed (see Table 3.3). These time series were subjectively chosen based on the four following list of criteria in order of importance: (1) the time displayed significant trend as displayed in Chapter 6; (2) the time series were obviously not consistently bounded by 0% or 100% (to help ensure error normality for significance tests); (3) the stations data was not supplemented with that of another station; and (4) the station experienced a relatively small elevation change due to any station relocation.

The second control method is similar to the methods employed by Svoma et al. (2010) and Hamlet et al. (2005). Specifically, I test for trend in the COOP percentage time series (which span multiple PDO phase changes) during three separate sub-periods representing transitions in the PDO. For example, the first twentieth century warm to cold phase transition of the PDO was considered as the period 1936 to 1960. Similarly, a cold to warm transition occurred from 1961 to 1987, and an indeterminable but potential warm to cold phase change occurred from 1988 to 2009 (Hare and Mantua 2000; Bond et al. 2003; Stewart et al. 2005; Knowles et al. 2006). If trends during these three sub-periods appeared to be more consistent with longer-term climate change than the inter-decadal changes expected from the PDO modulation of ENSO results, then it is

likely that the observed trends cannot be accounted for by variations in ENSO/PDO. For example, if for a given location I find that snow levels are lower during the warm phase of the PDO than the cold phase of the PDO, then I would expect the trends for the cold to warm transition to be negative. However, a positive trend would suggest that PDO is not responsible for the suggested increase in snow level.

Assuming that there are long term trends in the snow level data, one should not expect the methods for establishing the ENSO/PDO relationship with snow level described in Section 4.5 to be influenced by these trends. The ENSO cycles have short periods (Kestin et al. 1998) and therefore, it is a remote possibility that an uneven temporal distribution of El Niño or La Niña events would skew the general conclusions of statistical tests due to the assumed snow level trends. Additionally, the methods assessing the modulation of ENSO effects by PDO are employed separately for each PDO phase. Thus, the differing means/medians of snow levels by PDO phase due to the assumed long term trends in snow level would not affect the statistical conclusions about the ENSO relationship with snow level during each PDO phase the relationship between ENSO and snow level phase is determined with respect to mean/median snow level during the PDO phase of interest (i.e., not the overall mean/median that would not be representative of the PDO phase of interest due to the assumed long term trends in snow level).

4.8 Conclusion

To examine the natural climate variability (from El Niño–Southern Oscillation (ENSO) and Pacific Decadal Oscillation (PDO)) and a possible climate change signal in the elevation of snow level across the western US, I employed three methods to quantify both daily snow levels for each cold season (October through April) and interannual snow level variability:

(a) From 1958-2010, for ten rawinsonde locations (Figure 3.1; Table 3.1), interannual variability in wet-bulb zero (WBZ) height (the height above sea level that the wet-bulb temperature is 0^{o}C (Svoma 2011)) was represented by time series of cold season

median wet day WBZ heights. These were derived from records of wet day WBZ heights and below ground level WBZ heights.

(b) For ten watersheds each adjacent to a sounding location (Figure 3.2; Table 3.2), I created time series generally extending back to 1925 consisting of the percentage of wet days per cold season with snow levels above the elevation of stations in the National Weather Service Cooperative Observer network (COOP). These time series were derived from daily snowfall and rainfall reports at COOP stations of varying elevation, where snow level was estimated through the determination of the elevations between which rainfall transitioned to snowfall.

(c) From 1949-2009, I created times series consisting of wet day cold season averages and medians for 850 hPa temperature, 1000–850 hPa thickness, 850–700 hPa thickness and 1000–500 hPa thickness for each of 60 sixty grid points separated by 2.5^{o} latitude and 2.5^{o} longitude across the western US (Figure 3.3). These time series were derived from daily upper-air temperatures and geopotential heights obtained from National Center for Environmental Prediction/National Center for Atmospheric Research (NCEP/NCAR) reanalysis project. 850 hPa temperature, 1000–850 hPa thickness, 850–700 hPa thickness and 1000–500 hPa thickness have been found to effectively discriminate between frozen and liquid precipitation reaching the surface (Heppner 1992).

From the records of snow level produced by these three methods, I established the ENSO influence on snow level through correlation of the Southern Oscillation Index (SOI) and the time series of medians and percentages as well as through examining the shift in the center of the probability density functions of these variables from neutral ENSO conditions to La Niña/El Niño conditions. To determine the modulation of the ENSO influence on snow level by PDO, I repeated the ENSO analyses separately for each cold and warm phase of the PDO (warm: 1925-1946, cold: 1947-1976, warm: 1977-1998 (Stewart et al. 2005; Knowles et al. 2006)). The spatial variability in the statistical relationships between snow level and ENSO/PDO was assessed through the calculation and mapping of the local Moran's I values on correlation coefficients resulting from

the statistical analyses of WBZ heights, COOP derived percentages and reanalysis derived thickness/temperature variables.

Trends in the time series of median WBZ heights, COOP percentages of snow levels above station elevations, and average thickness/temperature values were determined through both Mann-Kendall non-parametric trend test and simple linear regression (note, a first-order autoregressive model was employed when serial autocorrelation was present in the error terms). The spatial variability in trends was assessed through the calculation and mapping of the local Moran's I values on regression coefficients resulting from the trend tests. Lastly, to put any significant trends in the context of natural climate variability, residual trends were analyzed after the statistical removal of ENSO/PDO variability through multiple and simple linear regression. Additionally, during various transitions of PDO phase, trends were examined for consistency with the expected trends from the results of the analysis of the ENSO/PDO relationship with snow level.

In summary, a variety of parametric and non-parametric statistical methods were executed on time series of snow level variables to establish the importance of natural climate variability and long term climate change to any apparent trends in snow level. In the following chapter, the relationship between snow level and ENSO/PDO is established for the western US as a whole, followed by a detailed analysis of the spatial variability of these relationships. The consistency of results between the three methods of snow level quantification (WBZ heights, COOP snow level approximations, and NCEP/NCAR derived upper-air data) is discussed to conclude the general relationship (and spatial patterns in the relationship) between snow level and ENSO/PDO.

Chapter 5: The El Niño–Southern Oscillation and Pacific Decadal Oscillation Relationship with Snow Levels

5.1 Introduction

In the previous chapter, I discussed the three separate methods that quantify daily snow levels (from October through April) and interannual snow level variability. The first method involves a climatology of wet day 850 hPa temperature, 1000–850 hPa thickness, 850–700 hPa thickness and 1000–500 hPa thickness for 60 grids across the western US from the NCEP/NCAR reanalysis output (Figure 3.4). The second method employs a climatology of wet day wet-bulb zero (WBZ) heights at ten rawinsonde sites across the western US (Figure 3.4). Lastly, a record of estimated snow level elevations for ten watersheds adjacent to the ten rawinsonde sites (Figure 3.4) was developed. Additionally, a methodology was introduced to statistically compare these snow level measures with El Niño–Southern Oscillation (ENSO) as well as Pacific Decadal Oscillation (PDO) along with the means of trend detection. Lastly, I detailed the method used to determine if any observed trends are outside the realm of natural climate variability (i.e., ENSO/PDO).

In this chapter, I seek to answer the following question introduced in Chapter 1: *What is the relationship between ENSO/PDO and snow level and how does this relationship vary across on the western US?* To accomplish this, normalized fall SOI values are used to quantify the ENSO state and identify El Niño events (normalized fall SOI <-0.4) and La Niña events (normalized fall SOI >0.4; see Figure A.1 in the Appendix). I first establish the existence of an ENSO signal in the NCEP/NCAR reanalysis temperature/thickness variables and the spatial variability thereof, followed by an analysis of the modulation of the ENSO signal by PDO phase. That leads to a discussion of similar analyses using the WBZ heights, and approximate watershed snow levels within the context of the observed ENSO/PDO signal in temperature/thickness. Lastly, I discuss the results with respect to the large body of previous research regarding the ENSO/PDO relationships with western US climate.

5.2 ENSO/PDO and Upper-Air Thickness/Temperature

5.2.1 The SOI Relationship with Temperature and Thickness

The analysis is initiated by statistical tests for error normality and constant variance. Rejections (at the 0.05 confidence level) of the error normality and constant error variance assumptions for Pearson product-moment correlations as determined by the Lilliefors test and Breusch-Pagan test respectively are displayed in Figure A.2 in the Appendix. Both assumptions appear valid at most grids and very few grids display significant deviations of these attributes for all four reanalysis variables (Figure A.2). Over the western US as a whole, all correlations between fall SOI and median winter temperature/thickness (i.e., 850 hPa temperature, 1000–850 hPa thickness, 850–700 hPa thickness and 1000–500 hPa thickness from the NCEP/NCAR reanalysis output) significantly deviate from zero (i.e., field significance < 0.05; see Table 5.1). Correlations are generally negative across the western US for both Pearson product-moment correlations (Table 5.2) and Kendall's Tau non-parametric correlations (Table 5.3). For both measures of correlation, at least 40 out of the 60 grids located in the western US display negative correlations with more than ten grids displaying significant (two-sided $p<0.05$) negative correlations for all four reanalysis variables. In contrast, for both measures of correlation and for all variables, only two locations display significant positive correlations. As negative fall SOI values indicate equatorial atmospheric conditions favoring warmer sea surface temperatures over the eastern equatorial pacific (i.e., El Niño type conditions), these results suggest higher 850 hPa temperature, 1000–850 hPa thickness, 850–700 hPa thickness and 1000–500 hPa thickness during El Niño events and the reverse for La Niña events across the western US.

Table 5.1: Field significance of Pearson product-moment correlation, Kendall's Tau correlation, the shift in the La Niña PDF, and the shift in the El Niño PDF over the entire western US for the temperature and thickness measures (1949-2009).

	r Field Significance	τ Field Significance	La Niña Anomaly Field Significance	El Niño Anomaly Field Significance
850 hPa Temperature	0.006	0.001	0.69	0.01
1000-850 hPa Thickness	0.003	0.004	0.61	0.01
850-700 hPa Thickness	0.011	0.005	0.72	0.03
1000-500 hPa Thickness	0.016	0.006	0.44	0.02

Table 5.2: Descriptive statistics for the Pearson product-moment correlation results for the 60 NCEP/NCAR reanalysis grid points (1949-2009).

	Median r	Max r	Min r	Number of grids with r<0	Number of grids with r<0 and two-sided p<0.05	Number of grids with r>0 and two-sided p<0.05
850 hPa Temperature	-0.10	0.35	-0.44	43	13	2
1000-850 hPa Thickness	-0.14	0.31	-0.43	40	15	2
850-700 hPa Thickness	-0.10	0.29	-0.42	41	14	2
1000-500 hPa Thickness	-0.07	0.25	-0.39	41	11	1

Table 5.3: As in Table 5.2, but for the Kendall's Tau correlation tests.

	Median τ	Max τ	Min τ	Number of grids with τ <0	Number of grids with τ <0 and two-sided p<0.05	Number of grids with τ >0 and two-sided p<0.05
850 hPa Temperature	-0.06	0.23	-0.28	44	16	2
1000-850 hPa Thickness	-0.07	0.20	-0.31	43	15	2
850-700 hPa Thickness	-0.08	0.18	-0.32	42	17	1
1000-500 hPa Thickness	-0.05	0.19	-0.32	42	13	1

The predominantly negative correlations appear to be a result of higher temperature/thickness values during cold seasons with low SOI values in the fall (i.e., normalized fall SOI values < -0.4) rather than lower temperature/thickness values during winters associated with high SOI values (i.e., normalized fall SOI > 0.4; see Table 5.4 and Table 5.5). For the sake of simplicity, winters associated with normalized fall SOI values below -0.4 (above 0.4) are represent winters coinciding with El Niño (La Niña) conditions (all other winters are considered neutral ENSO conditions) for the remainder of this chapter, however, it is important to note that the statistical tests are based on the normalized fall SOI values and not the occurrence of El Niño and La Niña events per se. Over the western US as whole, statistically significant (i.e., field significance < 0.05) shifts in the El Niño PDFs relative to the neutral ENSO PDFs are evident (Table 5.1). During El Niño events, greater than 50% of wet days were above the median value for neutral ENSO conditions (i.e., an increase in thickness/temperature) for at least 49 out of the 60 locations across the western US for all four reanalysis variables (Table 5.4). The number of locations that these shifts in the centers of the El Niño PDFs are significant (two-sided pseudo $p <$ 0.05) range from 9 locations for 850-700 hPa thickness to 18 locations for 850 hPa temperature. At more than half of the grid locations, for all temperature and thickness measures, more than 55% of the wet day values during El Niño events were above the neutral ENSO median with some locations displaying ~70% of wet day values greater than the neutral median (Table 5.4). In contrast, over the western US as whole, there is no evidence for significant shifts in the La Niña PDFs for any of the four variables (i.e., field significance > 0.05; see Table 5.1) and few locations display significant (two-sided pseudo $p < 0.05$) deviations from 50% (Table 5.5).

Table 5.4: As in Table 5.2, but for the percent of wet day cold season temperature/thickness values during El Niño events greater than the neutral ENSO median (1949-2009).

	Median %	Max %	Min %	Number of >50% grids	Number of Significant (two-sided pseudo p<0.05) >50% grids	Number of Significant (two-sided pseudo p<0.05) <50% grids
850 hPa Temperature	56.04	71.14	38.89	50	18	0
1000-850 hPa Thickness	55.48	68.22	38.89	49	13	0
850-700 hPa Thickness	55.06	70.62	39.48	50	9	0
1000-500 hPa Thickness	54.95	69.00	41.98	49	13	0

Table 5.5: As in Table 5.2, but for the percent of wet day cold season temperature/thickness values during La Niña events greater than the neutral ENSO median (1949-2009).

	Median %	Max %	Min %	Number of >50% grids	Number of Significant (two-sided pseudo p<0.05) >50% grids	Number of Significant (two-sided pseudo p<0.05) <50% grids
850 hPa Temperature	52.43	65.09	43.75	42	2	0
1000-850 hPa Thickness	51.76	65.82	37.50	38	2	0
850-700 hPa Thickness	52.20	68.73	40.95	41	2	0
1000-500 hPa Thickness	52.45	66.55	43.81	48	3	0

5.2.2 Spatial Variability in the SOI Relationship with Temperature and Thickness

For Pearson product-moment correlations, a prominent northwest to southeast gradient in the monotonic relationship between fall SOI and the cold season wet day medians of all four temperature/thickness variables exists over the western US (Figure 5.1). Significant (two-sided $p < 0.05$) negative correlations are largely confined to a significant cluster (jointly significant at the 0.05 level) in the Pacific Northwest (i.e., northern California, Oregon and Washington; see Table 5.6) and significant positive correlations confined to a significant cluster in the Southern Rockies

(i.e., southern Colorado and New Mexico; see Table 5.6) as illustrated by Figure 5.1. While a few isolated significant correlations exist outside these two regions (which are all negative correlations), correlation results are not nearly as spatially organized. As with Pearson correlations, Kendall's Tau correlations display the significant cluster of significantly negative correlations in the Pacific Northwest and the significant cluster of positive correlations in the Southern Rockies (Figure 5.2). For all four reanalysis variables, however, Kendall's Tau correlations display an additional significant cluster of significantly negative correlations in southern California (Figure 5.2).

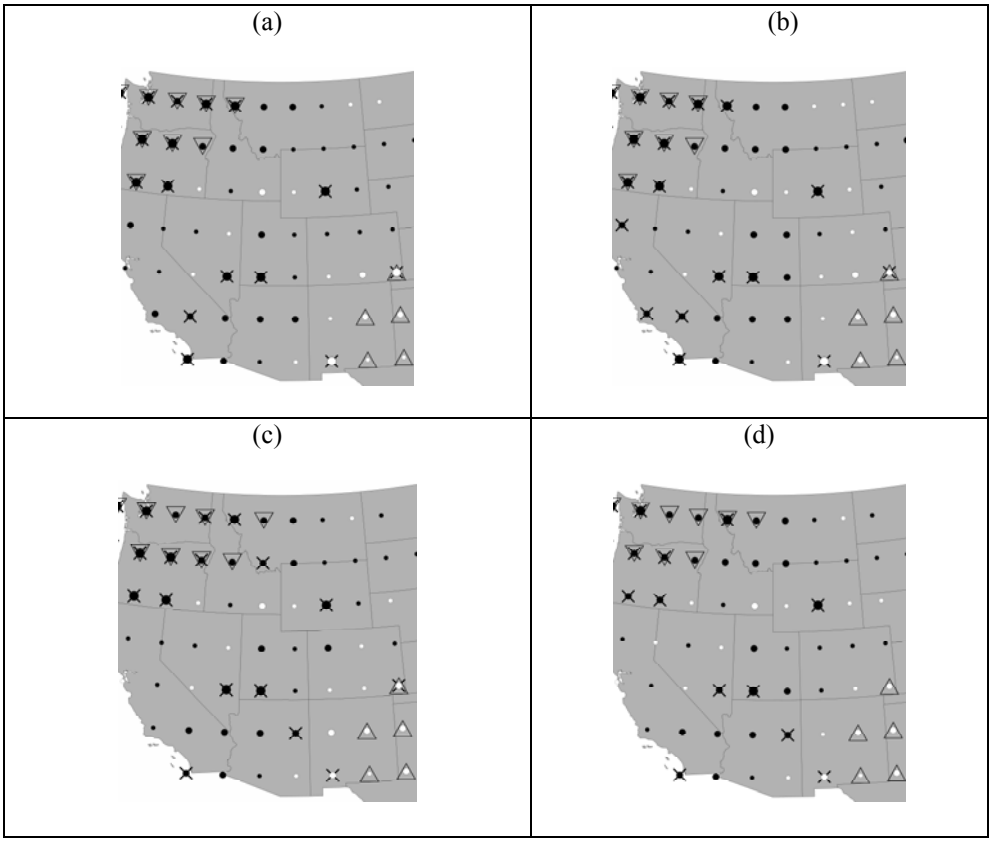

Figure 5.1: From 1949-2009, Pearson product-moment correlation coefficients between normalized fall SOI and cold season median wet day 850 hPa temperature (a), 1000-850 hPa thickness (b), 850-700 hPa thickness (c), and 1000-500 hPa thickness (d). Black (white) circles indicate negative (positive) correlation coefficients. Small circles indicate $0<|r|\leq 0.15$, medium circles indicate $0.15<|r|\leq 0.30$, and large circles indicate $0.30>|r|$. Significant correlation coefficients (two-sided $p<0.05$) are indicated by × and local Moran's I values jointly significant with 95% confidence indicating clustering of positive (negative) correlations are given by triangles (inverted triangles).

Table 5.6: Descriptions of the regions displaying homogeneous ENSO signals in temperature/thickness introduced in Section 5.2.

Region	Geographical Coverage
Southwest	southern California, western Arizona, southern Nevada, and southwestern Utah
Southern Rockies	New Mexico, southern Colorado
Central Rockies	northern Utah, northern Colorado, southern Idaho, and southern Wyoming
Northern Rockies	northern Idaho and Montana
Pacific Northwest	northern California, Oregon, and Washington

Considering the correlation results for the Pacific Northwest, it is not surprising that significant (two-sided pseudo $p < 0.05$) increases in temperature/thickness occur during El Niño events (Figure 5.3) and that temperature/thickness decreases occur during La Niña events (Figure 5.4). The reverse of this pattern is evident for the Southern Rockies (Figure 5.3 and Figure 5.4). Additionally, the significant correlations in southern California appear to be the result of increased temperature/thickness during El Niño events rather than decreased values during La Niña events over the Southwest (i.e., southern California, western Arizona, southern Nevada, and southwestern Utah; see Table 5.6) as illustrated in Figure 5.3 and Figure 5.4. The lack of evidence for monotonic relationships between fall SOI and temperature/thickness in regions outside of the Pacific Northwest, the Southern Rockies, and southern California is due to the lack of a La Niña signal that is opposite (in terms of lower/higher values than the neutral ENSO median) of the El Niño signal.

During El Niño events, nearly the entire western US (~50 out of 60 grids) displays higher wet day median temperature/thickness than during neutral ENSO conditions, except for the Southern Rockies. The largest and most significant (two-sided pseudo $p < 0.05$) increased values during El Niño events are mostly found in a significant cluster (jointly significant at the 0.05 level) of high values in the Southwest (Figure 5.3). Other significant increases during El Niño conditions

are seen in the Pacific Northwest and Northern Rockies (i.e., northern Idaho and Montana; see Table 5.6), however, these are not significantly clustered (Figure 5.3). Decreased temperature/thickness during El Niño events is significantly clustered over the Southern Rockies; however, there are no individual grids that display a significant shift (Figure 5.3).

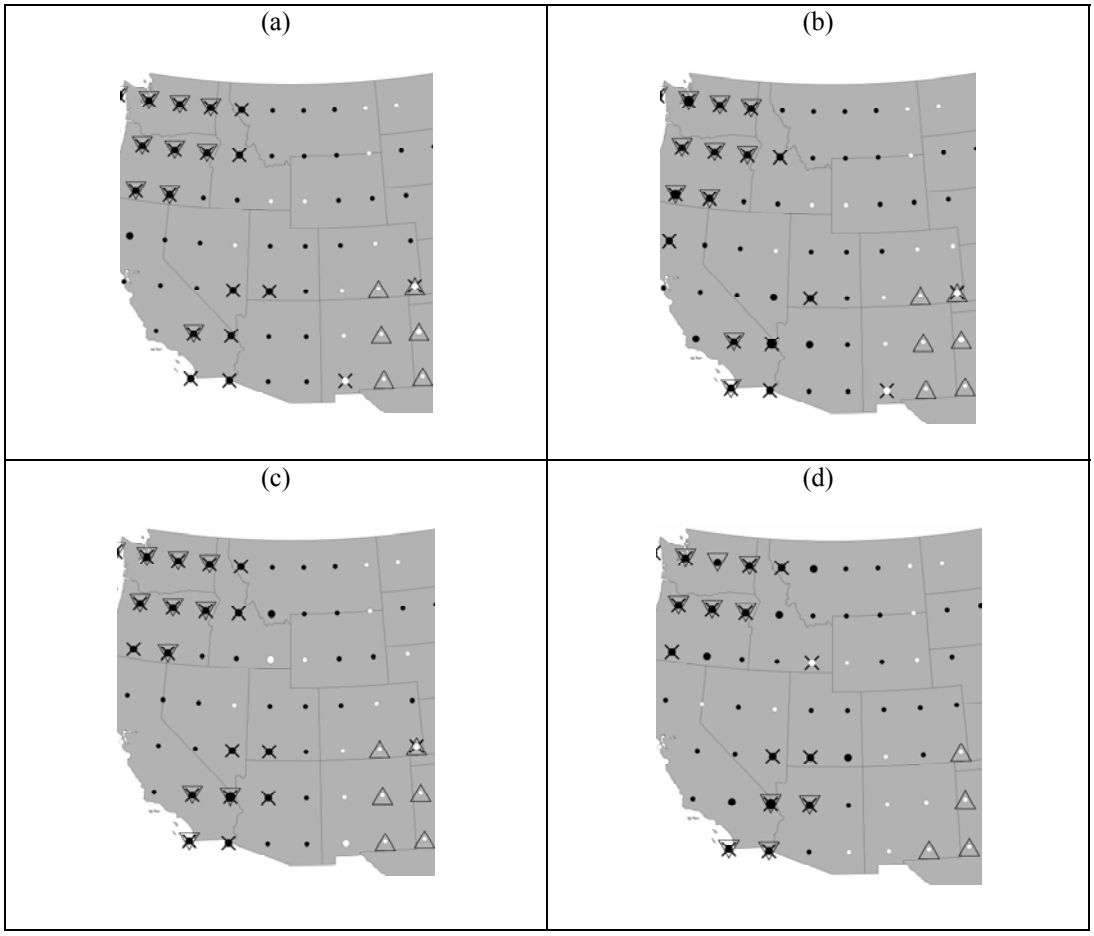

Figure 5.2: As in figure 5.1 but with Kendall's Tau non-parametric correlation coefficients.

During La Niña events, much of the western US displays increased temperature/thickness relative to neutral ENSO conditions yet few of these are significant (Figure 5.4). The few that are significant are surrounded by much lower magnitude PDF increases (or decreases), suggesting the lack of a coherent spatial pattern near these higher values (Figure 5.4). The only significant clustering is in the Pacific Northwest where a large region of decreased temperature/thickness

during La Niña events is apparent (Figure 5.4). Within this region, however, there is not a statistically significant decrease at any individual grid location.

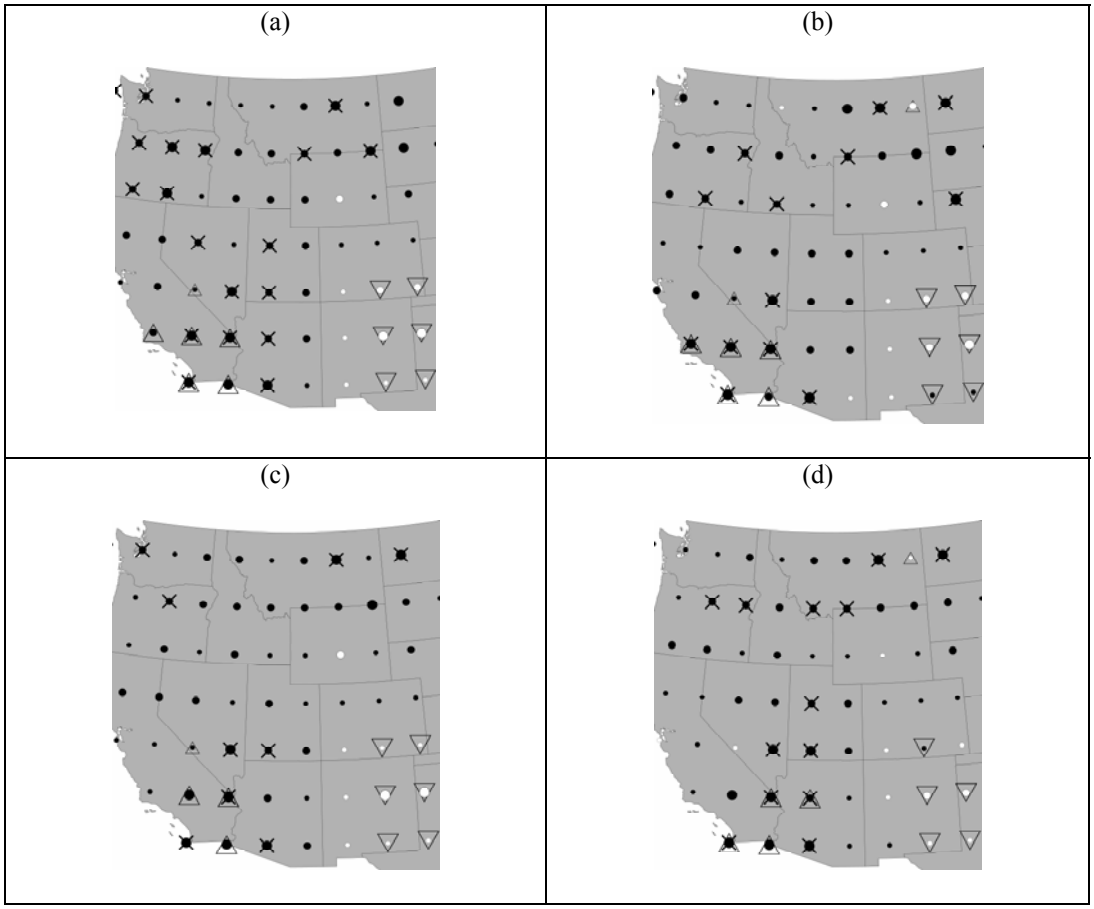

Figure 5.3: From 1949-2009, the percentage of winter wet day values during El Niño events (i.e., normalized fall SOI <-0.40) greater than the median value for neutral ENSO conditions for 850 hPa temperature (a), 1000-850 hPa thickness (b), 850-700 hPa thickness (c), and 1000-500 hPa thickness (d). Small black (white) circles indicate values >50% and ≤55% (≥45% and <50%), medium black (white) circles indicate values >55% and ≤60% (≥40% and <45%) and large black (white) circles indicate values >60% (<40%). Significant deviations from 50% (two-sided pseudo p<0.05) are indicated by ×. Local Moran's I values jointly significant with 95% confidence indicating clustering of higher(lower) values are given by large triangles (inverted triangles). Jointly significant local Moran's I indicating a low value surrounded by higher values are given by small triangles.

In summary, the Pacific Northwest, Southern Rockies, and southern California are the only locations displaying significant monotonic relationships between fall SOI and the cold season medians of the temperature/thickness variables. Outside these regions a spatially organized and significant shift toward higher temperature/thickness during El Niño events relative to neutral

ENSO events is present over western Arizona, southern Nevada and southwestern Utah (i.e., the remaining portions of the Southwest outside of southern California). The magnitude of the La Niña effects on temperature/thickness values is generally much less than that of the El Niño effects and there is little evidence over much of the western US for a significant La Niña effect on temperature/thickness outside of a significant cluster of decreased temperature/thickness (although insignificant for individual grids) in the Pacific Northwest.

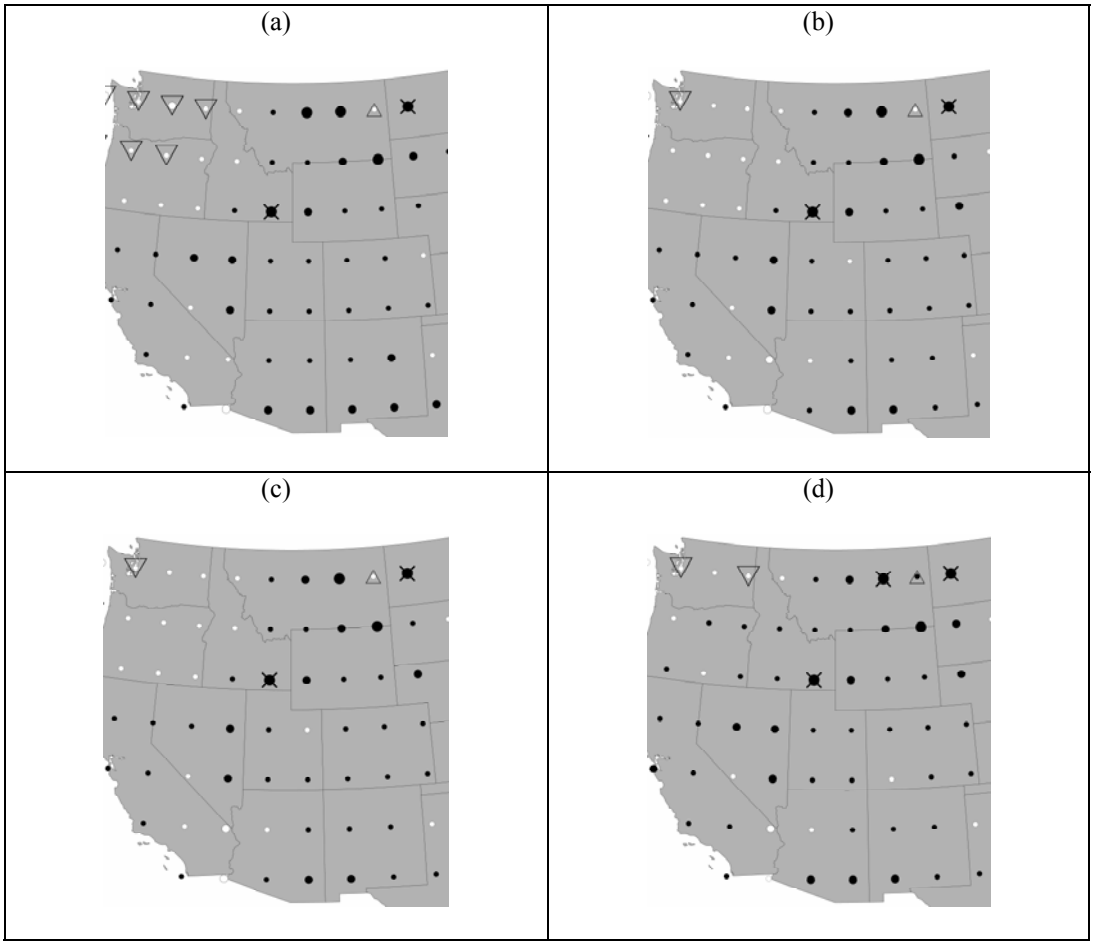

Figure 5.4: As in figure 5.3 but for La Niña conditions.

5.2.3 Modulation of the SOI Relationship with Temperature and Thickness by PDO.

For both cold PDO and warm PDO, violations of the error normality and constant error variance assumptions for Pearson product-moment correlations are less prevalent than for the entire period of record (in the Appendix, Figures A.3 and A.4). During the cold PDO, the western US as a whole the does not display significant (field significance < 0.05) correlations between fall SOI and the winter medians of 850 hPa temperatures, 1000–850 hPa thickness, 850–700 hPa thickness and 1000–500 hPa thickness for both Pearson product-moment correlation and Kendall's Tau correlation (Table 5.7). Additionally, for all four variables, around half of the 60 grid locations display positive/negative correlations and few correlations are significant (Table 5.8 and Table 5.9). This is in contrast to the correlations results for the entire period of record (i.e., 1949-2009; also referred to as the overall results) for which correlations are generally negative across the West and many (i.e., generally >10) are significant (Table 5.2 and Table 5.3).

Table 5.7: Field significance of Pearson product-moment correlation, Kendall's Tau correlation, the shift in the La Niña PDF, and the shift in the El Niño PDF over the entire western US for all temperature and thickness measures during the cold PDO (1949-1976).

	r Field Significance	τ Field Significance	La Niña Anomaly Field Significance	El Niño Anomaly Field Significance
850 hPa Temperature	0.786	0.684	0.29	0.02
1000-850 hPa Thickness	0.409	0.216	0.50	0.07
850-700 hPa Thickness	0.929	0.687	0.17	0.12
1000-500 hPa Thickness	0.784	0.904	0.16	0.08

Table 5.8: Descriptive statistics for the Pearson product-moment correlation results for the 60 NCEP/NCAR reanalysis grid points during the cold PDO (1949-1976).

	Median r	Max r	Min r	Number of grids with r<0	Number of grids with r<0 and two-sided p<0.05	Number of grids with r>0 and two-sided p<0.05
850 hPa Temperature	-0.01	0.34	-0.41	35	2	0
1000-850 hPa Thickness	-0.03	0.36	-0.41	35	3	0
850-700 hPa Thickness	-0.01	0.34	-0.41	32	1	0
1000-500 hPa Thickness	0.01	0.37	-0.39	28	1	0

Table 5.9: As in Table 5.8, but for the Kendall's Tau correlation tests.

	Median τ	Max τ	Min τ	Number of grids with τ <0	Number of grids with τ <0 and two-sided p<0.05	Number of grids with τ >0 and two-sided p<0.05
850 hPa Temperature	-0.03	0.25	-0.40	32	2	0
1000-850 hPa Thickness	-0.03	0.29	-0.42	34	3	2
850-700 hPa Thickness	-0.02	0.29	-0.41	31	1	1
1000-500 hPa Thickness	0.00	0.26	-0.45	30	1	0

Similar to the results for the entire period of record, during the cold PDO over the entire western US the shift in center of the El Niño PDF relative to the neutral ENSO PDF is fairly significant with field significance values ranging from 0.02 for 850 hPa temperature and 0.12 for 850-700 hPa thickness (Table 5.7). This shift is again a positive shift (i.e., higher values during El Niño relative to the neutral ENSO case) in temperature/thickness for ~47 out of 60 grids with significant positive shifts ranging from six locations for 1000-500 hPa Thickness to 13 locations for 850 hPa temperature and no significant negative shifts at any of the grids (Table 5.10). Again, similar to the results from the entire period of record, insignificant shifts in the La Niña PDFs are present over the western US as a whole for all four reanalysis variables (Table 5.7), however, the

large majority of shifts are positive (as with El Niño events) and about twice as many are significant positive shifts during PDO cold phase (Table 5.11) compared to the entire period of record (Table 5.5). For many of the grid locations (Table 5.11), the increased thickness/temperature during La Niña events (~55% of the wet day temperature/thickness values are greater than the neutral ENSO median) are comparable to increases during EL Niño events (~56% of the wet day temperature/thickness values are greater than the neutral ENSO median; Table 5.10). This supports the correlation results for the cold PDO, as the shifts in the El Niño and La Niña PDFs do not suggest a monotonic relationship between fall SOI and median winter wet day 850 hPa temperatures, 1000–850 hPa thickness, 850–700 hPa thickness and 1000–500 hPa thickness.

Table 5.10: Descriptive statistics for the percent of cold season wet day temperature/thickness values during El Niño events greater than the neutral ENSO median for the 60 NCEP/NCAR reanalysis grid points during the cold PDO (1949-1976).

	Median %	Max %	Min %	Number of >50% grids	Number of Significant (two-sided pseudo $p<0.05$) >50% grids	Number of Significant (two-sided pseudo $p<0.05$) <50% grids
850 hPa Temperature	57.22	76.11	40.59	47	13	0
1000-850 hPa Thickness	56.36	75.22	40.59	47	8	0
850-700 hPa Thickness	54.69	76.11	43.56	43	7	0
1000-500 hPa Thickness	54.27	76.11	41.82	47	6	0

Table 5.11: As in Table 5.10 but for La Niña events.

	Median %	Max %	Min %	Number of >50% grids	Number of Significant (two-sided pseudo p<0.05) >50% grids	Number of Significant (two-sided pseudo p<0.05) <50% grids
850 hPa Temperature	55.93	67.36	47.03	47	5	0
1000-850 hPa Thickness	54.87	68.25	45.24	49	3	0
850-700 hPa Thickness	54.52	68.25	46.27	53	5	0
1000-500 hPa Thickness	55.91	71.43	45.76	53	6	0

In contrast to the cold PDO, during the warm PDO, Pearson product-moment correlation results (Table 5.12 and Table 5.13) are similar to those results from the entire period of record (Table 5.1 and Table 5.2). Pearson correlations are field significant at the 0.05 level for 850 hPa temperature and 1000-850 hPa thickness and at the 0.1 level for 1000-500 hPa and 850-700 hPa thickness (Table 5.12). Additionally, for all four variables, ~45 out of 60 locations display negative correlations with fall SOI with 8 or more grids showing significant negative correlations (Table 5.13). The only difference between the Kendall's Tau correlations results (Table 5.14) and Pearson correlation results (Table 5.13) appears to be that of statistical significance. Considering the limited evidence that the warm PDO phase fall SOI and median winter temperature/thickness are not from a bivariate normal distributions (Figure A.4), this difference could be due to the lower power (i.e., the probability of correctly rejecting the null hypothesis given that the alternative is true) of the Kendall's Tau correlation tests under the smaller sample sizes associated with the warm PDO (n=22).

Table 5.12: Field significance of Pearson product-moment correlation, Kendall's Tau correlation, the shift in the La Niña PDF, and the shift in the El Niño PDF over the entire western US for all temperature and thickness measures during the warm PDO (1977-1998).

	r Field Significance	τ Field Significance	La Niña Anomaly Field Significance	El Niño Anomaly Field Significance
850 hPa Temperature	0.026	0.703	0.83	0.29
1000-850 hPa Thickness	0.005	0.460	1.00	0.37
850-700 hPa Thickness	0.096	0.451	0.86	0.17
1000-500 hPa Thickness	0.084	0.225	1.00	0.13

Table 5.13: Descriptive statistics for the Pearson product-moment correlation results for the 60 NCEP/NCAR reanalysis grid points during the warm PDO (1977-1998).

	Median r	Max r	Min r	Number of grids with r<0	Number of grids with r<0 and two-sided p<0.05	Number of grids with r>0 and two-sided p<0.05
850 hPa Temperature	-0.23	0.57	-0.62	46	9	1
1000-850 hPa Thickness	-0.26	0.55	-0.63	45	10	2
850-700 hPa Thickness	-0.19	0.50	-0.62	45	9	1
1000-500 hPa Thickness	-0.15	0.47	-0.62	45	8	1

Table 5.14: As in Table 5.13, but for the Kendall's Tau correlation results.

	Median τ	Max τ	Min τ	Number of grids with τ <0	Number of grids with τ <0 and two-sided p<0.05	Number of grids with τ >0 and two-sided p<0.05
850 hPa Temperature	-0.12	0.28	-0.37	45	2	0
1000-850 hPa Thickness	-0.11	0.31	-0.48	45	2	1
850-700 hPa Thickness	-0.11	0.24	-0.35	45	3	0
1000-500 hPa Thickness	-0.09	0.24	-0.39	41	5	0

In contrast to the results from the entire period of record, during the PDO warm phase, the significant monotonic relationships between fall SOI and the winter medians of all four reanalysis variables do not coincide with significant (field significance < 0.05) increases/decreases in temperature/thickness during La Niña and El Niño events over the western US as a whole (Table 5.12). Considering this, it is not surprising that few locations display significant positive shifts in El Niño PDFs (Table 5.15) in contrast to the results for both the entire period of record (Table 5.4) and the cold PDO (Table 5.10). Also in contrast to the results for the entire period of record and the cold PDO, is the prevalence of negative shifts in the La Niña PDFs, although insignificant (Table 5.16). The prevalence of increased temperature/thickness during El Niño conditions and decreased temperature/thickness during La Niña conditions across the western US during the warm PDO phase supports the correlation results (Table 5.13 and Table 5.14) suggesting a monotonic relationship between fall SOI and the median winter wet day 850 hPa temperature and 1000-850 hPa thickness, 1000-500 hPa thickness, 850-700 hPa thickness.

Table 5.15: Descriptive statistics for the percent of cold season wet day temperature/thickness values during El Niño events greater than the neutral ENSO median for the 60 NCEP/NCAR reanalysis grid points during the warm PDO (1977-1998).

	Median %	Max %	Min %	Number of >50% grids	Number of Significant (two-sided pseudo p<0.05) >50% grids	Number of Significant (two-sided pseudo p<0.05) <50% grids
850 hPa Temperature	52.71	69.57	34.87	38	3	1
1000-850 hPa Thickness	52.27	71.74	34.40	37	2	2
850-700 hPa Thickness	51.68	69.57	29.52	39	4	3
1000-500 hPa Thickness	51.95	72.83	31.43	37	6	0

Table 5.16: As in Table 5.15 but for La Niña events.

	Median %	Max %	Min %	Number of >50% grids	Number of Significant (two-sided pseudo p<0.05) >50% grids	Number of Significant (two-sided pseudo p<0.05) <50% grids
850 hPa Temperature	48.86	66.67	35.71	24	0	1
1000-850 hPa Thickness	47.08	65.22	28.57	19	0	0
850-700 hPa Thickness	47.39	83.33	34.62	20	1	0
1000-500 hPa Thickness	49.35	66.67	35.71	23	0	0

5.2.4 Spatial Variability in the Modulation of the SOI Relationship with Temperature and Thickness by PDO

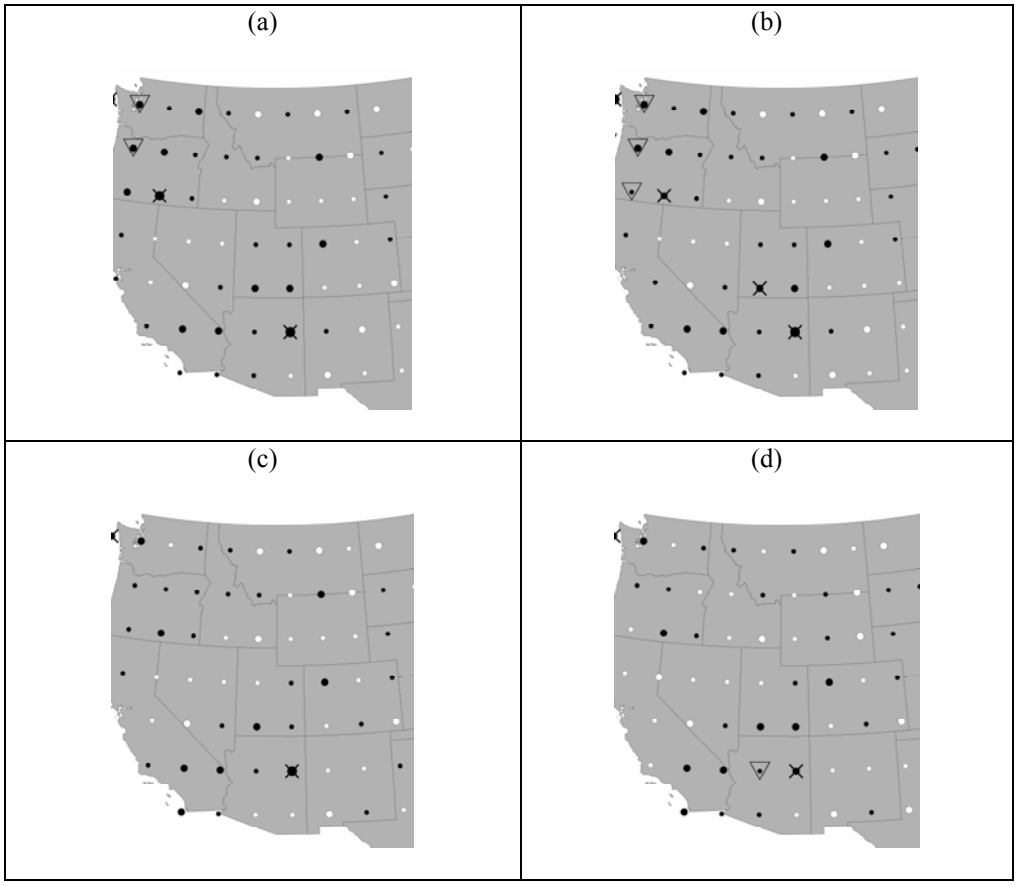

Figure 5.5: As in figure 5.1 but for the cold PDO (1949-1976). Black (white) circles indicate negative (positive) correlation coefficients. Small circles indicate $0<|r|\leq 0.20$, medium circles indicate $0.2<|r|\leq 0.40$, and large circles indicate $0.40<|r|$.

During the cold PDO, for both Kendall's Tau correlation and Pearson correlation results between fall SOI values and the median winter temperature/thickness, the negative correlations are in the Pacific Northwest and the Southwest (Figure 5.5 and Figure 5.6), however, unlike the results for the entire period of record, these correlations are insignificant and not significantly clustered. Outside the Pacific Northwest and the Southwest, insignificant negative and positive correlations are equally prevalent. This is in contrast to the results for the entire period of record displaying negative correlations for nearly the entire study area except for a significant cluster of negative correlations over the Southern Rockies.

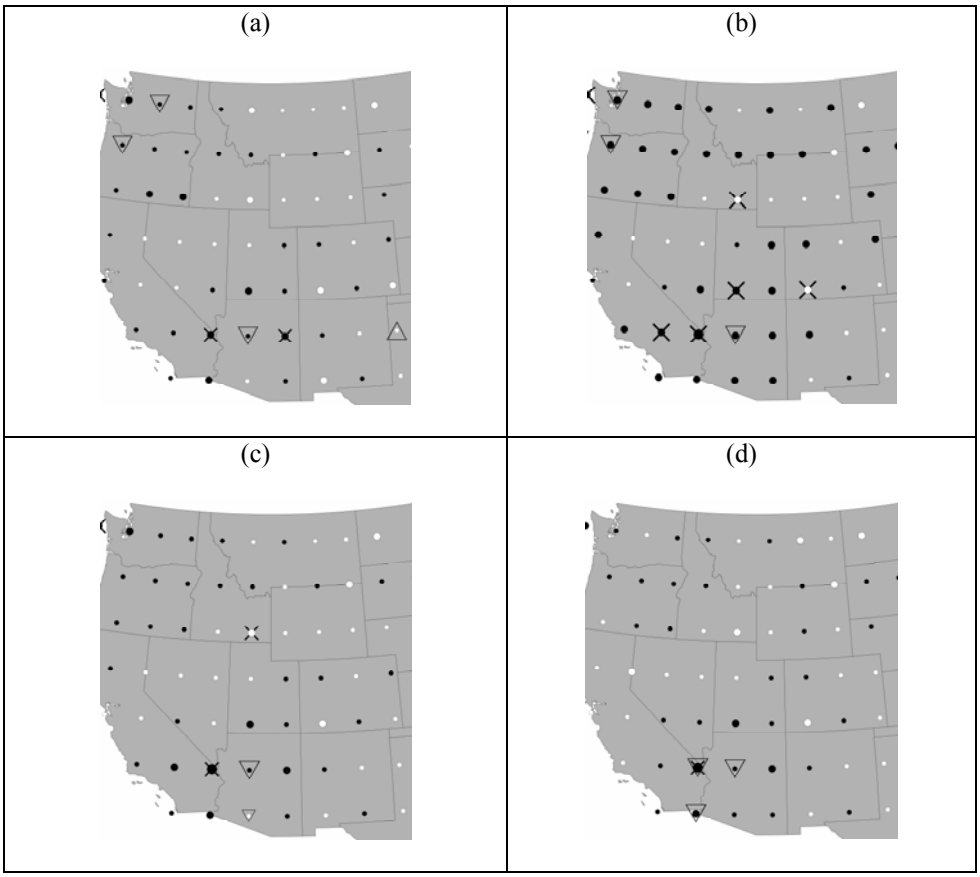

Figure 5.6: As in Figure 5.5 but for Kendall's Tau correlations. The small inverted triangle indicates a jointly significant with 95% confidence high values surrounded by low values.

As with the results for the entire period of record, during the cold PDO, the significant (two-sided pseudo $p < 0.05$) increases in temperature/thickness during El Niño events are located in a significant cluster (jointly significant at the 0.05 confidence level) in the Southwest (Figure 5.7). Other regions with significant positive shifts are Northern California and Oregon. A significant cluster of decreased 850 hPa temperature during El Niño conditions is centered over the Southern Rockies; however, this cluster is not as evident for the other three NCEP/NCAR reanalysis variables (Figure 5.7). Nearly the entire western US displays increased temperature/thickness during La Niña events occurring with the cold PDO, however, only a few of these are significant and there does not appear to be a significant clustering of the higher values (Figure 5.8).

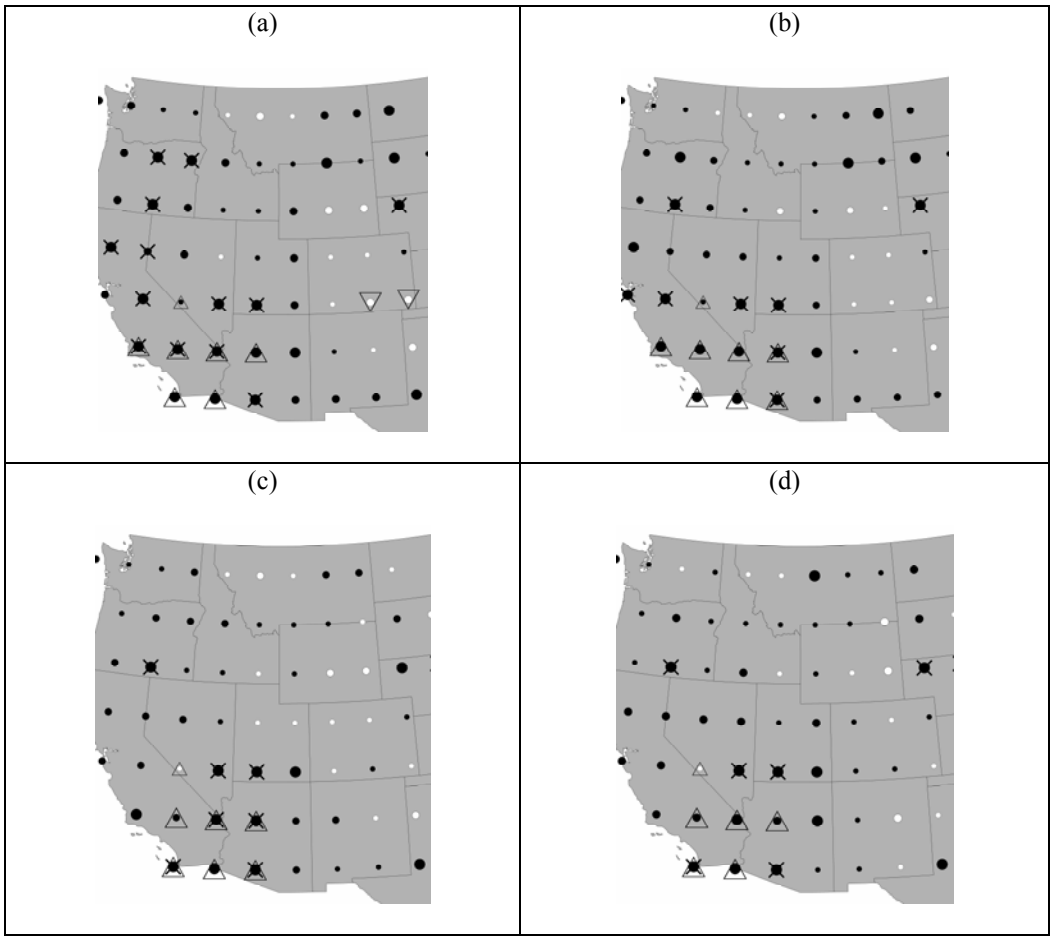

Figure 5.7: As in Figure 5.3 but for the cold PDO (1949-1976).

During the warm PDO, correlation results are very similar to the results for the entire period of record displaying significant negative correlations in portions of the Southwest and the Pacific Northwest and significant positive correlations over the Southern Rockies (Figures 5.9 and 5.10).These results, however, are not as spatially significant as the overall results with significant clustering only seen in the positive correlations over the Southern Rockies (Figures 5.9 and 5.10). Additionally, the Northern Rockies display significant clustering (jointly significant with 95% confidence) of significantly negative correlations which was not apparent in the overall results.

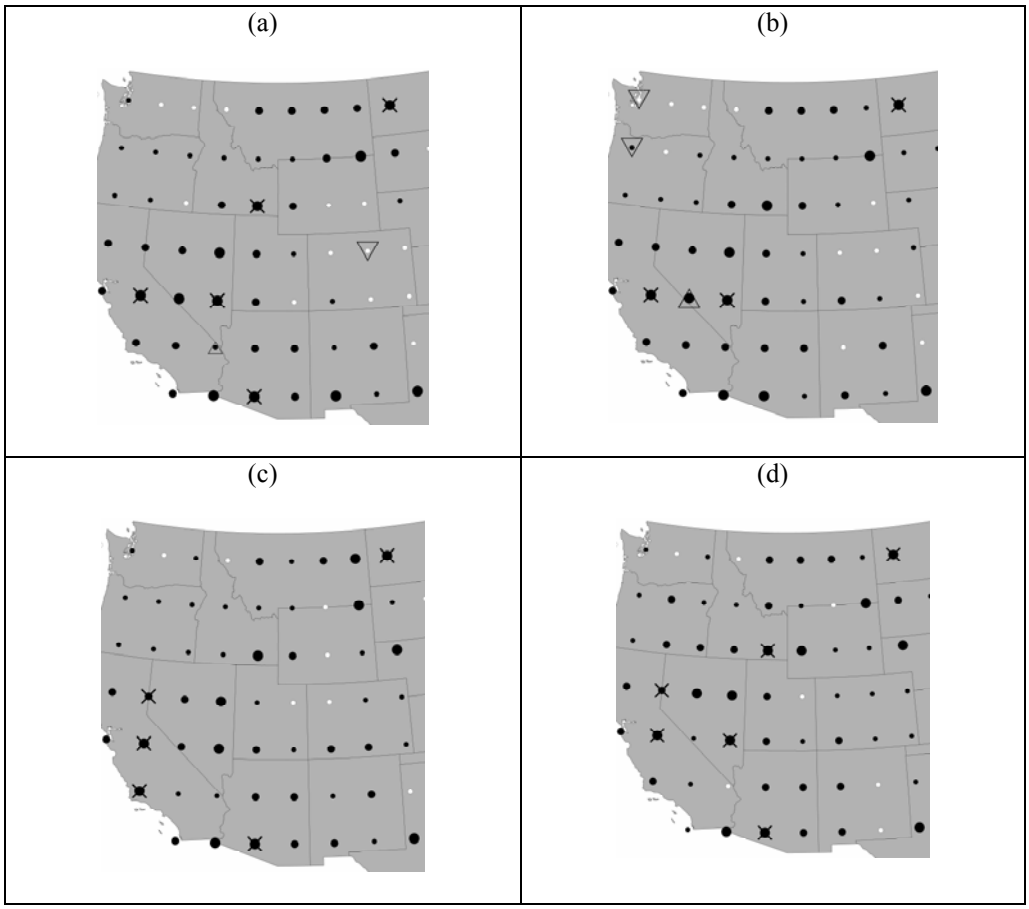

Figure 5.8: As in figure 5.4 but for the cold PDO (1949-1976).

During the warm PDO phase, the clustering of significant positive shifts in the El Niño PDFs evident for the entire period of record over the Southwest is not apparent (Figure 5.11). Also in contrast to the El Niño signal for the entire period of record, there is no evidence for significant positive shifts in the Pacific Northwest (Figure 5.11). Similar to the results for the entire period of record, significant clustering of increased thickness/temperature is evident over the Northern Rockies as is a significant cluster of negative shifts over the Southern Rockies (Figure 5.11). Similar to the overall La Niña signal, during the warm PDO phase, there is a large region of negative shifts in the Pacific Northwest (Figure 5.12). Lastly, regions displaying significantly increased values during La Niña events during the cold PDO phase (Figure 5.8) display no evidence for a spatially coherent and statistically significant La Niña signal during the warm PDO phase (Figure 5.12).

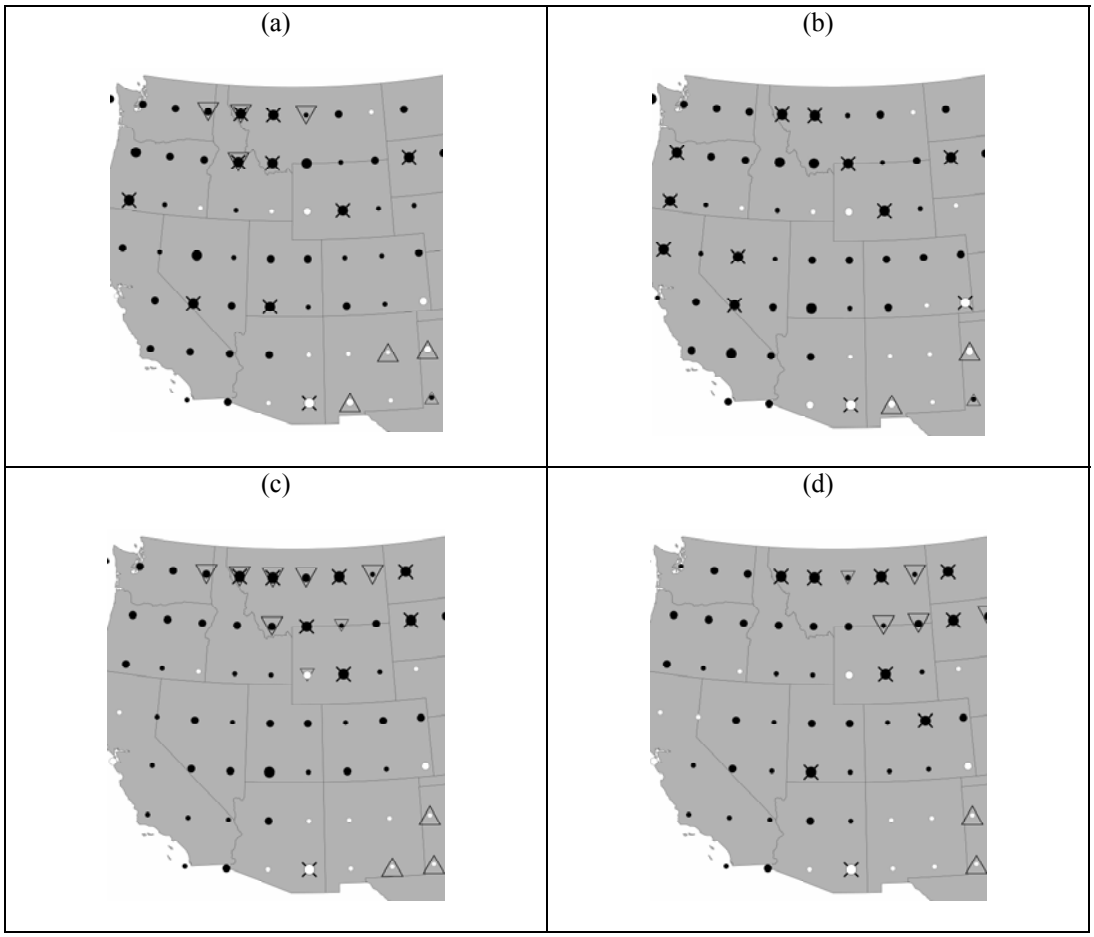

Figure 5.9: As in figure 5.5 but for the warm PDO (1977-1998). Additionally, the small triangle (inverted triangle) indicate jointly significant with 95% confidence low (high) values surrounded by high (low) values.

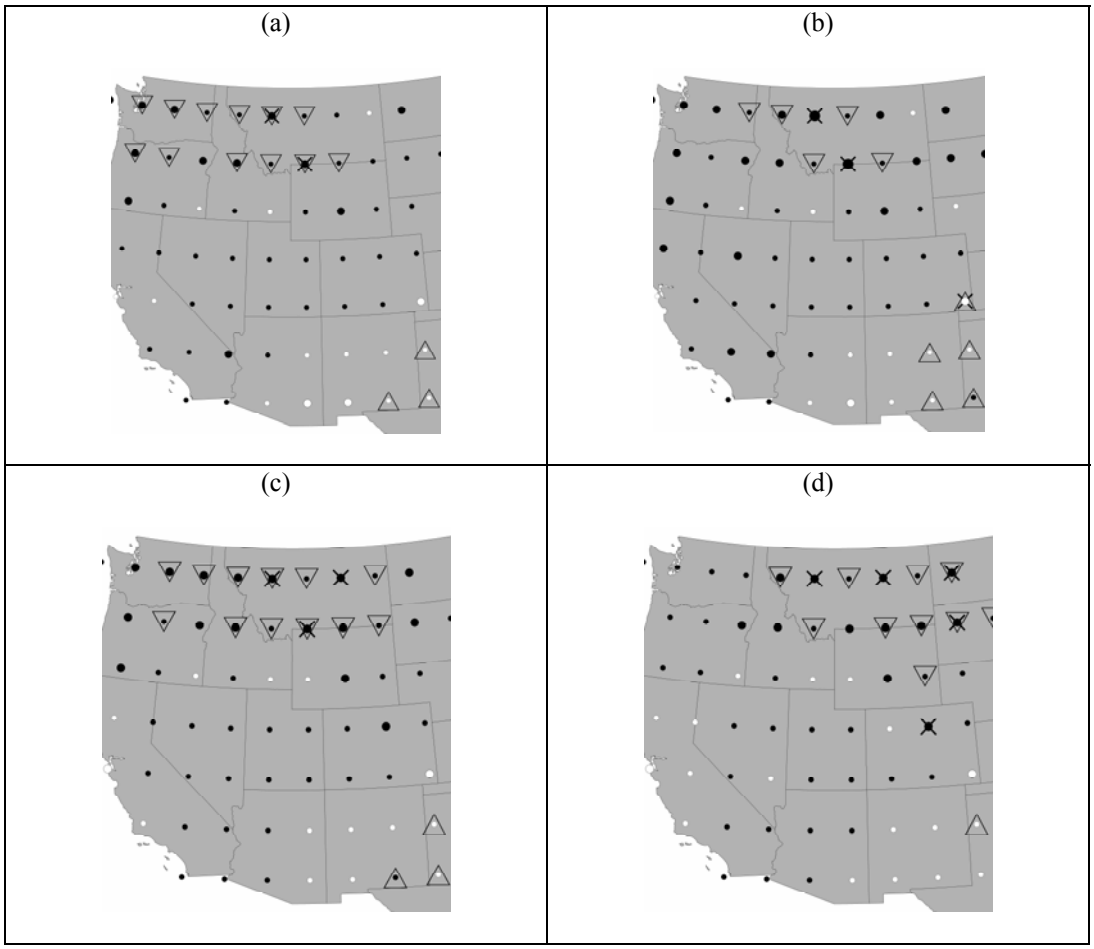

Figure 5.10: As in figure 5.6 but for the warm PDO (1977-1998).

5.2.5 Summary of ENSO/PDO relationship with Temperature and Thickness

The relationship between fall SOI and temperature/thickness across the western US differs between the warm and cold PDO phases as illustrated by Figure 5.13 displaying the results for 850-700 hPa thickness (note: the 850-700 hPa thickness are displayed to highlight the PDO modulation of the ENSO effects in a single figure). The overall ENSO pattern reveals significant increases in temperature/thickness during El Niño conditions in the Pacific Northwest and Southwest with less significant but spatially coherent decreases over the Southern Rockies (Figure 5.13). During the warm PDO, this El Niño signal is amplified over the Southern Rockies and the Northern Rockies display significant and spatially coherent increases temperature/thickness.

Outside these two regions, the El Niño signal is dampened (Figure 5.13). During the cold PDO, this El Niño signal appears slightly amplified over the Southwest while dampened over the remainder of the study area.

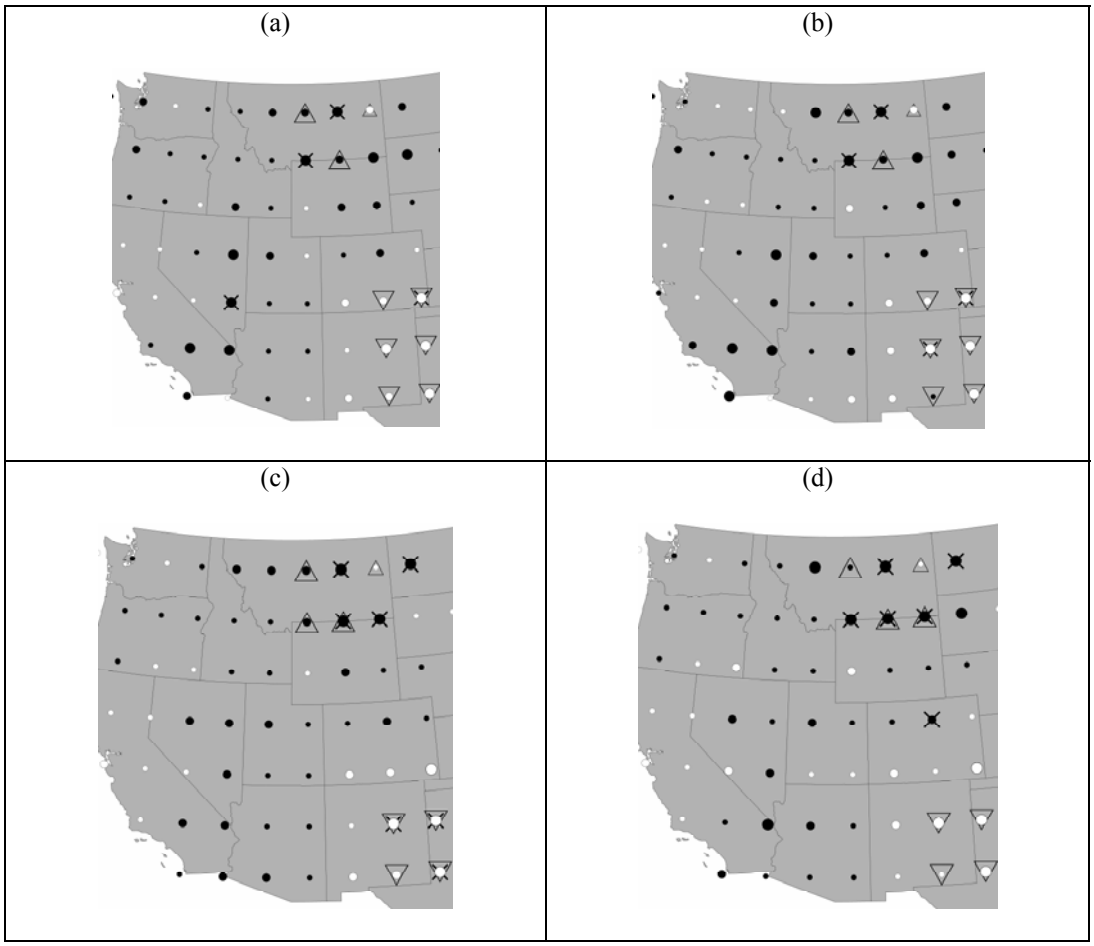

Figure 5.11: As in figure 5.3 but for the warm PDO (1977-1998).

The overall La Niña signal displays insignificant shifts in the temperature/thickness PDFs at individual grids; however, a significant cluster of decreased values is apparent in the Pacific Northwest (Figure 5.13). During the warm PDO, this signal amplifies in the Pacific Northwest. During the cold PDO, however, nearly the entire western US displays increased temperature/thickness during La Niña conditions and California, Arizona and Nevada display individual grids with significant increases, much like the El Niño signal during cold PDO only lacking spatial coherence (Figure 5.13).

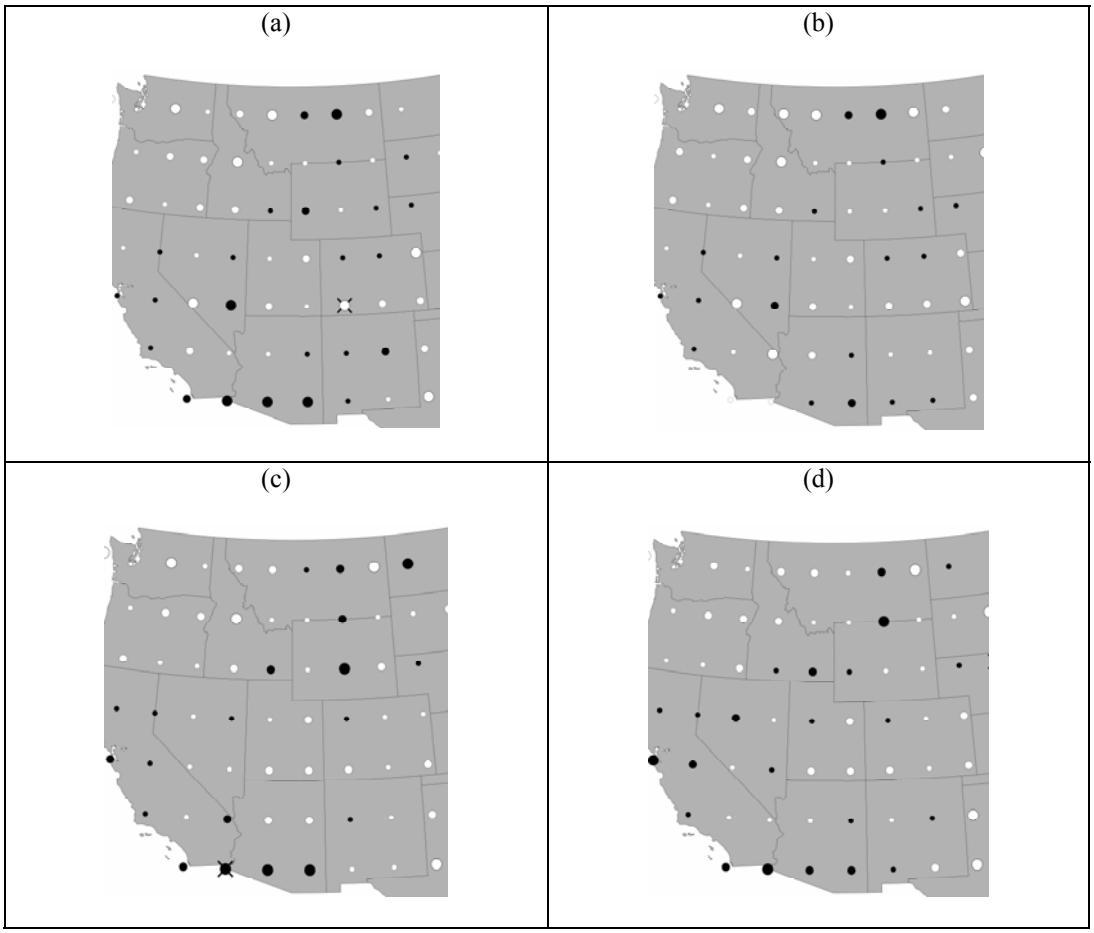

Figure 5.12: As in figure 5.4 but for the warm PDO (1977-1998).

In short, the results suggest in-phase (i.e., warm PDO and El Niño or cold PDO La Niña) amplification of the ENSO signal for the Southern Rockies, particularly for El Niño conditions during the warm PDO. In the Pacific Northwest, there appears to be an in-phase dampening of the ENSO signal along with an amplification of the La Niña signal during warm PDO. In the Southwest, the El Niño signal is most apparent during the cold PDO and least apparent during the warm PDO with La Niña conditions during the cold PDO similar to the overall El Niño signal. In the Northern Rockies, a subtle El Niño signal toward higher thickness/temperature appears to be amplified during the warm PDO and dampened during the cold PDO. Therefore, assuming no long-term trend, temperature/thickness appears to be higher during the cold PDO in the Southwest, Southern Rockies, and Pacific Northwest and lower over the Northern Rockies.

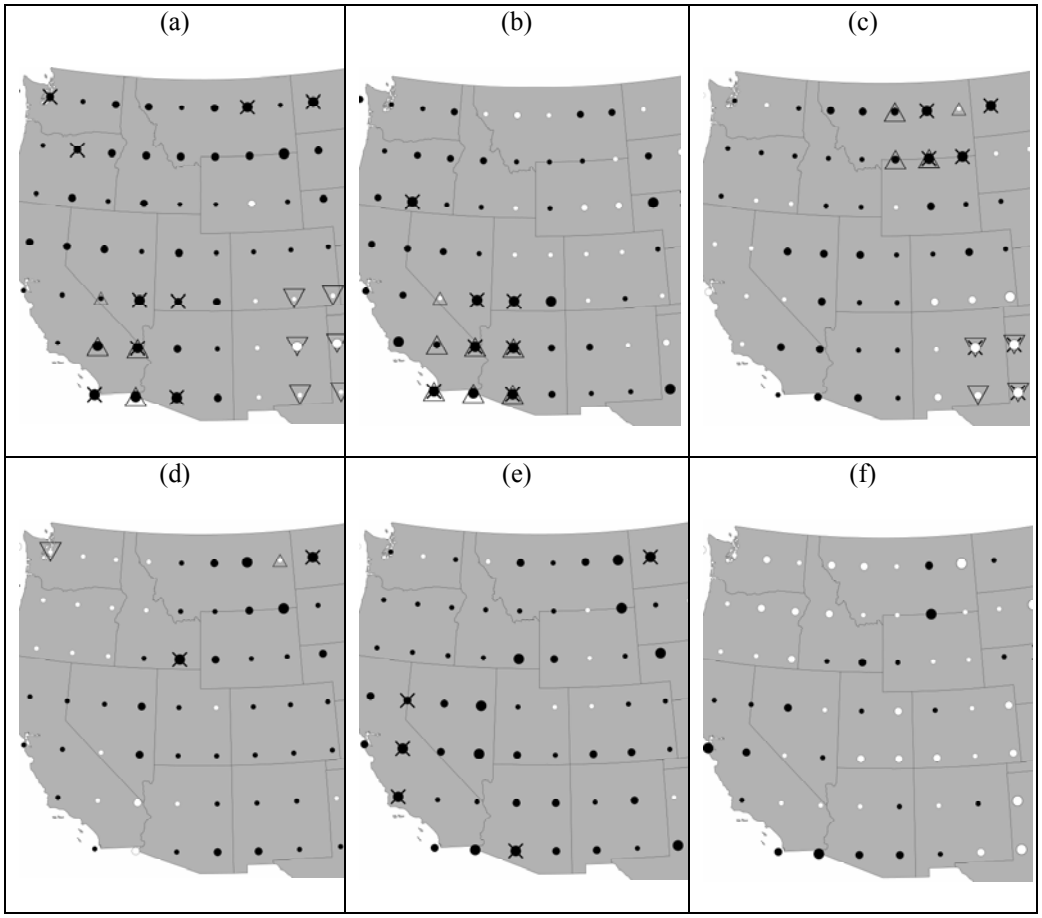

Figure 5.13: The 850-700 hPa thickness panel from Figure 5.3 (a), Figure 5.7 (b), Figure 5.11 (c), Figure 5.4 (d), Figure 5.8 (e), and Figure 5.12 (f) illustrating the modulation of the El Niño signal (top three panels a-c) and the La Niña signal (lower three panels d-f) by the cold PDO (middle panels b and e) and the warm PDO (right panels c and f).

5.3 ENSO/PDO and Wet-Bulb Zero Height

5.3.1 The Relationship between SOI and Wet-Bulb Zero Height

The error normality and constant error variance assumptions are valid for all correlations between median temperature/thickness and fall SOI as determined by the Lilliefors test and Breusch-Pagan test, respectively. Albuquerque, NM displays insignificant positive correlations (Table 5.17) which is consistent with the positive correlations in the Southern Rockies (Figure 5.13) as higher (lower) mean temperature in vertical layers of the atmosphere during El Niño (La Niña) events would suggest higher (lower) WBZ heights during El Niño (La Niña) events. Eight of the ten rawinsonde sites display negative correlations (Table 5.17). These negative correlations

are significant (two-sided $p < 0.05$) at Salem, OR, Grand Junction CO, and Boise ID for both the Pearson and Kendall's Tau tests and mildly significant (two-sided $p < 0.10$) at Medford, Oregon for the Kendall's Tau test and Salt Lake City, Utah for the Pearson test (Table 5.17). The prominence of negative correlations is consistent with the prominence of negative correlations found between temperature/thickness and fall SOI for areas of the western US outside the Southern Rockies, particularly the significant negative correlations at Salem, OR in the Pacific Northwest (Figure 5.14).

Table 5.17: From 1958-2010, for the ten rawinsonde sites (see Table 3.1 for location code definitions), the neutral ENSO median wet day 0000 UTC WBZ heights, the Pearson product-moment correlations (r), Kendall's Tau correlations (τ), and the percentage of winter wet days with 0000 UTC WBZ heights during El Niño (and La Niña) events greater than the neutral ENSO median. Values significant at the 0.10 and 0.05 significance level are indicated.

Location Code	Neutral ENSO Median WBZ (msl)	τ	r	El Niño %	La Niña %
TUS	2475	-0.08	-0.08	47.51	46.28
SLC	1786	-0.14	-0.23 (p<0.10)	49.67	45.63
ABQ	2388	0.07	0.13	49.03	51.88
GJT	2011	-0.19 (p<0.05)	-0.34 (p<0.05)	56.08 (p<0.10)	48.80
BOI	1488	-0.23 (p<0.05)	-0.29 (p<0.05)	57.55 (p<0.05)	49.54
OAK	1745	-0.08	-0.11	52.31	48.98
VGB	1872	0.03	-0.03	52.23	48.07
MFR	1640	-0.18 (p<0.10)	-0.21	53.50	47.76
SLE	1369	-0.32 (p<0.05)	-0.45 (p<0.05)	55.38 (p<0.05)	46.83
OTX/GEG	1108	-0.15	-0.22	54.19	48.28

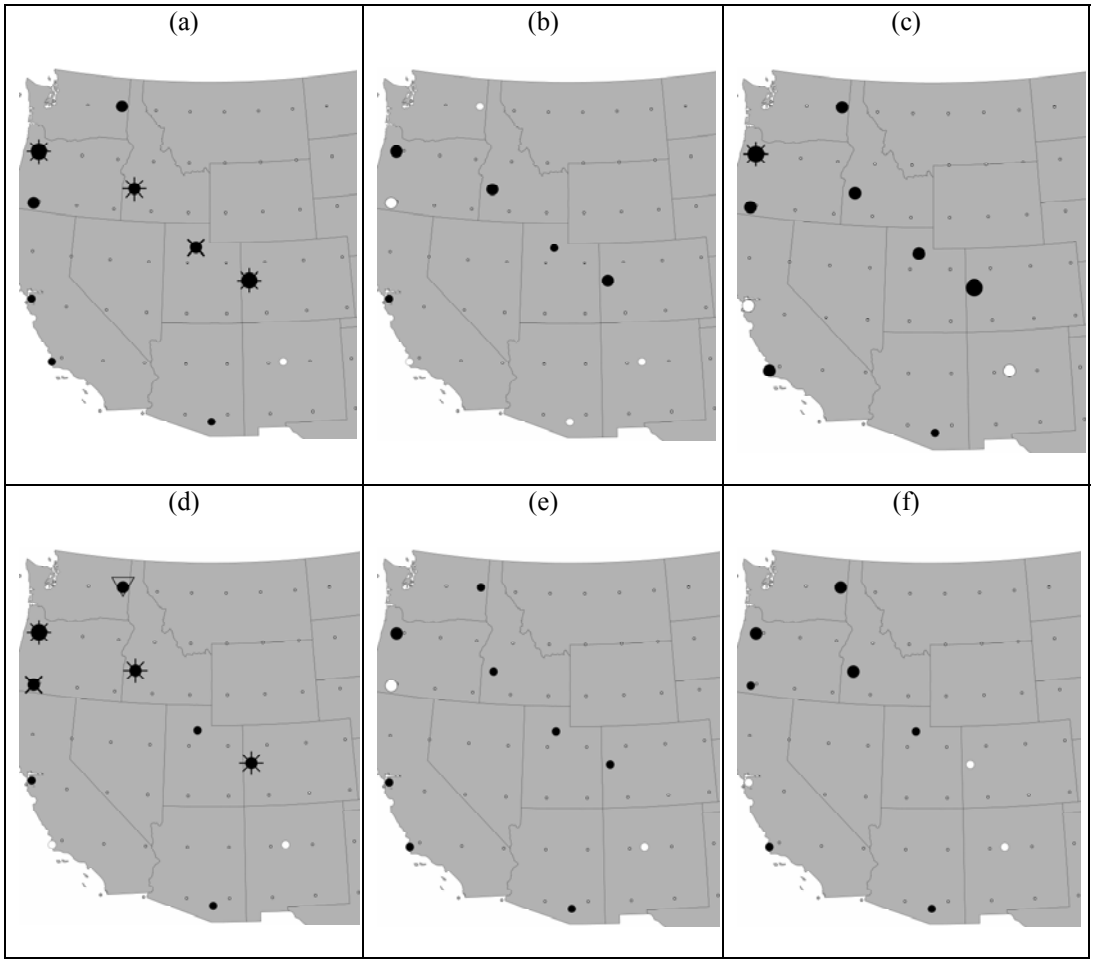

Figure 5.14: Pearson product-moment correlations between normalized fall SOI and winter median WBZ height (top panels a-c) and Kendall's Tau correlations between normalized fall SOI and winter median WBZ height (bottom d-f). Results for the entire period of record (1958-2010) are in the left panels (a and d) where black (white) circles indicate negative (positive) correlation coefficients. Within the left panels (a and d), small circles indicate $0<|r|\leq 0.15$, medium circles indicate $0.15<|r|\leq 0.30$, and large circles indicate $0.30>|r|$. Results for the cold PDO (warm PDO) are in the middle panels b and e (right panels c and f) Within the middle (b and e) and right panels (c and f) black (white) circles indicate negative (positive) correlation coefficients and small circles indicate $0<|r|\leq 0.20$, medium circles indicate $0.2<|r|\leq 0.40$, and large circles indicate $0.40>|r|$. Significant correlation coefficients at the 0.05 levels are indicated by asterisks (at the 0.10 level by ×). Local Moran's I values jointly significant with 95% confidence indicating clustering of lower values are given by inverted triangles. Dots represent the NCEP/NCAR reanalysis grids.

The neutral ENSO median wet day cold season (i.e., October through April) 0000 UTC WBZ heights are given in Table 5.17. As with the results for temperature/thickness, the prominence of negative correlations appears to be due to increased WBZ heights during El Niño conditions relative to neutral ENSO conditions rather than decreased WBZ heights during La Niña conditions. The increases in WBZ heights during El Niño conditions are mildly significant (two-sided pseudo $p < 0.10$) at Grand Junction, CO and significant (two-sided pseudo $p<0.05$) at Boise, ID and Salem, OR (Table 5.17). The rawinsonde sites with increased WBZ heights are located in the regions with increased temperature/thickness identified in Section 5.2.2, especially in the Pacific Northwest (Figure 5.15; note, 1200 UTC data are displayed in Figure A.5 in the Appendix). Also consistent with the temperature/thickness results in Section 5.2.2, is the decreased WBZ heights during El Niño at Albuquerque NM located in the Southern Rockies (Figure 5.15). Salt Lake City UT displays insignificant decreases in WBZ heights during El Niño conditions and is located in the central Rockies (Table 5.6), a region that did not display a noticeable El Niño signal in temperature/thickness (Figure 5.13). Tucson, AZ is located near the prominent cluster of grids with increased temperature/thickness in the Southwest (Figure 5.13) and displays insignificant decreases in WBZ heights, however, Tucson, AZ is located on the eastern fringe of this cluster of high temperature/thickness values (Figure 5.13 and Figure 5.15). During La Niña conditions, there are no significant increases/decreases in WBZ heights, however, only Albuquerque, NM displays an increase in WBZ heights which is consistent with the La Niña signal in the Southern Rockies for the temperature/thickness results. Also consistent with the temperature/results is the decreased (although insignificant) WBZ height in the Pacific Northwest during La Niña conditions. In short, as with the results for temperature/thickness, there is no significant evidence for a La Niña effect on WBZ heights.

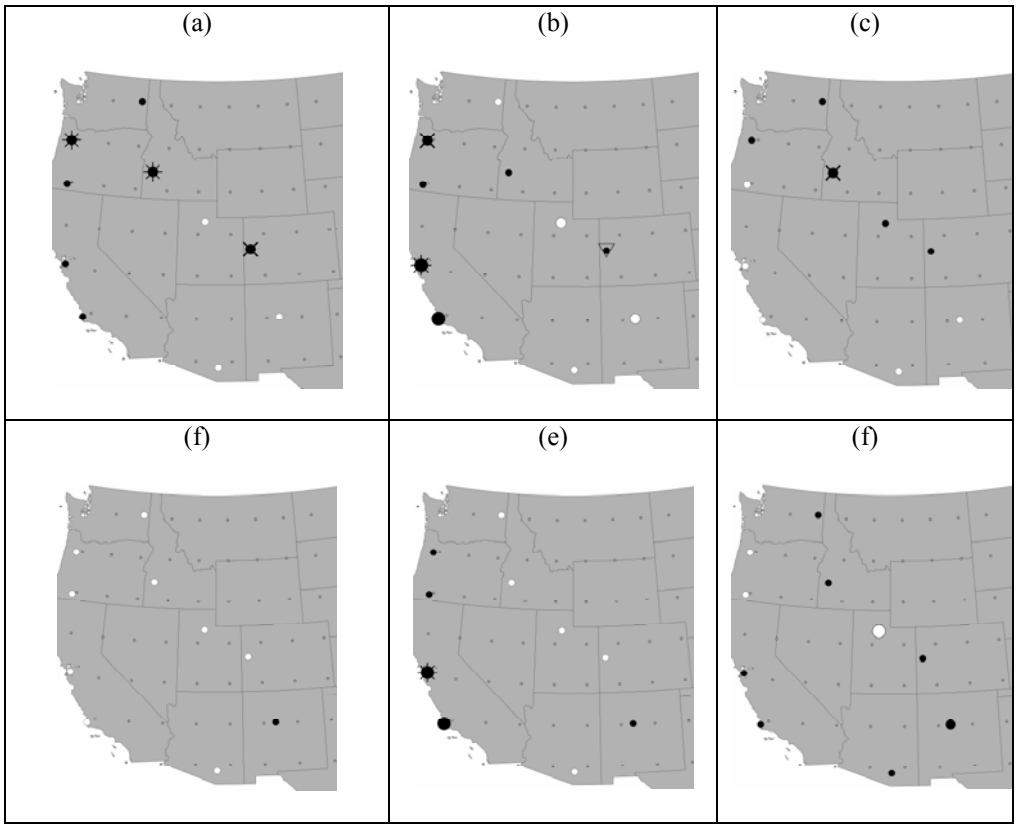

Figure 5.15: Percentage of winter wet day WBZ heights during El Niño events (top panels a-c) and La Niña events (bottom panels d-f) greater than the median value for neutral ENSO conditions for the entire period of record (left panels a and d), cold PDO (middle panels b and e) and warm PDO (right panels c and f) Small black (white) circles indicate values >50% and ≤55% (≥45% and <50%), medium black (white) circles indicate values >55% and ≤60% (≥40% and <45%) and large black (white) circles indicate values >60% (<40%). Significant deviations from 50% at the 0.05 levels are indicated by asterisks (at the 0.10 level by ×). Local Moran's I values jointly significant with 95% confidence indicating a high value surrounded by lower values are given by inverted triangles. Dots represent the NCEP/NCAR reanalysis grids.

The results for the relationship between fall SOI and WBZ height are largely consistent with the results for the relationship between fall SOI and temperature/thickness. Specifically, higher WBZ heights for rawinsonde sites located in the coastal states (particularly in the Pacific Northwest) during El Niño events and lower heights at Albuquerque, NM in the Southern Rockies during El Niño events. Unlike the temperature/thickness results, significant spatial clustering as determined by local Moran's I analysis is lacking in the WBZ results. This is likely due to the employed weight structure (i.e., inverse gravity weights with every rawinsonde site considered a neighbor of one another) as the sparse coverage of the study area resulted in assigning too little weight to the nearest neighbors in many cases. This problem could be remedied by altering the

weight structure; however, an analysis of optimal weight structure is beyond the scope of this dissertation. Additionally, unlike the temperature/thickness results where no significant ENSO signal is apparent in the central Rockies, Grand Junction, CO displays a significant ENSO signal consistent with the ENSO signal in the Pacific Northwest (Figure 5.15). This may be spurious significance, however, as Salt Lake City, UT (also located in the central Rockies) does not display this same signal (Figure 5.15). Lastly, Tucson, AZ does not display an ENSO signal consistent with the adjacent NCEP/NCAR reanalysis grid. Considering that the ENSO signal at Tucson, AZ and the adjacent grid are both insignificant, this suggests that the significant (two-sided pseudo $p < 0.05$) El Niño signal in temperature/thickness over the Southwest is not apparent for eastern Arizona and mainly confined to western Arizona and southern California.

5.3.2 The Modulation of the Relationship between SOI and Wet-Bulb Zero Height by PDO

For the cold PDO and warm PDO, the error normality and constant error variance assumptions are valid for all correlations as determined by the Lilliefors test and Breusch-Pagan test, respectively. During the cold PDO, correlations are negative at 8 rawinsonde sites for Kendall's Tau correlations and 5 sites for Pearson correlations; however, no correlations are significant (Table 5.18). As with the temperature/thickness results, the lack of significant correlations is due to the increase in WBZ heights during both El Niño and La Niña conditions relative to neutral conditions at 4 rawinsonde sites and the decrease during both El Niño and La Niña conditions at 3 rawinsonde sites (Table 5.18).

Table 5.18: For the cold PDO (1958-1976), the Pearson product-moment correlations (r), Kendall's Tau correlations (τ), and the percentage of winter wet days with 0000 UTC WBZ heights during El Niño (and La Niña) events greater than the neutral ENSO median for the ten rawinsonde sites (see Table 3.1 for location code definitions). Values significant at the 0.10 and 0.05 significance level are indicated.

Location Code	**τ**	**r**	**El Niño %**	**La Niña %**
TUS	-0.07	0.05	46.58	48.90
SLC	-0.11	-0.08	43.99	47.58
ABQ	0.11	0.15	43.56	52.99
GJT	-0.09	-0.30	53.46	49.44
BOI	-0.13	-0.20	51.37	46.88
OAK	-0.04	-0.10	67.99 (p<0.05)	62.93 (p<0.05)
VGB	-0.02	0.05	63.64	62.11
MFR	0.18	0.19	54.93	54.86
SLE	-0.17	-0.22	57.19 (p<0.10)	52.20
OTX/GEG	-0.06	0.02	49.73	48.76

For the cold PDO, the rawinsonde sites in the coastal states display an increase in WBZ during El Niño conditions that appears larger (panel (b) of Figure 5.15) than for the overall El Niño signal (panel (a) of Figure 5.15) with significant increases at Oakland, CA and Salem, OR. This is consistent with the results from the temperature/thickness analysis for which the increase in temperature/thickness during El Niño conditions in the cold PDO was similar to or greater than the overall El Niño signal over the Southwest and Pacific Northwest (Figure 5.13). Additionally, consistent with the temperature/thickness results is the cold PDO La Niña signal for the West Coast which displays increases in WBZ height (significant of the 0.05 level in Oakland, California) that are similar to the overall El Niño signal (Figure 5.13 and Figure 5.15). Apart from Boise, ID, for which the significant (two-sided pseudo p<0.05) increase in WBZ for the overall El Niño signal is not significant during the cold PDO, the rawinsonde sites outside of the West Coast do not display a clear modulation of the WBZ height ENSO signal by the cold PDO phase.

During the warm PDO, little evidence exists for a change in the correlation results relative to the entire period of record. The significant (two-sided pseudo p<0.10) negative

correlations at Salt Lake City, UT, Boise, ID, Medford, OR, Salem, OR, and Grand Junction CO for the entire period of record (Table 5.17) are negative during the warm PDO with the significance maintained at Salem, OR, for Pearson correlation (Table 5.19). Out of the ten rawinsonde sites, six display a La Niña signal opposite of the El Niño signal (i.e., an increase during La Niña conditions and a decrease during El Niño conditions or the reverse) suggesting a more monotonic relationship between fall SOI and WBZ height during the warm PDO compared to the cold PDO, which is consistent with the temperature/thickness results.

Table 5.19: As in Table 5.18 but for the warm PDO (1977-1998).

Location Code	**τ**	**r**	**El Niño %**	**La Niña %**
TUS	-0.07	-0.01	49.20	50.62
SLC	-0.11	-0.29	50.39	38.64
ABQ	0.19	0.18	48.33	57.02
GJT	0.02	-0.31	54.77	54.14
BOI	-0.22	-0.28	57.75 (p<0.10)	51.32
OAK	0.20	0.22	45.81	51.69
VGB	-0.05	-0.22	49.73	52.94
MFR	-0.06	-0.19	48.88	47.98
SLE	-0.25	-0.42 (p<0.05)	52.97	45.88
OTX/GEG	-0.17	-0.21	54.08	50.15

Similar, to the temperature/thickness results, the significant (two-sided pseudo $p < 0.05$) overall El Niño signal suggesting increased WBZ height over the West Coast is not apparent during the warm PDO (Table 5.19 and Figure 5.15). The La Niña signal during the warm PDO displays more increases (seven out of the ten sites) in WBZ height (Table 5.19 and Figure 5.15) while the overall La Niña signal displays only one increase. Considering that no increase or decrease is significant, there is little evidence for a modulation of the La Niña signal during the warm PDO.

There are four major similarities between the modulation of the ENSO signal in WBZ height by PDO phase and the modulation of the ENSO signal in temperature/thickness by the PDO phase. First, there is more evidence for a monotonic relationship between normalized fall SOI and median winter wet day temperature/thickness/WBZ height during the warm PDO than the cold PDO. Second, during the cold PDO the El Niño signal displaying an increase in WBZ height/temperature/thickness relative to neutral ENSO conditions is similar (or perhaps enhanced) when compared to the overall El Niño signal over the West Coast. Third, the La Niña signal during the cold PDO is similar to yet slightly weaker than the overall El Niño signal over the West Coast. Lastly, while there is some evidence for significant correlations during the warm PDO, the difference in the El Niño and La Niña PDFs from the neutral ENSO PDFs are largely insignificant throughout the western US. The single obvious difference between the temperature/thickness results and the WBZ height results is the decrease in temperature/thickness during El Niño conditions over the Southern Rockies that is more apparent and significant (two-sided pseudo $p < 0.05$) during the warm PDO. This is not more apparent during the warm PDO for WBZ heights over Albuquerque, NM.

5.4 ENSO/PDO and Winter Watershed Percentages

5.4.1 The Relationship between SOI and Winter Watershed Percentages

The error normality and constant error variance assumptions are valid for all correlations and t-tests applied to the entire period of record as determined by the Lilliefors test and Breusch-Pagan test, respectively. For both correlation tests between normalized fall SOI and the percentage of winter wet days with snow level above the elevations of the stations indicated by asterisks in Table 3.3 (referred to as watershed percentages), coefficients are negative for eight out the ten watersheds and significantly negative at five watersheds (Table 5.20). These results are consistent with the WBZ height and temperature/thickness results in the coastal states (Table 5.20 and Figure 5.16) as higher (lower) thickness and WBZ heights during El Niño (La Niña) events would suggest higher (lower) watershed percentages during El Niño (La Niña) events. The only positive correlations (and these are insignificant) are in the Upper Rio Grande Watershed in New Mexico and the Weber/Jordan watershed in Utah (Table 5.20) The positive correlation (although highly

insignificant) for the Upper Rio Grande located in Southern Rockies adjacent to Albuquerque, NM is consistent with the temperature/thickness and WBZ height results.

Table 5.20: For the ten watersheds, the neutral ENSO median percentage of precipitation days with snow level above the elevation of the stations given by asterisks in Table 3.3 (i.e., watershed percentages), the Pearson product-moment correlations (r), Kendall's Tau correlations (τ), and the difference in the means of watershed percentages for El Niño (and La Niña) conditions and neutral ENSO conditions. Values significant at the 0.10 and 0.05 significance level are indicated.

Adjacent US Rawinsonde Location Code	**Watershed**	**Neutral ENSO Median (%)**	**τ**	**r**	**$\mu_{\text{El Niño}} - \mu_{\text{neutral}}$ (%)**	**$\mu_{\text{La Niña}} - \mu_{\text{neutral}}$ (%)**
TUS	Salt/Lower Verde	32.12	-0.16 (p<0.10)	-0.14	15.20 (p<0.05)	4.30
SLC	Weber/Jordan	23.51	0.09	0.05	4.90 (p<0.10)	6.07 (p<0.05)
ABQ	Upper Rio Grande	18.82	0.01	0.01	-3.41	-3.82
GJT	Colorado Headwaters	42.93	-0.18 (p<0.05)	-0.30 (p<0.05)	4.11	-3.03
BOI	South Salmon/Payette/Weiser	17.57	-0.08	-0.18	6.28 (p<0.10)	0.60
OAK	San Joaquin	55.53	-0.12	-0.19	4.52	-2.79
VGB	Ventura-San Gabriel/Santa Ana	58.82	-0.18 (p<0.05)	-0.25 (p<0.05)	13.15 (p<0.05)	-0.29
MFR	Middle/Upper Rogue	64.81	-0.23 (p<0.05)	-0.33 (p<0.05)	9.16 (p<0.05)	-1.40
SLE	North Santium/ Molalla-Pudding/ Clackamas	60.34	-0.23 (p<0.05)	-0.36 (p<0.05)	7.03 (p<0.05)	-2.47
OTXGEG	Pend Orielle/Preist/Pend Orielle Lake	41.29	-0.17 (p<0.05)	-0.22 (p<0.05)	4.01	-1.73

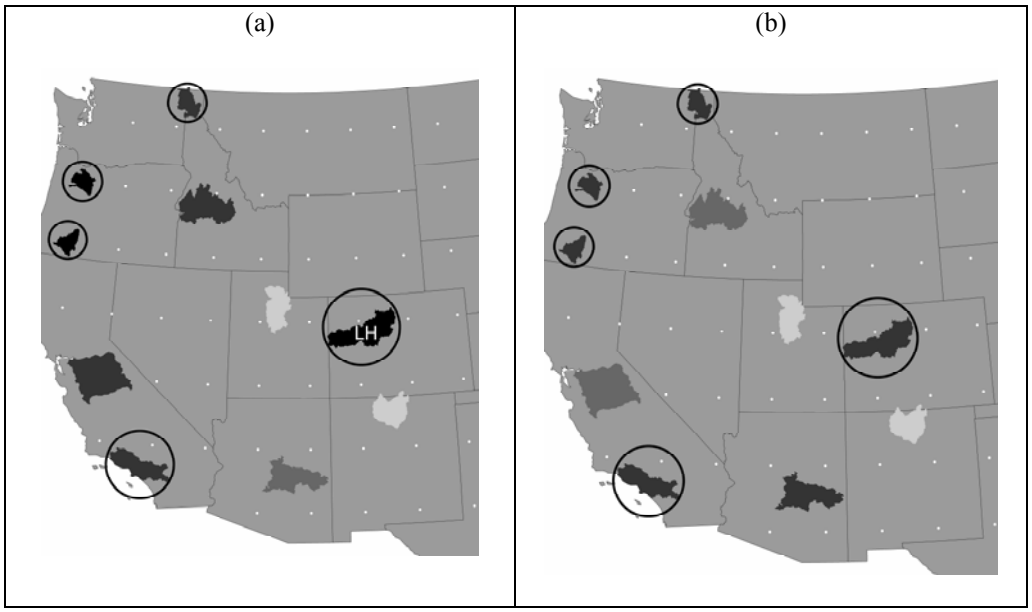

Figure 5.16: Pearson product-moment correlations (a) and Kendall's Tau correlations (b) between normalized fall SOI and winter percentage of winter wet days with snow level above the elevation of the station in each watershed (shaded polygons) indicated by asterisks in Table 3.3. Negative (positive) correlations are given by shading darker (lighter) than the base map (i.e., the states). Black polygons indicate that r <-0.30, dark gray polygons indicate that -0.30≤ r <-0.15, lighter gray polygons indicate -0.15≤ r <0, and the lightest gray polygons indicate 0< r ≤0.15. Circled polygons indicate significant (two-sided p<0.05) correlations and LH indicates a jointly significant with 95% confidence local Moran's I suggesting a low correlation surrounded by higher correlations.

The neutral ENSO median watershed percentages are given in Table 5.20. Consistent with the results for WBZ height and temperature/thickness, the prominence of negative correlations appears to be due to the increased percentages during El Niño conditions relative to neutral ENSO conditions rather than decreased percentages during La Niña conditions. Only the Upper Rio Grande displays decreased percentages during El Niño events while four watersheds display significant (two-sided pseudo p<0.05) increases in percentages during El Niño conditions (Table 5.20) including three in the west coast states (Figure 5.17). Similar to the WBZ/temperature/thickness results, there does not appear to be a significant La Niña signal in the watershed percentages (Figure 5.15), however, the watersheds in the Pacific Northwest display a decrease during La Niña events which is consistent with the temperature/thickness and WBZ height results.

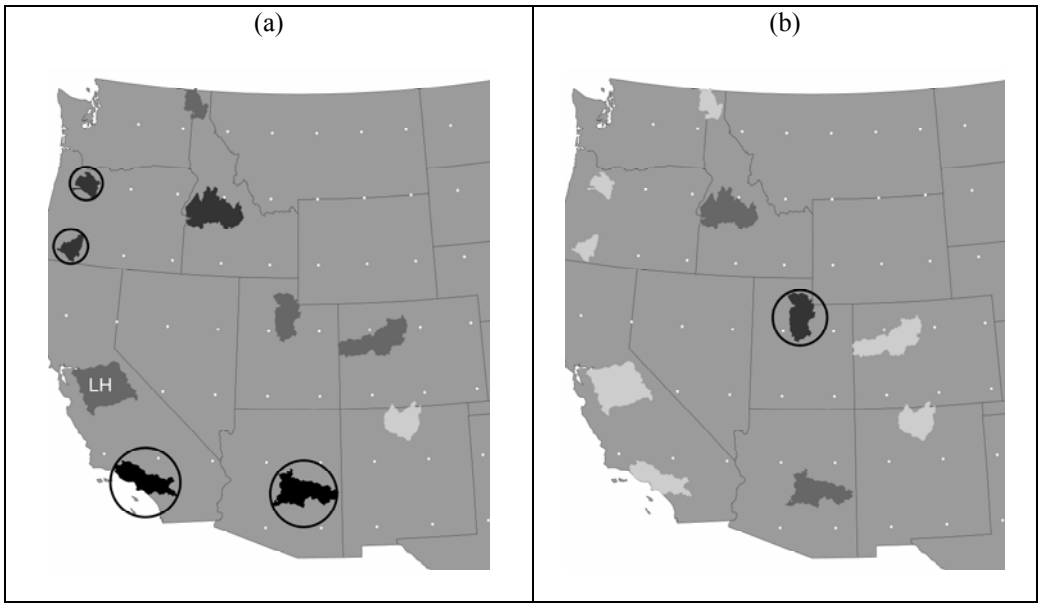

Figure 5.17: The difference in the means of the percentage of precipitation days with snow level above the elevation of the stations within each watershed given by asterisks in Table 3.3 for El Niño (a)/La Niña (b) conditions and neutral ENSO conditions. Polygons with shading that is lighter (darker) than the base map (i.e., the shading of the states) represent watershed with a higher (lower) mean during neutral ENSO conditions. Black polygons indicate $10\% < \mu_{\text{El Niño}} - \mu_{\text{neutral}}$, dark gray polygons indicate $5\% < \mu_{\text{El Niño}} - \mu_{\text{neutral}} \leq 10\%$ or $5\% < \mu_{\text{La Niña}} - \mu_{\text{neutral}} \leq 10\%$, lighter gray polygons indicate $0\% < \mu_{\text{El Niño}} - \mu_{\text{neutral}} \leq 5\%$ or $0\% < \mu_{\text{La Niña}} - \mu_{\text{neutral}} \leq 5\%$, and the lightest gray polygons indicate $-5\% \leq \mu_{\text{El Niño}} - \mu_{\text{neutral}} < 0\%$ or $-5\% \leq \mu_{\text{La Niña}} - \mu_{\text{neutral}} < 0\%$. Circled polygons indicate significant (two-sided pseudo $p<0.05$) difference in means and LH indicates a jointly significant with 95% confidence local Moran's I suggesting a low value surrounded by higher values.

Overall, the results for the relationship between fall SOI and winter watershed percentages are largely consistent with the results for the relationship between fall SOI and WBZ height/temperature/thickness. Specifically, higher percentages of winter wet days with snow level above the elevation of the stations within the watersheds located in the coastal states during El Niño events. Unlike the temperature/thickness results, significant spatial clustering as determined by local Moran's I analysis is lacking in the watershed percentage results, likely due to same reason given for the WBZ height results in Section 5.3.1 above. Additionally, unlike the temperature/thickness results where no significant ENSO signal is apparent in the central Rockies, Colorado Headwaters displays a significant ENSO signal similar to the ENSO signal in the Pacific Northwest (Figure 5.16) which is consistent with the WBZ height results. This may be spurious

significance; however, as the Weber/Jordan watershed (also located in the central Rockies) does not display this same signal (Figure 5.16). Lastly, the Salt/Lower Verde watershed in eastern Arizona displays a significant El Niño signal of increased percentages which is consistent with the temperature/thickness results at the adjacent NCEP/NCAR reanalysis grids but not the WBZ heights results at Tucson, AZ.

5.4.2 The Modulation of the Relationship between SOI and Winter Watershed Percentages by PDO

The error normality and constant error variance assumptions are valid for all correlations and t-tests applied to the entire period of record as determined by the Lilliefors and Breusch-Pagan tests, respectively, except for the Ventura-San Gabriel/Santa Ana watershed which displayed one violation of the error normality assumption for Pearson correlation. During the cold PDO, correlations are negative at eight of the ten rawinsonde sites; however, no correlations are significant (two-sided $p < 0.05$) for both correlation tests (Figure 5.18, Figure 5.19 and Table 5.21). As with the temperature/thickness results, the lack of significant correlations is due to the increase in watershed percentages during both El Niño and La Niña conditions relative to neutral conditions at seven out of ten watersheds (Table 5.21).

Table 5.21: For the cold PDO (1947-1976), the Pearson product-moment correlations (r), Kendall's Tau correlations (τ), and the difference in the means of the percentage of precipitation days with snow level above the elevation of the stations given by asterisks in Table 3.3 for El Niño (and La Niña) conditions and neutral ENSO conditions. Values significant at the 0.10 and 0.05 significance level are indicated.

Adjacent US Rawinsonde Location Code	**Watershed**	**τ**	**r**	**$\mu_{\text{El Niño}} - \mu_{\text{neutral}}$ (%)**	**$\mu_{\text{La Niña}} - \mu_{\text{neutral}}$ (%)**
TUS	Salt/Lower Verde	-0.04	-0.05	11.60	0.32
SLC	Weber/Jordan	0.22	0.33 (p<0.10)	2.09	0.55 (p<0.05)
ABQ	Upper Rio Grande	0.04	-0.01	-4.09	0.46
GJT	Colorado Headwaters	-0.11	-0.17	2.32	0.55
BOI	South Salmon/Payette/Weiser	-0.06	-0.13	2.76	0.55
OAK	San Joaquin	-0.01	-0.02	-0.99	0.90
VGB	Ventura-San Gabriel/Santa Ana	-0.20	-0.29	19.25 (p<0.05)	0.01
MFR	Middle/Upper Rogue	-0.11	-0.10	8.81	0.10
SLE	North Santium/ Molalla-Pudding/ Clackamas	-0.09	-0.10	1.73	0.75
OTXGEG	Pend Orielle/Preist/Pend Orielle Lake	-0.13	-0.04	-0.83	0.89

Unlike the WBZ height/temperature/thickness results during the cold PDO, the El Niño signal is less apparent over the west coast watersheds that display a significant El Niño signal (Table 5.21 and Figure 5.20). Consistent with the WBZ height and temperature/thickness results is the cold PDO La Niña signal for the West Coast which displays increases in watershed percentages (significant of the 0.05 level in the Weber/Jordan watershed in Utah) similar to the overall El Niño signal (Figure 5.13, Figure 5.15 and Figure 5.21).

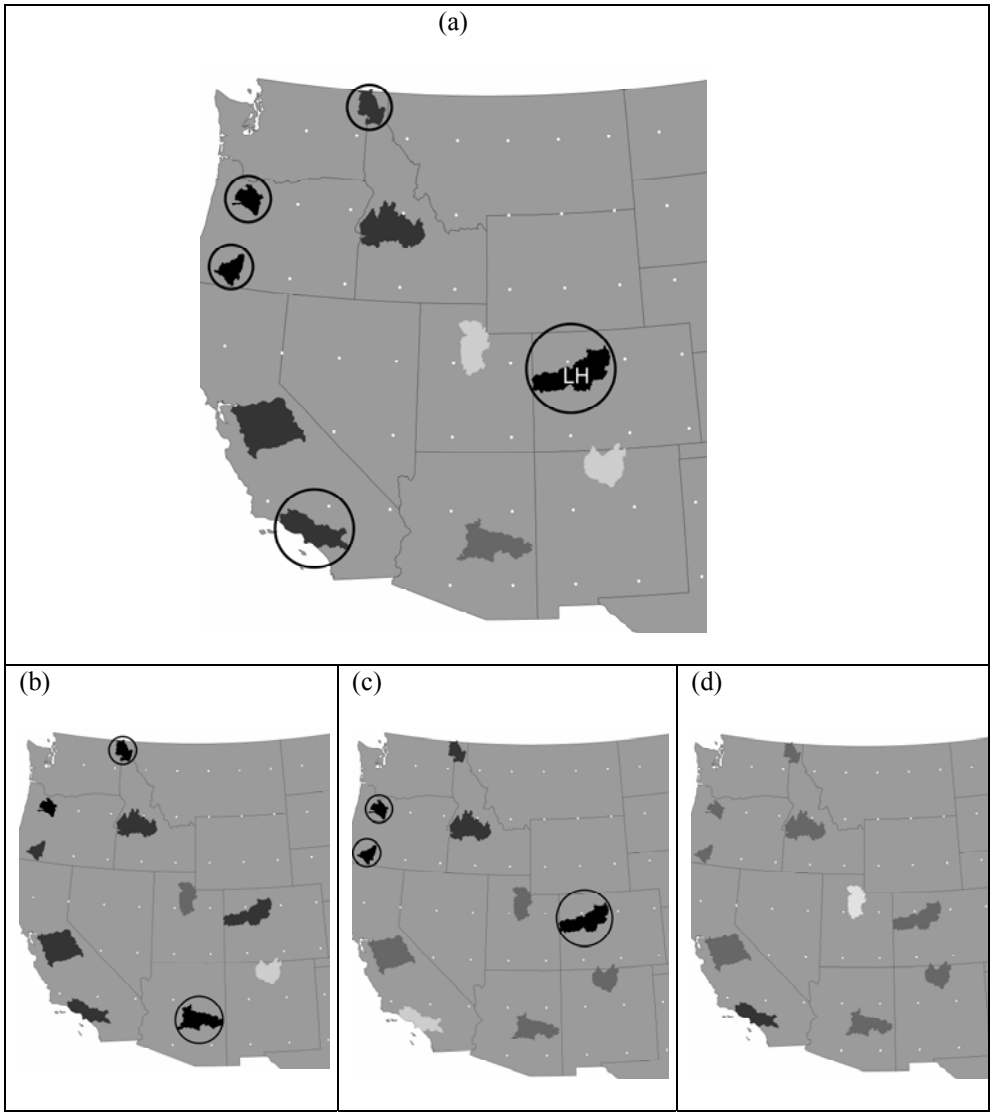

Figure 5.18: Pearson product-moment correlations between normalized fall SOI and winter percentage of winter wet days with snow level above the elevation of the station in each watershed (shaded polygons) indicated by asterisks in Table 3.3 for the entire available record (a), for the 1925-1946 warm PDO (b), for the 1977-1998 warm PDO (c) and for the 1947-1976 cold PDO (d). Map symbols for the panel (a) are defined in the caption for Figure 5.16. For the bottom panels (b-d), black polygons indicate that r <-0.40, dark gray polygons indicate that -0.40≤ r <-0.20, lighter gray polygons indicate -0.20≤ r <0, lighter gray polygons indicate 0< r ≤0.20 and the lightest gray polygons indicate 0.20< r ≤0.40. Circled polygons indicate significant (two-sided p<0.05) correlations.

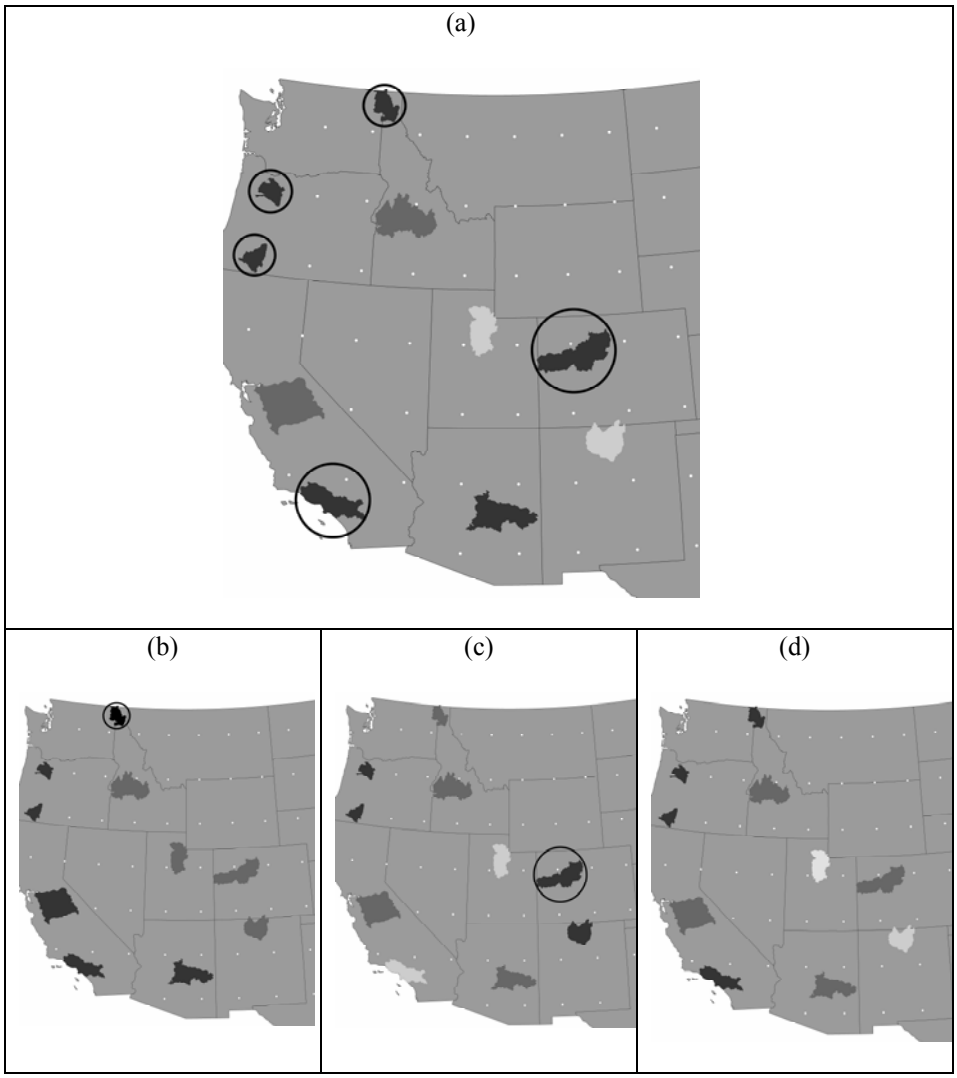

Figure 5.19: As in Figure 5.18 but for Kendall's Tau correlations.

During both warm phases of the PDO, the correlation results are similar to the overall correlation results (Table 5.22, Table 5.23, Figure 5.18, and Figure 5.19), except for only a slight loss of significance. This is similar to the results for the WBZ heights and temperature/thickness results displaying correlations during the warm PDO similar to overall correlations. Unlike, the results for the WBZ heights and temperature/thickness, there does not appear to be a dampening of the El Niño signal at the locations that displayed a significant increase in percents for the over El Niño signal, however, there is a loss of significance (Table 5.22; Table 5.23; Figure 5.20). Lastly, the largest decreases in watershed percentages occur for La Niña conditions during the two warm PDO phases (Figure 5.21) which is similar to the temperature and thickness results (Figure 5.13).

Table 5.22: As in Table 5.21 but for the 1925-1946 warm PDO. The asterisks indicate that that one of the Lilliefors tests resulted in the rejection of the error normality assumption.

Adjacent US Rawinsonde Location Code	**Watershed**	**τ**	**r**	**$\mu_{\text{El Niño}} - \mu_{\text{neutral}}$ (%)**	**$\mu_{\text{La Niña}} - \mu_{\text{neutral}}$ (%)**
TUS	Salt/Lower Verde	-0.32	-0.68 (p<0.05)	16.69	-2.82
SLC	Weber/Jordan	-0.11	-0.11	2.28	-0.37
ABQ	Upper Rio Grande	-0.02	0.02	-5.87	-6.18
GJT	Colorado Headwaters	-0.15	-0.21	-3.97	-10.22
BOI	South Salmon/Payette/Weiser	-0.15	-0.25	9.66	3.69
OAK	San Joaquin	-0.21	-0.30	4.37	-6.74
VGB	Ventura-San Gabriel/Santa Ana	-0.38 (p<0.10)	-0.33*	5.58	-4.57
MFR	Middle/Upper Rogue	-0.27 (p<0.10)	-0.39 (p<0.10)	13.52	2.23
SLE	North Santium/ Molalla-Pudding/ Clackamas	-0.22	-0.41	14.33	4.59
OTXGEG	Pend Orielle/Preist/Pend Orielle Lake	-0.42 (p<0.05)	-0.57 (p<0.05)	11.11 (p<0.05)	-2.98

There are three major similarities between the modulation of the ENSO signal in watershed percentages by PDO phase and the modulations of the ENSO signal in temperature/thickness by the PDO phase. First, there is more evidence for a monotonic relationship between normalized fall SOI and watershed percentages/temperature/thickness/ during the warm PDO than the cold PDO. Second, the La Niña signal during the cold PDO is similar to, yet slightly weaker than the overall El Niño signal over the West Coast. Lastly, outside of Arizona and southern California, the largest decreases in watershed percentages occur during the warm PDO under La Niña conditions.

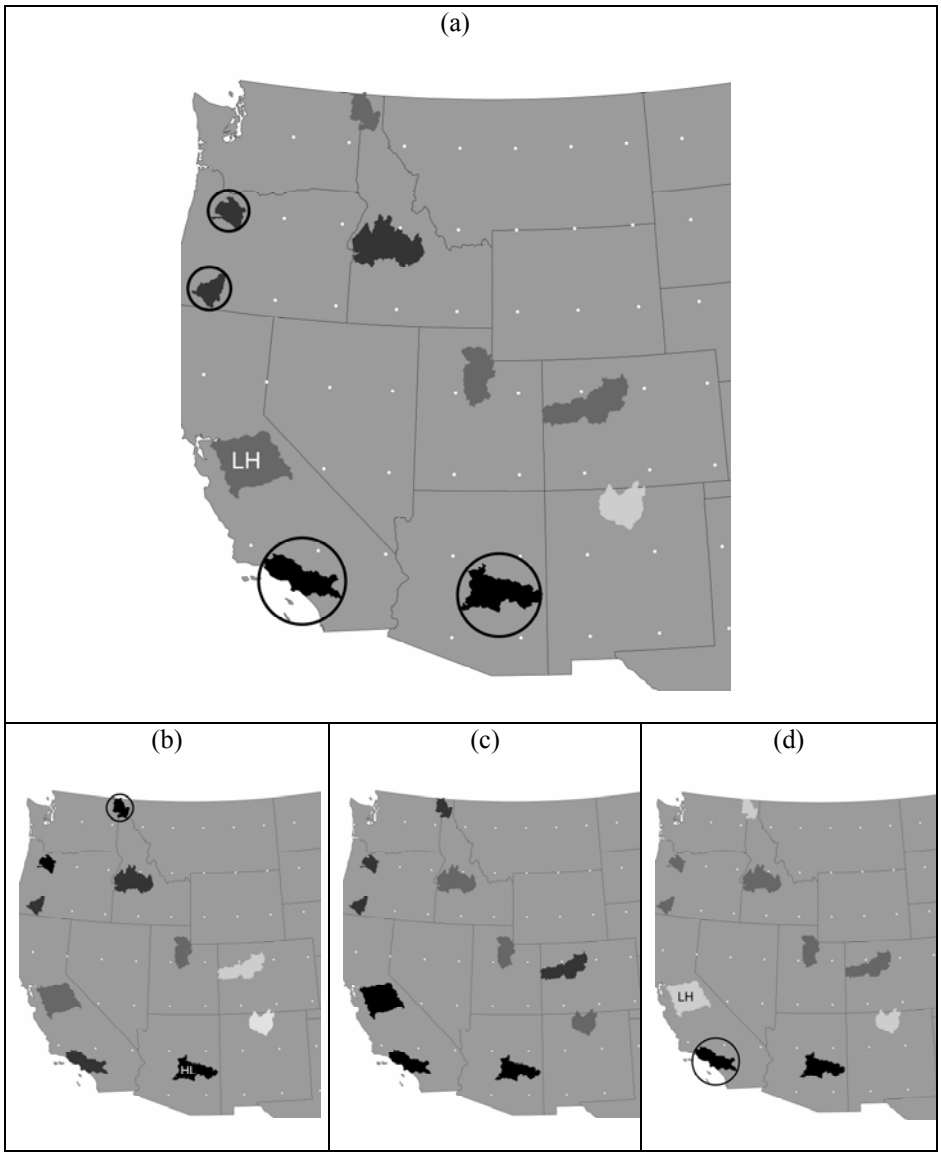

Figure 5.20: The difference in the means of the percentage of precipitation days with snow level above the elevation of the stations within each watershed given by asterisks in Table 3.3 for El Niño conditions and neutral ENSO conditions for the available record (a), for the 1925-1946 warm PDO (b), for the 1977-1998 warm PDO (c) and for the 1947-1976 cold PDO(d). Map symbols for the top panel (a) are defined in the caption for Figure 5.16, however, the lightest gray polygon (only occurs in panel b) indicates that $-10\% \leq \mu_{\text{El Niño}} - \mu_{\text{neutral}} < -5\%$.

Table 5.23: As in Table 5.21 but for the 1977-1998 warm PDO.

Adjacent US Rawinsonde Location Code	Watershed	τ	r	$\mu_{\text{El Niño}} - \mu_{\text{neutral}}$ (%)	$\mu_{\text{La Niña}} - \mu_{\text{neutral}}$ (%)
TUS	Salt/Lower Verde	-0.18	-0.01	19.86 (p<0.10)	22.51
SLC	Weber/Jordan	0.07	-0.16	2.91	2.05
ABQ	Upper Rio Grande	-0.21	-0.18	2.34	-1.96
GJT	Colorado Headwaters	-0.35 (p<0.05)	-0.52 (p<0.05)	8.04	-11.89 (p<0.10)
BOI	South Salmon/Payette/Weiser	-0.13	-0.30	2.97	-5.65
OAK	San Joaquin	-0.09	-0.18	10.79	2.90
VGB	Ventura-San Gabriel/Santa Ana	0.02	0.02	14.77 (p<0.10)	32.57 (p<0.05)
MFR	Middle/Upper Rogue	-0.28 (p<0.10)	-0.50 (p<0.05)	8.52 (p<0.10)	-1.94
SLE	North Santium/ Molalla-Pudding/ Clackamas	-0.28 (p<0.10)	-0.48 (p<0.05)	8.83 (p<0.10)	-0.36
OTXGEG	Pend Orielle/Preist/Pend Orielle Lake	-0.17	-0.29	5.90	1.42

There are three major differences between the temperature/thickness results and the watershed percentage results. First, while the decrease in temperature/thickness during El Niño conditions over the Southern Rockies that was more apparent and significant (two-sided pseudo $p < 0.05$) during the warm PDO, this was not more apparent during the warm PDO for the watershed percentages in the Upper Rio Grande in New Mexico (note, this dissimilarity was also found between the WBZ height results for Albuquerque, NM and the temperature/thickness results). Second, during the cold PDO, the enhancement of the El Niño signal displaying an increase in watershed percentages relative to neutral ENSO conditions is not apparent. Lastly, the evidence for a dampening of the El Niño signal at watersheds displaying an increase in percentages during both warm phases of the PDO is through a loss of statistical significance only, and not from obvious changes in the increases in percentages.

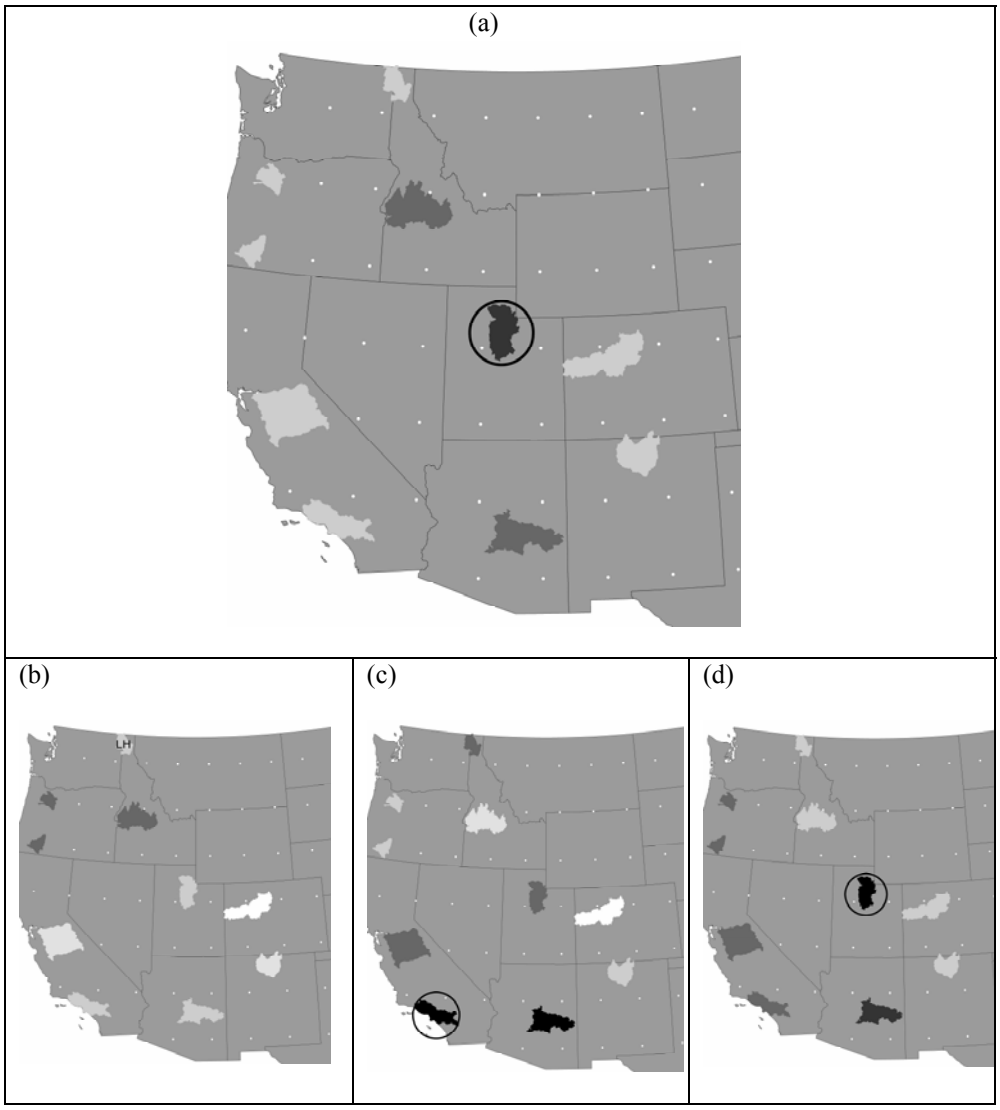

Figure 5.21: As in figure 5.20 but for La Niña conditions. Additionally, white polygons indicate $\mu_{\text{La Niña}} - \mu_{\text{neutral}} < -10\%$.

5.5 Similarities in the Three ENSO/PDO Analyses

Several key results have been identified regarding the ENSO/PDO analyses that are consistent between the temperature/thickness variables, WBZ heights, and watershed percentages.

1) The majority of the western US displays higher values of watershed percentages, WBZ heights, and temperature/thickness during El Niño events (i.e., winters preceded by normalized fall SOI < -0.4). These results are internally consistent as higher mean temperature in vertical layers of the atmosphere would lead to higher WBZ heights and percentages of days with estimated snow level above elevations within the watersheds. The only region of the western US consistently displaying lower values during El Niño events is the Southern Rockies.
2) Increased values during El Niño conditions are significant ($p < 0.05$) over the west coast locations (i.e., reanalysis grids, rawinsonde sites and watersheds in southern California and the Pacific Northwest).
3) The Pacific Northwest is the only region displaying a La Niña signal consistent for all three variables (i.e., watershed percentages, WBZ heights and temperature/thickness). The signal is a decrease in values during La Niña events, although generally statistically insignificant.
4) During the cold PDO, for southern California, the La Niña signal has a similar direction and magnitude than the El Niño signal described above (although less significant).
5) The in-phase (i.e., warm PDO/El Niño or cold PDO/La Niña) dampening of the ENSO signal over the West Coast (particularly the Pacific Northwest) is most obvious for the temperature/thickness results but supported by both WBZ height results and watershed percentage results (although only through a loss of statistical significance for the watershed percentage El Niño signal).

6) Over southern California, the amplification of the significant El Niño signal during the cold PDO is obvious for both temperature/thickness and WBZ height results, however, results for the watershed percentages are inconclusive.
7) For regions outside the West Coast, results for the PDO analysis are inconsistent between watershed percentages, temperature/thickness, and WBZ heights.

Considering these findings and assuming no long term trend in temperature/thickness, WBZ heights, and the percentage of days per winter with estimated snow level above specified elevations, these variables appear to be highest during the cold PDO, particularly in southern California and the Pacific Northwest.

5.6 Discussion of the ENSO Results

The convergent results from the three measures of interannual snow level variability discussed in the Section 5.5 suggest higher snow levels over much of the western US during El Niño, particularly over the coastal regions. The Pacific–North American (PNA) pattern identified by Wallace and Gutzler (1981) is characterized by differing (i.e., positive versus negative) geopotential height anomalies between the Pacific Ocean around 45°N and western North America (as well as western North America and the southeastern US). Deeper than normal troughs over the North Pacific and southeastern US coincident with a stronger than normal ridge over the Rocky Mountains is often referred to as the positive PNA (Renwick and Wallace 1996; Higgins et al. 2002; Yu and Zwiers 2007). The reverse of this situation (the negative PNA) results in more zonal upper-level flow across the North Pacific and North America (Sheppard et al. 2002).

During El Niño events, anomalously high sea surface temperatures in the eastern equatorial Pacific produce a large area of anomalous convection that affects circulation in the extratropics (Straus and Shukla 2002). Consequently, many studies suggest a link between ENSO and the PNA (e.g., Lau 1997; Dettinger et al. 1998), specifically, higher frequencies of positive PNA episodes during El Niño and higher frequencies of negative PNA episodes during La Niña

events (Sheppard et al. 2002). Other researchers have linked ENSO to geopotential height anomalies distinct from the PNA (e.g., Zhang et al. 1996; Straus and Shukla 2002) and winter weather characteristics over the western US are affected by east-west shifts of the upper-level ridge generally over the Rocky Mountains, specifically, the eastward shift of the ridge during El Niño events (Sheppard et al. 2002; Higgins et al. 2002; Straus and Shukla 2002). Consequently, during El Niño events, maritime air flow into the western US is more frequent and cold air masses from Canada are less frequent (Higgins et al. 2002), despite increased meridional flow from the positive PNA. Additionally, the preferred extratropical cyclone track can often split during El Niño events and storms making landfall in southern California are supplied by lower latitude moisture sources in the Pacific (Sheppard et al. 2002). Considering these previous investigations, one would expect to find higher snow level elevation during El Niño events, especially apparent over the coastal regions (i.e., the El Niño signal suggested by the results in Sections 5.2-5.4), in response to the higher frequency of maritime flow (rather than colder continental air flow) throughout the winter.

As suggested in Sections 5.2-5.4 above, this El Niño signal is less apparent with distance from the Pacific Ocean with evidence supporting slightly lower snow levels over the Southern Rockies. Air masses associated with winter mid-latitude cyclones crossing the numerous mountain barriers between the Pacific Ocean and the Southern Rockies begin to resemble continental air masses rather than maritime air masses (Mock 1995; Mock and Birkeland; 2000). As the air masses lose maritime characteristics, it is reasonable to assume that the more meridional upper-level flow during El Niño associated with positive PNA would result in lower snow levels over the Southern Rockies.

Considering the significant El Niño signal in snow level, one may expect a significant opposite signal during La Niña events due to the higher frequency of continental air flow. Contrarily, there is a lack of a significant La Niña signal across the western US. This suggests asymmetry in the ENSO influence on snow level in the western US. It is important to note that

previous studies have found asymmetries and nonlinearities in the ENSO relationship with mid-latitude flow (e.g., Straus and Shukla 2002).

Numerous studies have suggested cooler winters for the Southwest US during El Niño events (e.g., Ropelewski and Halpert 1986; Kahya and Dracup 1994; Gershunov 1998; Gershunov and Barnett 1998a; Higgins et al. 2002). The higher snow levels during El Niño indicated by this study is not contradictory to these previous studies as the coincident increase in winter storm frequency (e.g., Sheppard et al. 2002; Higgins et al. 2002) likely decreases the mean winter temperature in the Southwest US. Higher snow levels during El Niño simply suggest warmer temperatures during precipitation events.

5.7 Discussion of the Modulation of ENSO Results by PDO

The results from Sections 5.2-5.4 suggest that (1) during the cold PDO, for southern California, the La Niña signal is similar to the overall El Niño signal, (2) in phase (i.e., warm PDO/El Niño or cold PDO/La Niña) dampening of the ENSO signal over the West Coast (particularly the Pacific Northwest), and (3) the amplification of the significant El Niño signal during the cold PDO over southern California. Many previous investigators suggest an indirect PDO affect on western US weather through the modulation of the ENSO effect by PDO phase (e.g., Gershunov and Barnett 1998b; Gutzler et al. 2002; Brown and Comrie 2004; Yu et al. 2007; Yu and Zwiers 2007). The strength of the Aleutian low (and thus the PNA) is affected by sea surface temperature anomalies in the North Pacific displaying decadal variability (i.e., the PDO). During the warm phase of the PDO, waters in the northern and western Pacific are anomalously cool while waters in the eastern tropical Pacific and along the west coast of North America are warmer than normal (and the reverse for the cold PDO; Stoner et al 2009). During the warm phase of the PDO, the Aleutian low strengthens along with the PNA pattern resulting in more meridional upper-level flow over the western US, often serving to amplify the effects of El Niño events and dampen the effects of La Niña events (Gutzler et al. 2002; Brown and Comrie 2004; Yu and

Zwiers 2007; Yu et al. 2007; Goodrich 2007). Conversely, during cold PDO, the La Niña signal is strengthened and the El Niño signal is dampened, as PNA tends to be negative.

The results from Sections 5.2-5.4 are supported by this previous body of research. As the PNA tends to be positive (i.e., highly meridional flow over the western US) during the El Niño/warm PDO, one would expect a dampening of the El Niño signal during the warm PDO due to deeper troughs (Sheppard et al. 2002; Yu et al. 2007; Yu and Zwiers 2007) resulting in colder air flow and lower snow levels. The shallow troughs during cold PDO, as the upper-air flow is more zonal, along with the maritime air flow in the western US during El Niño supports the increase in snow level during El Niño/cold PDO. Lastly, as one would expect maritime air flow into southern California even during La Niña events, the shallow troughs during the cold PDO result in higher snow level elevations in southern California. Therefore, particularly over the West Coast, the zonal flow associated with the cold PDO is a likely catalyst for the increased snow level elevations relative to the warm PDO, as suggested by the modulation of the ENSO influence by PDO.

5.7 Conclusions

From three separate methods (WBZ heights, COOP snow level approximation for watersheds, upper-air reanalysis proxies) of quantifying daily snow level and interannual snow level variability, I have established the relationship between fall SOI/PDO phase and estimated snow levels from the watershed COOP stations, 850 hPa temperature, 850-700 hPa thickness, 1000-500 hPa thickness, 1000-850 hPa thickness and WBZ heights. There are three major findings that aid in addressing the research question introduced in Chapter 1: *What is the relationship between ENSO/PDO and snow level and how does this vary across on the western US?*

(1) In support of my hypothesis in Chapter 1 (specifically, *I expect snow levels to be the highest during El Niño events occurring in conjunction with the cold PDO*), the fall SOI relationship with 850 hPa temperature, 850-700 hPa thickness, 1000-500 hPa thickness, 1000-850 hPa thickness, WBZ heights, and watershed percentages suggest

higher snow levels over most of the western US (except the Southern Rockies) during El Niño, particularly over the coastal regions. Considering previous investigations, the higher frequency of maritime flow (as opposed to continental flow) into the western US during El Niño events results in increased snow level elevation. The distance from the Pacific Ocean weakens this El Niño signal and the Southern Rockies display decreased snow level elevations as the maritime air masses associated with mid-latitude cyclones following the enhanced meridional flow transition to continental air masses. The higher mean winter temperature during El Niño events suggested by previous researchers is not contradictory to these results as higher snow levels suggest higher temperatures during precipitation events, where as the frequency of troughing and precipitation would influence the mean winter temperature.

(2) Previous researchers suggest a link between the warm (cold) phase of the PDO and a strengthening (weakening) of the Aleutian low resulting in the in-phase amplification of the ENSO effects on winter weather in the western US through the enhancement (dampening) of the PNA. The highly positive PNA during the warm PDO/El Niño conditions suggests a deepening of troughs that occur over the western US and serves to dampen the El Niño signal of higher snow level over the West Coast. Similarly, the more zonal flow and shallower troughs associated with the cold PDO serves to amplify the El Niño signal over the West Coast. In addition, during the cold PDO, La Niña events resemble a weaker version of the El Niño signal over southern California (i.e., increased snow level elevation) likely due to the more zonal flow.

(3) Also supporting my hypothesis in Chapter 1 (specifically, *I expect snow levels to be the highest during El Niño events occurring in conjunction with the cold PDO*), the above results suggest that over the western US, assuming no long term trends, snow levels are higher during the cold PDO relative to the warm PDO likely due to the more zonal flow.

This chapter detailed the analyses of interannual and decadal variability in snow level as linked to ENSO and PDO. In the following chapter, the interannual snow level variability as quantified by the WBZ heights, NCEP/NCAR reanalysis temperature/thickness variables, and the estimated snow levels from the COOP stations within each watershed are examined for multi-decadal trend. Spatial variability in trends is also analyzed revealing the regions of the western US displaying coherent spatial patterns in snow level trend.

Chapter 6: Trends in Snow Level Elevation

6.1 Introduction

In previous chapter, I analyzed the interannual and decadal variability in snow level for the western United States, by establishing the relationship between snow level and El Niño–Southern Oscillation (ENSO), as well as the modulation of this relationship by Pacific Decadal Oscillation (PDO). In this chapter, I seek to answer the second question introduced in Chapter 1: *Do multi-decadal trends exist in the elevation of snow level, and if so, how do these vary across the western US?* I first establish the existence of trends in the NCEP/NCAR reanalysis temperature/thickness variables and the spatial variability thereof. That leads to a discussion of similar analyses using the wet-bulb zero (WBZ) heights, and approximated watershed snow levels within the context of the observed trends in temperature/thickness. Lastly, the convergent results between these measures of snow level with respect to the large body of previous research regarding trends in twentieth-century western US climate are discussed.

6.2 Trends in Winter Wet Day Temperature and Thickness

The trend analyses of mean winter wet day temperature and thickness are initiated by statistical tests for error normality, constant variance, and autocorrelation, as discussed in Chapter 3. Rejections (at the 0.05 confidence level) of the error normality, constant error variance, and independent error terms (i.e., $\rho = 0$ in the first-order autocorrelation model 4.26) assumptions for the simple linear regressions as determined by the Lilliefors test, Breusch-Pagan test, and Durbin-Watson test respectively are displayed in Figure A.6. The assumptions appear valid at most grids and very few grids display significant deviations of these attributes for all four reanalysis variables (Figure A.6). It is important to note, that first-order autocorrelation was successfully alleviated by the application of the Hildreth-Lu procedure in all cases and the simple linear slopes (Figure 6.1) for autocorrelated time series were derived from a first-order autoregressive model (4.26).

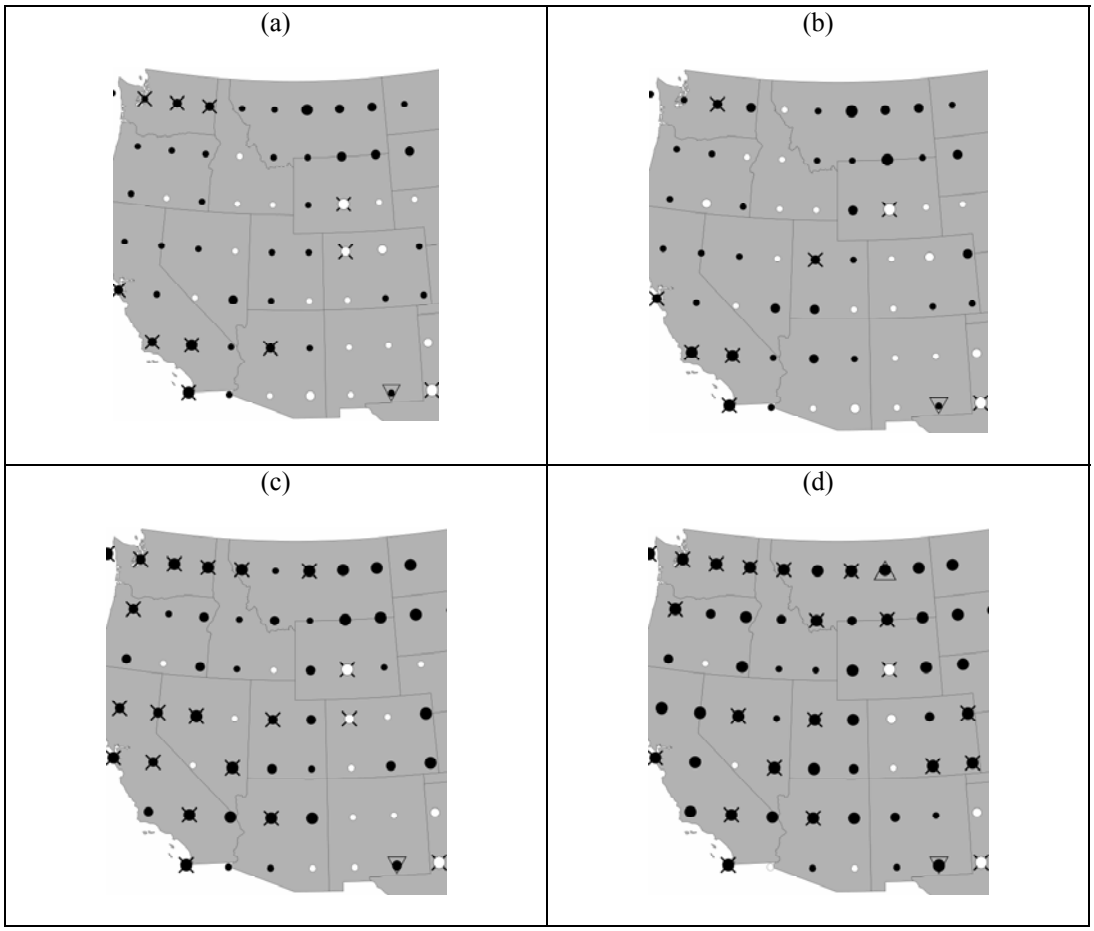

Figure 6.1: From 1949-2009, trends (b_1 for simple linear regression) in cold season median wet day 850 hPa temperatures (a), 1000-850 hPa thickness (b), 850-700 hPa thickness (c), and 1000-500 hPa thickness (d). Black (white) circles indicate positive (negative) trends. For 850 hPa temperatures (a), large circles indicate $|b_1|$ >0.3 K dec^{-1} , medium circles indicate 0.15<$|b_1|$ ≤0.3 K dec^{-1} , and small circles indicate 0.0<$|b_1|$ ≤0.15 K dec^{-1}. For 1000-850 hPa thickness (b) and 850-700 hPa thickness (c), large circles indicate $|b_1|$ >1.0 gpm dec^{-1} , medium circles indicate 0.5<$|b_1|$ ≤1.0 gpm dec^{-1} , and small circles indicate 0.0<$|b_1|$ ≤0.5 gpm dec^{-1}. For 1000-500 hPa thickness (d), large circles indicate $|b_1|$ >2.0 gpm dec^{-1} , medium circles indicate 0.1<$|b_1|$ ≤2.0 gpm dec^{-1} , and small circles indicate 0.0<$|b_1|$ ≤1.0 gpm dec^{-1}. Significant trends (p<0.05) are indicated by ×. Local Moran's I values jointly significant with 95% confidence indicating clustering of higher values are given by large right-side up triangles. Jointly significant local Moran's I indicating a high value surrounded by lower values are given by small inverted triangles.

Trend analyses of winter wet day temperature and thickness are nearly identical between the simple linear regression and Mann-Kendall test. For wet day 850 hPa temperature, 850–700 hPa thickness and 1000–500 hPa thickness, trends are field significant (pseudo $p < 0.05$) over the western US as a whole (Table 6.1). For 1000–850 hPa thickness, trends are slightly less significant for simple linear regressions (pseudo $p = 0.083$) and Mann-Kendall (pseudo $p = 0.106$) trend tests (Table 6.1). The field significance appears to be a result of increasing trends with significant (two-sided $p < 0.05$) increasing trends displayed for at least six out of the 60 grids for all temperature/thickness measures with at most 4 grids displaying significant decreasing trends (Table 6.2 and Table 6.3). 1000-500 hPa thickness displays the most evidence for increasing trend with more than 50 grids displaying positive trends (more than 15 of which are significant) while 1000-850 thickness displays the least evidence for increasing trends with less than 41 out 60 grids displaying positive trend (Table 6.2 and Table 6.3). Trend magnitudes are generally mild with about half of the grids displaying trends of less than 0.07 K dec^{-1} for 850 hPa temperature, less than 0.24 gpm dec^{-1} for 1000–850 hPa thickness, less than 0.77 gpm dec^{-1} for 850–700 hPa thickness and less than 2.87 gpm dec^{-1} for 1000–500 hPa thickness (Table 6.2).

Table 6.1: Field significance of simple linear regression (SLR) and Mann-Kendall (MK) trend tests for cold season median wet day temperature and thickness, over the entire western US since 1949.

	SLR Field Significance	MK Field Significance
850 hPa Temperature	0.035	0.022
1000-850 hPa Thickness	0.083	0.106
850-700 hPa Thickness	0.007	0.008
1000-500 hPa Thickness	0.003	0.004

Table 6.2: Descriptive statistics for the simple linear regression trend test results for cold season median wet day temperature and thickness at the 60 NCEP/NCAR reanalysis grid points since 1949.

	Median b_1 (K or gpm dec^{-1})	Max b_1 (K or gpm dec^{-1})	Min b_1 (K or gpm dec^{-1})	Number of grids with $b_1>0$	Number of grids with $b_1>0$ and two-sided $p<0.05$	Number of grids with $b_1<0$ and two-sided $p<0.05$
850 hPa Temperature	0.07	0.51	-0.72	40	8	3
1000-850 hPa Thickness	0.24	2.21	-3.18	38	6	2
850-700 hPa Thickness	0.77	2.85	-3.65	45	16	3
1000-500 hPa Thickness	2.87	9.89	-11.36	51	18	2

Table 6.3: Descriptive statistics for the Mann-Kendall trend test results for cold season median wet day temperature and thickness at the 60 NCEP/NCAR reanalysis grid points since 1949.

	Median τ	Max τ	Min τ	Number of grids with $\tau>0$	Number of grids with $\tau>0$ and two-sided $p<0.05$	Number of grids with $\tau<0$ and two-sided $p<0.05$
850 hPa Temperature	0.04	0.39	-0.27	39	8	4
1000-850 hPa Thickness	0.03	0.33	-0.24	40	5	2
850-700 hPa Thickness	0.09	0.34	-0.23	48	15	2
1000-500 hPa Thickness	0.12	0.35	-0.23	53	16	2

For 850–700 hPa thickness and 1000–500 hPa thickness, significant (two-sided $p <$ 0.05) increasing trends appear uniformly distributed across the western portion of the study are (Figures 6.1 and 6.2). For 850 hPa temperature and 1000–850 hPa thickness, significant increasing trends (Figures 6.1 and 6.2) are confined to the Pacific Northwest and the Southwest (see Table 5.6 for region definitions). All four thickness/temperature measures display significant decreasing trends confined to the central Rockies (Figure 6.1 and 6.2) and Mann-Kendall results indicate a significant cluster of decreases centered over southern Wyoming and northern Colorado. It is important to note that the trends in temperature/thickness do not appear to be in response to the

trends in the portion of wet days sampled during coldest part of the winter season, namely December-February (Figure A.7). While five out of the 60 grids display significant (two-sided $p <$ 0.05) decreasing trends in the percentage of sampled wet days occurring during December-February (one would expect this to contribute to increasing trends in average wet day temperature/thickness during October-April), most of the grids display highly insignificant trends and nearly all of California and Nevada (a region with significant increases in temperature/thickness) displays positive trends (Figure A.7).

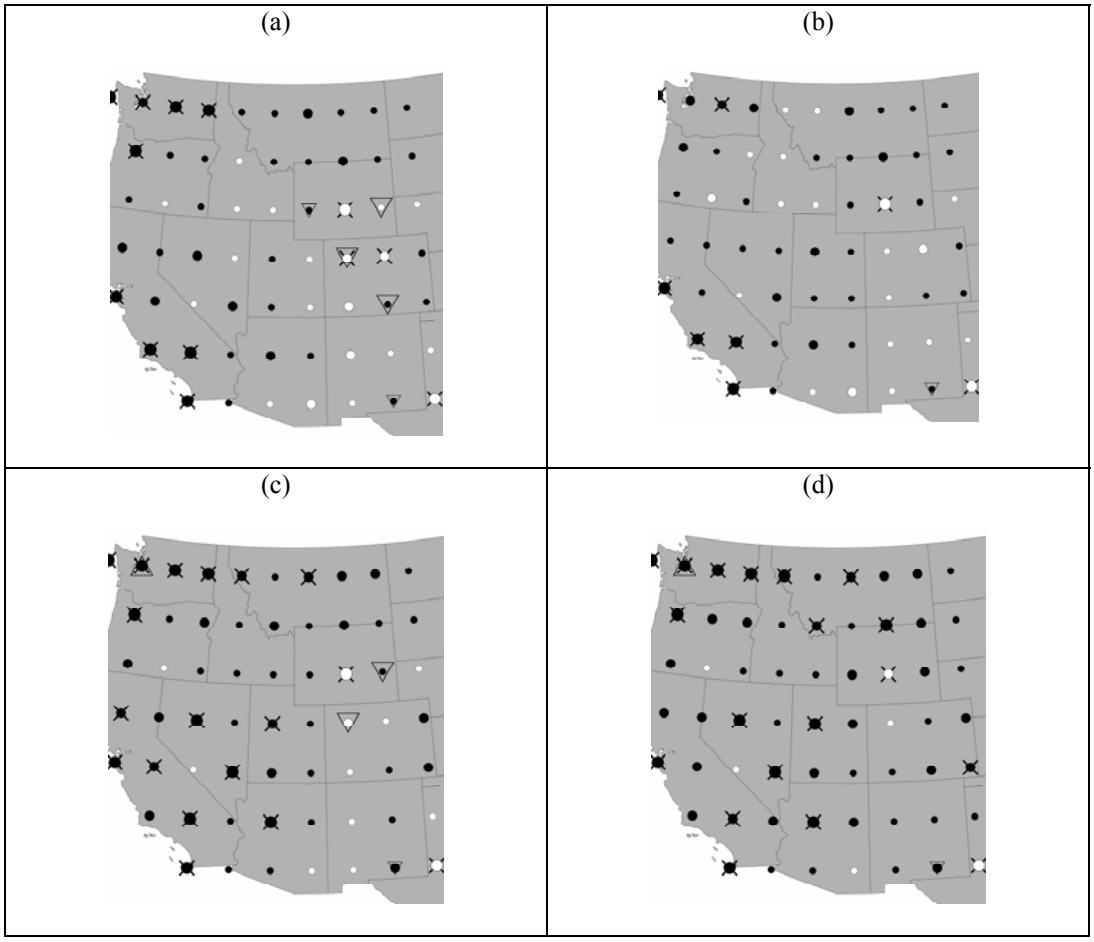

Figure 6.2: As in Figure 6.1 but Mann-Kendall trend test. Black (white) circles indicate positive (negative) trends. Large circles indicate $|\tau|$ >0.2, medium circles indicate 0.1< $|\tau|$ ≤0.2, and small circles indicate 0.0< $|\tau|$ ≤0.1. Significant trends (p<0.05) are indicated by ×. Local Moran's I values jointly significant with 95% confidence indicating clustering of higher(lower) values are given by large triangles (inverted triangles). Jointly significant local Moran's I indicating a high value surrounded by lower values are given by small inverted triangles.

6.3 Trends in Winter Wet Day WBZ Height

The simple linear regressions of median wet day winter 0000 UTC WBZ height versus year for all rawinsonde sites, display little evidence to support the rejection of the error normality, constant error variance, and the independent error terms (i.e., $\rho = 0$ in the first-order autocorrelation model 4.26) assumptions as determined by the Lilliefors test, Breusch-Pagan test, and Durbin-Watson test respectively. For the ten rawinsonde sites, trend results from the Mann-Kendall test and simple linear regression are very similar (Table 6.4). Trends in WBZ height range from -3.80 m dec^{-1}(highly insignificant) at Oakland, CA (Figure 6.3; Table 6.4) to 65.38 m dec^{-1} (two-sided $p < 0.01$) at Albuquerque, NM (Figure 6.4; Table 6.4) with modest yet insignificant trends of 28.2 m dec^{-1} ($p = 0.13$) at Salt Lake City, UT (Figure 6.5; Table 6.4), 27.8 m dec^{-1} ($p = 0.13$) at Grand Junction, CO (Figure 6.4; Table 6.4), 20.4 m dec^{-1} ($p = 0.15$) at Medford, OR (Figure 6.6; Table 6.4) and 11.3 m dec^{-1} ($p = 0.36$) at Salem, OR (Figure 6.7; Table 6.4). Therefore, there is more evidence for increasing winter wet day WBZ heights (significant at two sites per the Mann-Kendall test) than decreasing WBZ heights which is consistent with the temperature/thickness results, as increased mean temperature in vertical layers of the atmosphere would suggest increased WBZ heights. It is important to note that the trend results for the 0000 UTC are similar to the trend results for the 1200 UTC soundings (Figure A.8).

Table 6.4: Mann-Kendall and simple linear regression trend test results for cold season median wet day WBZ height at the ten rawinsonde sites. Significant deviations from the null hypothesis (i.e., no trend) are indicated by p-values in parenthesis and simple linear fits for cold season 1958 (the beginning of the period of record) are given in the $\hat{Y}[1958]$ column.

Location Code	**τ**	b_1 **(m dec^{-1})**	$\hat{Y}[1958]$ **(msl)**
TUS	-0.04	-2.26	2458
SLC	0.09	28.2	1664
ABQ	0.24 (p<0.05)	65.38 (p<0.01)	2214
GJT	0.22 (p<0.05)	27.77	1984
BOI	-0.02	-0.58	1531
OAK	-0.08	-3.80	1756
VGB	0.01	0.71	2237
MFR	0.11	20.36	1593
SLE	0.09	11.34	1350
OTX/GEG	-0.02	3.90	1124

A notable contrast between the trends in temperature/thickness and the trends in WBZ heights is the significant positive trends in WBZ heights at Grand Junction, CO and Albuquerque, NM (Figure 6.8). The rawinsonde site at Grand Junction, CO is adjacent to NCEP/NCAR reanalysis grids that display decreases (some significant with 95% confidence in northern Colorado and southern Wyoming) in winter wet day values of temperature/thickness (Figures 6.1 and 6.2). Similarly, the rawinsonde site at Albuquerque, NM is adjacent to NCEP/NCAR reanalysis grids that display decreases (although insignificant) in winter wet day 850 hPa temperature, 850–700 hPa thickness and 1000–850 hPa thickness (Figures 6.1 and 6.2). As with the temperature/thickness analysis, the trends in the wet day WBZ height data do not appear to be explained by trends in the percentage of sampled wet days per winter occurring in December-February (Figure A.9). As this latent variable does not appear to account for the contrasting results

between the WBZ height and temperature/thickness analyses in Colorado and New Mexico, trend results for the estimated snow levels in the Upper Rio Grande watershed and the Colorado Headwaters watershed discussed in the next section can strengthen the findings of either of these two contrasting data sources.

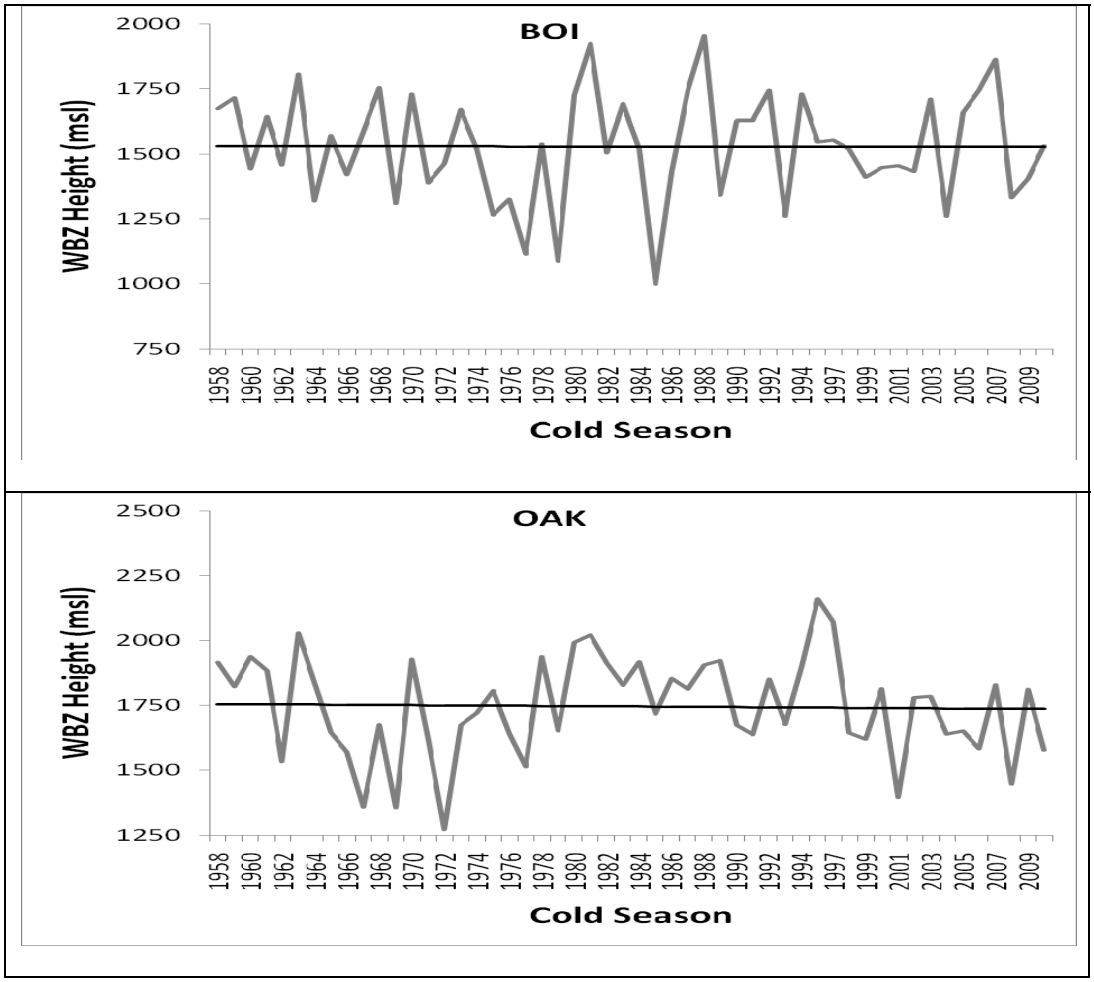

Figure 6.3: Cold season median 0000 UTC WBZ heights (thick gray line) and simple linear fits (thin black line) for the rawinsonde sites near Boise, ID and Oakland, CA. Refer to Table 6.4 for details about each time series.

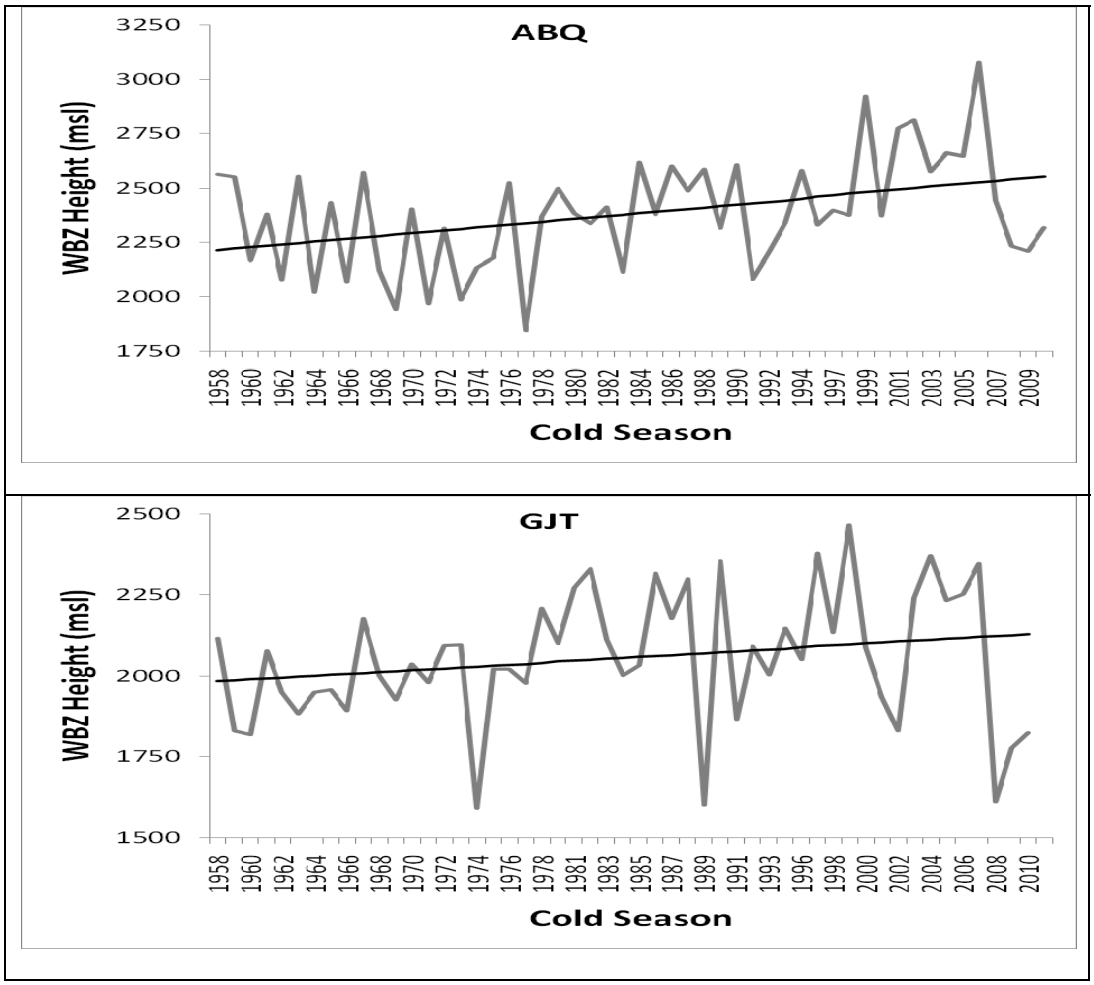

Figure 6.4: As in Figure 6.3 but for the rawinsonde sites near Albuquerque, NM and Grand Junction, CO.

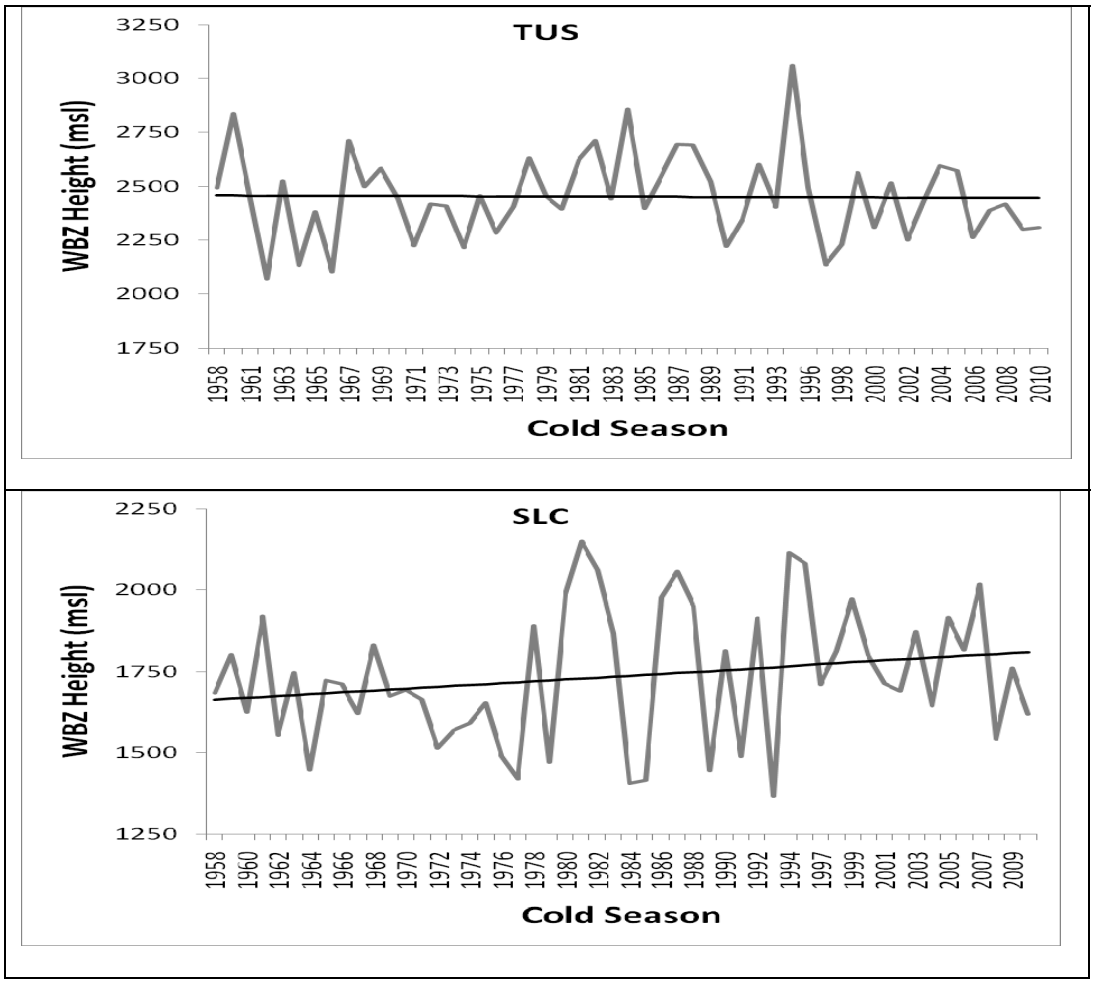

Figure 6.5: As in Figure 6.3 but for the rawinsonde sites near Tucson, AZ and Salt Lake City, UT.

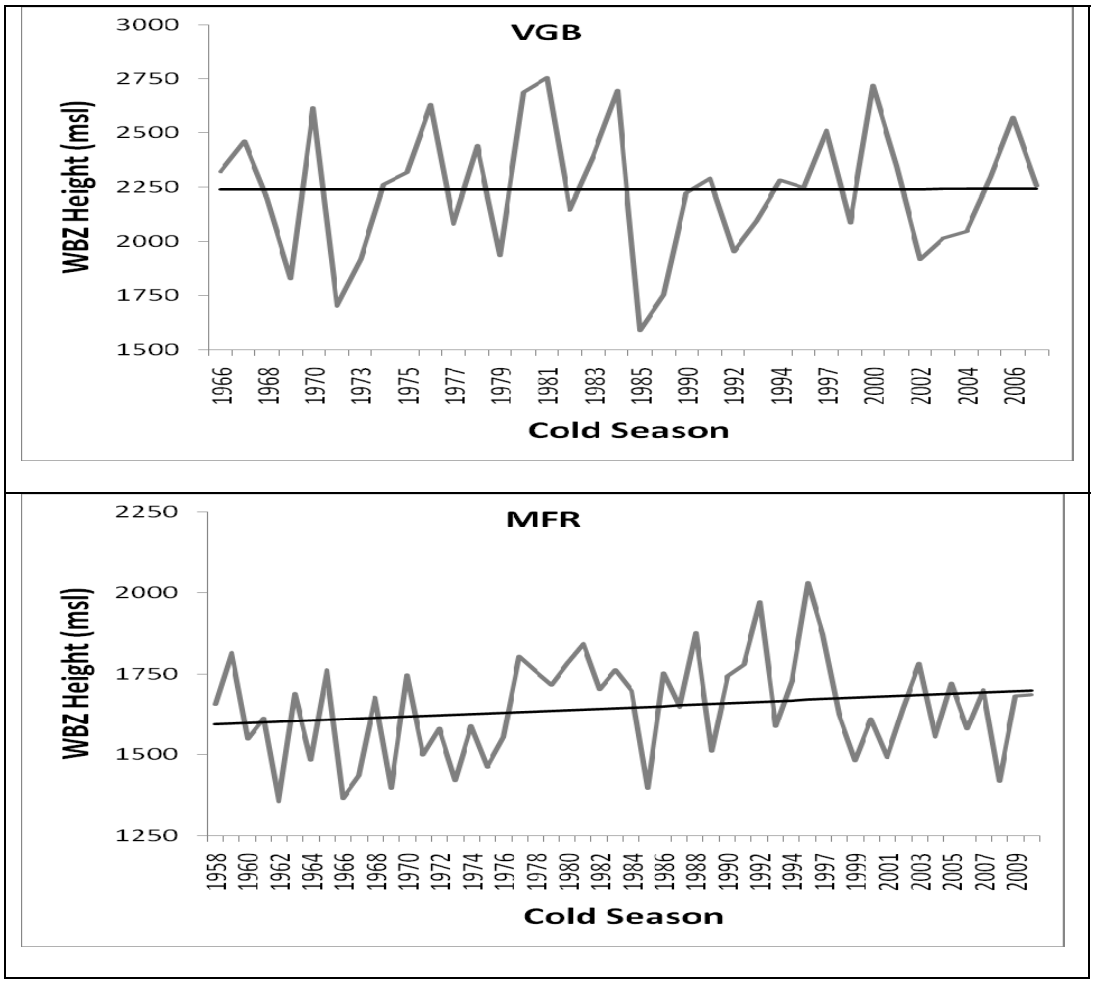

Figure 6.6: As in Figure 6.3 but for the rawinsonde sites near Vandenberg Air Force Base, CA and Medford, OR.

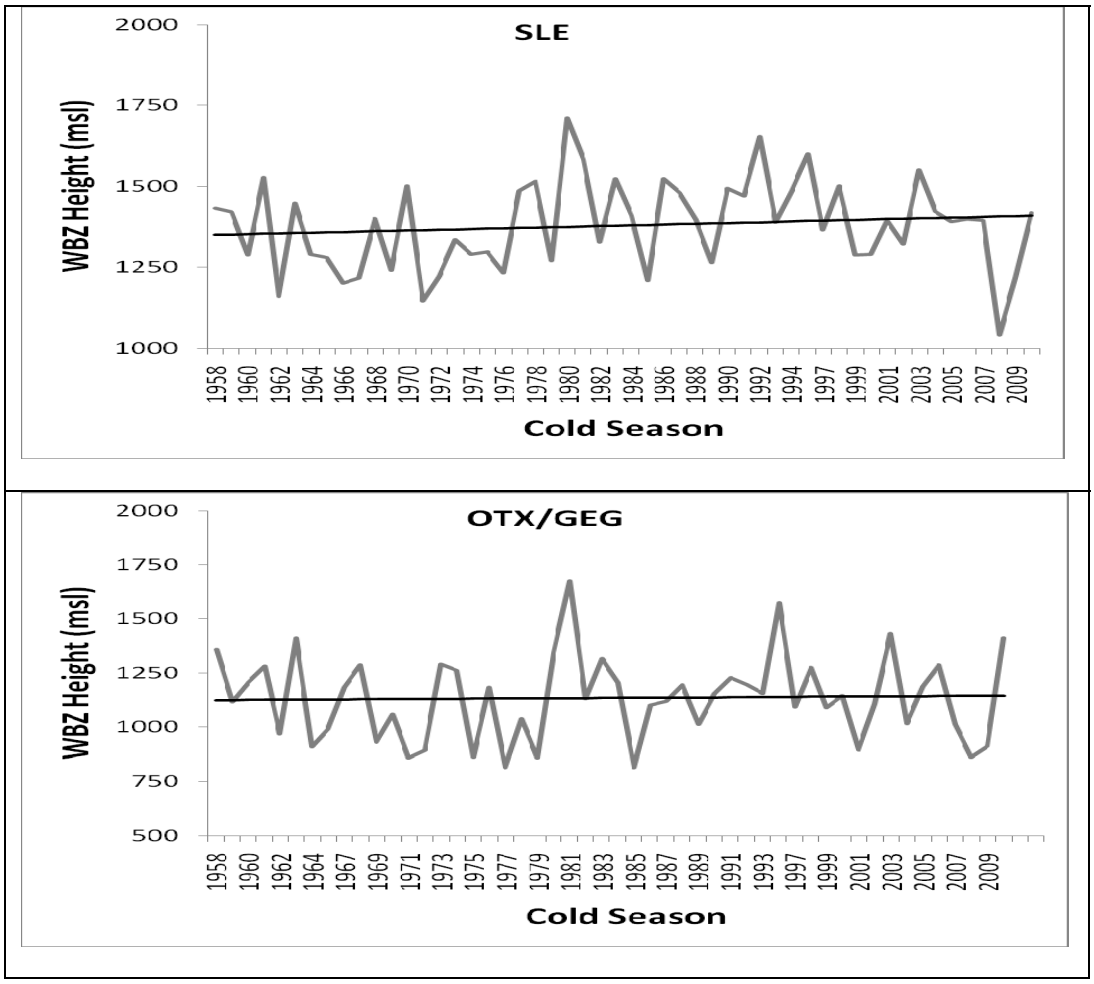

Figure 6.7: As in Figure 6.3 but for the rawinsonde sites near Salem, OR and Spokane, WA.

Figure 6.8: From 1958-2009, trends in cold season median wet day 0000 UTC WBZ height for simple linear regression (b_1) (a) and Mann-Kendall trend test (τ) (b). Black (white) circles indicate positive (negative) trends. For simple linear regression (left), large circles indicate $|b_1|$ >40.0 m dec^{-1} , medium circles indicate 20.0<$|b_1|$ ≤40.0 m dec^{-1} , and small circles indicate 0.0<$|b_1|$ ≤20.0 m dec^{-1}. For Mann-Kendall test (right), large circles indicate $|\tau|$ >0.2, medium circles indicate 0.1<$|\tau|$ ≤0.2, and small circles indicate 0.0<$|\tau|$ ≤0.1. Significant trends (p<0.05) are indicated by ×.

Table 6.5: Mann-Kendall (τ) and simple linear regression (b_1) trend test results for the ten watersheds. Significant deviations from the null hypothesis (i.e., no trend) are indicated by p-values in parenthesis. Simple linear fits for cold season 1925 are given in the $\hat{Y}[1925]$ column (note: for the sake of comparability, the fits are extrapolated for some time series as not all time series extend back to 1925, see Table 3.3). Blank cells indicate nearly constant time series at 100%. Regressions for which the error normality assumption was rejected at the 0.05 significance level are indicated by @, regressions for which the constant error variance assumption was rejected are indicated by #, and regressions with first-order positively autocorrelated error terms are indicated by $. Note, the slopes for the autocorrelated time series are derived from a first-order autoregressive model (4.26) which relieved autocorrelation in all cases.

	Elev (msl)	**τ**	b_1 **(% dec^{-1})**	$\hat{Y}[1925]$ **(%)**
Salt/Lower Verde	374	-	-	-
	524-555	-	-	-
	674-677	-	-	-
	807	0.04	0.10$^{@}$	96.39
	1054	0.05	0.19$^{@}$	95.01
	1085	0.32 (p<0.01)	1.80 (p<0.01)$^{@}$	83.04
	1268	0.46 (p<0.01)	5.66 (p<0.01)	55.88
	1560	0.40 (p<0.01)	5.95 (p<0.01)	27.84
	1984	0.27 (p<0.01)	4.23 (p<0.01)	11.55
	2146	0.35 (p<0.01)	5.32 (p<0.01)$^{\#}$	1.03
	2441	0.21 (p<0.01)	1.55$^{@\#\$}$	1.55
	Elev (msl)	**τ**	b_1 **(% dec^{-1})**	$\hat{Y}[1925]$ **(%)**
Weber/Jordan	1302	0.23 (p<0.01)	2.29 (p<0.01)	55.70
	1512	0.22 (p<0.01)	2.23 (p<0.01)	33.72
	1557	0.13	1.30	31.29
	1652	0.12	1.31 (p<0.05)	23.26

Table 6.5 Continued

	1701	0.01	0.30	21.43
	1817	0.15	1.20 (p<0.05) [#]	13.31
	1953	0.25 (p<0.01)	1.25 (p<0.01) [#]	8.93
	2655	0.07	0.10[@]	0.62
Upper Rio Grande	**Elev (msl)**	**τ**	**b_1 (% dec^{-1})**	$\hat{Y}$[1925] **(%)**
	1695	0.33 (p<0.01)	2.51 (p<0.01) [$]	25.69
	1862	0.24 (p<0.01)	1.84 (p<0.01) [$]	18.93
	2122	0.22 (p<0.01)	1.37 (p<0.01)	12.18
	2234	0.07	0.21[@]	4.51
	2457	-0.03	-0.06[@]	4.52
Colorado Headwaters	**Elev (msl)**	**τ**	**b_1 (% dec^{-1})**	$\hat{Y}$[1925] **(%)**
	1365	0.18 (p<0.05)	1.36 (p<0.05)	45.88
	1475	0.17 (p<0.05)	1.00 (p<0.05)	36.55
	1752	0.21 (p<0.05)	1.92 (p<0.01) [$]	24.60
	1901	0.22 (p<0.01)	1.33 (p<0.05) [$]	17.06
	2060	0.23 (p<0.01)	0.83 (p<0.01) [@]	4.83
	2411	0.08	0.13	2.39
	2679	0.00	-0.01[@]	0.61
	Elev (msl)	**τ**	**b_1 (% dec^{-1})**	$\hat{Y}$[1925] **(%)**
	722	0.14	1.50 (p<0.05)	50.52

Table 6.5 Continued

South Salmon/Payette/Weiser	893	0.30 (p<0.01)	3.28 (p<0.01)	35.94
	1176	0.22 (p<0.01)	1.80 (p<0.01)	17.79
	1533	0.06	0.00	8.97
	1797	0.24 (p<0.01)	0.58 (p<0.01)	4.63
San Joaquin	**Elev (msl)**	**τ**	**b_1 (% dec^{-1})**	$\hat{Y}$[1925] **(%)**
	532	0.37 (p<0.01)	1.94 (p<0.01) [@]	83.58
	606	0.24 (p<0.01)	1.74 (p<0.01) [@#]	81.21
	801	0.33 (p<0.01)	2.42 (p<0.01) [@#]	76.20
	1179	0.07	0.40	53.24
	1210	0.13	1.20	41.66
	1377	0.15	1.70 (p<0.05)	30.67
Ventura-San Gabriel/Santa Ana	**Elev (msl)**	**τ**	**b_1 (% dec^{-1})**	$\hat{Y}$[1925] **(%)**
	402	0.22 (p<0.01)	0.47[@#$]	92.83
	792	0.27 (p<0.01)	0.94[@$]	89.03
	933	0.33 (p<0.01)	2.12 (p<0.01) [@]	79.02
	1523	0.23 (p<0.01)	3.45 (p<0.01)	43.89
	2060	0.15	1.86[#$]	15.94
	Elev (msl)	**τ**	**b_1 (% dec^{-1})**	$\hat{Y}$[1925] **(%)**
	201	0.24 (p<0.01)	0.89 (p<0.05) [@#$]	90.95

Table 6.5 Continued

Middle/Upper Rogue	280	0.25 (p<0.01)	0.86 (p<0.05) [@#$]	89.75
	532	0.37 (p<0.01)	2.04 (p<0.01) [@#$]	80.29
	755	0.30 (p<0.01)	2.79 (p<0.01) [#$]	64.35
	Elev (msl)	**τ**	**b_1 (% decade^{-1})**	$\hat{Y}$[1925] **(%)**
North Santium/Molalla-Pudding/Clackamas	124	0.27 (p<0.01)	0.88 (p<0.01) [@#$]	92.15
	228	0.38 (p<0.01)	1.52 (p<0.01) [@#$]	85.69
	341	0.36 (p<0.01)	2.00 (p<0.01) [#$]	79.20
	731	0.25 (p<0.01)	1.75 (p<0.05) [$]	58.35
	Elev (msl)	**τ**	**b_1 (% decade^{-1})**	$\hat{Y}$[1925] **(%)**
Pend Orielle/Priest/ Pend Orielle Lake	402	-0.22 (p<0.01)	-1.87 (p<0.01)	55.27
	500	-0.21 (p<0.01)	-1.63 (p<0.01)	47.31
	539	-0.19 (p<0.05)	-1.44 (p<0.05)	41.64
	651	-0.18 (p<0.05)	-1.27 (p<0.05) [@]	37.15
	725	-0.14	-1.06[$]	30.59

6.4 Trends in Estimated Snow Levels

The simple linear fits for cold season 1925 (i.e., $\hat{Y}[1925]$) highlight the inter-watershed consistency of the COOP snow level approximation method (Table 6.5) yielding similar percentages of wet days per winter with snow level estimated as above (i.e., the watershed percentages) similar elevations at similar latitudes. For example, for elevations ranging from~1500 msl to ~2700 msl, $\hat{Y}[1925]$ ranges from ~34% to 0.62% for the Weber/Jordan watershed and from ~37% to 0.61% for the Colorado Headwaters watershed, interior mountain watersheds at similar latitudes (Table 6.5). With the exception of the South Salmon/Payette/Weiser watershed, the watersheds display time series of percentages with non-normal error distributions or inconstant error variance (Table 6.5). This is expected, considering that many of the time series representing relatively low elevations (high elevations) are bounded by 100% (0%). Therefore, more weight should be given to the Mann-Kendall trend results for these time series (Table 6.5). Additionally, the Durbin-Watson test revealed numerous time series with error terms that are first-order autocorrelated (Table 6.5); however, the Hildreth-Lu procedure successfully removed the autocorrelation in all cases.

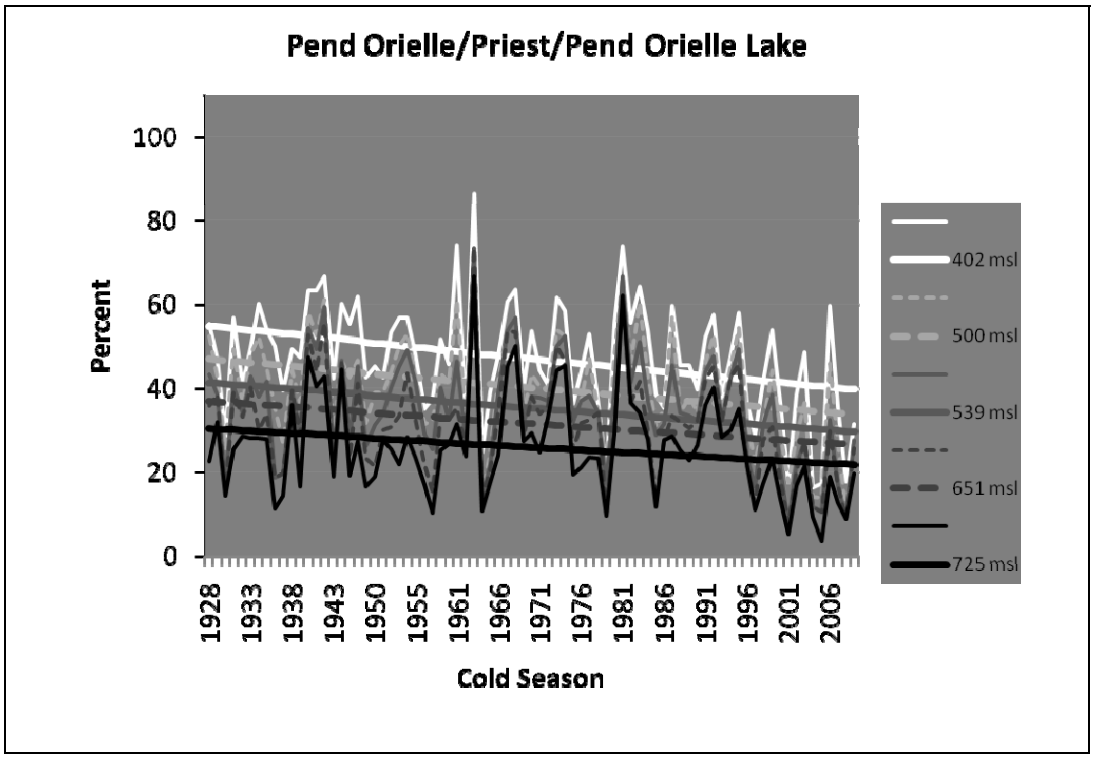

Fig 6.9: For the Pend Orielle/Priest /Pend Orielle Lake watershed, observed time series (thin lines) and simple linear regression fits (thick lines) of the percentage of wet days per cold season with snow level estimated above the specified elevations.

Highly significant (two-sided $p < 0.01$) increasing trends (Table 6.5) in watershed percentages are evident for all watersheds except the Pend Orielle/Priest/Pend Orielle Lake watershed located near Spokane, WA which only displays highly significant decreasing trends (Figure 6.9). The prominence of increasing trends is consistent with the temperature/thickness results and WBZ height results as increased temperature in vertical layers of the atmosphere and increased heights of the wet-bulb freezing level would suggest increases in the elevation at which rain transitions to snowfall. The largest trends within each watershed range from 1.92 % dec^{-1} (two-sided $p < 0.01$) at an elevation of 1752 msl in the Colorado Headwaters watershed to 5.95 % dec^{-1} (two-sided $p < 0.01$) at an elevation of 1560 msl in the Salt/Lower Verde watershed in Arizona (Table 6.5).

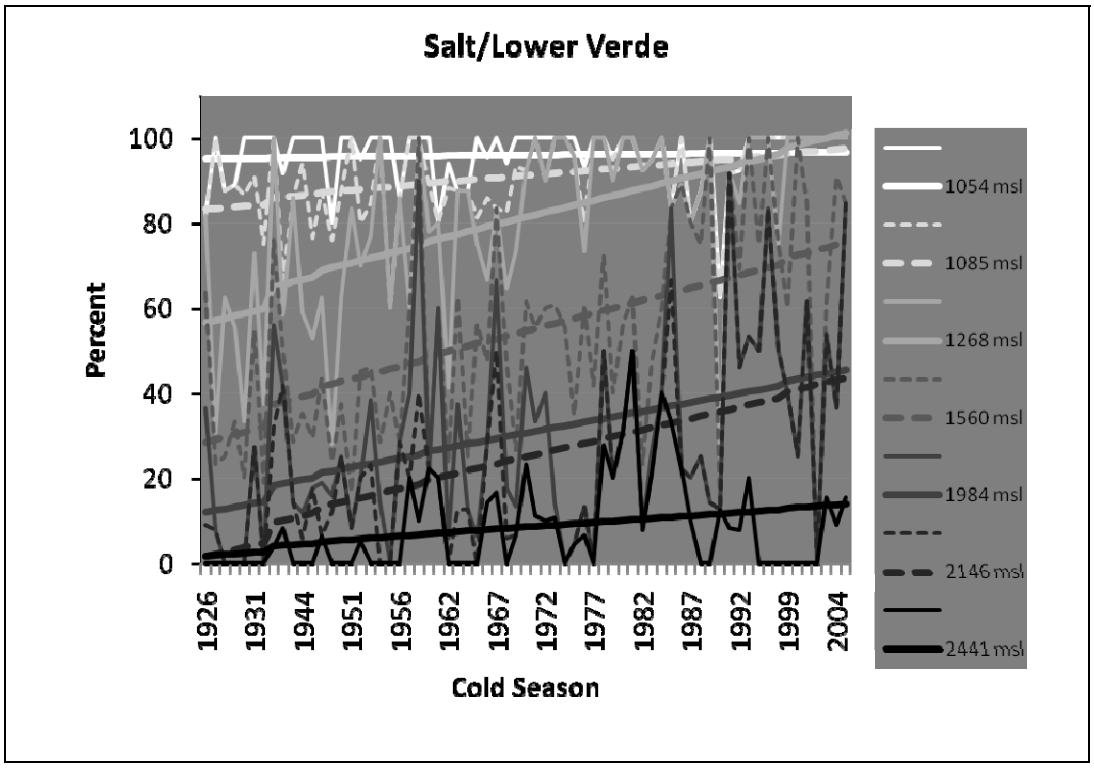

Fig 6.10: As in Figure 6.9 but for the Salt/Lower Verde watershed. The four lowest elevation stations are not shown as the large majority of cold seasons display values of 100%.

For many watersheds, the magnitude and significance of the increasing trends is obviously dependent on elevation. In Salt/Lower Verde watershed in Arizona, the largest and most significant increases are found between 1085 msl and 2146 msl (Table 6.5; Figure 6.10). This suggests that snowfall was too rare throughout the period of record at lower elevations (<1085 msl) for significant trends to be discerned and that estimated snow levels did not consistently reach high enough elevations (>2146 msl) for significant trends to be discerned. This same pattern is apparent for the Venture-San Gabriel/Santa Ana watershed in southern California (Table 6.5; Figure 6.11). Similarly, trends are least evident at the highest elevations of the Weber/Jordan watershed (Table 6.5; Figure 6.12), the Upper Rio Grande watershed (Table 6.5; Figure 6.13), the Colorado Headwaters watershed (Table 6.5; Figure 6.14). Trends are evident throughout the entire range of sampled elevations in the South Salmon/Payette/Weiser watershed (Table 6.5; Figure 6.15), the San Joaquin watershed (Table 6.5; Figure 6.16), the Middle/Upper Rogue watershed (Table 6.5; Figure 6.17), and the North Santium, Molalla-Pudding, Clackamas watershed (Table 6.5; Figure 6.18).

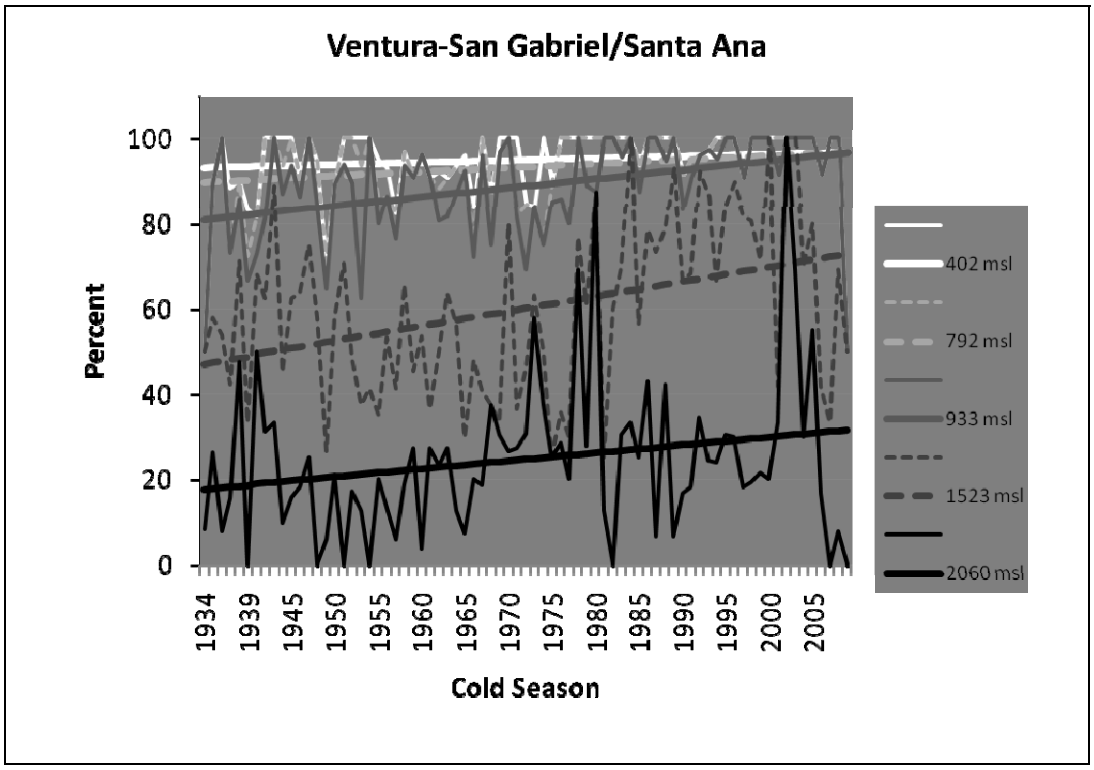

Fig 6.11: As in Figure 6.9 but for the Ventura-San Gabriel /Santa Ana watershed.

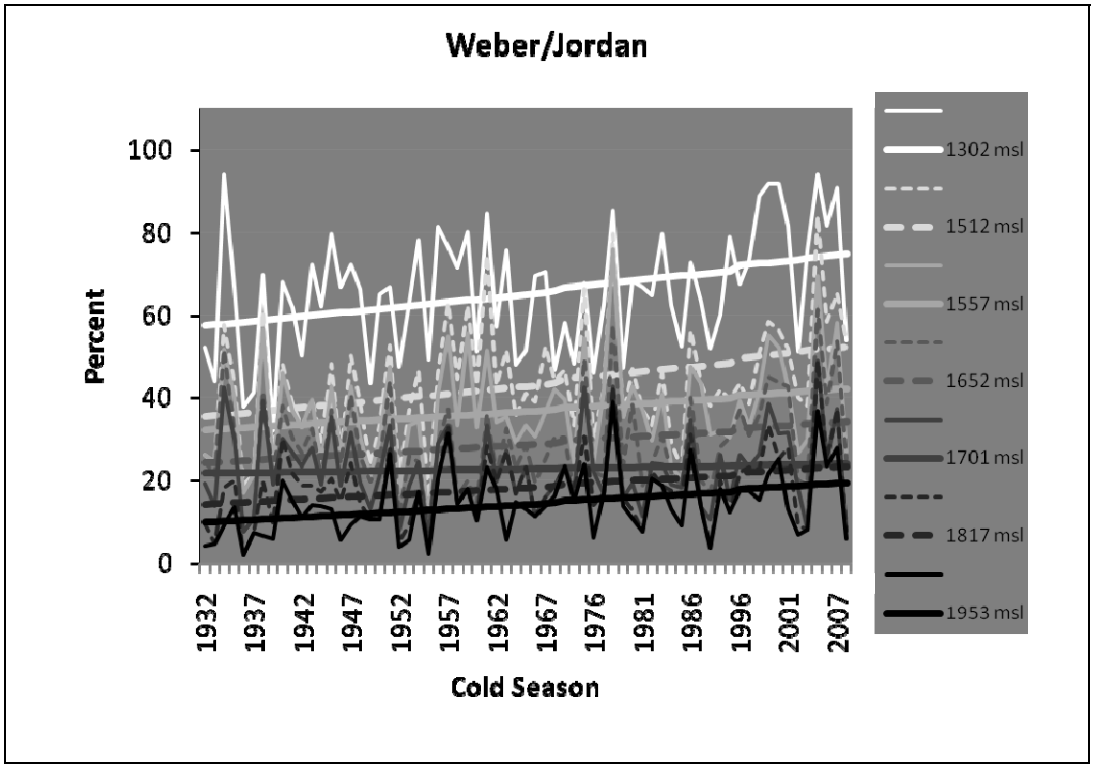

Fig 6.12: As in Figure 6.9 but for the Weber/Jordan watershed. The highest elevation station (2655 msl) is not shown as the large majority of cold seasons display values near 0%.

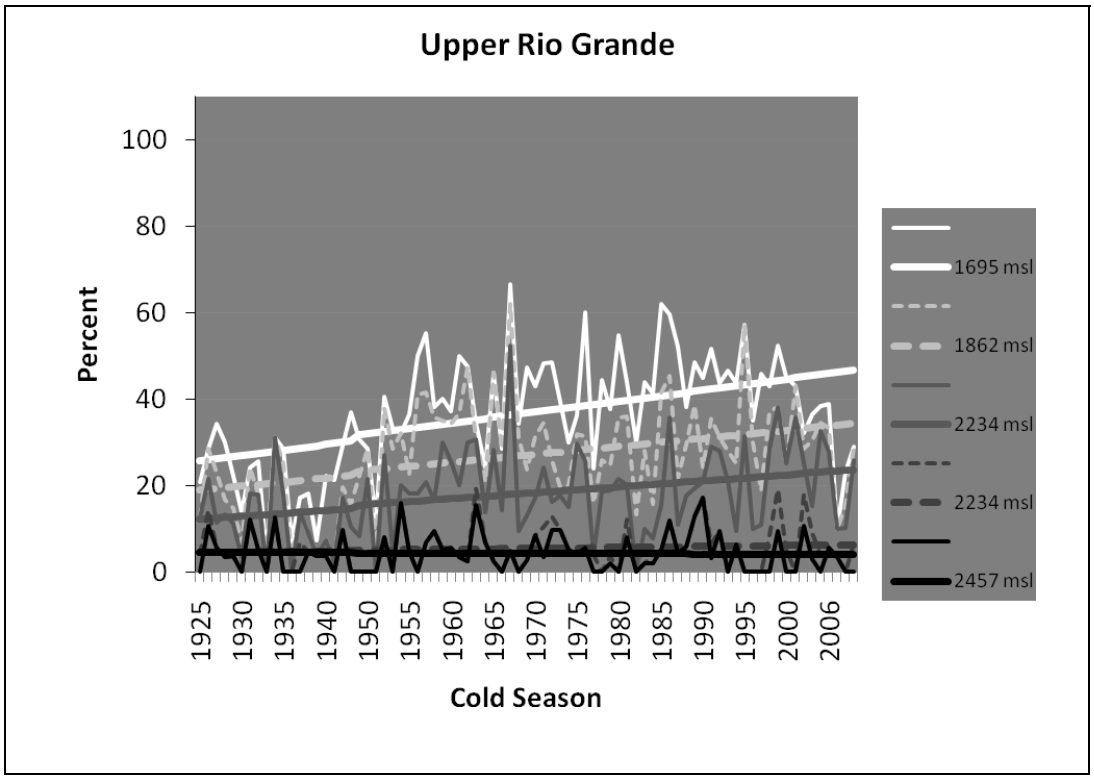

Fig 6.13: As in Figure 6.9 but for the Upper Rio Grande watershed.

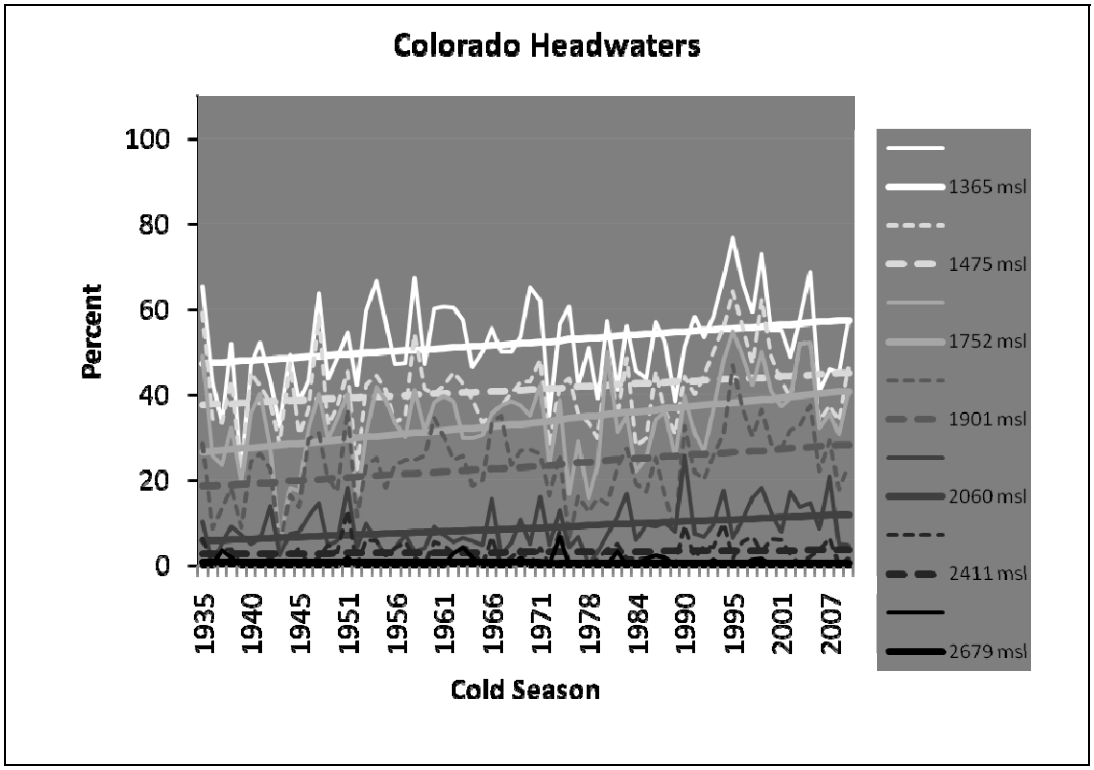

Fig 6.14: As in Figure 6.9 but for the Colorado Headwaters watershed. The elevations correspond to the lower bound of the elevation ranges in Table 6.5.

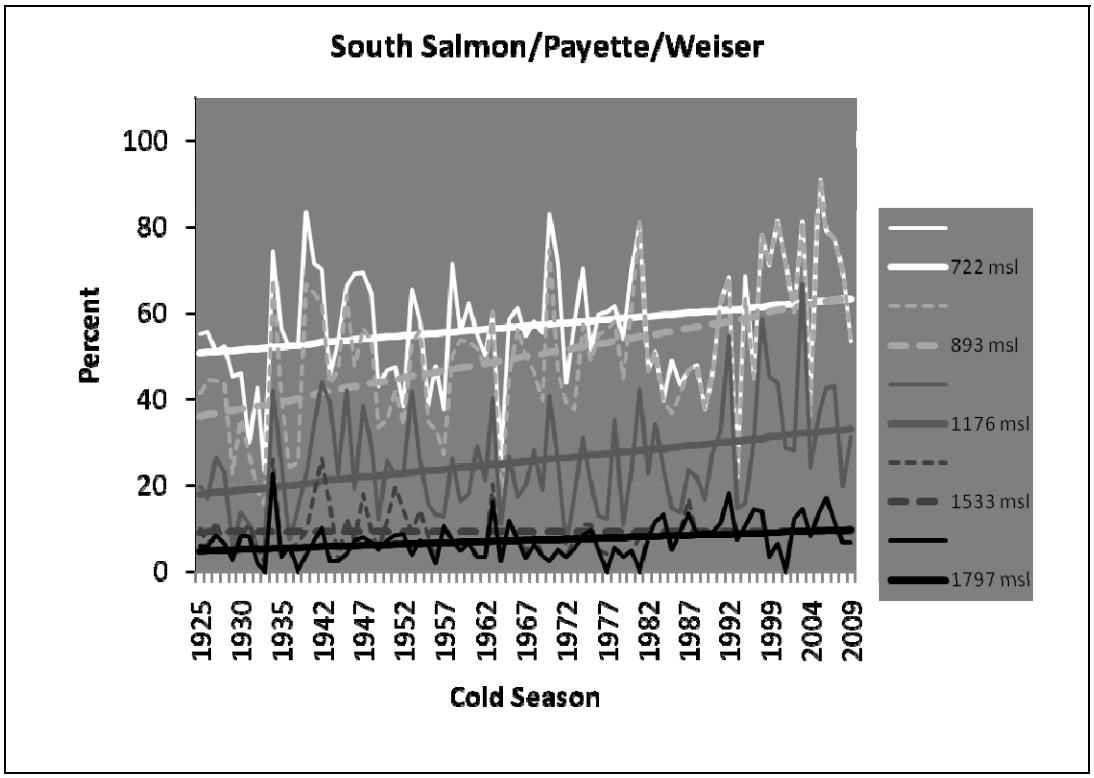

Fig 6.15: As in Figure 6.9 but for the South Salmon/Payette/Weiser watershed.

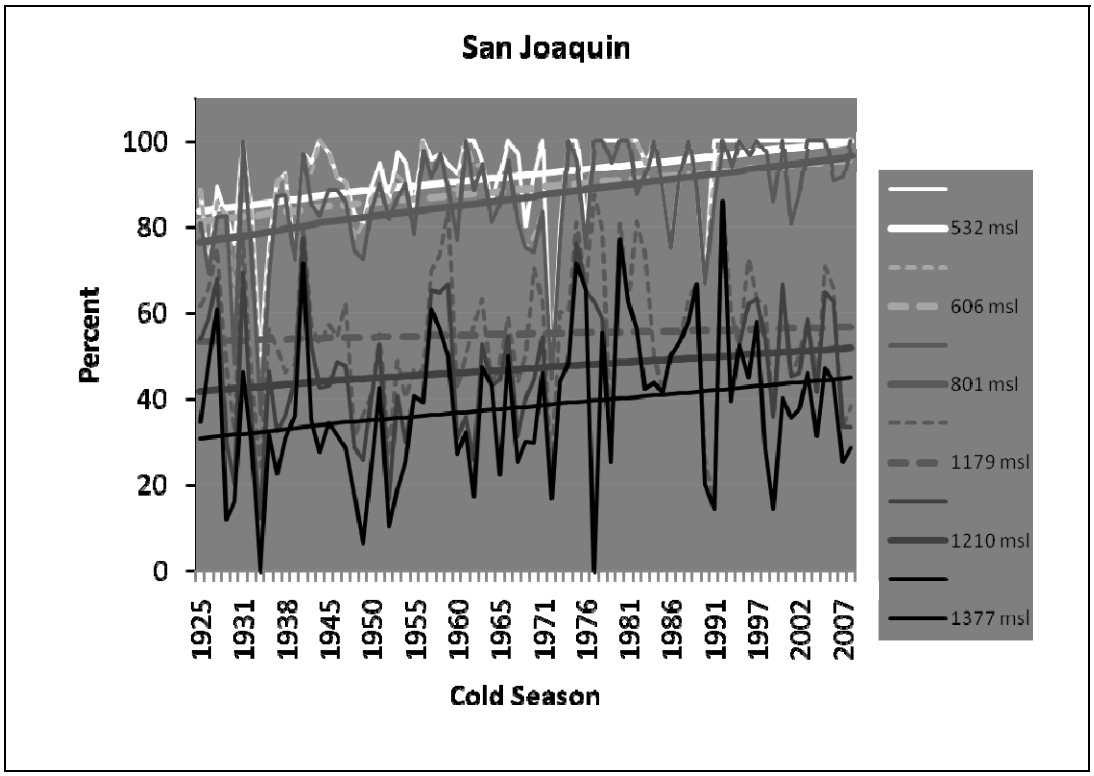

Fig 6.16: As in Figure 6.9 but for the San Joaquin watershed.

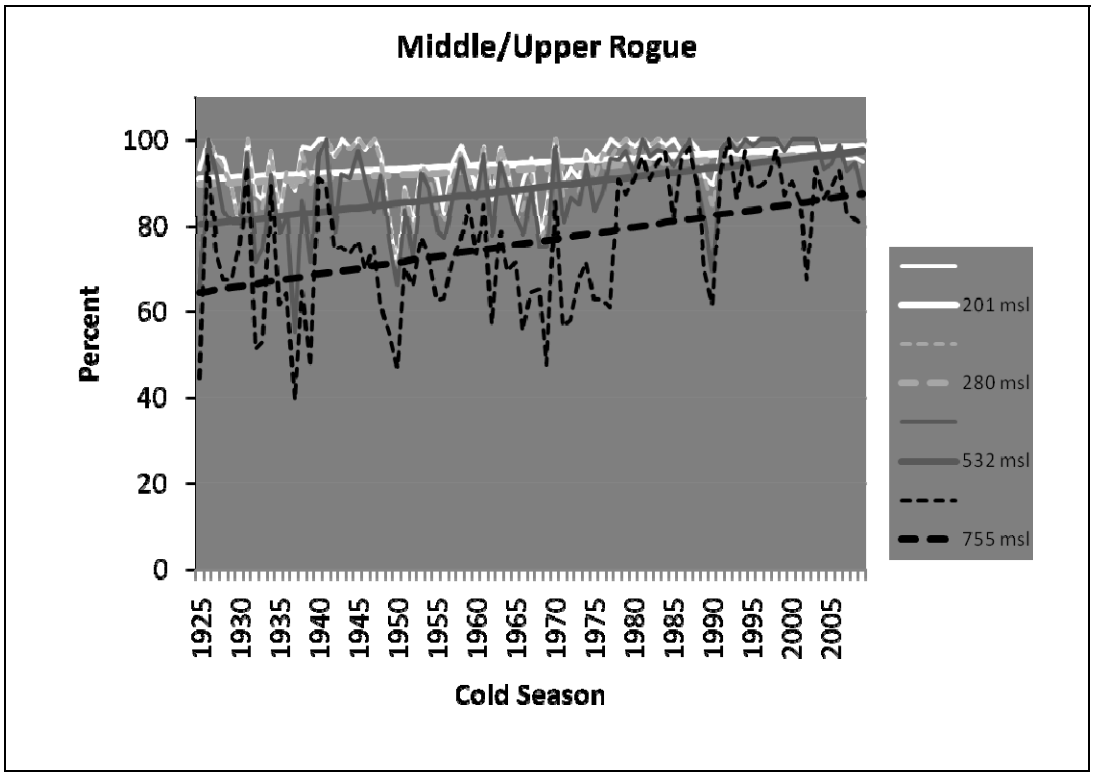

Fig 6.17: As in Figure 6.9 but for the Middle/Upper Rogue watershed.

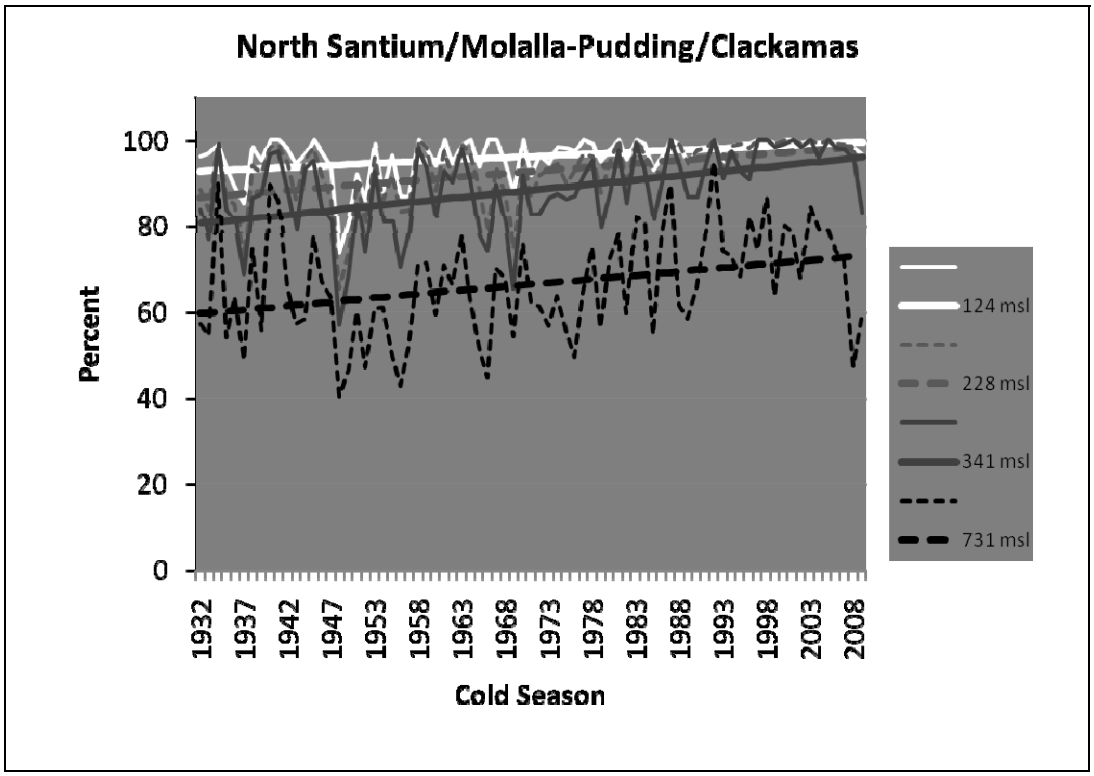

Fig 6.18: As in Figure 6.9 but for the North Santium/Molalla-Pudding/Clackamas watershed.

As seen in Figure A.10, for eight out of the 10 watersheds, there appear to be slight decreases in the percentage of cold season snow levels estimated during the height of winter (i.e., December-February). These decreases appear to be substantial for the Salt/Lower Verde watershed, the South Salmon/Payette/Weiser watershed and the Ventura-San Gabriel/Santa Ana watershed (Figure A.10). While it is certainly possible that the decreases in the percentage of snow levels estimated during December-February may have amplified the magnitude of the numerous increasing trends, I argue that this is not the sole cause of these trends for two reasons. First, the decreases in the percentage of estimated snow levels during December-January (Figure A.10) are much less apparent than the increases in the watershed percentages (Figures 6.10-6.18). Second, for all watersheds, the percentage of snow levels estimated during December-January remained greater than 50% throughout the periods of record (according to the simple linear fits), therefore, one would expect that similar analyses focusing strictly on snow levels estimated during December-February would yield similar results.

6.5 Similarities in the Three Trend Analyses

Several key results have been identified in the trend analyses that are consistent between at least two of the three snow level quantification measures (i.e., the temperature/thickness variables, WBZ heights, and watershed percentages).

(1) Over the western US as whole, the trend analyses from the three different snow level quantification methods are consistent with one another. Specifically, significant increasing trends are evident in measures of the temperature of the vertical layers of the atmosphere (i.e., temperature/thickness), wet-bulb temperature freezing level (WBZ height), and estimated snow levels (watershed percentages).

(2) Significant increasing trends are apparent for WBZ heights and watershed percentages in Colorado (Grand Junction and Colorado Headwaters watershed) and New Mexico (Albuquerque and Upper Rio Grande watershed).

(3) Significant increasing trends are apparent for watershed percentages and temperature/thickness at adjacent NCEP/NCAR reanalysis grids in California (Ventura-San Gabriel/Santa Ana watershed as well as the San Joaquin watershed), Utah (Weber/Jordan watershed), and Oregon (Middle/Upper Rogue as well as the North Santium, Molalla-Pudding, Clackamas watershed). In these areas, trends in WBZ heights are insignificant.

There are two major contrasting results in the trend analyses from the three different snow level quantification methods.

(1) The significant increasing trends in WBZ heights and watershed percentages in Colorado (Grand Junction and Colorado Headwaters watershed) are adjacent to NCEP/NCAR reanalysis grid displaying significant decreasing trends in temperature/thickness.

(2) The reanalysis grids over northeastern Washington and northern Idaho display significant increases in thickness/temperature yet the Pend Orielle, Priest, and Pend Orielle Lake watershed near Spokane, WA displays significant decreases in watershed percentages.

Considering the evidence for increasing trends in WBZ heights and watershed percentages in Colorado/New Mexico and the increasing trends in WBZ heights and significantly increasing watershed percentages in Oregon (adjacent to Washington), it is likely that the decreasing temperature/thickness in southern Wyoming/northern Colorado and the decreasing watershed percentages in the Pend Orielle, Priest, and Pend Orielle Lake watershed near Spokane, WA are spuriously significant.

Lastly, there does not appear to be a discernable spatial pattern in the convergent results from trend analyses. While there is some evidence for significant clustering of increasing trends in temperature/thickness in the Pacific Northwest (Figure 6.2), the highly insignificant WBZ height

trends at Spokane, WA and the decreasing trends in watershed percentages over the Pend Orielle, Priest, and Pend Orielle Lake watershed do not support this cluster of increasing temperature/thickness. Similarly, the cluster of decreasing trends in temperature/thickness in southern Wyoming and northern Colorado (Figure 6.2) is in contrast to the significantly positive trends in WBZ heights at Grand Junction, CO and watershed percentages in the Colorado Headwaters watershed.

6.6 Discussion

The convergent results from the three measures of interannual snow level variability discussed in the Section 6.5 suggest increasing snow levels across much of the western US. These findings are consistent with a large body of literature documenting both increasing winter temperature over the western US and decreasing snowfall likely due to increasing frequencies of rainfall events during winter (e.g., Vincent et al. 1999; Barnett et al. 2005; Knowles et al. 2006; Feng and Hu 2007; Barnett et al. 2008 Pierce et al. 2008; Raushcer et al. 2008; Hidalgo et al. 2009). Specifically, from 1979-2005 linear trends in December-January surface air temperature range from +0.1 - +0.9°C dec^{-1} (IPCC 2007). Numerous researchers have attributed this warming to decreases in western US snowpack (e.g., Hamlet et al. 2005; Mote et al. 2008; Barnett et al. 2008 Pierce et al. 2008).

On a more related note, Knowles et al. (2006), as well as Feng and Hu (2007) recently analyzed trends in snowfall to rainfall ratios across the western and northern US. These investigators found wide spread decreasing trends over the western US that were most evident for locations with the highest warming rates and where temperatures were generally warm enough to change precipitation form (specifically, the Pacific Northwest and the Southwest). In the Rocky Mountains, however, the results from Knowles et al. (2006) and Feng and Hu (2007) were not nearly as conclusive. In this region, trends in snowfall to rainfall ratios were adjacent to increasing trends likely due to the high elevations of the measurement sites. Similar results were found by

Kunkel et al. (2009a) indicating decreasing snowfall totals across the Pacific Northwest and the Southwest along with both increasing and decreasing snowfall totals in the Rocky Mountains.

The results from these previous investigators support the increasing snow levels suggested by the results presented in Sections 6.2-6.4 above. Specifically, over the western US, one should expect increasing snow levels to coincide with widespread twentieth century warming and higher frequencies of rainfall at the expense of snowfall. As mentioned in Chapter 2, a shortcoming of the previous trend analysis of snowfall to rainfall ratios (i.e., Knowles et al. 2006; Feng and Hu 2007) is that the high elevations of the snowfall/precipitation measurement sites in the Rocky Mountains inhibited inferences about snow level elevation trends. The results presented in Section 6.3 and 6.4 above indicate predominantly increasing trends in snow level in the Rocky Mountains since ~1925 and supplement these previous investigations.

6.7 Conclusion

Through three separate methods of quantifying daily snow level and interannual snow level variability (WBZ heights, COOP snow level approximation for watersheds, upper-air reanalysis proxies), recent trends were established in the estimated snow levels from the watershed COOP stations, 850 hPa temperature, 850-700 hPa thickness, 1000-500 hPa thickness, 1000-850 hPa thickness and WBZ heights. Two major results aid in addressing the research question introduced in Chapter 1: *Do multi-decadal trends exist in the elevation of snow level, and if so, how do these vary across the western US?*

(1) Over the western US, there are significant (two-sided $p < 0.05$) increasing trends in measures of the temperature of vertical layers of the atmosphere (i.e., temperature/thickness), wet-bulb temperature freezing level (WBZ height), and estimated snow levels (watershed percentages) suggesting increasing snow level over the western US since ~1925.

(2) Convergent results from the three separate methods of snow level quantification do not support an obvious spatial pattern in snow level trend over the western US.

In the previous chapter, I established the interannual and decadal variability in snow level as linked to ENSO and PDO. In this chapter, multi-decadal increasing trends in snow level were established. In the following chapter, I explore the likelihood that the increasing trends in snow level are due to forcing independent of ENSO/PDO (i.e., possibly anthropogenic forcing).

Chapter 7: Are Trends in Snow Level Elevation Explained by Natural Climate Variability?

7.1 Introduction

The results from the previous chapter suggest multi-decadal increasing trends in snow level for much of the western United States. In this chapter, I seek to answer another question introduced in Chapter 1: *Are multi-decadal trends in snow level outside the realm of natural climate variability (e.g., variations in ENSO/PDO)?* I first establish the trends in temperature/thickness, WBZ heights, and estimated snow levels not accounted for by variations in ENSO. Similarly, in the ensuing section, trends in these three snow level measures are analyzed through the statistical removal of variations in both ENSO and PDO from the response variables, followed by a brief alternative control method through trend analyses during periods coincident with PDO phase changes. Lastly, I discuss the expected trends in snow level due to variations in ENSO and PDO alone in the context of the findings in Chapter 5 and those of previous investigators.

7.2 Trends with ENSO Variability Removed

As highlighted in Chapter 5, for many areas of the western US, Pearson product-moment correlation coefficients between normalized fall SOI and cold season median wet day temperature/thickness and 0000 UTC WBZ heights as well as COOP percentages (i.e., the percentage of winter wet days per cold season with snow level estimated above given elevations) indicate that normalized fall SOI accounts for a significant (two-sided $p < 0.05$) amount of variance in the interannual variability of the these snow level proxies. This was particularly evident in the Pacific Northwest and the Southwest (Figures 5.1, 5.14 and 5.16). Additionally, as highlighted in Chapter 6, increasing trends (many with two-sided $p < 0.05$) in temperature/thickness, WBZ heights, and COOP percentages are prevalent across the western US (Figures 6.1, 6.8, and 6.10-6.18).

Before a discussion of residual trend results, it is important to note that the results regarding the tests of error normality, constant error variance, and first-order error autocorrelation are virtually identical to those of the simple linear trend tests in Chapter 6 for all three snow level measures indicating that error-normality, constant error variance, and independent error terms are valid assumptions. The residuals resulting from the regression of a given snow level proxy against fall SOI represent the interannual variability in the proxy not accounted for by fall SOI. Over the western US as a whole, these residual trends in temperature/thickness remain field significant (pseudo $p < 0.05$) for all temperature/thickness measures for both the Mann-Kendall test and simple linear regression (Table 7.1). Additionally, these trends remain predominantly positive and trend magnitudes are reduced only slightly (e.g., a median of 0.07 K dec^{-1} (0.06 K dec^{-1}) over the 60 grids for the raw (residual) trends) while at least 8 out of the 60 grids display significant positive residual trends (Table 7.2 and 7.3). Lastly, the spatial variability in the residual trends in temperature/thickness (Figure 7.1) is nearly identical to the trends with fall SOI variability not removed (Figure 6.1), with increasing trends particularly apparent in the Pacific Northwest and the Southwest but evident in nearly all areas of the western US.

Table 7.1: Field significance of simple linear regression (SLR) and Mann-Kendall (MK) trend tests on the residuals resulting from regressing cold season median wet day temperature/thickness against fall SOI over the entire western US since 1949.

	SLR Field Significance	MK Field Significance
850 hPa Temperature	0.001	0.001
1000-850 hPa Thickness	0.029	0.017
850-700 hPa Thickness	0.001	0.001
1000-500 hPa Thickness	0.001	0.001

Table 7.2: Descriptive statistics for the simple linear regression trend tests on the residuals resulting from regressing cold season median wet day temperature/thickness against fall SOI at the 60 NCEP/NCAR reanalysis grid points since 1949.

	Median b_1 (K or gpm dec^{-1})	Max b_1 (K or gpm dec^{-1})	Min b_1 (K or gpm dec^{-1})	Number of grids with $b_1>0$	Number of grids with $b_1>0$ and two-sided $p<0.05$	Number of grids with $b_1<0$ and two-sided $p<0.05$
850 hPa Temperature	0.06	0.49	-0.71	40	9	3
1000-850 hPa Thickness	0.21	2.23	-3.14	37	5	2
850-700 hPa Thickness	0.70	2.83	-3.55	45	15	3
1000-500 hPa Thickness	2.80	9.82	-11.03	51	17	2

Table 7.3: As in Table 7.2 but for the Mann-Kendall trend test.

	Median τ	Max τ	Min τ	Number of grids with $\tau>0$	Number of grids with $\tau>0$ and two-sided $p<0.05$	Number of grids with $\tau<0$ and two-sided $p<0.05$
850 hPa Temperature	0.04	0.41	-0.27	37	8	4
1000-850 hPa Thickness	0.03	0.35	-0.23	38	6	2
850-700 hPa Thickness	0.09	0.35	-0.22	47	14	2
1000-500 hPa Thickness	0.12	0.34	-0.24	53	16	2

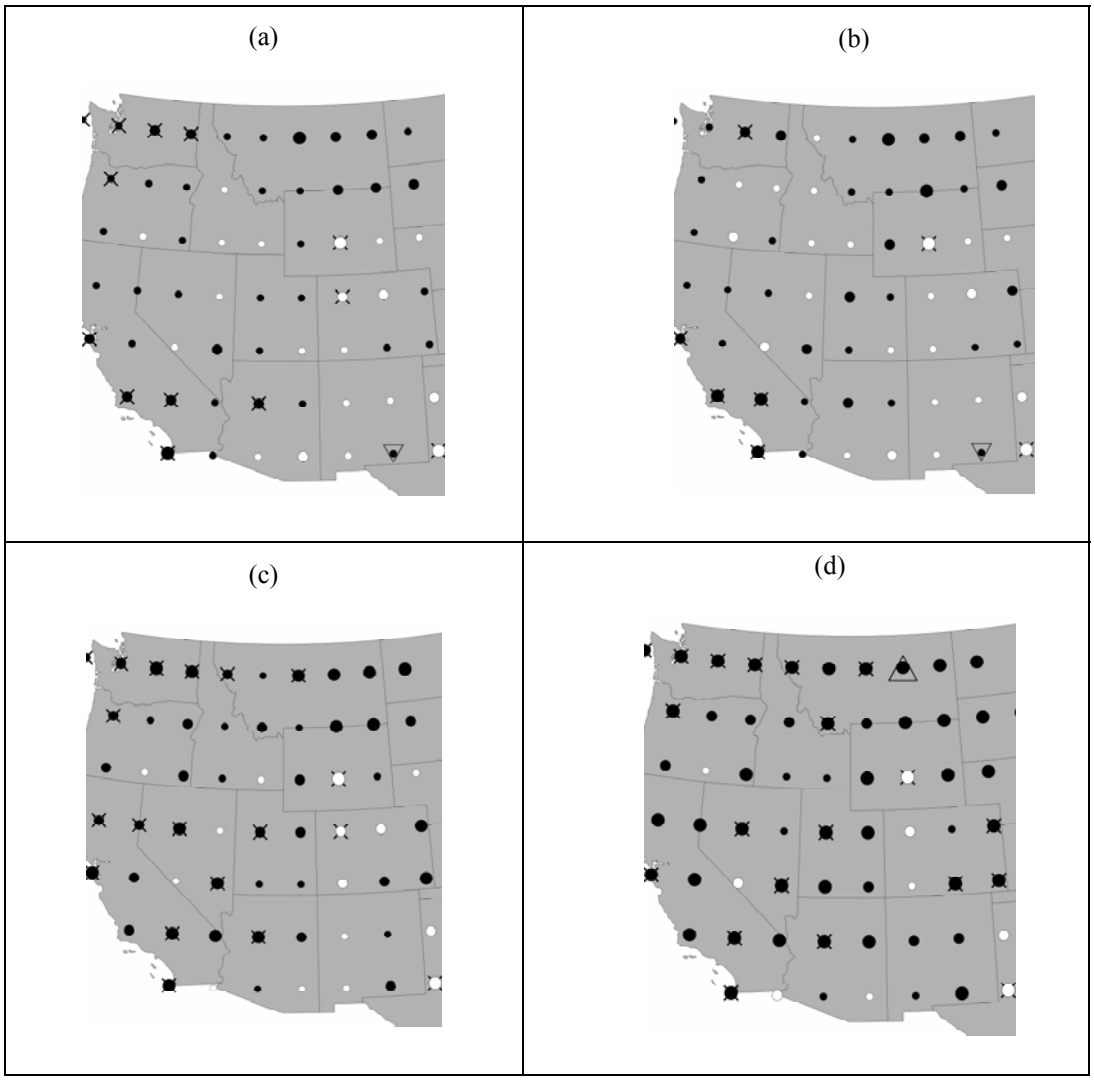

Figure 7.1: From 1949-2009, residual trends (b_1 for simple linear regression) in cold season median wet day values resulting from regressing 850 hPa temperatures (a), 1000-850 hPa thickness (b), 850-700 hPa thickness (c), and 1000-500 hPa thickness (d) against fall SOI. Black (white) circles indicate positive (negative) trends. For 850 hPa temperatures, large circles indicate $|b_1|$ >0.3 K dec^{-1}, medium circles indicate 0.15< $|b_1|$ ≤0.3 K dec^{-1}, and small circles indicate 0.0< $|b_1|$ ≤0.15 K dec^{-1}. For 1000-850 hPa thickness and 850-700 hPa thickness, large circles indicate $|b_1|$ >1.0 gpm dec^{-1}, medium circles indicate 0.5< $|b_1|$ ≤1.0 gpm dec^{-1}, and small circles indicate 0.0< $|b_1|$ ≤0.5 gpm dec^{-1}. For 1000-500 hPa thickness, large circles indicate $|b_1|$ >2.0 gpm dec^{-1}, medium circles indicate 0.1< $|b_1|$ ≤2.0 gpm dec^{-1}, and small circles indicate 0.0< $|b_1|$ ≤1.0 gpm dec^{-1}. Significant trends (two-sided p<0.05) are indicated by ×. Local Moran's I values jointly significant with 95% confidence indicating clustering of higher values are given by large triangles. Jointly significant local Moran's I indicating a high value surrounded by lower values are given by small inverted triangles.

Similar to the temperature/thickness residual trends, there is very little difference between the 0000 UTC WBZ height trend analyses with the raw data and with SOI variability removed (Table 6.4 and 7.4). Trends are positive at seven out of the ten rawinsonde locations and are significant (two-sided $p < 0.01$) at Albuquerque, NM (Table 7.4) with a slope of 65 m dec^{-1}. Similarly, each COOP station within each watershed that displayed significant (two-sided $p < 0.05$) positive trend in the raw percentage time series also displays significant positive trends in the residual time series (Table 7.5). Again, trend magnitudes are relatively unaffected by the removal of the SOI variability from the percentage time series. For example, the largest change in trend magnitude occurred at the COOP station that is ~1523 msl in the Ventura-San Gabriel/Santa Ana watershed which displayed a 3.45 % dec^{-1} increasing trend in the raw data and a 3.38 % dec^{-1} increasing trend in the SOI adjusted data. In summary, there is little evidence that the statistical removal of the variability in the response variables (i.e., the snow level measures) accounted for by normalized fall SOI results in a de-trending of the snow level measures.

Table 7.4: From 1958-2009, results for the Mann-Kendall and simple linear regression trend tests on the residuals resulting from regressing cold season median wet day 0000 UTC WBZ heights against fall SOI. Significant deviations from the null hypothesis (i.e., no trend) are indicated by * (two-sided $p<0.05$) and ** (two-sided $p<0.01$).

Location Code	**τ**	**Linear trend (m dec^{-1})**
TUS	-0.04	-2.22
SLC	0.14	28.66
ABQ	0.25 **	65.06 **
GJT	0.19	28.37
BOI	-0.03	-0.01
OAK	-0.08	-3.60
VGB	0.02	1.26
MFR	0.11	20.68
SLE	0.12	11.93
OTX/GEG	0.00	5.27

Table 7.5 From ~1925-2009, results for the Mann-Kendall and simple linear regression trend tests on the residuals resulting from regressing cold season percentages of estimated snow levels above the given elevations against fall SOI. Significant deviations from the null hypothesis (i.e., no trend) are indicated by two-sided p-values. Regressions for which the error normality assumption was rejected at the 0.05 significance level are indicated by @, regressions for which the constant error variance assumption was rejected are indicated by #, and regressions with first-order positively autocorrelated error terms are indicated by $. Note, the slopes for the autocorrelated time series are derived from a first-order autoregressive model (4.26) which relieved autocorrelation in all cases.

Watershed	**Elev (msl)**	**τ**	***Linear trend* (% dec^{-1})**
Salt/Lower Verde	1560	0.40 (p<0.01)	5.93 (p<0.01)
Weber/Jordan	1652	0.12	1.32 (p<0.05)
Upper Rio Grande	1862	0.24 (p<0.01)	1.84$^{\$}$ (p<0.01)
Colorado Headwaters	1475	0.16	1.01 (p<0.05)
South Salmon/Payette/Weiser	1176	0.21 (p<0.01)	1.81 (p<0.01)
San Joaquin	1377	0.15 (p<0.05)	1.69 (p<0.05)
Ventura-San Gabriel/Santa Ana	1523	0.24 (p<0.01)	3.38 (p<0.01)
Middle/Upper Rogue	755	0.35 (p<0.01)	2.99$^{@\#}$ (p<0.01)
North Santium/ Molalla-Pudding/ Clackamas	731	0.27 (p<0.01)	1.86 (p<0.01)
Pend Orielle/Preist/Pend Orielle Lake	500	-0.21 (p<0.01)	-1.64 (p<0.01)

7.3 Trends with ENSO and PDO Variability Removed

The multiple linear regression model (model 4.33) with normalized fall SOI (X_1), the PDO phase indicator variable (X_2=1 (0) if PDO is in a cold (warm) phase), and the SOI PDO interaction variable (i.e., $X_3 = X_1 * X_2$) results in a significant ($p < 0.05$) amount of explained variance in at least 16 of the 60 NCEP/NCAR grids for all thickness/temperature measures when PDO is assumed to be in a warm phase from 1977-2009 (Table 7.6) and when PDO is assumed to have transitioned to a cold phase in 1999 (Table 7.7). Given that normalized fall SOI is already in

model 4.33, the number of grids displaying significant ($p < 0.05$) additional variance explained in the interannual variability of each temperature/thickness measure by the addition of X_2 and X_3 into the model ranges from seven grids for 1000-850 hPa thickness assuming PDO is currently in a warm phase to 15 grids for 850-700 hPa thickness assuming PDO is currently in a warm phase and for 1000-850 hPa thickness assuming PDO is currently in a cold phase. This suggests that the addition of the PDO indicator and interaction variables are valuable predictors of temperature/thickness across the western US in that the additional explained variance may account for the observed trends.

Table 7.6: Assuming that the PDO has remained in its warm phase, descriptive statistics for the multiple linear regression model 4.33 results for temperature/thickness over the 60 NCEP/NCAR reanalysis grid points since 1949. b_1 is the estimated coefficient for fall SOI (X_1), b_2 is the estimated coefficient for the PDO phase indicator variable (X_2), and b_3 is the estimated coefficient for the interaction effects variable (i.e., X_3 , or the product of X_1 and X_2). Extra R^2 refers to the addition of X_2 and X_3 to the model with X_1 already included. Coefficient significance refers to two-sided p-values less than 0.05. For 850 hPa temperature, b_1 and b_3 are in units of K/normalized fall SOI and b_2 is in units of K. For the thickness measures, b_1 and b_3 are in units of m/normalized fall SOI and b_2 is in units of m.

	Number of significant grids		Number of grids with negative coefficients			Number of grids with significant negative coefficients			Number of grids with significant positive coefficients			Median				
	R^2	extra R^2	b_1	b_2	b_3	b_1	b_2	b_3	b_1	b_2	b_3	R^2	extra R^2	b_1	b_2	b_3
850 hPa Temperature	20	12	46	27	24	12	10	0	0	5	1	0.10	0.04	-0.24	0.04	0.07
1000-850 hPa Thickness	19	7	47	28	22	18	6	0	0	5	1	0.09	0.03	-1.41	0.43	0.43
850-700 hPa Thickness	20	15	47	43	21	13	14	0	0	3	2	0.09	0.03	-1.23	-1.32	0.78
1000-500 hPa Thickness	16	11	47	46	21	10	16	0	0	1	1	0.08	0.04	-3.64	-7.01	2.66

Table 7.7: As in Table 7.6 but assuming that the PDO entered a cold phase in 1999

	Number of significant grids		Number of grids with negative coefficients			Number of grids with significant negative coefficients			Number of grids with significant positive coefficients			Median				
	R^2	extra R^2	b_1	b_2	b_3	b_1	b_2	b_3	b_1	b_2	b_3	R^2	extra R^2	b_1	b_2	b_3
850 hPa Temperature	23	14	50	19	23	8	4	1	1	12	2	0.11	0.04	-0.30	0.46	0.06
1000-850 hPa Thickness	20	15	51	17	21	10	2	1	1	13	1	0.10	0.03	-1.67	1.87	0.39
850-700 hPa Thickness	21	14	48	23	21	9	7	1	1	8	3	0.10	0.04	-1.65	1.36	0.57
1000-500 hPa Thickness	17	10	49	26	22	6	6	1	1	7	3	0.08	0.04	-4.78	1.26	1.95

Table 7.8: Assuming that the PDO has remained in its warm phase, the multiple linear regression model 4.33 results for cold season median 0000 UTC WBZ heights and the trends in the resulting residuals since 1958. b_1 is the estimated coefficient for fall SOI (X_1), b_2 is the estimated coefficient for the PDO phase indicator variable (X_2), and b_3 is the estimated coefficient for the interaction effects variable (i.e., X_3 , or the product of X_1 and X_2). Extra R^2 refers to the addition of X_2 and X_3 to the model with X_1 already included. Coefficient significance refers to two-sided p-values. Significant values are indicated by * (p<0.05) and ** (p<0.01).

Location Code	R^2	Extra R^2	b_1 (m/SOI)	b_2 (m)	b_3 (m/SOI)	τ	Linear trend (m dec^{-1})
TUS	0.04	0.04	-22.79	-74.84	32.79	-0.12	-20.99
SLC	0.13 *	0.08	-61.45	-112.67	52.67	-0.01	0.07
ABQ	0.17 *	0.15 *	58.28	-203.23 **	-26.50	0.06	11.74
GJT	0.20	0.09	-74.90 *	-122.27 *	37.76	0.01	-3.16
BOI	0.10	0.01	-80.09 *	16.15	48.75	0.01	4.90
OAK	0.04	0.03	-13.80	-72.64	-5.46	-0.16	-22.59
VGB	0.01	0.00	-22.57	-18.30	34.58	0.00	-3.39
MFR	0.27 **	0.22 **	-58.18 *	-131.51 **	83.42 *	-0.08	-12.36
SLE	0.33 **	0.13 *	-76.52 **	-92.37 **	53.14	-0.08	-11.36
OTX/GEG	0.09	0.04	-72.11	-23.93	76.28	-0.03	-0.23

Table 7.9: As in Table 7.8 but assuming PDO entered a cold phase in 1999.

Location Code	R^2	Extra R^2	b_1 (m/SOI)	b_2 (m)	b_3 (m/SOI)	τ	Linear trend (m dec^{-1})
TUS	0.08	0.07	-1.85	-111.74	3.11	-0.04	-8.11
SLC	0.09	0.04	-80.00	-44.69	65.89	0.10	24.26
ABQ	0.02	0.00	36.08	-6.25	-2.57	0.25 **	64.76 **
GJT	0.15	0.03	-58.32	-78.65	1.20	0.14	23.54
BOI	0.09	0.01	-72.28	29.03	16.01	-0.01	1.26
OAK	0.18 *	0.17 *	36.83	-163.13 **	-63.12	-0.10	-11.45
VGB	0.04	0.04	-70.98	7.62	112.78	0.04	1.28
MFR	0.27 **	0.23 **	-28.11	-151.74 **	25.28	0.10	11.10
SLE	0.35 **	0.15 **	-54.31 *	-108.67 **	12.53	0.10	5.22
OTX/GEG	0.06	0.01	-45.58	-30.63	10.88	0.00	3.36

Table 7.10: Assuming that the PDO has remained in its warm phase, the multiple linear regression model 4.33 results for cold season percentages of estimated snow levels above the given elevations and the trends in the resulting residuals since ~1925. b_1 is the estimated coefficient for fall SOI (X_1), b_2 is the estimated coefficient for the PDO phase indicator variable (X_2), and b_3 is the estimated coefficient for the interaction effects variable (i.e., X_3 , or the product of X_1 and X_2). Extra R^2 refers to the addition of X_2 and X_3 to the model with X_1 already included. Coefficient significance refers to two-sided p-values. Significant values are indicated by * (p<0.05) and ** (p<0.01) for the multiple regression results and two-sided p-values for the trend results. Simple linear regressions for which the error normality assumption was rejected at the 0.05 significance level are indicated by @, regressions for which the constant error variance assumption was rejected are indicated by #, and regressions with first-order positively autocorrelated error terms are indicated by $. Note, the slopes for the autocorrelated time series are derived from a first-order autoregressive model (4.26) which relieved autocorrelation in all cases.

Watershed	**Elev (msl)**	**R^2**	**Extra R^2**	**b_1 (%/SOI)**	**b_2 (%)**	**b_3 (%/SOI)**	**τ**	**Linear trend (% dec^{-1})**
Salt/Lower Verde	1560	0.06	0.04	-2.95	-11.02	1.88	0.38 (p<0.01)	5.32 (p<0.01)
Weber/Jordan	1652	0.06	0.05	-1.31	-5.05	3.05	0.11	1.05
Upper Rio Grande	1862	0.10	0.10 *	-1.11	7.86 **	0.98	0.33 (p<0.01)	2.15 (p<0.01)
Colorado Headwaters	1475	0.11	0.01	-3.53 *	-0.59	2.20	0.18 (p<0.05)	0.97 (p<0.05)
South Salmon/Payette/Weiser	1176	0.05	0.02	-2.85	-3.59	1.59	0.19	1.69 (p<0.01)
San Joaquin	1377	0.05	0.04	-4.13	-4.33	7.25	0.14	1.46 (p<0.01)
Ventura-San Gabriel/Santa Ana	1523	0.26 **	0.20 **	-2.86	-18.66 **	-1.52	0.17 (p<0.05)	1.76
Middle/Upper Rogue	755	0.27 **	0.16 **	-5.95 **	-12.48 **	4.83	0.34 (p<0.01)	2.58$^{\#}$ (p<0.01)
North Santium/ Molalla-Pudding/ Clackamas	731	0.30 **	0.17 **	-5.42 **	-10.47 **	4.32	0.17 (p<0.05)	1.18 (p<0.05)
Pend Orielle/Preist/Pend Orielle Lake	500	0.10 *	0.05	-4.99 **	3.62	4.50	-0.21 (p<0.01)	-1.49 (p<0.01)

Table 7.11: As in Table 7.10 but assuming PDO entered a cold phase in 1999.

Watershed	Elev (msl)	R^2	Extra R^2	b_1 (%/SOI)	b_2 (%)	b_3 (%/SOI)	τ	Linear trend (% dec^{-1})
Salt/Lower Verde	1560	0.03	0.01	-6.02	-3.43	5.68	0.41 (p<0.01)	5.90 (p<0.01)
Weber/Jordan	1652	0.03	0.03	-2.55	0.94	3.90	0.12	1.23 (p<0.05)
Upper Rio Grande	1862	0.13 *	0.13 **	-2.55	8.55 **	2.95	0.20 (p<0.01)	1.42$^{\$}$ (p<0.05)
Colorado Headwaters	1475	0.13 *	0.04	-4.78 **	1.34	3.73	0.17 (p<0.05)	0.88
South Salmon/Payette/Weiser	1176	0.07	0.03	-4.74*	3.96	3.00	0.18 (p<0.05)	1.52 (p<0.01)
San Joaquin	1377	0.04	0.03	-3.61	-4.89	5.07	0.17 (p<0.05)	1.70 (p<0.05)
Ventura-San Gabriel/Santa Ana	1523	0.15 **	0.09 *	-2.69	-12.40 **	-1.33	0.28 (p<0.01)	3.59 (p<0.01)
Middle/Upper Rogue	755	0.19 **	0.08 *	-8.30 **	-5.27	7.64 *	0.38 (p<0.01)	2.99$^{\#}$ (p<0.01)
North Santium/ Molalla-Pudding/ Clackamas	731	0.21 **	0.07 *	-6.1 4 **	-5.68 *	4.40	0.27 (p<0.01)	1.89 (p<0.01)
Pend Orielle/Preist/Pend Orielle Lake	500	0.09	0.04	-4.41 *	-3.69	4.24	-0.21 (p<0.01)	-1.59 (p<0.01)

For both classifications of PDO phase in the last decade, the introduction of the variables related to PDO into model 4.33 explains a significant amount of variance in 0000 UTC WBZ height at Medford and Salem, OR (Table 7.8 and 7.9). Additionally, for both recent PDO phase classifications, R^2 adjusted for model 4.33 is higher than R^2 for with only X_1 in the model for at least five of the rawinsonde sites. Similarly, for both recent PDO classifications the introduction of X_2 and X_3 into the model explains significant additional variance in the COOP percentages at the Upper Rio Grande, Ventura-San Gabriel/Santa Ana, Middle/Upper Rogue, and North Santium/ Molalla-Pudding/ Clackamas watersheds (Table 7.10 and 7.11). Additionally, for both recent PDO phase classifications, R^2 adjusted for model 4.33 is higher than R^2 for with only X_1 in the model for at least six of the rawinsonde sites. Therefore, similar to the multiple linear regression results for temperature/thickness, the addition of the PDO indicator and interaction variables are useful predictors of 0000 UTC WBZ heights and COOP percentages in that the additional explained variance may account for the observed trends.

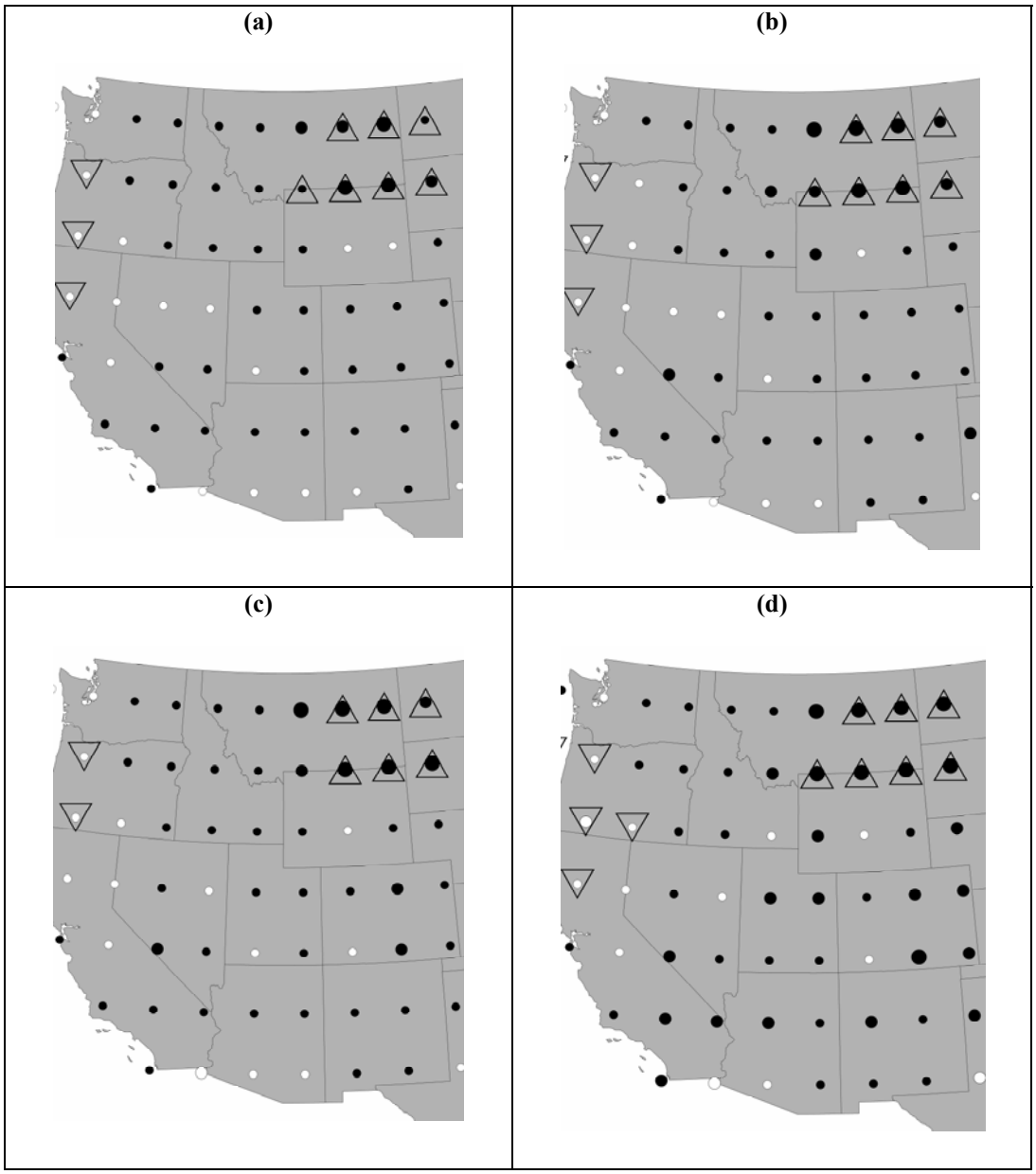

Figure 7.2: Assuming that the PDO has remained in its warm phase, residual trends (b_1 for simple linear regression) when 850 hPa Temperature (a), 1000-850 hPa Thickness (b), 850-700 hPa Thickness (c), and 1000-500 hPa Thickness (d) are regressed against fall SOI (X_1), the PDO phase indicator variable (X_2), and the interaction effects variable (i.e., the product of X_1 and X_2; see model 4.33). Additionally, local Moran's I values jointly significant with 95% confidence indicating clustering of lower values are given by large inverted triangles.

Table 7.12: Assuming that the PDO has remained in its warm phase, field significance of simple linear regression (SLR) and Mann-Kendall (MK) trend tests on the residuals resulting from regressing cold season median wet day values of temperature/thickness against fall SOI (X_1), the PDO phase indicator variable (X_2), and the interaction effects variable (i.e., the product of X_1 and X_2) as in the multiple regression model 4.33 over the entire western US since 1949.

	SLR Field Significance	MK Field Significance
850 hPa Temperature	>>0.05	>>0.05
1000-850 hPa Thickness	>>0.05	>>0.05
850-700 hPa Thickness	>>0.05	>>0.05
1000-500 hPa Thickness	>>0.05	>>0.05

For the temperature/thickness measures, the trends in the residuals resulting from multiple linear regression through model 4.33 assuming that the PDO has been in a warm phase from 1977-2009 are insignificant over the western US as a whole (Table 7.12) and there are no grids displaying significant (two-side $p < 0.05$) residual trends for simple linear regression (Table 7.13; Figure 7.2) and only one grid displaying significant trend for Mann-Kendall test for 1000-500 hPa thickness (Table 7.14). Contrarily, assuming the PDO transitioned to a cold phase in 1999, the trends in the residuals resulting from multiple linear regression are highly significant (pseudo $p < 0.01$) over the western US as a whole for all temperature/thickness measures (Table 7.15). Additionally, there is little difference between the trends in the raw data (Table 6.2) and the residual trends with at least 8 grids displaying significant positive trends for all thickness/temperature measures for both the simple linear regression (Table 7.16) and Mann-Kendall trend tests (Table 7.17). Additionally, the spatial variability in the residual trend assuming that the PDO transitioned to a cold phase in 1999 is nearly identical (Figure 7.3) to the trend in the raw data (Figure 6.1).

Table 7.13: Assuming PDO as remained in a warm phase, descriptive statistics of residual trends (b_1 for simple linear regression) when temperature/thickness is regressed against fall SOI (X_1), the PDO phase indicator variable (X_2), and the interaction effects variable (i.e., the product of X_1 and X_2; see model 4.33).

	Median b_1 (K or gpm dec^{-1})	Max b_1 (K or gpm dec^{-1})	Min b_1 (K or gpm dec^{-1})	Number of grids with $b_1>0$	Number of grids with $b_1>0$ and two-sided $p<0.05$	Number of grids with $b_1<0$ and two-sided $p<0.05$
850 hPa Temperature	0.03	0.38	-0.09	43	0	0
1000-850 hPa Thickness	0.15	1.93	-0.41	44	0	0
850-700 hPa Thickness	0.18	2.04	-0.75	45	0	0
1000-500 hPa Thickness	0.66	6.82	-1.43	46	0	0

Table 7.14: Assuming PDO as remained in a warm phase, descriptive statistics of residual trends (τ Mann-Kendall test) when temperature/thickness is regressed against fall SOI (X_1), the PDO phase indicator variable (X_2), and the interaction effects variable (i.e., the product of X_1 and X_2; see model 4.33).

	Median τ	Max τ	Min τ	Number of grids with $\tau>0$	Number of grids with $\tau>0$ and two-sided $p<0.05$	Number of grids with $\tau<0$ and two-sided $p<0.05$
850 hPa Temperature	0.03	0.15	-0.08	42	0	0
1000-850 hPa Thickness	0.03	0.16	-0.06	46	0	0
850-700 hPa Thickness	0.03	0.17	-0.08	43	0	0
1000-500 hPa Thickness	0.03	0.19	-0.10	46	1	0

Table 7.15: As in 7.12 but assuming that the PDO entered a cold phase in 1999.

	SLR Field Significance	MK Field Significance
850 hPa Temperature	0.001	0.001
1000-850 hPa Thickness	0.001	0.005
850-700 hPa Thickness	0.001	0.001
1000-500 hPa Thickness	0.001	0.001

Table 7.16: Assuming that the PDO entered a cold phase in 1999, descriptive statistics of residual trends (b_1 for simple linear regression) when temperature/thickness is regressed against fall SOI (X_1), the PDO phase indicator variable (X_2), and the interaction effects variable (i.e., the product of X_1 and X_2; see model 4.33).

	Median b_1 (K or gpm dec^{-1})	Max b_1 (K or gpm dec^{-1})	Min b_1 (K or gpm dec^{-1})	Number of grids with $b_1>0$	Number of grids with $b_1>0$ and two-sided $p<0.05$	Number of grids with $b_1<0$ and two-sided $p<0.05$
850 hPa Temperature	0.08	0.53	-0.47	42	11	1
1000-850 hPa Thickness	0.32	2.64	-1.99	45	9	0
850-700 hPa Thickness	0.67	3.02	-2.39	51	14	2
1000-500 hPa Thickness	2.50	10.86	-7.51	52	20	1

Table 7.17 Assuming that the PDO entered a cold phase in 1999, descriptive statistics of residual trends (τ Mann-Kendall test) when temperature/thickness is regressed against fall SOI (X_1), the PDO phase indicator variable (X_2), and the interaction effects variable (i.e., the product of X_1 and X_2; see model 4.33).

	Median τ	Max τ	Min τ	Number of grids with $\tau>0$	Number of grids with $\tau>0$ and two-sided $p<0.05$	Number of grids with $\tau<0$ and two-sided $p<0.05$
850 hPa Temperature	0.07	0.32	-0.21	43	10	2
1000-850 hPa Thickness	0.06	0.28	-0.16	44	8	0
850-700 hPa Thickness	0.12	0.33	-0.19	51	12	2
1000-500 hPa Thickness	0.13	0.38	-0.18	55	19	1

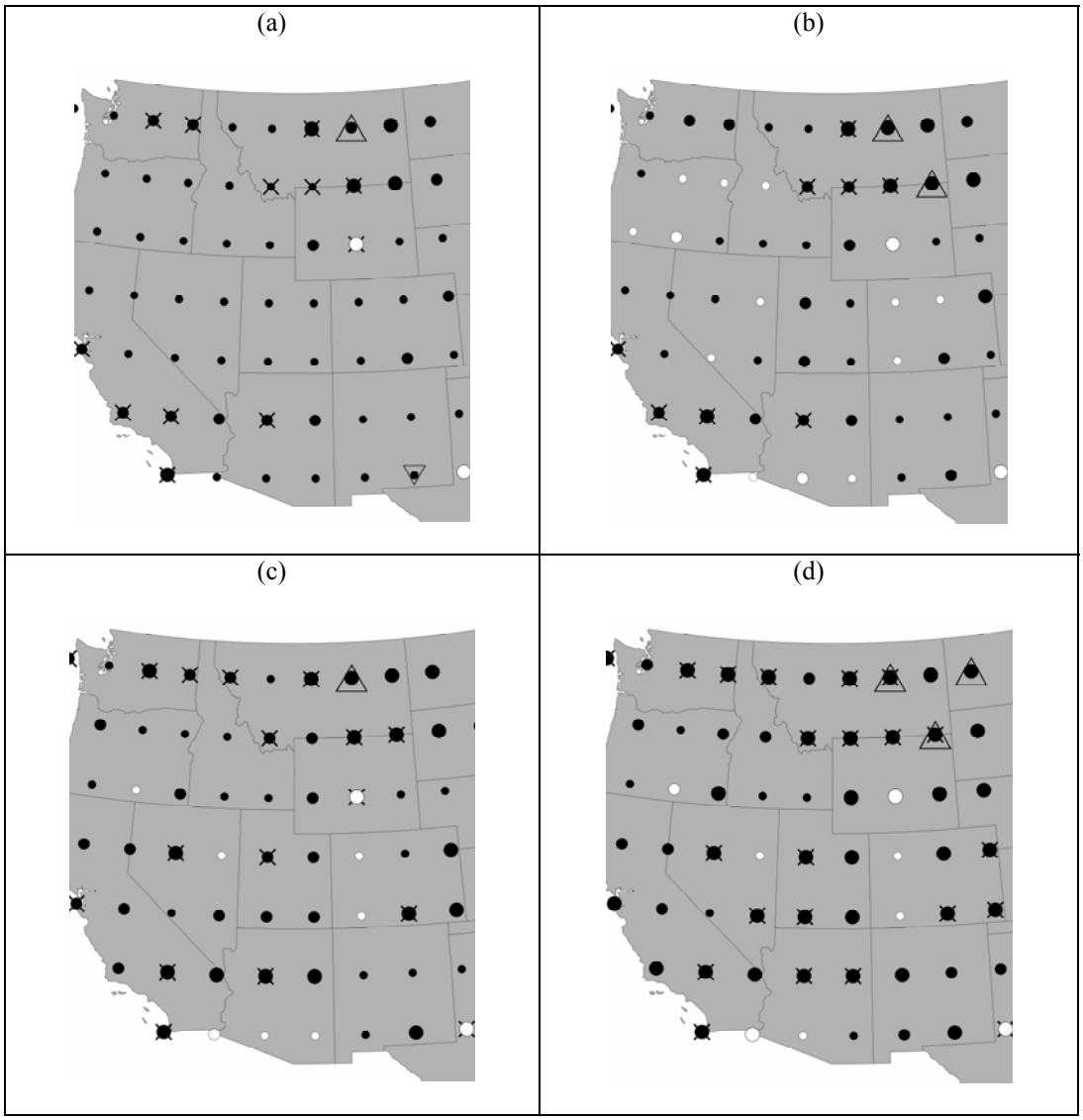

Figure 7.3: Assuming that the PDO entered its cold phase in 1999, residual trends (b_1 for simple linear regression) when 850 hPa Temperature (a), 1000-850 hPa Thickness (b), 850-700 hPa Thickness (c), and 1000-500 hPa Thickness (d) are regressed against fall SOI (X_1), the PDO phase indicator variable (X_2), and the interaction effects variable (i.e., the product of X_1 and X_2; see model 4.33).

A similar discrepancy between the two PDO classifications of the recent decade is apparent in the WBZ height residual trends. The assumption that PDO has remained in a warm phase results in a de-trending of the positive trends in the 0000 UTC WBZ height data (Table 7.8) particularly for Albuquerque, NM which displays a significant trend of +65.38 m dec^{-1} in the raw data but an insignificant trend of 11.74 m dec^{-1} in the residuals (Table 7.8). If one assumes that PDO did transition to a cold phase recently, the residual trend is a significant +64.76 m dec^{-1} at

Albuquerque and trends are similar at the other 9 locations to the raw data with only two negative trends (both insignificant; Table 7.9).

This discrepancy between the two PDO classifications is not apparent in the residual trends in the COOP derived percentage time series (Table 7.10 and 7.11). Nearly identical to the raw data (Table 6.5), for both PDO classifications of the previous decade, significant positive residual trends are displayed at for eight of the ten watersheds (Table 7.10 and 7.11). The discrepancies in residual trends between the two recent PDO classifications for temperature/thickness and WBZ heights is due to the shorter periods of record (1949-2009 and 1958-2010 respectively) when compared to the COOP percentages which extend back to ~1925. Under the assumption that the PDO has been in a warm phase since 1977, X_2 in the model 4.33 has a value of one for roughly first half of the WBZ height and temperature/thickness time series and a value of zero for the latter portion. As the representation of PDO in model 4.33 does not model the effects of cold and warm PDO specifically, rather the effects of simply a difference in PDO phase, one would expect the representation of only two PDO phases to result in the removal of any trends in the response variable when residual trends are examined. This is evidenced by the prominence of significantly negative values of b_2 in the temperature/thickness data (Table 7.6) and the WBZ height data (Table 7.8) assuming that PDO is currently in warm phase. In contrast, assuming that PDO entered a cold phase in 1999, there are more significant positive values of b_2 across the western US for the temperature/thickness measures than significant negative values (Table 7.7). This discrepancy between the two PDO classifications is not apparent for the COOP data due to the long period of record which spans more than two PDO phases regardless of the PDO classification of the last decade. Consequently, the coefficients are similar for each classification of PDO phase in the last decade (Table 7.10 and 7.11) as are the residual trends as discussed above. In summary, there is little evidence that the statistical removal of the variability in the response variables (i.e., the snow level measures) accounted for by normalized fall SOI and PDO variability results in a de-trending of the snow level measures.

7.4 Trends in COOP Percentages During Three Different Transitions of PDO

In this section, I highlight trend analyses results during three separate sub-periods of the COOP percentages time series. Specifically, the 1936 to 1960 warm to cold PDO transition, the 1961-1987 cold to warm transition and the disputed 1988-2009 transition. As a major focus of this chapter is to determine if the increasing trends in Chapter 6 are can be linked to transitions in PDO phase, I primarily focus on the modulation of the significant increasing trends through the three sub-periods in the remainder of this section. It is important to note that violations of error-normality and constant error variance are relatively frequent in the simple linear regression results displayed in Table 7.18, particularly for time series bounded by 0% or 100%. Therefore, more weight should be given to the Mann-Kendall trend results for such time series.

COOP stations displaying significant increasing trends in percentages for the entire length of record also display positive trends during the PDO transition from warm to cold (i.e., 1936 to 1960) in the Salt/Lower Verde, Weber/Jordan, Upper Rio Grande, Colorado Headwaters, and San Joaquin watersheds (Table 7.18 and 7.19). Negative trends from 1936 to 1960 are evident at the North Santium/Molalla-Pudding/Clackamas and South Salmon/Payette/Weiser watersheds (Table 7.18 and 7.19). COOP stations displaying positive trends during the PDO transition from cold to warm (i.e.,1961 to 1987) are present in the Salt/Lower Verde, Ventura-San Gabriel/Santa Ana , San Joaquin, Middle/Upper Rogue and the North Santium/Molalla-Pudding/Clackamas watersheds (Table 7.18 and 7.19). Negative trends from 1961 to 1987 are evident at Weber/Jordan, Upper Rio Grande, Colorado Headwaters watersheds. COOP stations displaying positive trends during the possible recent PDO transition from warm to cold (i.e.,1988 to 2009) are located in the Salt/Lower Verde, Weber/Jordan, South Salmon/Payette/Weiser San Joaquin and Middle/Upper Rogue watersheds (Table 7.18 and 7.19). Negative trends from 1998 to 2009 are evident at Upper Rio Grande, Colorado Headwaters and Ventura-San Gabriel/Santa Ana watersheds.

There are only three time series significant for the entire length of record that display obvious positive trends (Table 7.18 and 7.19) during the warm to cold transition and the potential

recent warm cold transition with negative trends during the cold to warm transition (a signal consistent with the results regarding the PDO/ENSO affect on snow level in Chapter 5 assuming PDO entered a cold phase in 1999). These are the COOP stations at 1512 msl in the Weber/Jordan watershed, and 1752-1800 msl and 1901-1963 msl in the Colorado Headwaters watershed (Table 7.18 and 7.19). Furthermore, the Salt/Lower Verde, Weber/Jordan, San Joaquin, and Ventura-San Gabriel/Santa Ana watershed all display time series with positive trends during all three sub-periods (Table 7.18 and 7.19). Additionally, the significant positive trends overall in the Ventura-San Gabriel/Santa Ana and the Middle/Upper Rogue watersheds appear to mainly be the result of highly significant (two-sided $p < 0.01$) increases during the cold to warm transition. Finally, over the ten watersheds, there is equal evidence for increasing trends during the early warm to cold PDO transition and the recent disputable cold to warm transition (Table 7.18 and 7.19).

Table 7.18: For the three sub-periods (i.e., the first warm to cold PDO transition, the cold to warm PDO transition, and the possible most recent warm to cold PDO transition), simple linear regression trend test results for the ten watersheds. Blank cells indicate nearly constant time series at 100%. Significant trends are indicated by two-sided p-values. Bold rows indicate times series with significant positive trend over the entire period of record (Table 6.5). Regressions for which the error normality assumption was rejected at the 0.05 significance level are indicated by @, regressions for which the constant error variance assumption was rejected are indicated by #, and regressions with first-order positively autocorrelated error terms are indicated by $. Note, the slopes for the autocorrelated time series are derived from a first-order autoregressive model (4.26) which relieved autocorrelation in all cases.

		Warm to Cold	**Cold to Warm**	**Indeterminable Warm to Cold**
		1936-1960	**1961-1987**	**1988-2009**
	Elev (msl)	***Linear trend* (% dec^{-1})**	***Linear trend* (% dec^{-1})**	***Linear trend* (% dec^{-1})**
Salt/Lower Verde	374	-	-	-
	524	-	-	-
	674	-	-	-
	807	1.54$^{@}$	-2.18$^{@\#}$	7.83$^{@\#}$
	1054	0.24$^{@}$	-0.93$^{@\$}$	8.76$^{@\#}$ (p<0.05)
	1085	**3.43**	**3.86 (p<0.05)**	**8.76$^{@\#}$ (p<0.05)**
	1268	**6.31**	**8.79 (p<0.01)**	**14.62$^{@\#}$**
	1560	**1.50**	**7.93**	**-3.74**
	1984	**12.19$^{\#\$}$**	**1.95**	**6.70**
	2146	**2.45$^{\$}$**	**8.87 (p<0.05)**	**6.70**
	2441	8.89$^{\$}$	10.79$^{\#\$}$ (p<0.01)	1.05$^{\$}$
		Warm to Cold	**Cold to Warm**	**Indeterminable Warm to Cold**
		1936-1960	**1961-1987**	**1988-2009**
	Elev (msl)	***Linear trend* (% dec^{-1})**	***Linear trend* (% dec^{-1})**	***Linear trend* (% dec^{-1})**
	1302	**7.82$^{@}$ (p<0.05)**	**0.55**	**0.81$^{\$}$**
	1512	**5.96**	**-4.09**	**11.70 (p<0.05)**

Table 7.18 Continued

Weber/Jordan	1557	2.61	0.29	7.20[#]
	1652	**-1.80**	**-0.07**	**7.64**
	1701	-2.07	-0.18	4.09
	1817	**0.56[@#]**	**-1.05[@]**	**6.76[@]**
	1953	**3.41**	**0.77**	**4.42**
	2655	-0.56	0.07	-0.03
Upper Rio Grande	**Elev (msl)**	**Warm to Cold 1936-1960 *Linear trend* (% dec^{-1})**	**Cold to Warm 1961-1987 *Linear trend* (% dec^{-1})**	**Indeterminable Warm to Cold 1988-2009 *Linear trend* (% dec^{-1})**
	1695	**12.29 (p<0.01)**	**3.09**	**-10.29 (p<0.01)**
	1862	**14.12 (p<0.01)**	**-3.93**	**-3.98**
	2122	**7.31 (p<0.01)**	**-4.30**	**0.45**
	2234	1.23	-0.49	-1.66
	2457	1.86	-0.49	-3.35
Colorado Headwaters	**Elev (msl)**	**Warm to Cold 1936-1960 *Linear trend* (% dec^{-1})**	**Cold to Warm 1961-1987 *Linear trend* (% dec^{-1})**	**Indeterminable Warm to Cold 1988-2009 *Linear trend* (% dec^{-1})**
	1365	**8.25 (p<0.01)**	**-3.21**	**-2.81[$]**
	1475	**2.48**	**-1.34[#]**	**-3.89[$]**
	1752	**5.10**	**-3.02**	**1.37[$]**
	1901	**5.51 (p<0.05)**	**-3.11[$]**	**-0.21[$]**
	2060	**-0.05**	**0.85**	**-0.51**
	2411	1.41	-0.60	-0.87
	2679	-0.38[@#]	-0.15[@]	-0.30[@#]

Table 7.18 Continued

	Elev (msl)	Warm to Cold 1936-1960 *Linear trend* (% dec^{-1})	Cold to Warm 1961-1987 *Linear trend* (% dec^{-1})	Indeterminable Warm to Cold 1988-2009 *Linear trend* (% dec^{-1})
South Salmon/Payette/Weiser	**722**	**-6.89$^{\$}$**	**-1.28**	**12.83 (p<0.05)**
	893	**-5.58$^{\$}$**	**0.97**	**12.86 (p<0.05)**
	1176	**-6.28$^{\$}$**	**-0.99**	**4.95**
	1533	-2.94$^{\$}$	1.32	-0.44
	1797	**1.05**	**0.99$^{@}$**	**-0.44**
	Elev (msl)	**Warm to Cold 1936-1960 *Linear trend* (% dec^{-1})**	**Cold to Warm 1961-1987 *Linear trend* (% dec^{-1})**	**Indeterminable Warm to Cold 1988-2009 *Linear trend* (% dec^{-1})**
San Joaquin	**532**	**2.20**	**0.03**	**4.90$^{@\#}$**
	606	**0.31**	**4.99$^{\$}$**	**2.65$^{@}$**
	801	**1.40**	**4.72$^{\$}$**	**3.31$^{@}$**
	1179	0.43$^{\$}$	3.53	-2.45
	1210	-1.82$^{\$}$	5.77	-1.28
	1377	**-0.65$^{\$}$**	**8.63**	**-8.78$^{\#}$**
	Elev (msl)	**Warm to Cold 1936-1960 *Linear trend* (% dec^{-1})**	**Cold to Warm 1961-1987 *Linear trend* (% dec^{-1})**	**Indeterminable Warm to Cold 1988-2009 *Linear trend* (% dec^{-1})**
Ventura-San Gabriel/Santa Ana	402	1.95$^{\$}$	3.52$^{@}$ (p<0.01)	-5.01$^{@\#}$
	792	2.08	5.24$^{@\$}$ (p<0.05)	-5.01$^{@\#}$
	933	**2.34**	**5.35 (p<0.05)**	**-3.47$^{@\#}$**
	1523	**-4.89**	**11.44 (p<0.05)**	**-12.21**

Table 7.18 Continued

	2060	-5.78[#]	3.40[@#]	0.76[$]
Middle/Upper Rogue	**Elev (msl)**	**Warm to Cold 1936-1960 *Linear trend* (% dec^{-1})**	**Cold to Warm 1961-1987 *Linear trend* (% dec^{-1})**	**Indeterminable Warm to Cold 1988-2009 *Linear trend* (% dec^{-1})**
	201	**-4.03[@$]**	**4.31[#] (p<0.01)**	**0.10[@#$]**
	280	**-4.29[$]**	**4.43[#] (p<0.01)**	**-0.98[#$]**
	532	**1.77[#]**	**5.92[#] (p<0.01)**	**0.73[@#$]**
	755	**3.21[#$]**	**15.46[$] ($p$<0.01)**	**0.54[#$]**
North Santium/Molalla-Pudding/Clackamas	**Elev (msl)**	**Warm to Cold 1936-1960 *Linear trend* (% dec^{-1})**	**Cold to Warm 1961-1987 *Linear trend* (% dec^{-1})**	**Indeterminable Warm to Cold 1988-2009 *Linear trend* (% dec^{-1})**
	124	**-1.87[$]**	**0.29**	**0.68[@]**
	228	**-0.82[$]**	**2.17**	**-3.34[@#$]**
	341	**-1.84[$]**	**2.66**	**0.62[$]**
	731	**-5.66[$]**	**4.80**	**-5.12[$]**
Pend Orielle/Priest/ Pend Orielle Lake	**Elev (msl)**	**Warm to Cold 1936-1960 *Linear trend* (% dec^{-1})**	**Cold to Warm 1961-1987 *Linear trend* (% dec^{-1})**	**Indeterminable Warm to Cold 1988-2009 *Linear trend* (% dec^{-1})**
	402	-4.27[$]	-1.43	-9.78 (p<0.05)
	500	-0.69	0.58	-10.17 (p<0.05)
	539	0.61	-0.33	-12.08 (p<0.01)
	651	-2.58	-3.10	-12.23[$] ($p$<0.01)
	725	-3.11[#]	-2.14	-11.02[$] ($p$<0.01)

Table 7.19 For the three sub-periods (i.e., the first warm to cold PDO transition, the cold to warm PDO transition, and the possible most recent warm to cold PDO transition), Mann-Kendall trend test results for the ten watersheds. Blank cells indicate nearly constant time series at 100%. Significant values are indicated by * (two-sided $p<0.05$) and ** (two-sided $p<0.01$). Bold rows indicate times series with significant positive trend over the entire period of record (Table 6.5).

		Warm to Cold	**Cold to Warm**	**Indeterminable Warm to Cold**
		1936-1960	**1961-1987**	**1988-2009**
	Elev (msl)	**τ**	**τ**	**τ**
Salt/Lower Verde	374	-	-	-
	524	-	-	-
	674	-	-	-
	807	0.13	-0.14	0.28*
	1054	0.04	0.06	0.38**
	1085	**0.16**	**0.28***	**0.38****
	1268	**0.21**	**0.28***	**0.33***
	1560	**-0.04**	**0.20**	**-0.07**
	1984	**0.10**	**0.06**	**0.13**
	2146	**0.03**	**0.26**	**0.13**
	2441	**0.15**	**0.37****	**0.09**
		Warm to Cold	**Cold to Warm**	**Indeterminable Warm to Cold**
		1936-1960	**1961-1987**	**1988-2009**
	Elev (msl)	**τ**	**τ**	**τ**
Weber/Jordan	**1302**	**0.28**	**0.02**	**0.27**
	1512	**0.21**	**-0.19**	**0.42***
	1557	0.11	0.04	0.20
	1652	-0.11	-0.09	0.28

Table 7.19 Continued

	1701	-0.12	-0.07	0.14
	1817	-0.05	-0.17	0.27
	1953	**0.17**	**0.01**	**0.14**
	2655	-0.08	0.06	-0.07
Upper Rio Grande	**Elev (msl)**	**Warm to Cold 1936-1960 τ**	**Cold to Warm 1961-1987 τ**	**Indeterminable Warm to Cold 1988-2009 τ**
	1695	**0.65 ****	**0.12**	**-0.46****
	1862	**0.62 ****	**-0.16**	**-0.13**
	2122	**0.45 ****	**-0.18**	**0.06**
	2234	0.15	0.00	-0.14
	2457	0.25	-0.03	-0.25
Colorado Headwaters	**Elev (msl)**	**Warm to Cold 1936-1960 τ**	**Cold to Warm 1961-1987 τ**	**Indeterminable Warm to Cold 1988-2009 τ**
	1365	**0.39****	**-0.21**	**-0.06**
	1475	**0.12**	**-0.07**	**-0.01**
	1752	**0.26**	**-0.22**	**0.13**
	1901	**0.40****	**-0.26**	**0.12**
	2060	**-0.04**	**0.10**	**-0.02**
	2411	0.29*	-0.12	-0.10
	2679	-0.13	-0.03	-0.16

Table 7.19 Continued

	Elev (msl)	Warm to Cold 1936-1960 τ	Cold to Warm 1961-1987 τ	Indeterminable Warm to Cold 1988-2009 τ
South Salmon/Payette/Weiser	722	-0.21	-0.14	0.33*
	893	**-0.11**	**-0.04**	**0.31**
	1176	**-0.14**	**-0.05**	**0.16**
	1533	-0.16	0.28*	-0.01
	1797	**0.16**	**0.18**	**-0.01**
	Elev (msl)	**Warm to Cold 1936-1960 τ**	**Cold to Warm 1961-1987 τ**	**Indeterminable Warm to Cold 1988-2009 τ**
San Joaquin	**532**	**0.09**	**-0.01**	**0.20***
	606	**-0.10**	**0.09**	**0.11**
	801	**0.13**	**0.08**	**0.13**
	1179	0.01	0.15	-0.14
	1210	0.02	0.20	-0.07
	1377	0.10	0.26	-0.20
	Elev (msl)	**Warm to Cold 1936-1960 τ**	**Cold to Warm 1961-1987 τ**	**Indeterminable Warm to Cold 1988-2009 τ**
Ventura-San Gabriel/Santa Ana	**402**	**-0.01**	**0.32****	**0.07**
	792	**0.01**	**0.35****	**0.07**
	933	**0.12**	**0.35****	**0.18**
	1523	**-0.17**	**0.24**	**-0.23**

Table 7.19 Continued

	2060	-0.14	0.13	-0.08
Middle/Upper Rogue	**Elev (msl)**	**Warm to Cold 1936-1960 τ**	**Cold to Warm 1961-1987 τ**	**Indeterminable Warm to Cold 1988-2009 τ**
	201	**-0.25**	**0.46****	**-0.10**
	280	**-0.24**	**0.40****	**0.01**
	532	**0.02**	**0.42****	**0.00**
	755	**0.10**	**0.45****	**-0.17**
North Santium/Molalla-Pudding/Clackamas	**Elev (msl)**	**Warm to Cold 1936-1960 τ**	**Cold to Warm 1961-1987 τ**	**Indeterminable Warm to Cold 1988-2009 τ**
	124	**-0.09**	**0.04**	**0.16**
	228	**-0.02**	**0.16**	**0.10**
	341	**-0.07**	**0.17**	**0.16**
	731	**-0.14**	**0.20**	**-0.01**
Pend Orielle/Priest/ Pend Orielle Lake	**Elev (msl)**	**Warm to Cold 1936-1960 τ**	**Cold to Warm 1961-1987 τ**	**Indeterminable Warm to Cold 1988-2009 τ**
	402	-0.17	-0.02	-0.31*
	500	-0.01	0.01	-0.44**
	539	0.05	-0.01	-0.44**
	651	-0.01	-0.11	-0.45**
	725	-0.02	-0.03	-0.49**

7.5 Summary of Results

There are two key results consistent between all three methods of snow level quantification (i.e., temperature/thickness, WBZ heights, and COOP percentages).

1) Residual trends in the measures of snow level are nearly identical to the trends when the variability due to normalized fall SOI is not statistically removed through simple linear regression.

2) Assuming that the PDO transitioned to a cold phase in 1998/1999, residual trends in the measures of snow level are nearly identical to the trends when the variability due to normalized fall SOI and PDO is not statistically removed through multiple linear regression.

Furthermore, assuming that the PDO has remained in a warm phase, residual (from multiple regression analysis) trends in the COOP percentages are nearly identical to the trends in the raw values. The elimination of increasing trends in the WBZ and temperature/thickness data is likely a result of the de-trending expected from modeling response variables that only span two PDO phases. Lastly, for times series of COOP percentages that display significant positive trend overall, trends during the warm to cold, cold to warm and the disputed warm to cold PDO transitions do not display a clear PDO signal and are more indicative of sustained positive trends.

7.6 Discussion

As previous research has suggested that the strength and/or frequency of El Niño events as quantified by SOI has increased in recent years (Power and Smith 2007) and considering the results from Chapter 5 suggesting higher snow levels during El Niño events over much of the western US (excluding the Southern Rockies) it is entirely possible that the increasing trends in snow level highlighted in Chapter 6 are due in part to variations in ENSO. However, the results

presented above suggest that the increasing trends in snow level across the western US are not due to variations in ENSO.

While some researchers have suggested a transition of the PDO to its cold phase in 1999 (Hare and Mantua 2000; Schwing et al. 2000), more recent investigations consider the PDO to be in a warm phase (St Jacques et al. 2010, Ellis et al. 2010). For example, Khaliq and Gachon (2010) used several change point techniques to suggest that the PDO has not change phase since 1977 and remains in a warm phase as of 2007. Furthermore, monthly measures of the PDO phase transitioned to positive values in the fall of 2009 (indicative of the warm phase) after two years of sustained negative values (Baringer et al. 2010) suggesting that PDO has not clearly entered a cold phase as of fall 2009.

The results in Chapter 5 suggest that snow levels are higher over the western US during the cold PDO due to less troughing and more zonal flow from the weakening of the Aleutian low. Therefore, assuming that the PDO is in its warm phase currently, one would expect decreases in snow level for periods spanning only two PDO phases with the latter a warm phase. Similarly, one would expect no trend in snow level during periods spanning three PDO phases beginning and ending in with a warm phase. Considering only this information, it appears that the trends in snow level suggested in Chapter 6 are not well explained by variations in PDO. Additionally, the results in Section 7.3 indicate that the trends in snow level measures since ~1925 persist when ENSO variability and the modulation of ENSO effects by PDO phase are removed statistically, regardless of the PDO phase classification of the last decade. If one assumes that the PDO entered a cold phase in 1999, the trends in snow level measures since 1949 and 1958 remained positive after the statistical removal of ENSO/PDO effects. Lastly, there is more evidence that increasing trends in estimated snow levels span all three PDO phase changes since the mid 1930s rather than increase during transitions to cold PDO and decrease during transitions to warm PDO. Therefore, the suggested trends in snow level elevation over the western US is not well explained by PDO.

As mentioned in Chapter 2, there are only a few previous studies that enable inferences about trends in snow level elevation across the western US. Knowles et al. (2006) as well as Feng and Hu (2007) analyzed trends in snowfall to rainfall ratios and noted a prominence of decreasing trends, consistent with increasing trends in snow level. As with trends in snow level suggested in this study, Knowles et al. (2006) highlight that the decreases in snowfall to rainfall ratio are not well explained by variations in PDO, saying "…the PDO warm phase lasting from about 1925 through 1946 was characterized by lower temperatures and higher [ratios] than the most recent 1977–1998 PDO warm phase… suggesting that the trends reported here are at least partially attributable to still longer term climate shifts."

7.7 Conclusion

From the increasing trends established in three separate snow level measures (WBZ heights, COOP snow level approximation for watersheds, upper-air reanalysis proxies), I examined the contribution of variations in ENSO and PDO to the observed trends to answer the following research question introduced in Chapter 1: *Are multi-decadal trends in snow level outside the realm of natural climate variability (e.g., variations in ENSO/PDO)?* Several major results suggest that the increasing trends in snow level are indeed multi-decadal and not well explained by ENSO/PDO.

1) Trends in snow level measures remain positive when variations in ENSO are accounted for by the statistical removal of the variability in snow level measures modeled by normalized fall SOI.

2) With the removal of the ENSO effects and the modulation of the ENSO effects by PDO trends in the snow level measures remain positive and significant.

3) It is appears more likely that the increases in estimated snow levels span all PDO phase changes since the mid1930s rather than increase with transitions to cold PDO and decrease with transitions to warm PDO.

In the following chapter, I briefly summarize the gap in the literature filled by the answers to three research questions of focus in this dissertation. Then I briefly discuss the employed data and methods followed by a summary of results. Lastly, I end the dissertation with recommendation for future research.

Chapter 8: Conclusion

8.1 Summary of Research Problem

Water resources for many major cities throughout the western US are dependent on reservoirs filled from major rivers with high elevation headwaters (Raushcer et al. 2008; Hidalgo et al. 2009). From a water budget perspective, snowfall is more beneficial than rainfall due to its slower rate of return to the atmosphere as water vapor. Additionally, for the majority of streams throughout the western US, snowmelt accounts for 75% percent of the annual discharge (Cayan 1996). Consequently, the focus of this dissertation has been on interannual snow level elevation variability which is directly related to the variability in the land area receiving snowfall (Svoma 2011; Casola et al. 2009). The response of spring snow water equivalent and date of maximum spring runoff have been examined extensively for multi-decadal trends, as well as for interannual and decadal variability in response to sea surface temperature oscillations such as El Niño-Southern Oscillation (ENSO) and Pacific Decadal Oscillation (PDO) (e.g., Gershunov and Barnett 1998b; Gutzler et al. 2002; Brown and Comrie 2004; Hamlet et al. 2005; Stewart et al. 2005). Snow level has been examined indirectly in this context through the analysis of records of snowfall to rainfall ratios at sites across the western US (Knowles et al. 2006; Feng and Hu; 2007), however, there is a lack of published research explicitly regarding snow levels over the western US (Svoma 2011).

Therefore, the goal of this study has been to evaluate the following three hypotheses:

1) Higher frequencies of maritime air flow into the western US during El Niño events along with more zonal air flow during cold PDO phases (Higgins et al. 2002; Brown and Comrie 2004) result in the highest snow levels occurring during El Niño events in conjunction with the cold PDO.

2) Considering the numerous studies indicating trends in twentieth century climate across the western US consistent with large scale warming (e.g., Mote et al. 2008; Rauscher et

al. 2008; Barnett et al. 2008, Pierce et al. 2008; Hidalgo et al. 2009), trends in snow level are predominantly increasing across the western US.

3) Knowles et al. (2006) found snowfall to rainfall ratios across the western US to be lower during the more recent warm phase of the PDO (1977-1998) than the earlier warm phase (1925-1946). As such, one should expect the climate change signal in snow level to be outside the realm of variations in PDO. Additionally, the numerous recent studies suggesting that changing climate in the western US is due to increased temperature from anthropogenic forcing (e.g., Barnett et al. 2008; Pierce et al. 2008) suggest that increasing snow levels are not well explained by the potential increase in the frequency and strength of El Niño events.

8.2 Summary of Data and Methods

Snow level elevation was estimated at daily resolution using three separate methods of snow level quantification from three independent datasets.

1) The first is a collection of daily wet-bulb zero (WBZ) heights (i.e., an estimator of the vertical distance above sea level where frozen precipitation transitions to liquid precipitation (Gedzelman and Arnold 1993; Albers et al. 1996; Bourgouin 2000; Wetzel and Martin 2001)) from 1957-2010 at ten rawinsonde locations across the western US.
2) Second, I empirically estimated snow level at daily resolution from ~1924-2009, from daily snowfall and precipitation totals from the National Weather Service Cooperative Observer (COOP) Network as a measure of daily precipitation type over various elevations across each of ten watersheds adjacent to the rawinsonde sites.
3) Lastly, from National Center for Environmental Prediction/National Center for Atmospheric Research reanalysis data at 2.5^{o} resolution across the western US, I used the 850 hPa temperature, the 1000–500 hPa thickness, the 1000–

850 hPa thickness and the 850–700 hPa thickness (Heppner 1992) for each day from 1948-2009 to effectively discriminate between frozen and liquid precipitation at the surface (Heppner 1992).

Time series representing the interannual variability in these snow level proxies were subject to various statistical techniques to determine the influence of ENSO/PDO on snow level, linear trends in snow level, and to explore the likelihood that observed trends in snow level are outside the influences of ENSO/PDO.

8.3 Summary of Results

Results from the statistical analysis of the three data sets discussed in Section 8.2 suggest three key characteristics of interannual snow level variability that support the first hypothesis in Section 8.1:

1) Snow levels are higher over most of the western US (except in the Southern Rockies) during El Niño, particularly over the coastal regions. Considering previous investigations, the increased snow levels may be a result of higher frequencies of maritime flow (as opposed to continental flow) into the western US during El Niño events (Higgins et al. 2002). Distance from the Pacific Ocean weakens the El Niño signal and the Southern Rockies display decreased snow level elevations likely due to the maritime air masses associated with mid-latitude cyclones following the enhanced meridional flow transitioning to continental air masses (Mock 1995; Mock and Birkeland; 2000).
2) Previous investigations (e.g., Gutzler et al. 2002; Brown and Comrie 2004), have suggested a link between the warm (cold) phase of the PDO and a strengthening (weakening) of the Aleutian low resulting in the in-phase amplification of the ENSO effects on winter weather in the western US through the enhancement (dampening) of differential troughing/ridging between the Rocky Mountains and the North Pacific (i.e., the Pacific–North American

(PNA) pattern). During warm PDO/El Niño conditions, troughs that occur over the western US tend to be deeper and may serve to dampen the El Niño signal of higher snow level over the West Coast (Gutzler et al. 2002; Brown and Comrie 2004). Similarly, more zonal flow and shallower troughs associated with the cold PDO (Gutzler et al. 2002; Brown and Comrie 2004) may amplify the El Niño signal over southern California in particular. Lastly, during the cold PDO, La Niña events resemble a weaker version of the typical El Niño signal over the West Coast again likely due to the more zonal flow.

3) Therefore, assuming no long term trends in snow level, snow levels are most likely higher during the cold PDO relative to the warm PDO due to the more zonal flow.

The second hypothesis is supported by convergent results between the three measures of snow level (temperature/thickness, WBZ heights, and estimated snow levels) which suggest increasing snow levels across the western US with no obvious spatial pattern in snow level trend. Lastly, results from the trend control methods support the third hypothesis in following ways:

1) Snow level proxy trends remain positive when variations in ENSO and PDO are accounted for by the statistical removal of the variability in snow level measures modeled by normalized fall SOI and PDO phase.

2) There is more evidence that the increases in estimated snow levels span all PDO phase changes since ~1925 rather than increase with transitions to cold PDO and decrease with transitions to warm PDO.

Therefore, recent trends in snow level elevation are not well explained by ENSO/PDO and may be a result of longer term climate change.

8.4 Future Research

While the empirical evidence of a clear influence of ENSO/PDO on snow level over the western US is supported by theory provided by previous investigators, this study does not make a

direct link between the influence of ENSO/PDO on the characteristics and tracks of cold season extra-tropical cyclones and snow level elevation. It may be difficult to empirically establish this direct link due to the few separate PDO phases observed over the last century, however, a detailed empirical analysis of the variability in upper-air flow and low-level moisture flow associated with ENSO/PDO variations would greatly aid in understanding the snow level response to these sea surface temperature oscillations.

The few PDO phase changes seen in the last century also confound statistical analyses regarding the contribution of ENSO/PDO to recent snow level trends. For example, without eliminating trend, it is difficult to statistically remove a potential PDO signal in time series of response variables that span only two PDO phases. As the periods of record of climatic databases increase in the future and span multiple changes in PDO phase, the separation of a cyclical PDO signal from multi-decadal trend will become more feasible. Furthermore, modeling studies akin to Barnett et al. (2008) and Pierce et al. (2008) (who focus on snow water equivalent) focusing on measures of snow level would greatly aid in the attribution of snow level trends to anthropogenic forcing or natural climate variability.

The three major empirical findings of this study can serve as a base for the future research directions suggested above. Specifically, (1) snow level elevations are higher across much of the western United States during El Nino events (as opposed to neutral ENSO or La Nina conditions), particularly for areas near the Pacific Ocean. (2) Snow level elevations are highest during the cold PDO over the entire western United States, again particularly over the coastal areas. (3) Lastly, the prominent increasing trends in snow level across the western United States are not well explained by variations in ENSO/PDO.

REFERENCES

Albers, S.C., J.A. McGinley, D.L. Birkenheuer, and J.R. Smart, 1996. The Local Analysis and Prediction System (LAPS): Analyses of Clouds, Precipitation, and Temperature. Weather and Forecasting 11: 273-287.

Adam, J. C., A. F. Hamlet, and D. P. Lettenmaier, 2009: Implications of global climate change for snowmelt hydrology in the twenty-first century. Hydrological Processes, 23, 962-972.

Baringer, M. O., D. S. Arndt, and M. R. Johnson, 2010: State of the climate in 2009. Bulletin of the American Meteorological Society, 91, 1-122.

Barnett, T., J. Adam, D. Lettenmaier. 2005. Potential impacts of a warming climate on water availability in snow-dominated regions. Nature. 438: 303-309.

Barnett, T. P., and D. W. Pierce, 2009: Sustainable water deliveries from the Colorado River in a changing climate. Proceedings of the National Academy of Sciences of the United States of America, 106, 7334-7338.

Barnett, T. P., and Coauthors, 2008: Human-induced changes in the hydrology of the western United States. Science, 319, 1080-1083.

Bavay, M., M. Lehning, T. Jonas, and H. Lowe, 2009: Simulations of future snow cover and discharge in Alpine headwater catchments. Hydrological Processes, 23, 95-108.

Baxter, M. A., C. E. Graves, and J. T. Moore, 2005: A climatology of snow-to-liquid ratio for the contiguous United States. Weather and Forecasting, 20, 729-744.

Bourgouin, P., 2000. A Method to Determine Precipitation Types. Weather and Forecasting 15: 583-592.

Brown, D. P., and A. C. Comrie, 2004: A winter precipitation 'dipole' in the western United States associated with multidecadal ENSO variability. Geophysical Research Letters, 31, 4.

Brown, R. D., 2000: Northern hemisphere snow cover variability and change, 1915-97. Journal of Climate, 13, 2339-2355.

Budikova, D., 2005: Impact of the Pacific Decadal Oscillation on relationships between temperature and the Arctic Oscillation in the USA in winter. Climate Research, 29, 199-208.

Burakowski, E. A., C. P. Wake, B. Braswell, and D. P. Brown, 2008: Trends in wintertime climate in the northeastern United States: 1965-2005. Journal of Geophysical Research-Atmospheres, 113.

Casola, J. H., L. Cuo, B. Livneh, D. P. Lettenmaier, M. T. Stoelinga, P. W. Mote, and J. M. Wallace, 2009: Assessing the Impacts of Global Warming on Snowpack in the Washington Cascades. Journal of Climate, 22, 2758-2772.

Cayan D. 1996. Interannual climate variability and snowpack in the western United States. Journal of Climate, 9, 928-948.

Cayan, D. R., S. A. Kammerdiener, M. D. Dettinger, J. M. Caprio, and D. H. Peterson, 2001: Changes in the onset of spring in the western United States. Bulletin of the American Meteorological Society, 82, 399-415.

Cerveny, R. S., B. M. Svoma, and R. S. Vose, 2010: Lunar tidal influence on inland river streamflow across the conterminous United States. Geophysical Research Letters, 37.

Chu, P. S., and J. B. Wang, 1997: Recent climate change in the tropical western Pacific and Indian Ocean regions as detected by outgoing longwave radiation records. Journal of Climate, 10, 636-646.

Cohen, J., and D. Rind, 1991: The effect of snow cover on the climate. Journal of Climate, 4, 689-706.

Dettinger, M. D., D. R. Cayan, H. F. Diaz, and D. M. Meko, 1998: North-south precipitation patterns in western North America on interannual-to-decadal timescales. Journal of Climate, 11, 3095-3111.

Durand, Y., G. Giraud, M. Laternser, P. Etchevers, L. Merindol, and B. Lesaffre, 2009: Reanalysis of 47 Years of Climate in the French Alps (1958-2005): Climatology and Trends for Snow Cover. Journal of Applied Meteorology and Climatology, 48, 2487-2512.

Ellis A.W., G.B. Goodrich, G.M. Garfin. 2010. A hydroclimatic index for examining patterns of drought in the Colorado River Basin. International Journal of Climatology 30: 236-255.

Feng, S., and Q. Hu, 2007: Changes in winter snowfall/precipitation ratio in the contiguous United States. Journal of Geophysical Research-Atmospheres, 112, 12.

Garcia, J. A., M. C. Gallego, A. Serrano, and J. M. Vaquero, 2007: Trends in block-seasonal extreme rainfall over the Iberian Peninsula in the second half of the twentieth century. Journal of Climate, 20, 113-130.

Gedzelman, S., R. Arnold. 1993. The form of cyclonic precipitation and its thermal impact. Monthly Weather Review 121: 1957-1978.

Gershunov, A., 1998: ENSO influence on intraseasonal extreme rainfall and temperature frequencies in the contiguous United States: Implications for long-range predictability. Journal of Climate, 11, 3192-3203.

Gershunov, A., and T. P. Barnett, 1998a: ENSO influence on intraseasonal extreme rainfall and temperature frequencies in the contiguous United States: Observations and model results. Journal of Climate, 11, 1575-1586.

——, 1998b: Interdecadal modulation of ENSO teleconnections. Bulletin of the American Meteorological Society, 79, 2715-2725.

Goodrich, G. 2007. Influence of the Pacific decadal oscillation on winter precipitation and drought during years of neutral ENSO in the western United States. Weather and Forecasting, 22, 116-124.

Green, K., and C. M. Pickering, 2009: The Decline of Snowpatches in the Snowy Mountains of Australia: Importance of Climate Warming, Variable Snow, and Wind. Arctic Antarctic and Alpine Research, 41, 212-218.

Groisman, P. Y., R. W. Knight, T. R. Karl, D. R. Easterling, B. M. Sun, and J. H. Lawrimore, 2004: Contemporary changes of the hydrological cycle over the contiguous United States: Trends derived from in situ observations. Journal of Hydrometeorology, 5, 64-85.

Gutzler, D. S., D. M. Kann, and C. Thornbrugh, 2002: Modulation of ENSO-based long-lead outlooks of Southwestern US winter precipitation by the Pacific decadal oscillation. Weather and Forecasting, 17, 1163-1172.

Hamlet, A. F., and D. P. Lettenmaier, 1999: Columbia River streamflow forecasting based on ENSO and PDO climate signals. Journal of Water Resources Planning and Management-Asce, 125, 333-341.

Hamlet, A. F., P. W. Mote, M. P. Clark, and D. P. Lettenmaier, 2005: Effects of temperature and precipitation variability on snowpack trends in the western United States. Journal of Climate, 18, 4545-4561.

——, 2007: Twentieth-century trends in runoff, evapotranspiration, and soil moisture in the western United States. Journal of Climate, 20, 1468-1486.

Hanley, D. E., M. A. Bourassa, J. J. O'Brien, S. R. Smith, and E. R. Spade, 2003: A quantitative evaluation of ENSO indices. Journal of Climate, 16, 1249-1258.

Hare, S. R., and N. J. Mantua, 2000: Empirical evidence for North Pacific regime shifts in 1977 and 1989. 103-145.

Harrison, D. E., and N. K. Larkin, 1997: Darwin sea level pressure, 1876-1996: Evidence for climate change? Geophysical Research Letters, 24, 1779-1782.

Harshburger, B., H. Ye, and J. Dzialoski, 2002: Observational evidence of the influence of Pacific SSTs on winter precipitation and spring stream discharge in Idaho. Journal of Hydrology, 264, 157-169.

Heppner, P. O. G., 1992: Snow versus rain - looking beyond the magic numbers. Weather and Forecasting, 7, 683-691.

Hidalgo, H. G., and J. A. Dracup, 2003: ENSO and PDO effects on hydroclimatic variations of the Upper Colorado River basin. Journal of Hydrometeorology, 4, 5-23.

Hidalgo, H. G., and Coauthors, 2009: Detection and attribution of streamflow timing changes to climate change in the western United States. Journal of Climate, 22, 3838-3855.

Higgins, R.W., A. Leetmaa, V. E. Kousky. 2002. Relationships between climate variability and winter temperature extremes in the United States. Journal of Climate. 15: 1555-1572.

Hollander, M., and D. A.Wolfe, 1999: Nonparametric Statistical Methods. Wiley-Interscience, 787 pp.

Huschke R.W., 1959: Glossary of Meteorology. Bulletin of the American Meteorological Society. Available from: http://amsglossary.allenpress.com/glossary.

IPCC, 2007: Climate Change 2007: The Physical Science Basis. Contribution of Working Group I to the Fourth Assessment Report of the Intergovernmental Panel on Climate Change [Solomon, S., D. Qin, M. Manning, Z. Chen, M. Marquis, K.B. Averyt, M.Tignor and H.L. Miller (eds.)]. Cambridge University Press,Cambridge, United Kingdom and New York, NY, USA

Kalnay, E., and Coauthors, 1996: The NCEP/NCAR 40-year reanalysis project. Bulletin of the American Meteorological Society, 77, 437-471.

Kalra, A., T. C. Piechota, R. DavieS, and G. A. Tootle, 2008: Changes in US streamflow and western US snowpack. Journal of Hydrologic Engineering, 13, 156-163.

Kahya, E., J. Dracup. 1994. The influences of type-1 El-Nino and La-Nina events on streamflows in the Pacific-Southwest of the United-States. Journal of Climate. 7: 965-976.

Kanae, S., T. Oki, and K. Musiake, 2001: Impact of deforestation on regional precipitation over the Indochina Peninsula. Journal of Hydrometeorology, 2, 51-70.

Ke, C. Q., T. Yu, K. Yu, G. D. Tang, and L. King, 2009: Snowfall trends and variability in Qinghai, China. Theoretical and Applied Climatology, 98, 251-258.

Keyantash, J., and J. A. Dracup, 2002: The quantification of drought: An evaluation of drought indices. Bulletin of the American Meteorological Society, 83, 1167-1180.

Kestin, T., D. Karoly, J. Yang, et al. 1998. Time-frequency variability of ENSO and stochastic simulations. Journal of Climate. 11: 2258-2272.

Khaliq, M. N., and P. Gachon, 2010: Pacific Decadal Oscillation Climate Variability and Temporal Pattern of Winter Flows in Northwestern North America. Journal of Hydrometeorology, 11, 917-933.

Kim, J., T. Kim, R. Arritt et al. 2002. Impacts of increased atmospheric CO2 on the hydroclimate of the western United States. Journal of Climate, 15, 1926-1942.

Knowles, N., M. D. Dettinger, and D. R. Cayan, 2006: Trends in snowfall versus rainfall in the Western United States. Journal of Climate, 19, 4545-4559.

Kunkel, K., et al., 2007. Trend identification in twentieth-century US snowfall: The challenges. Journal of Atmospheric and Oceanic Technology, 24, 64-73.

Kunkel, K. E., M. Palecki, L. Ensor, K. G. Hubbard, D. Robinson, K. Redmond, and D. Easterling, 2009a: Trends in Twentieth-Century U. S. Snowfall Using a Quality-Controlled Dataset. Journal of Atmospheric and Oceanic Technology, 26, 33-44.

Kunkel, K. E., M. A. Palecki, L. Ensor, D. Easterling, K. G. Hubbard, D. Robinson, and K. Redmond, 2009b: Trends in Twentieth-Century US Extreme Snowfall Seasons. Journal of Climate, 22, 6204-6216.

Kutner, M.H., C.J. Nachtsheim, J. Neter, and W. Li, 2005: Applied Linear Statistical Models. McGraw-Hill, 1396 pp.

Lau, N. C., 1997: Interactions between global SST anomalies and the midlatitude atmospheric circulation. Bulletin of the American Meteorological Society, 78, 21-33.

Leung, L. R., Y. Qian, X. D. Bian, W. M. Washington, J. G. Han, and J. O. Roads, 2004: Mid-century ensemble regional climate change scenarios for the western United States. Climatic Change, 62, 75-113.

Lilliefors, H., 1967: On Kolmogorov-Smirnov test for normality with mean and variance unknown. Journal of the American Statistical Association, 62, 399-405.

Mantua, N., S. Hare, Y. Zhang, et al. 1997. A pacific interdecadal climate oscillation with impacts on salmon production. Bulletin of the American Meteorological Society, 78, 1069-1079.

Marty, C., 2008: Regime shift of snow days in Switzerland. Geophysical Research Letters, 35.

McCabe, G. J., and D. M. Wolock, 2009: Snowpack in the Context of Twentieth-Century Climate Variability. Earth Interactions, 13.

McGinnis, D. L., 2000: Synoptic controls on upper Colorado River basin snowfall. International Journal of Climatology, 20, 131-149.

Micu, D., 2009: Snow pack in the Romanian Carpathians under changing climatic conditions. Meteorology and Atmospheric Physics, 105, 1-16.

Minder, J. R., 2010: The Sensitivity of Mountain Snowpack Accumulation to Climate Warming. Journal of Climate, 23, 2634-2650.

Mock, C. J., 1995: Avalanche climatology of the continental zone in the southern Rocky-Mountains. Physical Geography, 16, 165-187.

Mock, C. J., and K. W. Birkeland, 2000: Snow avalanche climatology of the western United States mountain ranges. Bulletin of the American Meteorological Society, 81, 2367-2392.

Mote, P., A. Hamlet, and E. Salathe, 2008: Has spring snowpack declined in the Washington Cascades? Hydrology and Earth System Sciences, 12, 193-206.

Mote, P. W., 2003: Trends in snow water equivalent in the Pacific Northwest and their climatic causes. Geophysical Research Letters, 30.

——, 2006: Climate-driven variability and trends in mountain snowpack in western North America. Journal of Climate, 19, 6209-6220.

Mote, P. W., A. F. Hamlet, M. P. Clark, and D. P. Lettenmaier, 2005: Declining mountain snowpack in western North America. Bulletin of the American Meteorological Society, 86, 39-+.

Pierce, D. W., and Coauthors, 2008: Attribution of declining western us snowpack to human effects. Journal of Climate, 21, 6425-6444.

Power, S. B., and I. N. Smith, 2007: Weakening of the Walker Circulation and apparent dominance of El Nino both reach record levels, but has ENSO really changed? Geophysical Research Letters, 34.

Rackauskas, A., and D. Zuokas, 2007: New tests of heteroskedasticity in linear regression model. Lithuanian Mathematical Journal, 47, 248-265.

Rajagopalan, B., U. Lall, and M. A. Cane, 1997: Anomalous ENSO occurrences: An alternate view. Journal of Climate, 10, 2351-2357.

Rauscher, S. A., J. S. Pal, N. S. Diffenbaugh, and M. M. Benedetti, 2008: Future changes in snowmelt-driven runoff timing over the western US. Geophysical Research Letters, 35.

Redmond, K. T., and R. W. Koch, 1991: Surface climate and streamflow variability in the western united-states and their relationship to large-scale circulation indexes. Water Resources Research, 27, 2381-2399.

Renwick, J. A., and J. M. Wallace, 1996: Relationships between North Pacific wintertime blocking, El Nino, and the PNA pattern. Monthly Weather Review, 124, 2071-2076.

Rodgers, K. B., P. Friederichs, and M. Latif, 2004: Tropical pacific decadal variability and its relation to decadal modulations of ENSO. Journal of Climate, 17, 3761-3774.

Ropelewski, C., M. Halpert. 1986. North-American precipitation and temperature patterns associated with the El Nino Southern Oscillation (ENSO). Monthly Weather Review, 114, 2352-2362.

Schoner, W., I. Auer, and R. Bohm, 2009: Long term trend of snow depth at Sonnblick (Austrian Alps) and its relation to climate change. Hydrological Processes, 23, 1052-1063.

Schwing, F. B., C. S. Moore, S. Ralston, and K. M. Sakuma, 2000: Record coastal upwelling in the California Current in 1999. California Cooperative Oceanic Fisheries Investigations Reports, 41, 148-160.

Sheffield, J., and E. F. Wood, 2008: Global trends and variability in soil moisture and drought characteristics, 1950-2000, from observation-driven Simulations of the terrestrial hydrologic cycle. Journal of Climate, 21, 432-458.

Sheppard, P. R., A. C. Comrie, G. D. Packin, K. Angersbach, and M. K. Hughes, 2002: The climate of the US Southwest. Climate Research, 21, 219-238.

Sinha, T., and K. A. Cherkauer, 2008: Time Series Analysis of Soil Freeze and Thaw Processes in Indiana. Journal of Hydrometeorology, 9, 936-950.

Solow, A. R., and A. Huppert, 2003: On non-stationarity of ENSO. Geophysical Research Letters, 30.

Steinskog, D. J., D. B. Tjostheim, and N. G. Kvamsto, 2007: A cautionary note on the use of the Kolmogorov-Smirnov test for normality. Monthly Weather Review, 135, 1151-1157.

Stewart, I. T., 2009: Changes in snowpack and snowmelt runoff for key mountain regions. Hydrological Processes, 23, 78-94.

Stewart, I., D. Cayan, M. Dettinger. 2005. Changes toward earlier streamflow timing across western North America. Journal of Climate, 18, 1136-1155.

St Jacques, J.M., D.J. Sauchyn, Y. Zhao. 2010. Northern Rocky Mountain streamflow records: Global warming trends, human impacts or natural variability. Geophysical Research Letters 37: L06407

Stoner, A. M. K., K. Hayhoe, and D. J. Wuebbles, 2009: Assessing General Circulation Model Simulations of Atmospheric Teleconnection Patterns. Journal of Climate, 22, 4348-4372.

Straus, D. M., and J. Shukla, 2002: Does ENSO force the PNA? Journal of Climate, 15, 2340-2358.

Svoma, B. M., Balling, R.C., Ellis, A.W. 2010. Analysis of soil moisture trends in the Salt River watershed of central Arizona, Theoretical and Applied Climatology, DOI: 10.1007/s00704-010-0255-1

Svoma, B.M. 2011. Trends in snow level elevation in the mountains of central Arizona, International Journal of Climatology, 31 (1): 87-94. DOI 10.1002/joc.2062

Trenberth, K. E., and T. J. Hoar, 1996: The 1990-1995 El Nino Southern Oscillation event: Longest on record. Geophysical Research Letters, 23, 57-60.

Troup, A. J., 1965: Southern oscillation. Quarterly Journal of the Royal Meteorological Society, 91, 490-&.

Wallace, J. M., and D. S. Gutzler, 1981: Teleconnections in the geopotential height field during the Northern Hemisphere winter. Monthly Weather Review, 109, 784-812.

Wetzel S, Martin J. 2001. An operational ingredients-based methodology for forecasting mid-latitude winter season precipitation. Weather and Forecasting, 16, 156–167.

Williams, C. J., J. P. McNamara, and D. G. Chandler, 2009: Controls on the temporal and spatial variability of soil moisture in a mountainous landscape: the signature of snow and complex terrain. Hydrology and Earth System Sciences, 13, 1325-1336.

Wolter, K., R. M. Dole, and C. A. Smith, 1999: Short-term climate extremes over the continental united states and ENSO. Part I: Seasonal temperatures. Journal of Climate, 12, 3255-3272.

Wunsch, C., 1999: The interpretation of short climate records, with comments on the North Atlantic and Southern Oscillations. Bulletin of the American Meteorological Society, 80, 245-255.

Xu, Z. X., Z. F. Liu, G. B. Fu, and Y. N. Chen, 2010: Trends of major hydroclimatic variables in the Tarim River basin during the past 50 years. Journal of Arid Environments, 74, 256-267.

Ye, H. C., and M. Ellison, 2003: Changes in transitional snowfall season length in northern Eurasia. Geophysical Research Letters, 30.

Yu, B., and F. W. Zwiers, 2007: The impact of combined ENSO and PDO on the PNA climate: a 1,000-year climate modeling study. Climate Dynamics, 29, 837-851.

Yu, B., A. Shabbar, and F. W. Zwiers, 2007: The enhanced PNA-like climate response to Pacific interannual and decadal variability. Journal of Climate, 20, 5285-5300.

Zhang, T., K. Stamnes, and S. A. Bowling, 2001: Impact of the atmospheric thickness on the atmospheric downwelling longwave radiation and snowmelt under clear-sky conditions in the Arctic and Subarctic. Journal of Climate, 14, 920-939.

Zhang, Y., J. M. Wallace, and N. Iwasaka, 1996: Is climate variability over the North Pacific a linear response to ENSO? Journal of Climate, 9, 1468-1478.

APPENDIX A

SUPPLEMENTARY FIGURES

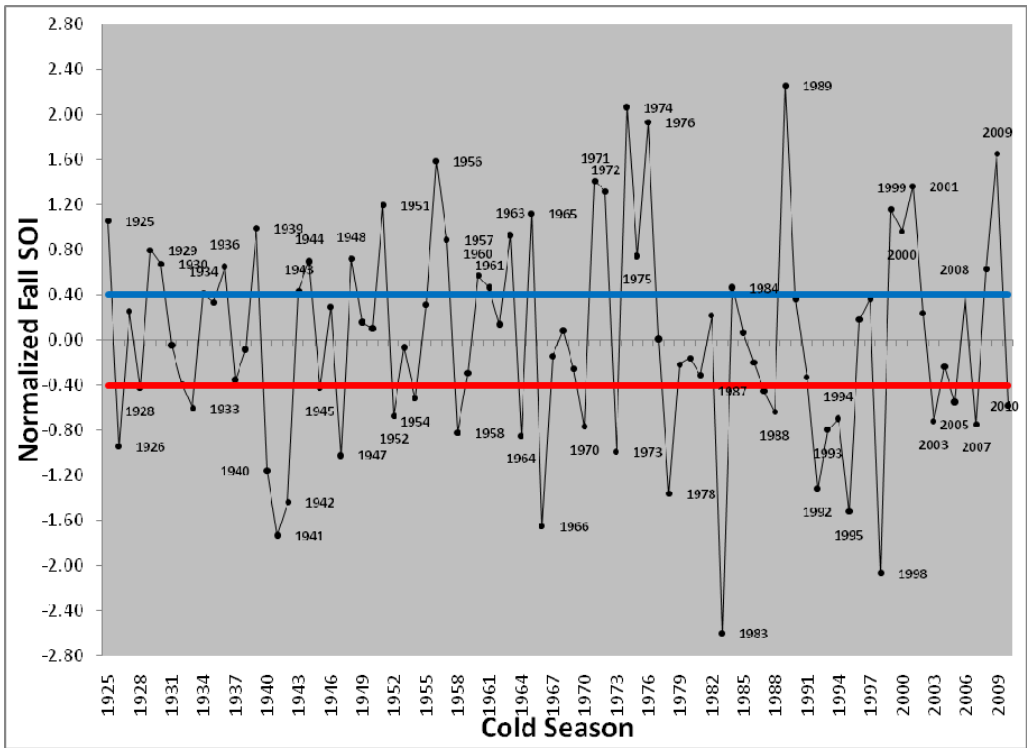

Figure A.1: Normalized fall SOI values used to quantify ENSO. Values below the red line (i.e., <-0.4) indicate El Niño events and values above the blue line (i.e., >0.4) indicate La Niña events. El Niño and La Niña events are labeled by water year (i.e., 1925 represents the winter of 1924/1925 and the normalized SOI from the fall of 1924).

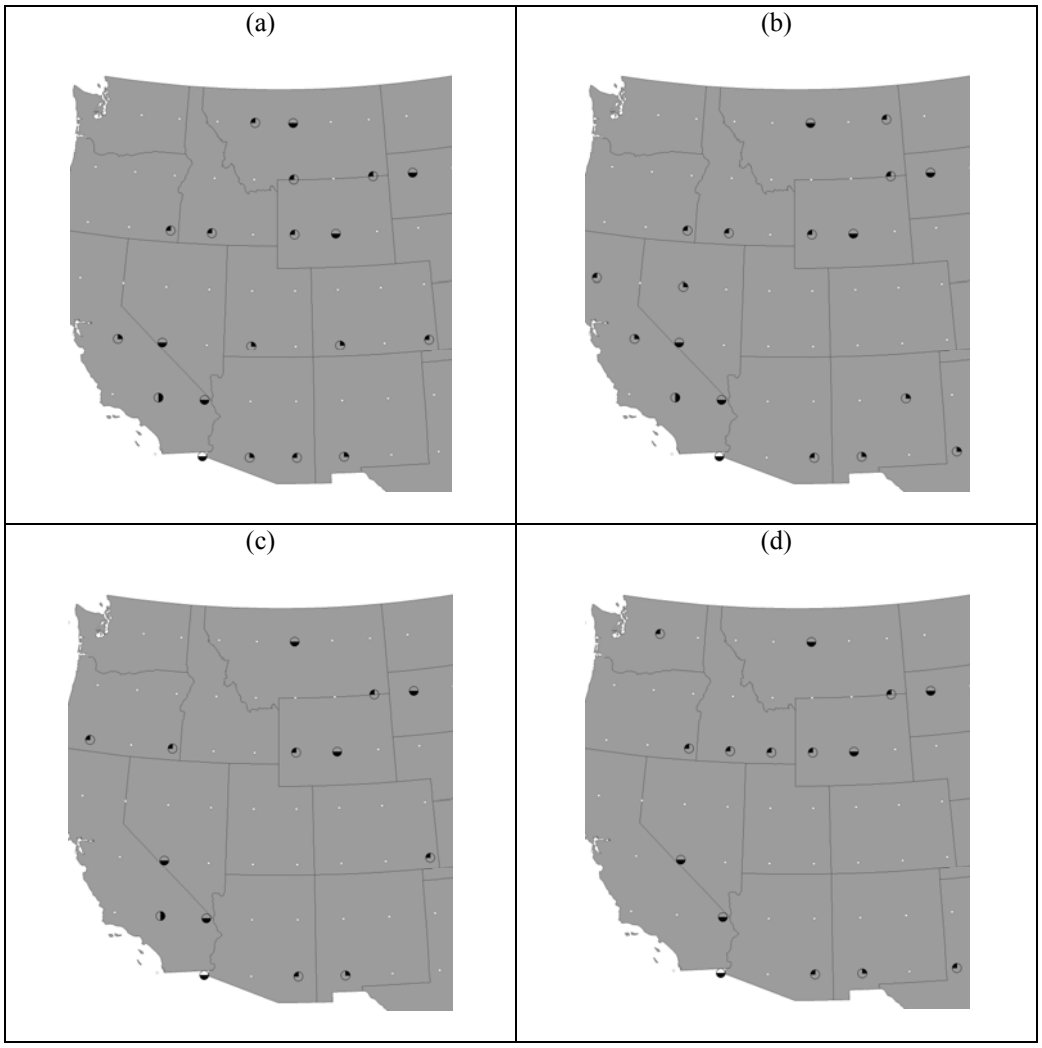

Figure A.2: Results for the Lilliefors test for error normality and the Breusch-Pagan test for constant error variance for the Pearson product-moment correlations between normalized fall SOI and winter median wet day 850 hPa temperature (a), 1000-850 hPa thickness (b), 850-700 hPa thickness (c), and 1000-500 hPa thickness (d). The dots represent NCEP/NCAR reanalysis grids displaying no significant violations of the error normality and constant error variance assumptions. Rejections of the error normality assumption at the 0.05 level for one Lilliefors test are indicated by circles filled with black in the upper-right quarter. Rejection of the error normality assumption for both Lilliefors tests are indicated by circles filled with black in the right half. Rejections of the constant error variance assumption at the 0.05 level for one Breusch-Pagan test are indicated by circles filled with black in the upper-left quarter. Rejections of the error normality assumption for one Lilliefors tests and the constant error variance assumption for one Breusch-Pagan test are indicated by circles filled with black in lower half.

Figure A.3: As in Figure A.2 but for the cold PDO.

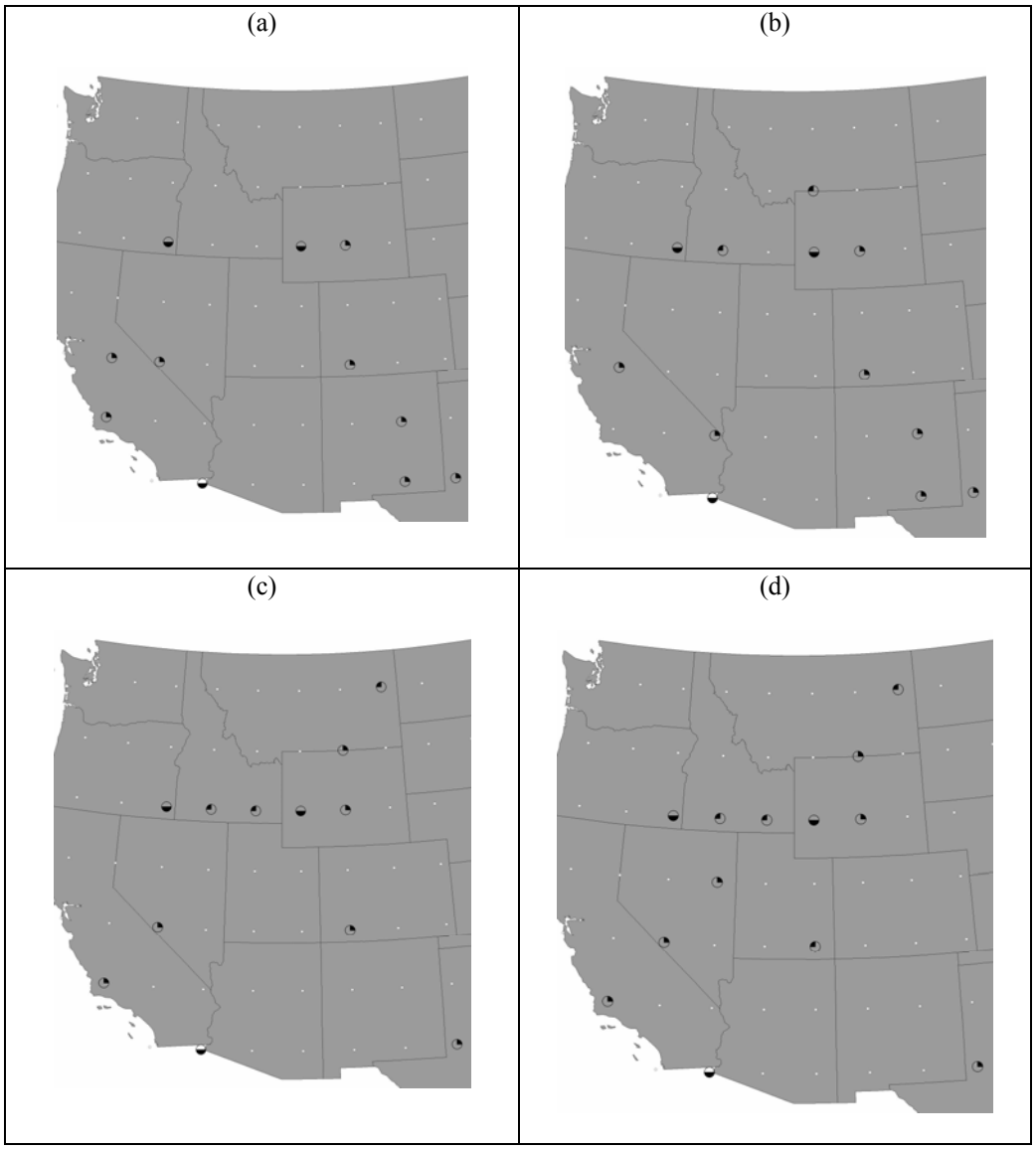

Figure A.4: As in Figure A.2 but for the warm PDO

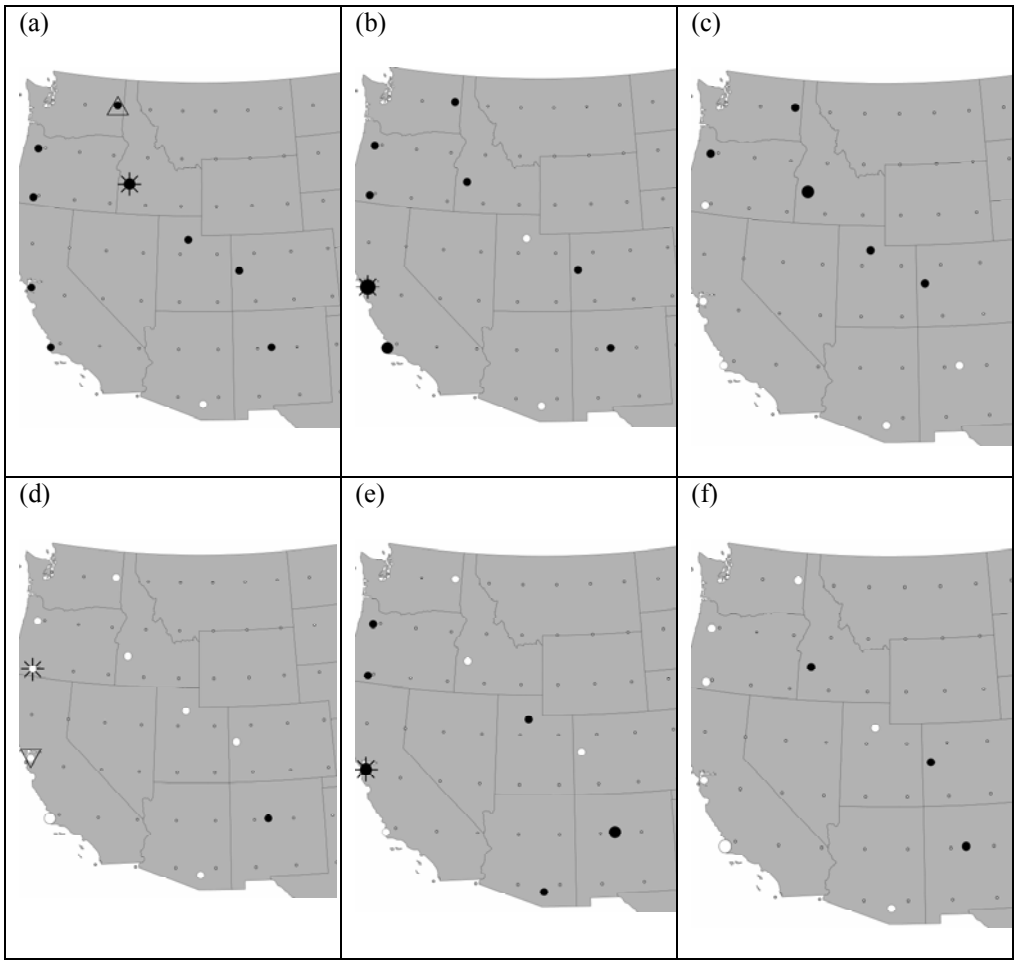

Figure A.5: As in Figure 5.15 but for the 1200 UTC soundings. Note, for the sake of simplicity, the 1200 UTC correlation results are not displayed and should be inferred from the panels be below.

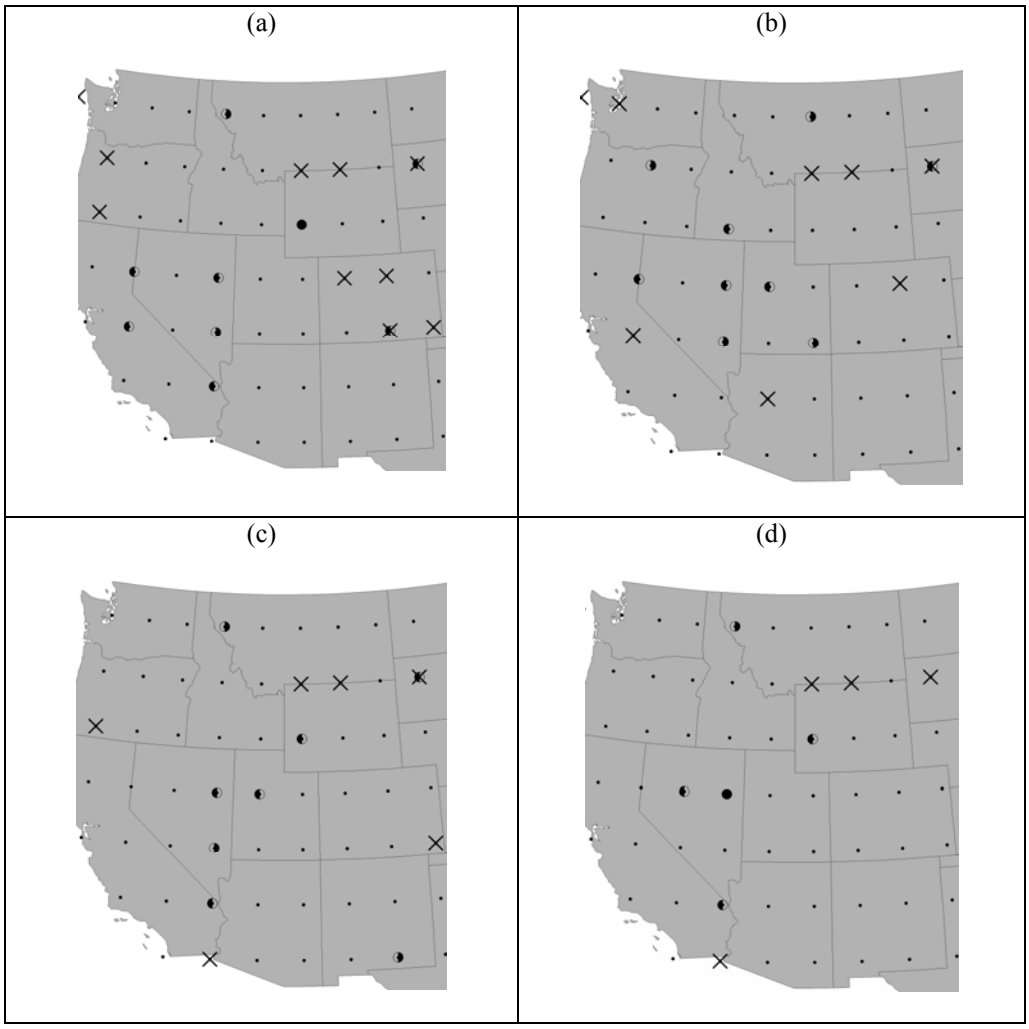

Figure A.6: Results for the Lilliefors test for error normality, the Breusch-Pagan test for constant error variance, and the Durbin-Watson test of independent error terms for the simple linear regression trend tests for cold season median wet day 850 hPa temperature (a), 1000-850 hPa thickness (b), 850-700 hPa thickness (c), and 1000-500 hPa thickness (d). The dots represent NCEP/NCAR reanalysis grids displaying no significant violations of the error normality, constant error variance, and independent error term assumptions. Rejections of the error normality assumption at the 0.05 level are indicated by circles filled with black in the right half. Rejections of the constant error variance assumption at the 0.05 level are indicated by circles filled with black in the left half. Grids displaying significant first-order autocorrelation in the error terms as determined by the Durbin-Watson test are indicated as × (note, autocorrelation was successfully alleviated by the Hildreth-Lu procedure in all cases).

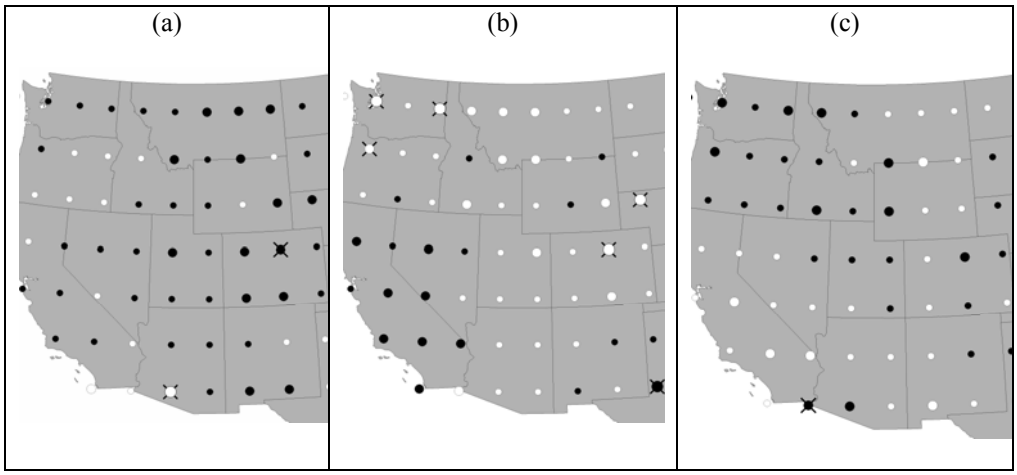

Figure A.7: Mann-Kendall trend test results for the percentage of sampled wet days per cold season occurring in October-November (a), December-January (b), and March-April (c). Black (white) circles indicate positive (negative) trends. Large circles indicate $|\tau|$>0.2, medium circles indicate 0.1<$|\tau|$≤0.2, and small circles indicate 0.0<$|\tau|$≤0.1. Significant trends ($p<0.05$) are indicated by ×.

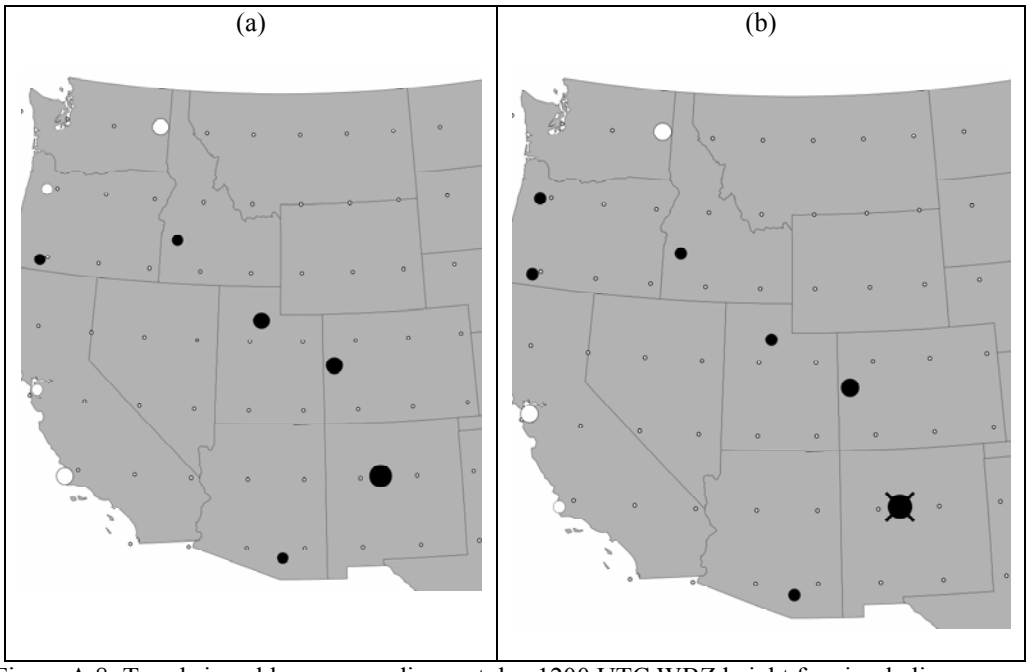

Figure A.8: Trends in cold season median wet day 1200 UTC WBZ height for simple linear regression (b_1) (a) and Mann-Kendall trend test (τ) (b). Black (white) circles indicate positive (negative) trends. For simple linear regression (a), large circles indicate $|b_1|$ >40.0 m dec^{-1}, medium circles indicate 20.0< $|b_1|$ ≤40.0 m dec^{-1}, and small circles indicate 0.0< $|b_1|$ ≤20.0 m dec^{-1}. For Mann-Kendall test (b), large circles indicate $|\tau|$ >0.2, medium circles indicate 0.1< $|\tau|$ ≤0.2, and small circles indicate 0.0< $|\tau|$ ≤0.1. Significant trends (p<0.05) are indicated by ×.

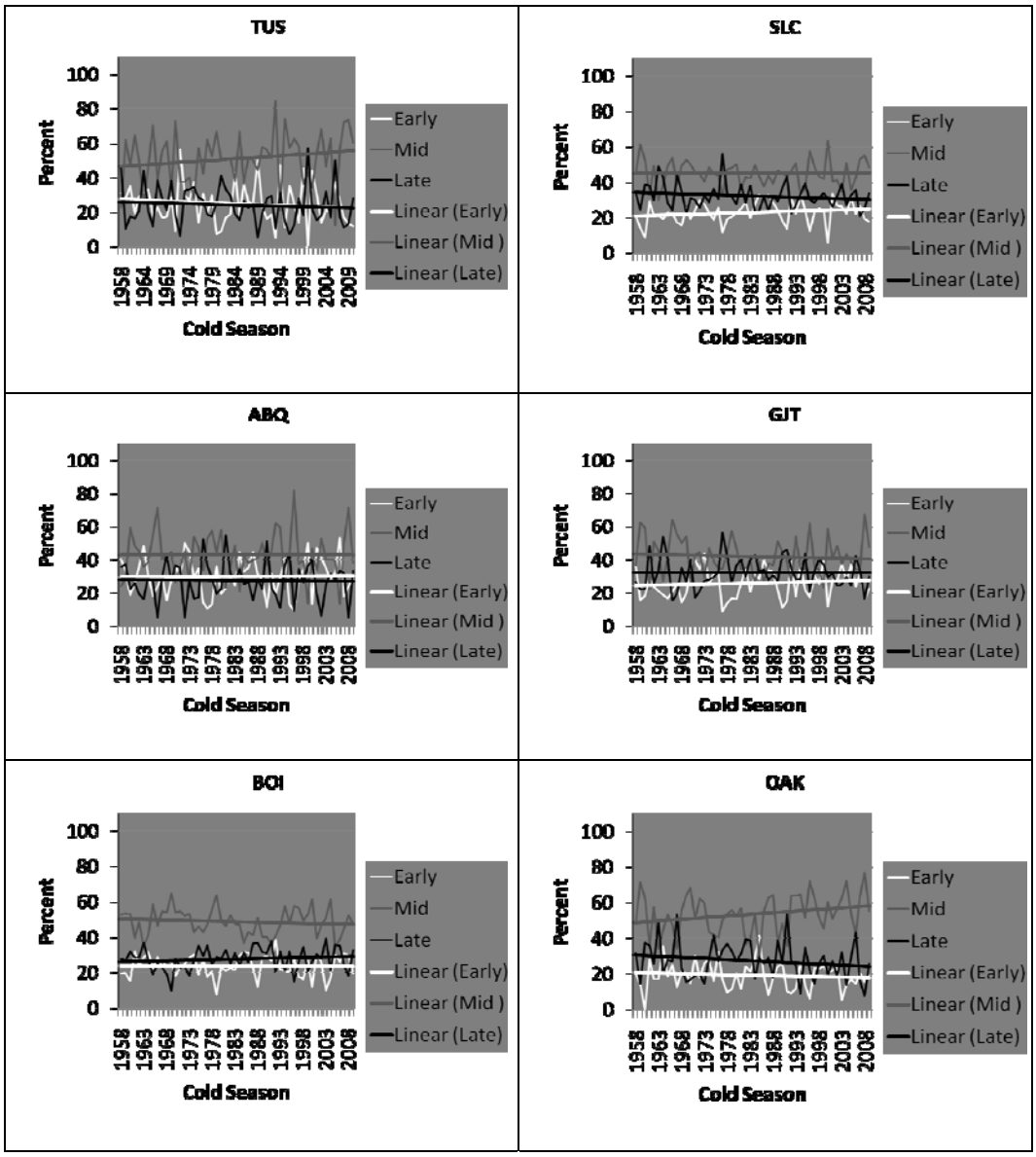

Figure A.9: For the ten rawinsonde sites, the percentages of wet days per cold season (thin lines) and linear fits (thick lines) during October-November (early period; white lines), December-February (middle period; gray lines) and March-April (late period; black lines).

Figure A.9 Continued

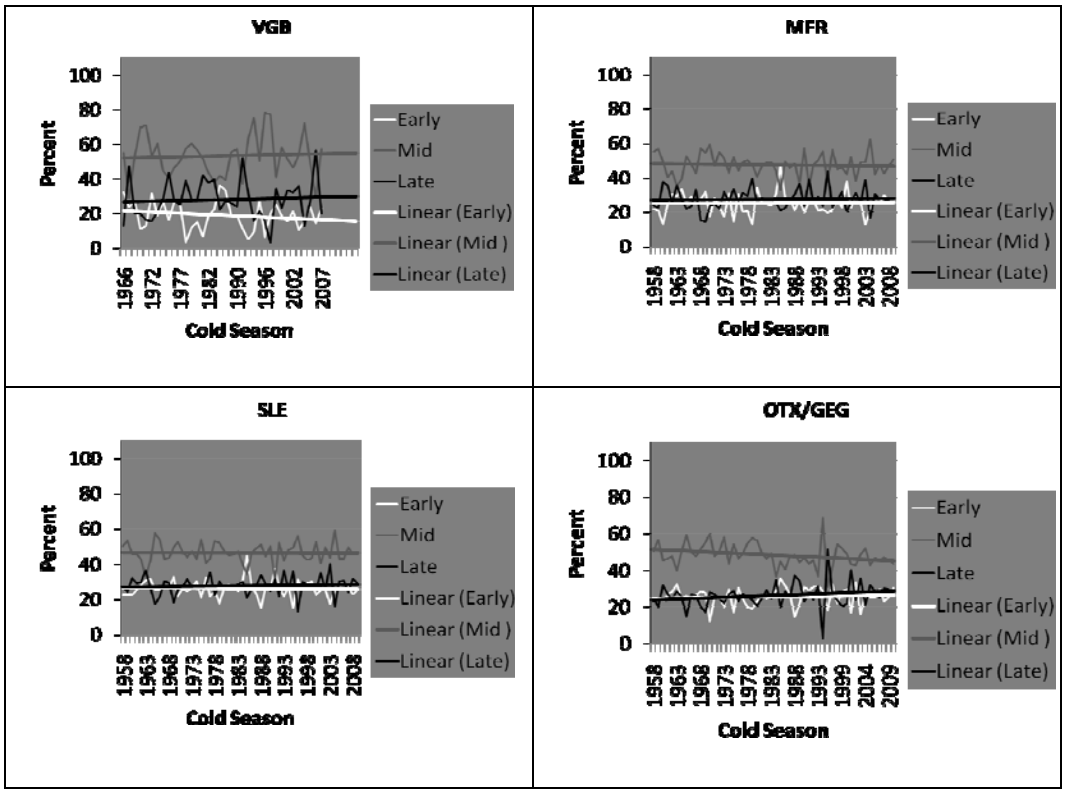

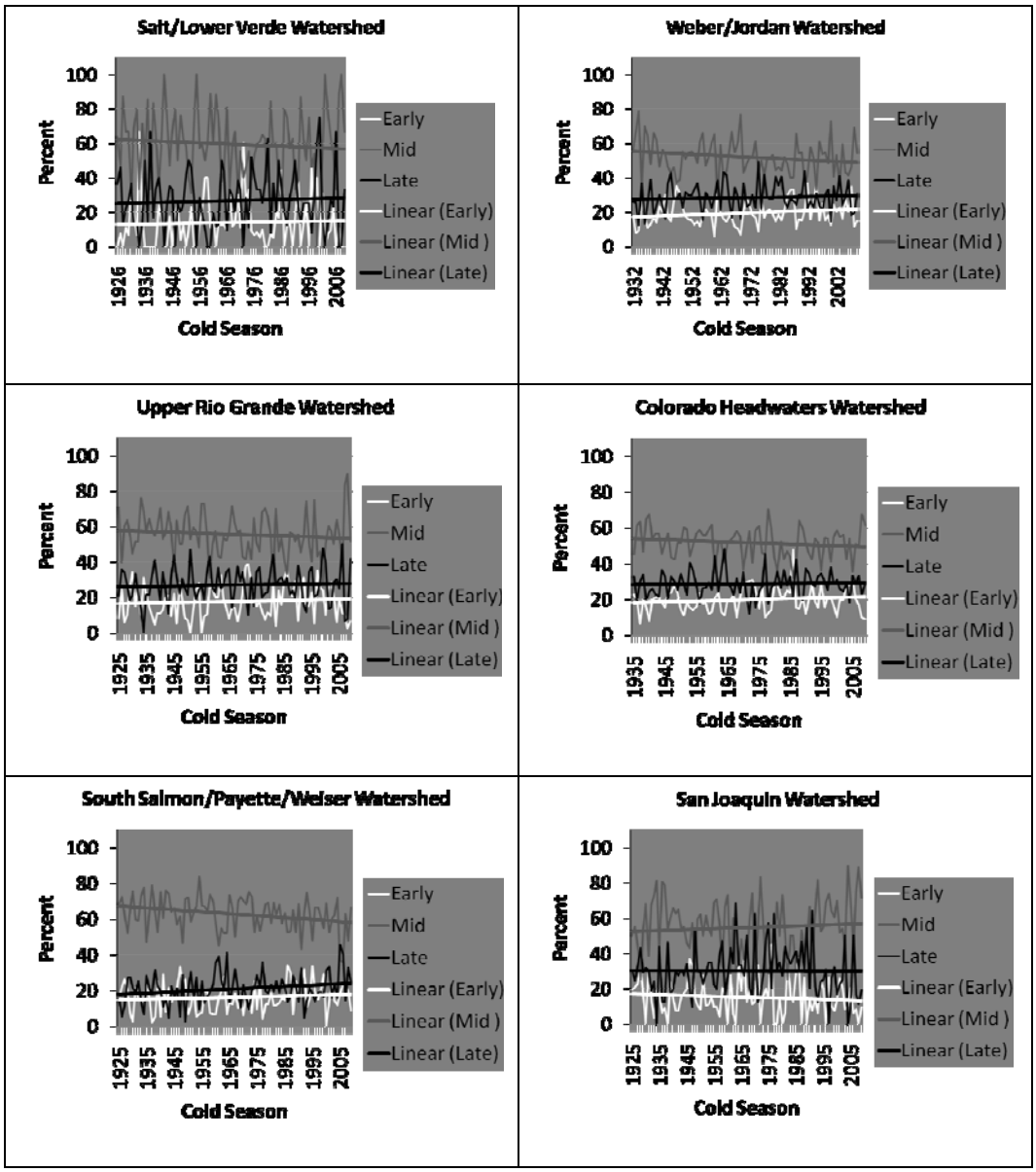

Figure A.10: For the ten watersheds, the percentages of days per cold season (thin lines) and linear fits (thick lines) with snow levels estimated during October-November (early period; white lines), December-February (middle period; gray lines) and March-April (late period; black lines).

Figure A.10 Continued